EXCHANGE PROCESSES BETWEEN STRATOSPHERE AND TROPOSPHERE

by A.D. CHRISTIE

Department of Meteorology

Imperial College of Science and Technology

A thesis submitted for the degree of Ph.D., in the University of London. April, 1964.

'Show us not the aim without the way,
For ends and means on earth are so entangled
That changing one, you change the other too;
Each different path brings other ends in view.'

Ferdinand Lassalle.

ABSTRACT

Following a critical appraisal of tracer properties and data, an attempt is made to elucidate the nature and amount of trans-tropopause exchange directly, and using ozone profiles for Liverpool obtained during the I.G.Y., together with simultaneous profiles of potential temperature, and horizontal and vertical wind components.

Circulation models in the troposphere and lower stratosphere are critically appraised and a favoured system presented. A model of trans-tropopause transfer is postulated from analysis of velocity components. The computed mean vertical transfer is the same order as the net transfer inferred from stratospheric residence times, suggesting the eddy mass transfers make a minor contribution.

Climatological analysis of the Liverpool profiles suggest:

1. Total ozone observations may not be used to infer information on ozone profiles.

2. There are two apparently distinct maxima in the seasonal mean ozone at standard levels in the upper troposphere and lower stratosphere. The later one (June/July) was found to increase in magnitude with approach to the tropopause.

We attempted verification of the nature of local (and mean) transverse circulations about the jet, inferred from evidence of other investigations, by interpreting horizontal profiles of mean ozone across the jet in the troposphere and in the 100 mb super-tropopause layer, endeavouring to subdue the effects of seasonal and jet level variations. The profiles indicated almost uniform

ozone in the 100 mb layer above the tropopause, but within the troposphere higher ozone to the right of the jet looking downstream, with a secondary though smaller ozone high to the left. Using similar techniques we then essayed construction of characteristic cross sections of ozone, potential temperature, and horizontal and vertical wind components.

The contribution of both vertical and horizontal components of enthalpy flux divergence to tropopause formation were found to be negligible, though of correct sign.

The evidence was interpreted as implying a mean direct (Hadley) cell penetrating the tropopause in the tropics and sub-tropics, and an indirect cell centred 150 mb below the polar front wind maximum, with local transverse circulations in entrance and exit regions of the jet contributing to transfer by large scale eddy mixing.

CONTENTS

Chapter 8 Exchange of Air Between the Troposphere and the Stratosphere

CHAPTER 1

Introduction

1.1 Statement of the Problem

The problem to be investigated in this thesis is the exchange of air between the stratosphere and the troposphere. This is part of the larger problem of the general circulation of the atmosphere and will be presented in this context.

In this chapter we shall review very briefly the nature of the problem, and the techniques available for investigating transfer.

The division of the atmosphere into stratosphere and troposphere is based on static stability, with a very stable stratosphere surmounting a troposphere in which the lapse rate is still broadly stable but comparable with the adiabatic. This thermal structure and its maintainance will be considered more fully in succeeding chapters; at present suffice to say that the two regimes are separated on most thermal profiles by a sharp lapse rate discontinuity. The concept that this lapse discontinuity, defined as a tropopause, constitutes a continuous impermeable boundary isolating the two lapse rate regimes but fluctuating in level in association with the fields of motion, has been treated with increasing scepticism in recent years and observations now show that the concept must be discarded.

Certain physical properties of a fluid and trace constituents of the atmosphere may be conservative under limiting conditions discussed later in some detail, and may be used to infer information on transfers. Water vapour, ozone mixing ratio and artificially produced radioisotopes (after initial rapid fallout due to gravitational sedimentation) may all be considered conservative in the lower stratosphere and upper troposphere.

Observations of the vertical distribution of water vapour over southern England by the British Met. Research Flight, summarised by Tucker (1957), show that there is generally a rapid decrease of mixing ratio with pressure near the tropopause and that in conditions of large thermal lapse rate discontinuities a small frost point lapse discontinuity may exist. The technique is not however well adapted to demonstrating the existence of a sharp transition of hygrolapse.

Ozone in the atmosphere is produced predominantly by photochemical processes with a minor contribution from lightening discharge. Since the high energy solar radiation effective in producing ozone has been absorbed in its downward path to mid-stratosphere the major ozone source is at or above this level. Chemical reactions, predominantly at the earth's surface to which the ozone is transported, are continuously destroying ozone. Estimates by Kroening and Ney (1961), of the rate of ozone removal at the earth's surface of 6×10^{10} atoms/cm^2/sec., show that the ozone destroyed there in the course of a year is of the same order of magnitude as the total hemispheric store. Since the latter is mainly in the lower and middle stratosphere, this gives a measure of the mass exchange taking place between that region and the troposphere and indicates that the mean life of lower and mid-stratospheric material is somewhat less than a year.

The ozone profiles over England measured by the Met. Research Flight and by Brewer and Milford (1960), and Brewer(1960), from radiosondes show rapid increase in concentration with height above a level roughly corresponding to the tropopause. Discontinuities

in concentration lapse rates and thermal lapse rates frequently occurred at different levels.

With the introduction of radioactive isotopes into the atmosphere by nuclear explosions, the problem of estimating atmospheric storage and drainage rates became one of biological as well as physical interest. Since the rate of surface deposition was observed to increase with time in the wake of extended periods of (in part) high level injection of artificially produced radioisotopes, it was logical to look to the atmosphere as a reservoir of activity. Estimates of the lifetime of radioisotopes within the troposphere reviewed by Sheppard (1963), vary from a few days to a month - a time scale much less than that inferred in the long term studies of deposition. Thus it was logical to consider the stratosphere as a store with a finite leakage of activity by mass exchange with the troposphere.

Estimates of the stratospheric residence times have ranged from several years (Stewart et al, 1958), to a year or less (Martell, 1959, Machta and List, 1959, Feely, 1960, Feely and Spar, 1960, and Staley, 1960).

The more recent and perhaps more reliable estimates of the period required for the removal of the activity of air whose origin is above the tropopause suggest that the mass transfer from stratosphere to troposphere in the course of a year is about the order of the mass of the stratosphere, which is consistent with the data on ozone.

The evidence (Martell, 1959), is for a more rapid transfer from the polar than from the tropical stratosphere.

An investigation of transfer mechanisms ideally involves following a preselected parcel of air. The simplest device, if physically realizeable, would be a zero lift balloon which would faithfully record the resultant motion of all systems to which it was exposed, of scale greater than the balloon. The practical alternative is the labelling of the parcel by means of some conservative property which may be used as a tracer.

Transfer of material between the stratosphere and troposphere may be effected by either mean or eddy motions, the spatio-temporal scale of mean defining the possible implication of eddy. Their relative contributions have yet to be established and the details of the processes have not yet been elaborated.

1.2 The Equations Governing Atmospheric Transfer

We will now present the various smoothed equations specifying fluid flow in the atmosphere, and see what their implications are in investigating transfer.

In all subsequent sections the following notation will be used:

ρ : density

α : specific volume

p : pressure

$\underline{V}$: velocity

u : zonal component of velocity

v : meridional component of velocity

ω : vertical companent of velocity

S : any conservative entity in amount per unit mass of air

$\underline{\Omega}$: angular velocity of the earth's rotation

ψ : potential energy

T : temperature

θ : potential temperature

C_p : specific heat at constant pressure

R : gas constant for 1 gm. dry air

K : $\frac{R}{C_p}$

q : energy added to unit mass of system by diabatic heating.

λ : latitude

ϕ : longitude

η : vorticity

$\underline{P}$: potential vorticity

$\underline{F}$: frictional force

$\underline{\mathbb{T}}_x$: $\underline{i}\tau_{xx} + \underline{j}\tau_{xy} + \underline{k}\tau_{xz}$ is the x component of the viscous stress tensor where $\underline{i}$, $\underline{j}$, and $\underline{k}$ are unit vectors in the x, y, and z directions respectively.

Vector quantities are denoted by means of a sub-bar, eg., $\underline{V}$ A mean value is defined by an integral of the form $\overline{p} = \frac{1}{\tau}\int_{t+\frac{\tau}{2}}^{t+\frac{\tau}{2}} p.dt$, and at any instant the field may be represented by two components, the mean and the deviation as follows $p = \overline{p} + p'$ where p' is the instantaneous departure from the mean value.

In the atmosphere $\frac{\rho'}{\rho} \doteq 10^{-3}$ whereas $\frac{V'}{V} \doteq 1$ which allows the approximation $\rho \doteq \overline{\rho}$ in most instances.

The equation of continuity of mass is:

$$\frac{\partial \rho}{\partial t} + \nabla.\rho\underline{V} = 0$$

By introducing the notation of means and deviations then, smoothing, we obtain:

$$\frac{\partial \overline{\rho}}{\partial t} + \nabla.\overline{\rho}\,\overline{\underline{V}} = 0 \quad \ldots\ldots\ldots\ldots\ldots\ldots\ldots\ldots\ldots\ldots 1.1$$

If we postulate the existence of any conservative entity S per unit mass of air

$$\frac{\partial \rho s}{\partial t} = -\nabla . \rho s \underline{V}$$

$$\frac{\partial \bar{\rho}(\bar{s}+s')}{\partial t} = -\nabla . \bar{\rho}(\bar{s}+s')(\underline{\bar{V}}+\underline{V}')$$

$$\frac{\partial \bar{\rho}\bar{s}}{\partial t} + \frac{\partial \overline{\rho' s'}}{\partial t} = -\nabla . \bar{\rho}\bar{s}\underline{\bar{V}} - \nabla . \bar{\rho}\bar{s}\underline{V}' - \nabla . \bar{\rho} s' \underline{\bar{V}} - \nabla . \overline{\rho' s' \underline{V}'}$$

Taking means of both sides this becomes:

$$\frac{\partial \bar{\rho}\bar{s}}{\partial t} = -\nabla . (\bar{\rho}\bar{s}\underline{\bar{V}}) - \nabla . (\overline{\rho' s' \underline{V}'})$$

or

$$\frac{d \bar{\rho}\bar{s}}{dt} = -\bar{\rho}\bar{s}\nabla . \underline{\bar{V}} - \nabla . (\overline{\rho' s' \underline{V}'})$$

i.e.

$$\bar{\rho}\frac{d\bar{s}}{dt} = -\bar{s}\left(\frac{d\bar{\rho}}{dt} + \bar{\rho}\nabla . \underline{\bar{V}}\right) - \nabla . (\overline{\rho' s' \underline{V}'}) = -\nabla . (\overline{\rho' s' \underline{V}'}) \quad \ldots\ldots 1.2.$$

The equation of motion, for a unit mass of air derived from Newton's law of rate of change of momentum, in terms of velocities measured relative to a system of axes rotating with the earth, may be expressed as follows:

$$\frac{d\underline{\bar{V}}}{dt} = -2\underline{\Omega} \wedge \underline{\bar{V}} - \nabla\psi - \bar{\alpha}\nabla\bar{p} + \bar{\alpha}\nabla . \quad \ldots\ldots 1.3.$$

	i	j	k
i	$\tau_{xx} - \bar{\rho}\overline{u'u'}$	$\tau_{xy} - \bar{\rho}\overline{u'v'}$	$\tau_{xz} - \bar{\rho}\overline{u'w'}$
j	$\tau_{xy} - \bar{\rho}\overline{u'v'}$	$\tau_{yy} - \bar{\rho}\overline{v'v'}$	$\tau_{yz} - \bar{\rho}\overline{v'w'}$
k	$\tau_{xz} - \bar{\rho}\overline{u'w'}$	$\tau_{yz} - \bar{\rho}\overline{v'w'}$	$\tau_{zz} - \bar{\rho}\overline{w'w'}$

where the forces acting on the unit mass are, in order of appearance on the righthand side of this equation:

1. The coriolis force resulting from the rotation of the system.
2. The geopotential resulting from the net component of gravity and centrifugal force.

3. The pressure gradient force.

4. The frictional force $\underline{F}$ resulting from the divergence of the viscous stresses τ_{ij} and the virtual eddy stresses $\overline{\rho}\,\overline{u'v'}$ etc.

This equation may be converted into the absolute vorticity equation by taking the curl of both sides.

$$\frac{d\eta}{dt} = -\eta(\nabla.\underline{\bar{v}}) + (\eta.\nabla)\underline{\bar{v}} - \nabla\bar{\alpha}\wedge\nabla\bar{p} + \nabla\wedge\bar{\alpha}\underline{F} \qquad \text{1.4.}$$

Since the atmosphere is not autobarotropic, ie. $\nabla\bar{\alpha}\wedge\nabla\bar{p} \neq 0$, we will consider an alternative function, the potential vorticity which removes this term from the equation. By first adding the smoothed continuity equation $\frac{d\bar{\alpha}}{dt} = \bar{\alpha}\nabla.\underline{\bar{v}}$ to 1.4 then multiplying by $\bar{\alpha}\nabla\bar{\theta}$ (θ is potential temperature) the equation becomes:

$$\frac{d}{dt}\{\bar{\alpha}\nabla\bar{\theta}.\eta\} - \bar{\alpha}\eta.\frac{d\nabla\bar{\theta}}{dt} - \bar{\alpha}\nabla\bar{\theta}.\eta.\nabla\underline{\bar{v}} + \bar{\alpha}\nabla\bar{\theta}.\nabla\bar{\alpha}\wedge\nabla\bar{p} - \bar{\alpha}\nabla\bar{\theta}\,\nabla\wedge\bar{\alpha}\underline{F} = 0.$$

or $$\frac{d}{dt}\{\bar{\alpha}\nabla\bar{\theta}.\eta\} = \underset{1.}{\bar{\alpha}\eta.\nabla\left(\frac{d\bar{\theta}}{dt}\right)} \underset{2.}{-\bar{\alpha}\nabla\bar{\theta}.\nabla\bar{\alpha}\wedge\nabla\bar{p}} + \underset{3.}{\bar{\alpha}\nabla\bar{\theta}.\nabla\wedge\bar{\alpha}\underline{F}}$$

In this equation term 2 is identically zero since θ is a function of α and p thus the complete equation of potential vorticity may be written:

$$\frac{dP}{dt} \equiv \frac{d}{dt}\left(\bar{\alpha}\nabla\bar{\theta}.\eta\right) = \bar{\alpha}.\eta.\nabla\left(\frac{d\theta}{dt}\right) + \bar{\alpha}\nabla\bar{\theta}.\nabla\wedge\bar{\alpha}\underline{F} \qquad \text{1.5}$$

The thermal transfer equation may be derived by subtracting the dynamic energy equation, obtained from 1.3, from the first law of thermodynamics:

$$\frac{dT}{dt} = \frac{1}{C_p}\left[\alpha\frac{dp}{dt} + \frac{dq}{dt} + \alpha\left\{\underline{\tau}_x.\frac{\partial\underline{v}}{\partial x} + \underline{\tau}_y.\frac{\partial\underline{v}}{\partial y} + \underline{\tau}_z.\frac{\partial\underline{v}}{\partial z}\right\}\right] \qquad \text{1.6.}$$

where $\frac{dq}{dt}$ is the rate of diabatic heating per unit mass of air.

Introducing the potential temperature enables us effectively to combine the individual rate of change of temperature and the adiabatic temperature change resulting from pressure variations

as follows:

$$\frac{d\theta}{dt} = \frac{1}{C_p}\left(\frac{p_0}{p}\right)^K \left[\frac{dq}{dt} + \alpha \left\{ \underline{\tau}_x \cdot \frac{\partial \underline{v}}{\partial x} + \underline{\tau}_y \cdot \frac{\partial \underline{v}}{\partial y} + \underline{\tau}_z \cdot \frac{\partial \underline{v}}{\partial z} \right\} \right] \quad \ldots\ldots\ldots 1.7.$$

Smoothing this becomes:

$$\frac{d\bar{\theta}}{dt} \doteq \frac{1}{C_p}\left(\frac{p_0}{p}\right)^K \left[\frac{d\bar{q}}{dt} + \overline{\underline{v}' \cdot \nabla q'} + \alpha \overline{\left\{ \underline{\tau}_x \cdot \frac{\partial \underline{v}}{\partial x} + \underline{\tau}_y \cdot \frac{\partial \underline{v}}{\partial y} + \underline{\tau}_z \cdot \frac{\partial \underline{v}}{\partial z} \right\}} \right] \quad \ldots\ldots 1.8$$

Clearly none of the properties whose total derivatives are evaluated in the above equations in the smoothed system, may be considered conservative, unless the terms appearing on the right of the equations equate to zero. In the appropriate sections we will consider under what conditions we are justified in making this assumption for various tracers or properties.

1.3 Proposed Procedure of Analysis

We must investigate to what extent we can clarify the transfer mechanisms and their connection with the observed fields of wind and temperature by the use of tracers.

The transfer equations which are superficially simplest are those associated with the mass continuity equation.

Here the investigation is one largely of scale, the scale dependence being associated with the smoothing process involved in the data measurement and analysis. Since we are concerned with investigating the transfer between stratosphere and troposphere the problem is further complicated by the lack of knowledge concerning the processes forming and maintaining the tropopause discontinuity itself. This complexity does not necessarily make the problem intractable for even if individual paths of parcels cannot be determined it may be possible, and is of great interest, to determine the integrated exchange across the mean tropopause

level by either, or a combination of, the mean and eddying motion at various times and locations.

In order to elucidate the climatology of the transfer processes, we will collate and present systematically, information on the atmospheric flow and transfer data from a survey of the literature, and interpret it in terms of consistency with alternative transfer models. In order to clarify the physics of the processes, a survey will be made of the current knowledge relating characteristic tracer distributions with specified synoptic situations. An attempt will then be made to analyse recent measurements of selected tracers, made over the U.K., and present them in such a manner as will assist in the exploration of the stratospheric-tropospheric transfer mechanisms.

CHAPTER 2 Climatological Analysis of Velocity, Temperature and Flux Distributions

2.1 General

Any enquiry into the nature of the mechanisms of exchange of air between troposphere and stratosphere requires that we first obtain a coherent description of the nature of the boundary between the two domains and of the fields of wind and temperature above and below it. We shall present the current state of knowledge on these matters.

The three dimensional specification of thermal and flow fields may be presented by either: a series of hemispheric charts of streamlines, isotachs and isotherms at finite pressure intervals or a number of equally spaced meridional cross sections of wind components and temperature, or preferably by both.

We observe obvious zonal assymetry in the temporal mean temperature distribution on isobaric surfaces over the northern hemisphere in 1950, (eg., figs. 2.1 and 2.2 from Piexoto, 1960). Similar standing waves occur in the temporaly smoothed streamline analysis of Heastie and Stevenson (1960), for high latitudes, and may be inferred in low latitudes from Krishnamurti's (1961), analysis of the subtropical jet stream of winter. Thus in order to construct representative mean meridional sections, we must perform a zonal smoothing by integrating around circles of latitude i.e., $[\bar{\psi}] = \frac{1}{2\pi}\int_0^{2\pi} \bar{\psi}\, d\lambda$ where $\bar{\psi} = \frac{1}{\tau}\int_{t-\frac{\tau}{2}}^{t+\frac{\tau}{2}} \psi\, dt$.

Any scaler property may now be expressed in the form $\psi = [\bar{\psi}] + \bar{\psi}^* + \psi'$ where $\bar{\psi}^*$ is the deviation of the temporal mean value of ψ at a selected longitude from the zonal mean value, i.e., the contribution from standing waves, while ψ' is the component resulting from transient eddies.

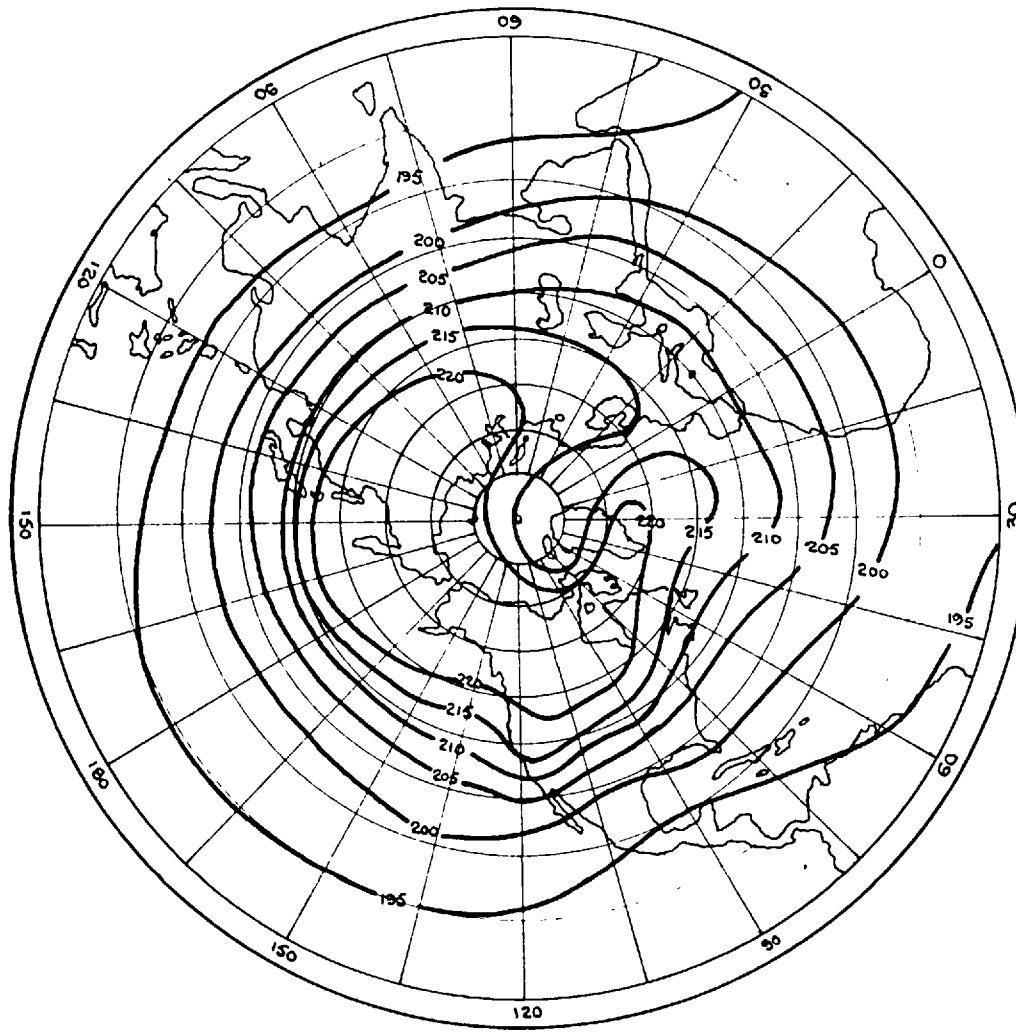

Figure 2.1. Distribution of 3 monthly mean temperature (°K) in winter at 100mb over the northern hemisphere (Piexoto, 1960).

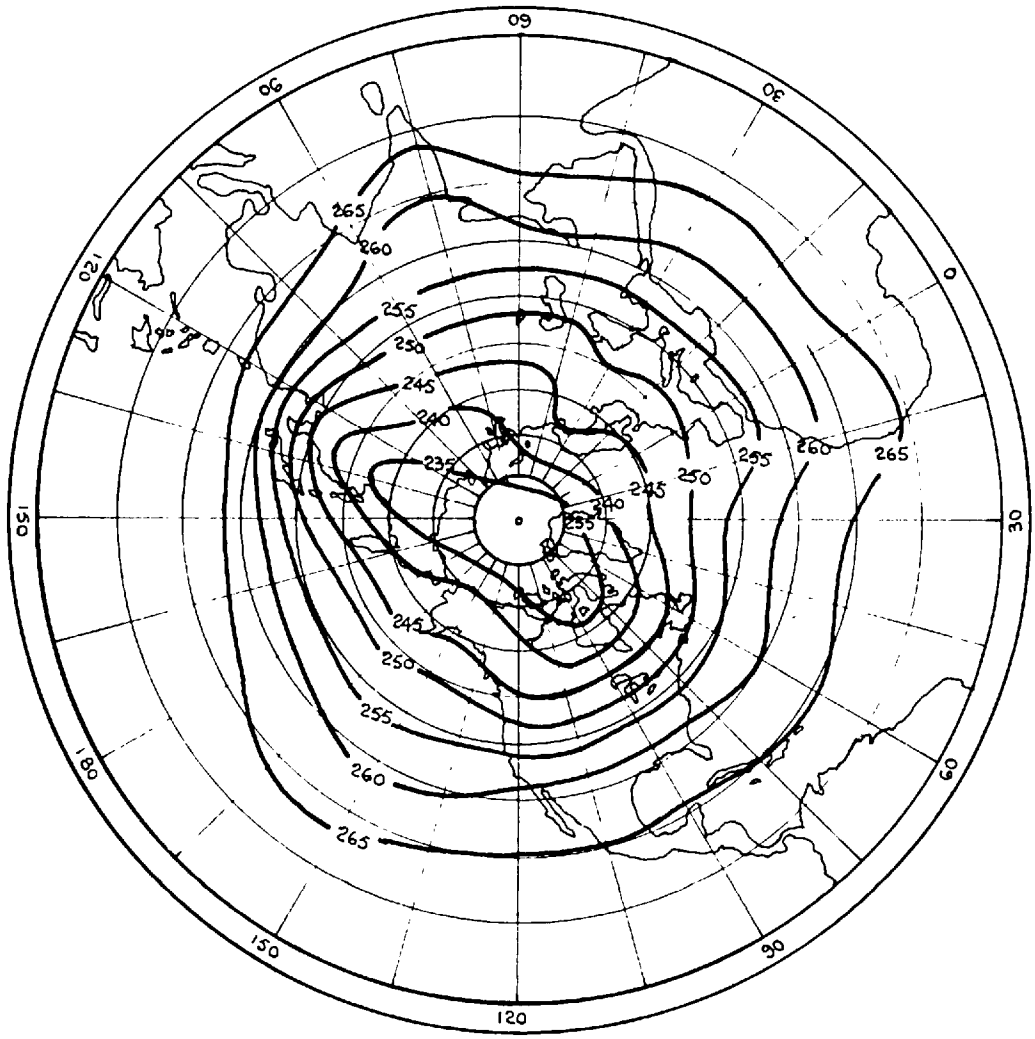

Figure 2.2. Distribution of 3 monthly mean temperature (°K) in winter at 500 mb over the northern hemisphere (Riexoto, 1960)

2.2 Mean Distributions

2.2.1 Wind

A chronological survey of analysis of meridional sections of temporal mean value of winds is presented in Table 2.1, together with a note on the area restrictions on the observations from which the means were derived.

The Crutcher (1961) analyses, illustrated for selected latitudes and seasons in figs. 2.3 and 2.4, show a persistent low latitude west wind maximum situated close to the 200 mb level. This maximum remains obvious on the winter zonal mean section in fig. 2.5, constructed from values computed from Crutcher's (1961) individual sections.

A second west wind maximum situated in higher latitudes is evident at certain selected meridians but absent from others and also from the zonal mean section. This maximum reflects the influence of migratory temperate zone jet streams which execute wavelike oscillations of large amplitude. In averaging, the zonal component is spread more or less uniformly over the whole latitude range of the oscillation.

Hemispheric charts of the seasonal mean values of maximum wind constructed from the Crutcher (1961) meridional cross sections show an apparent spiral pattern of jet streams circulating about a point displaced from the geographic pole towards east Asia and the Aleutians. This agrees with the 200 mb. isotach analysis of Wege (1957), but Krishnamurti (1961) claims the subtropical jet of winter is continuous around the world.

The zonal mean value of mean meridional wind, from Tucker's

Table 2.1 Summary of meridional sections of wind components for the troposphere, lower and middle stratosphere

Analysis Reference		Zonal Wind	Meridional Wind	Area of Analysis
			Tropospheric Analyses	
Mintz	(1954)	*		Geostrophic approximation from zonal mean contours
Tucker	(1959)		*	160W-0-40°E, mean value
Heastie & Stephenson	(1960)	*		20° intervals, zonal mean.
Crutcher	(1961)	*	*	10° intervals
Palmén & Vuorela	(1963)		*	winter zonal mean
			Lower stratospheric Analyses	
Mintz	(1954)	*		Geostrophic approximation from zonal mean contours
Kochanski	(1955)	*		Near 80°W
Pant	(1956)	*		Near 80°W
Wege et al	(1958)	*		Zonal mean
			Middle Stratospheric Analyses	
Pant	(1956)	*		Near 80°W
Murgatroyd	(1957)	*		All available observations

Table 2.2 Summary of meridional sections of temperature, T, and potential temperature, θ, for the troposphere, lower and middle stratosphere.

Analysis Reference.		Temperature T.	Poti Temp θ	Area of Analysis
			Tropospheric Analyses	
Bjerknes	(1934)	*		Eurasia
Willett	(1944)	*		U S A.
Hess	(1948)	*		Near 80°W.
Kochanski	(1955)	*		Near 80°W
Goldie et al	(1958)	*		80°W, 0°, 80°E, 140°E
Heastie & Stephenson	(1960)		*	20° intervals - zonal mean
Kochanski	(1955)	*		Near 80°W
Wege et al	(1958)	*		Zonal mean
Murgatroyd	(1957)	*		All available observations

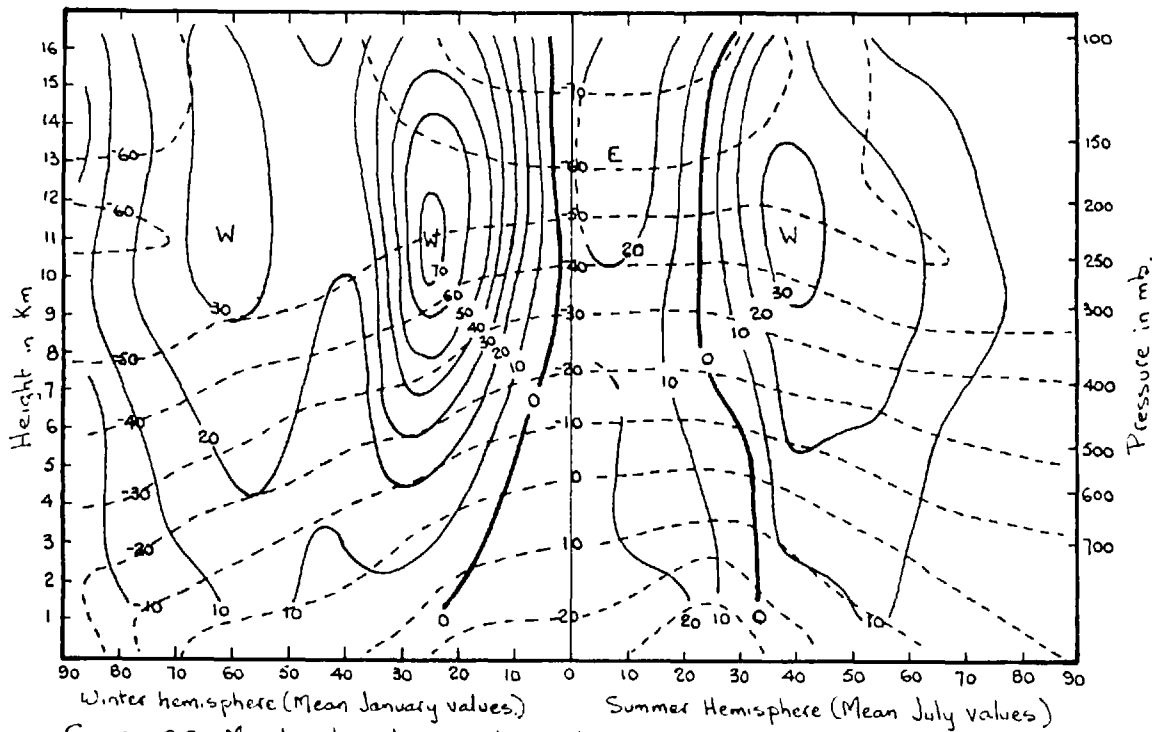

Figure 2.3. Meridional sections of temperature and zonal wind component for 0° W.

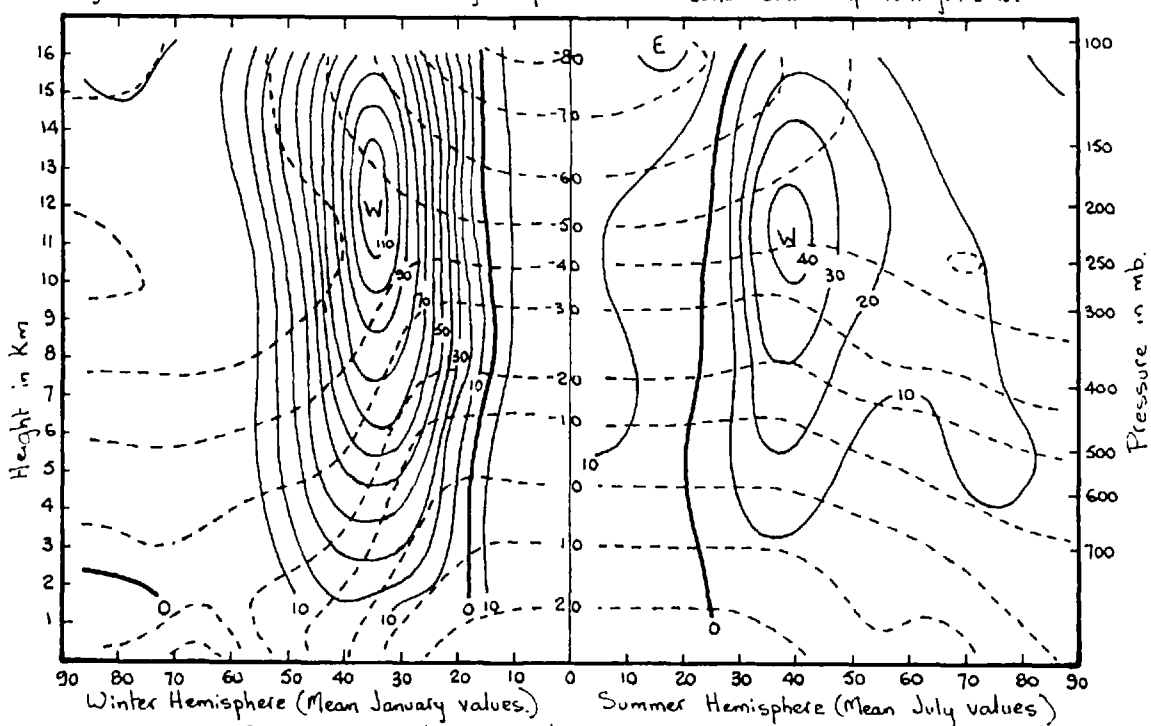

Figure 2.4. Meridional sections of temperature and zonal wind component for 140° E. for the northern hemisphere in winter and summer. Temperatures are in °C and winds in knots.

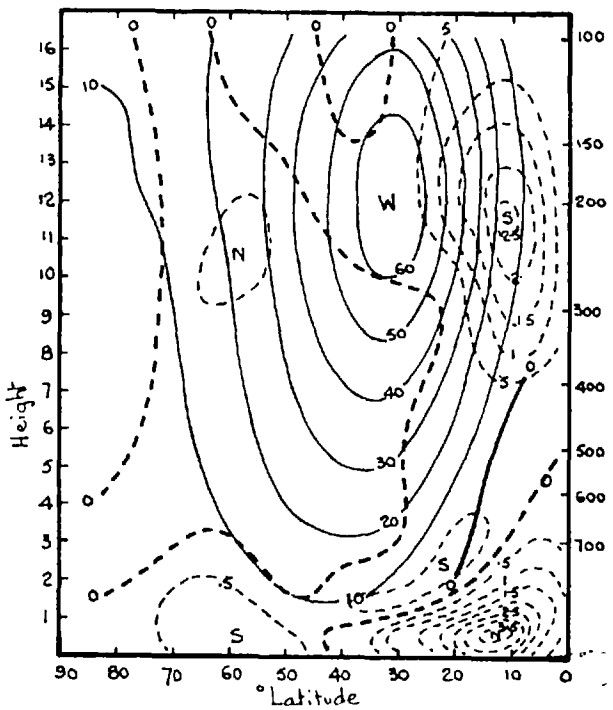

Figure 2.5. Meridional section of mean zonal (continuous lines) and meridional (dashed lines) wind components for the northern hemisphere in winter (from Crutcher, 1961, data)

(1959)analysis, are shown in fig. 2.6, and show good qualitative agreement with the more recent analysis of Palmén and Vuorela (1963) in fig. 2.5, made using the Crutcher (1961) meridional velocities. They indicate a direct circulation in low latitudes and an indirect cell in middle latitudes but evidence is not yet available about the sense or magnitude of the motions in the lower stratosphere.

Above 50 mb. the wind sampling has been much more sporadic. The most comprehensive survey currently available is that of Murgatroyd (1957), shown in fig. 2.7, in which he incorporated all the observations then available, from a variety of locations and utilising several measurement techniques, in characteristic seasonal sections. Since these sections were prepared much additional information on the wind field has been collected by releasing parachutes, plastic balloons, or chaff, from rockets between 60 and 80 km., above ground, and tracking their descent. (aumf Kampe, 1960, Masterson et al, 1961), and the Joint Scientific Advisory Group of the Meteorological Rocket Network, (1961).

2.2.2 Temperature

A chronological survey of mean meridional analyses of temperature is shown in Table 2.2.

From the characteristic seasonal cross sections of temperature in fig. 2.7 (from Murgatroyd, 1957), it is apparent that the atmosphere may be divided into strata with different thermal characteristics. These are:

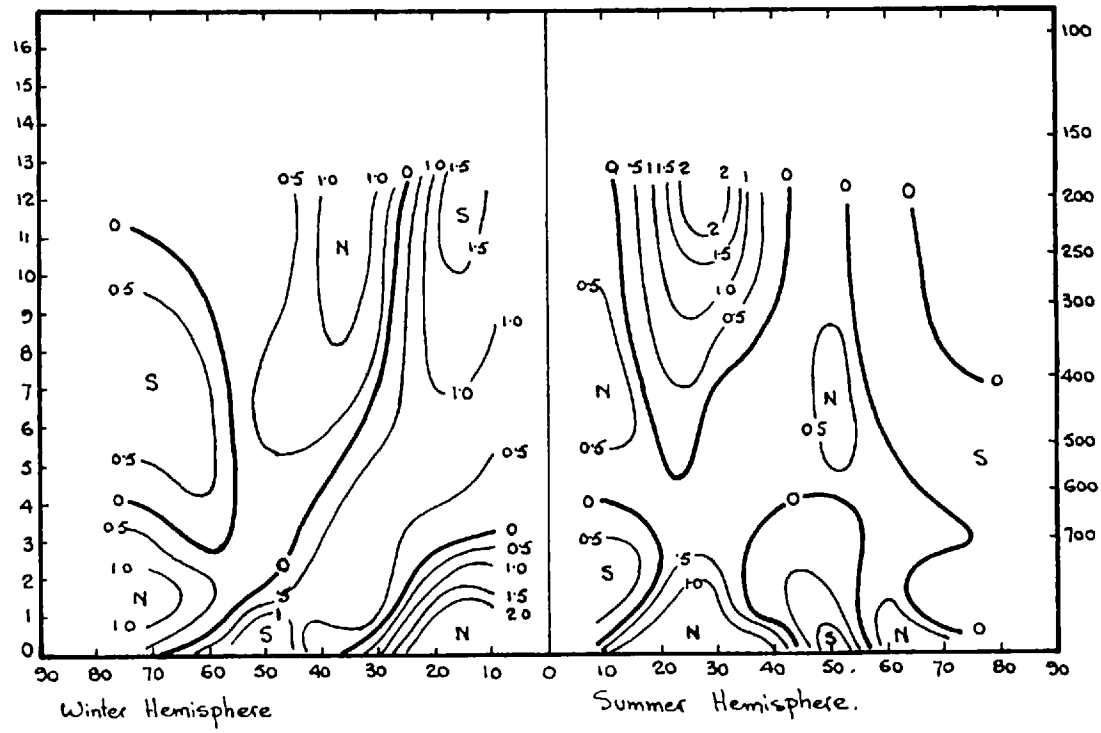

Figure 2.6. Mean meridional wind distribution in winter and summer over the northern hemisphere (from Tucker, 1959). Velocity units - m.sec^{-1}.

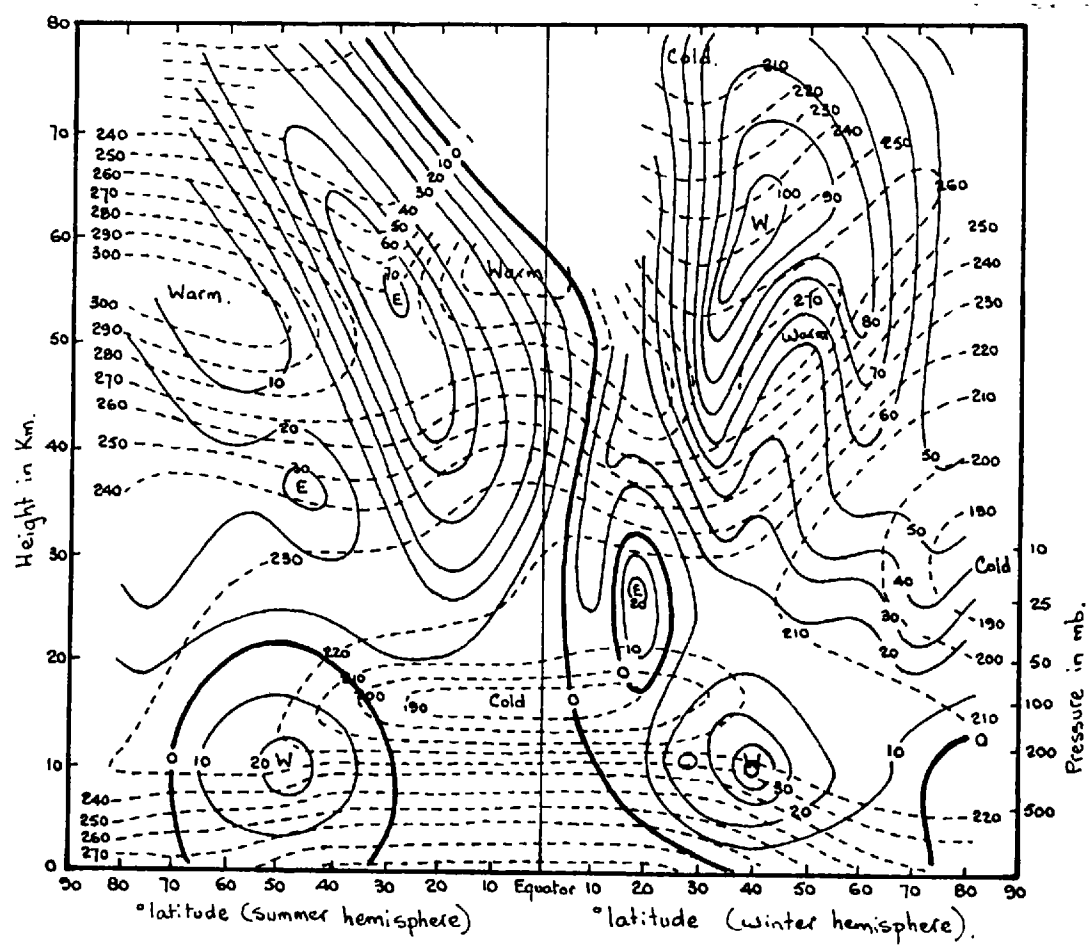

Figure 2.7. Meridional distribution of mean zonal wind (solid lines, in m. sec^{-1}) and temperature (dashed lines, in °K) in summer and winter, to a height of 80 km. (from Murgatroyd, 1957).

1. The troposphere - below 10-15 km., the thermal lapse rate is close to that for pseudo-adiabatic ascent, 7-10°K $km.^{-1}$ and horizontal gradient of temperature directed towards the equator in both winter and summer hemispheres.

2. The lower stratosphere - from 10-20 km., the thermal lapse rate drops to 1°K $km.^{-1}$ over the winter pole, becomes isothermal in winter mid-latitudes, and becomes negative over the tropics and in the summer hemisphere. Since the lapse rate change occurs at a higher level over the tropics than over the poles, the lapse rate reversal in the summer hemisphere ensures there a poleward directed horizontal temperature gradient. In the winter hemisphere the horizontal temperature gradient is directed polewards in the tropics but reverses in high latitudes consistent with the increase of lapse rate with latitude.

3. The middle stratosphere - from 20-30 km. The temperature continues to drop with height at about 1°K $km.^{-1}$ over the winter pole to a minimum between 25-30 km. of 190°K. In the summer hemisphere the temperature increases at about 0.5°K $km.^{-1}$ resulting in a horizontal temperature gradient directed from the winter to the summer pole, the magnitude of the gradient increasing with height.

4. The upper stratosphere - from 30-55 km. The temperature increases with height at a rate of approximately 3°K $km.^{-1}$ Since the lapse rate does not vary greatly with latitude the horizontal gradient remains directed from winter to summer hemisphere throughout the region.

The directions of the meridional gradients of mean temperature in the troposphere and lower stratosphere are readily observable in the zonal mean sections of potential temperature in winter and summer in fig. 2.8 from Heastie and Stevenson (1960).

2.3 Turbulent Mixing as a Transfer Process.

There is considerable turbulence associated with the above mean motions, the dynamical necessity for which was first demonstrated by Jeffreys (1926), and it has been discussed by Eady (1950), and Sheppard (1954). Further deductions on the existence and nature of transfer by both mean and eddy motion may be made from observations on the thermal and flow fields in two ways: by studies of balance requirements in meridional transfer of energy and momentum and by direct analysis of simultaneous zonal meridional and vertical components of velocity.

2.3.1 Information on atmospheric transfer from balance studies.

The transfer of an entity, S, per unit mass into unit volume is given by the flux convergence $-\nabla.\rho\underline{V}S$. In chapter 1 we saw how the transfer of various tracers might be expressed in the form:

$$\frac{\partial(\rho s)}{\partial t} = -\nabla.\rho\underline{V}S + \text{non conservative terms}$$

Integrating over an arbitrary volume, υ, with surface area, Σ, this becomes:

$$\frac{\partial}{\partial t}\iiint \rho S\, d\upsilon = -\iint \rho V_n S\, d\Sigma + \text{non conservative terms}$$

If the flux is evaluated over a zonal annular ring, the zonal component will vanish identically and the transfer equation for a complete annular ring may now be written:

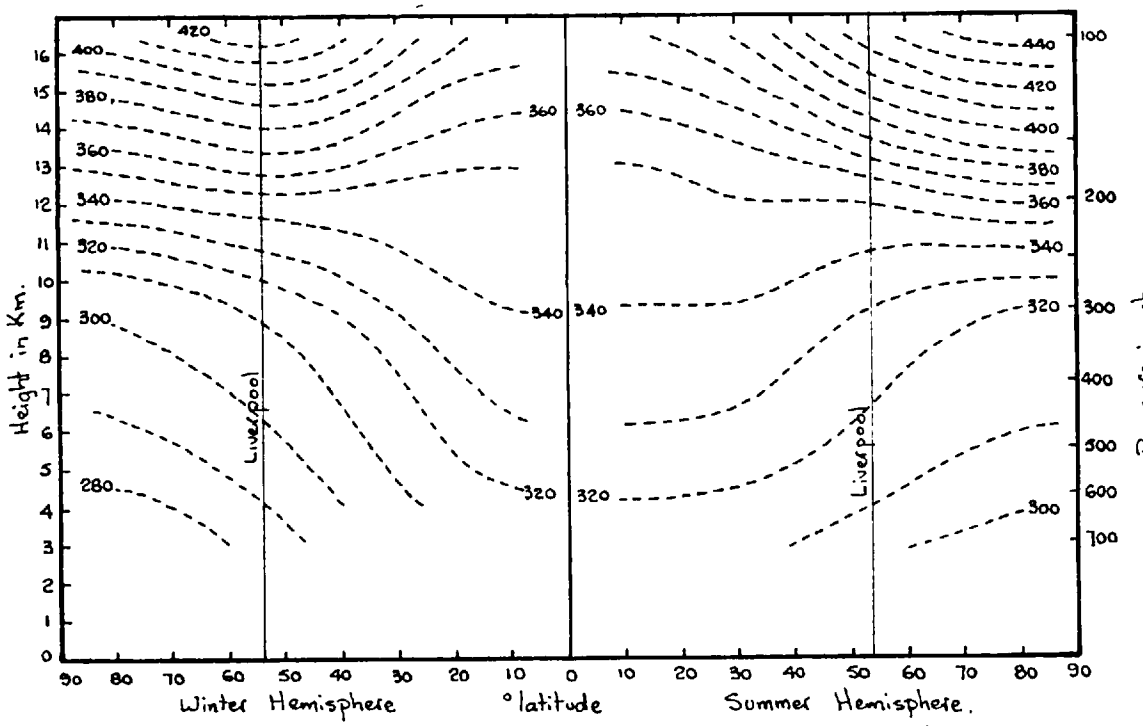

Figure 2.8 . Mean meridional sections of potential temperature (°K) in January and July for the northern hemisphere (from Heastie & Stephenson, 1960.)

$$\frac{\partial}{\partial t}\int_v \rho s\,dv = \left\{\int_{z_m}^{z_{m+1}} [\rho s v]\,dz\right\}_{y_m}^{y_{m+1}} + \left\{\int_{y_m}^{y_{m+1}} [\rho s w]\right\}_{z_m}^{z_{m+1}} + [\text{non-conservative terms}].$$

where the integrals within the brackets are evaluated over the interval specified after the bracket.

In practise the flux integrals are evaluated by considering spatial mean values of the properties inside the integral as dictated by the size of annulus considered. The accuracy of this approximation is clearly limited by the correlation between the variables in the integral within the integrating interval, and their respective variances.

Studies of balance are of two kinds - those involving net meridional transfers over the complete depth of the atmosphere and those involving transfers through annular rings of finite depth.

The studies of energy and angular momentum transfer will now be briefly considered.

2.3.2. Energy Balance Studies

Energy enters the atmosphere by short and long wave radiation and by convection of sensible ($C_p T$) and latent (Lr) heat. The heat budget for any volume is determined by the vertical fluxes of radiation together with the vertical and meridional fluxes of latent and sensible heat, neglecting viscous dissipation.

The radiative fluxes are functions of the distribution of absorbers, emitters and temperature; the type, thickness and amount of cloud, and the spectra, which are pressure and temperature dependent, of the contributory radiating gases.

London (1957), utilised a statistical model of the cloud, water vapour and temperature distributions to compute the net radiative sources and sinks of energy below 100 mb. for four seasons (fig. 2.9). We observe a resultant cooling of from 0 to 2°K day^{-1} with a maximum cooling mainly in the lower troposphere (2-5 km.).

Mean annual rates of temperature change due to Manabe and Möller (1961), are shown in fig. 2.10.

Calculations of the radiative cooling rates in the stratosphere have been made by Ohring (1958), Brooks (1958), and Murgatroyd and Goody (1958), to altitudes of 55, 50 and 90 km., respectively. Their results presented graphically in fig. 2.11, suggest a level of maximum rate of cooling 1.2°K day^{-1} at 25 km., from 10° - 70° N in winter and 1.1°K day^{-1} at 20 km., from 60° - 90° N in summer.

Now having evaluated the radiative effects it should be possible to estimate the mean and eddy components of the transport of energy in the forms: sensible ($c_p T$), potential (gz), and latent (Lr), necessary for balance.

At present only meridional balance studies of energy have been attempted and since much the greater energy source is the lower troposphere, the conclusions drawn will only apply to tropospheric transfer.

The thermal transfer equation 1.6 may be written:

$$\rho \frac{d}{dt}(c_p T + gz + Lr) = \rho \frac{dq}{dt} + \left\{ \mathbb{I}_x \cdot \frac{\partial v}{\partial x} + \mathbb{I}_y \cdot \frac{\partial v}{\partial y} + \mathbb{I}_z \cdot \frac{\partial v}{\partial z} \right\}$$

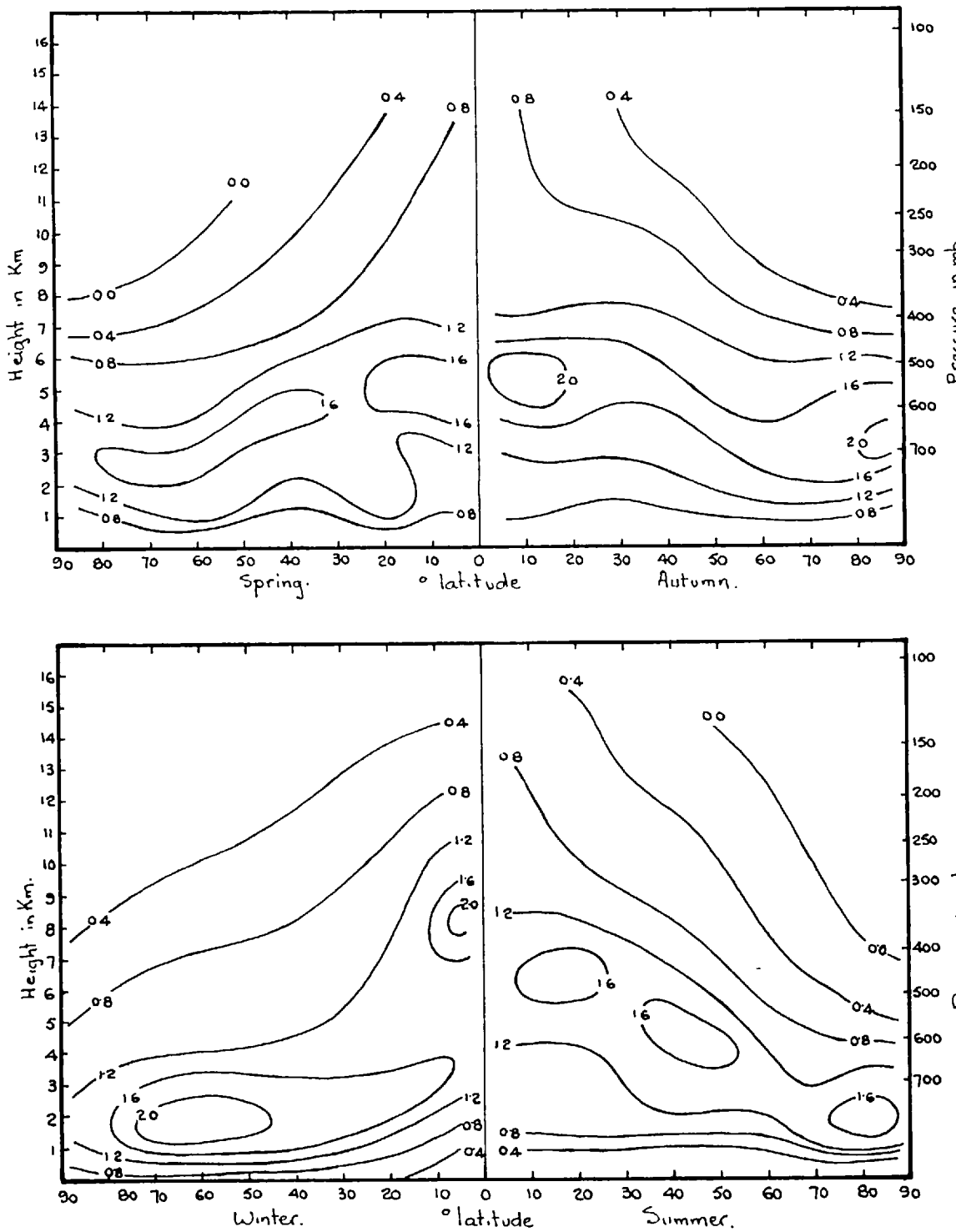

Figure 2.9. Meridional sections of net radiative cooling (in °K day^{-1}) in each season (from London, 1957.)

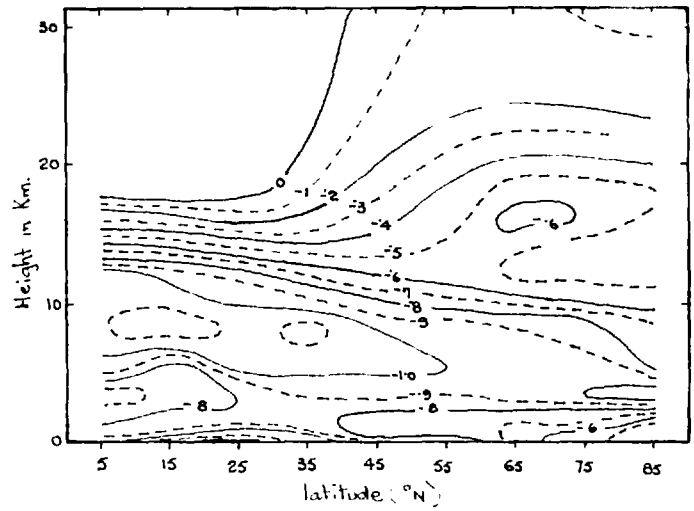

Figure 2.10. Computed distribution of annual mean rate of temperature change (°K day^{-1}) by radiation (Manabe and Möller, 1961)

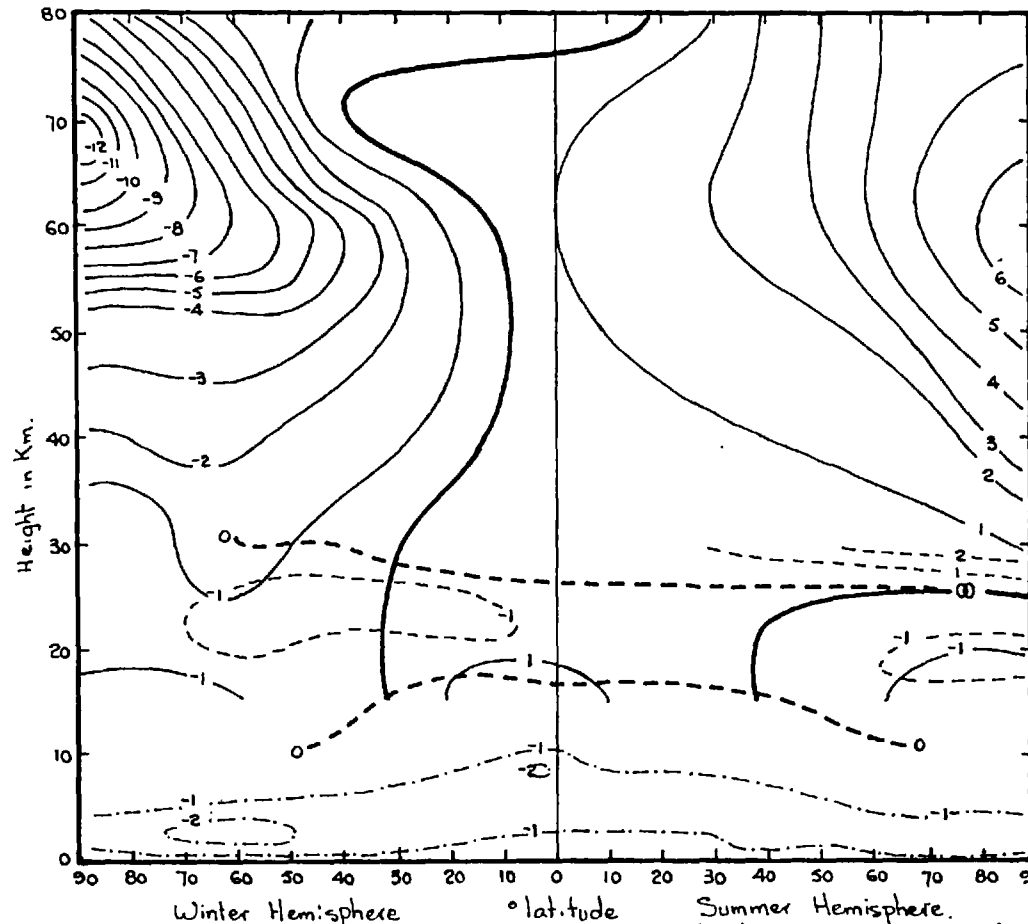

Figure 2.11. Meridional distribution of radiative heating rates in °K day^{-1} in winter and summer for the northern hemisphere. Continuous lines in the stratosphere from Murgatroyd & Singleton, (1961), dashed lines in the lower stratosphere from Brooks, (1958) and dash-dot lines in the troposphere from London (1957).

This reduces, after adding the product of the energy function in the round brackets and the mass continuity equation, to:

$$\frac{\partial \rho (c_p T + gz + Lr)}{\partial t} + \nabla \cdot \rho \underline{v} (c_p T + gz + Lr) = \rho \frac{dq}{dt} + \left\{ \underline{\tau}_x \cdot \frac{\partial \underline{v}}{\partial x} + \underline{\tau}_y \cdot \frac{\partial \underline{v}}{\partial y} + \underline{\tau}_z \cdot \frac{\partial \underline{v}}{\partial z} \right\} \quad \ldots\ldots 2.2.$$

Considering the net meridional flux across vertical walls extending from the surface to infinite height in a form indicated by equation 2.1 and substituting for each flux integral the appropriate mean and eddy terms (e.g. $\int_{\Sigma} \rho c_p T v_n \, d\Sigma \doteq \{[\bar{\rho}][\bar{c}_p][\bar{T}][\bar{v}] + [\bar{\rho}][\bar{c}_p][\overline{T'v'}]\}_{\phi_m}^{\phi_{m+1}}$). it becomes clear that the eddy contribution to energy transfer is effected by the sensible and latent heat transfers.

Starr and White (1954) estimated the contributions of the eddy transfers of sensible and latent heat to the energy transport. Their values are shown in fig. 2.12 together with estimated values of the northward energy transport required for balance, derived from calculations of the vertically integrated net budget of radiative heating. These show the energy transport to be almost entirely due to eddy flux in middle and high latitudes but a meridional circulation to be necessary in low latitudes.

2.3.3 Momentum Balance Evidence of Transport by Mean Meridional Circulation.

For the pattern of zonal motion shown in fig. 2.3 and 2.4, we see surface friction extracts westerly momentum from the mid-latitude atmosphere and injects it into the lower latitude atmosphere. This source and sink must therefore be balanced by the mean and eddy components of the horizontal fluxes.

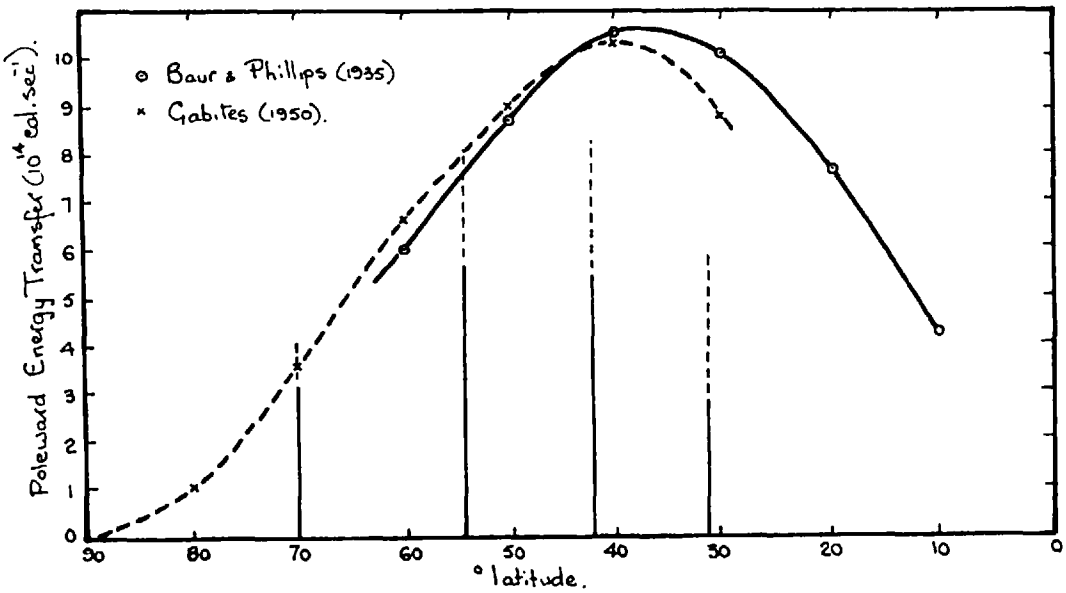

Figure 2.12. Estimated meridional profiles of net northward energy transport required for balance of vertically integrated radiative heat sources and sinks. The vertical lines represent zonal mean values of the eddy flux of energy— continuous lines, sensible heat, E', and dashed lines, latent heat, L', from Starr & White (1954).

Widger (1949), showed the balance equation of absolute angular momentum per unit mass might be written:

$$\frac{\partial}{\partial t}\int_v \rho M\, dv = \int_\Sigma \rho M . V\, d\Sigma + \int_\sigma p r_e\, d\sigma + \int_\Sigma r_e \mathbb{T}_x\, d\Sigma \quad \cdots\cdots\cdots 2.3.$$

where $M = \omega r_e + \Omega r_e^2$ is the absolute angular momentum, r_e the distance from the earth's axis, $d\sigma$ the projection of $d\Sigma$ on the meridional plane and $\mathbb{T}_x$ the total zonal frictional stress at the boundary.

The balance equation for an annular ring ~~with horizontal surfaces~~ bounded by the pressure surfaces p_m and p_{m+1} and vertical surfaces of latitudes ϕ_m and ϕ_{m+1} may be written:

$$0 = \left\{\int_{p_m}^{p_{m+1}} [\rho u r_e v]\, dz + \int_{p_m}^{p_{m+1}} [\rho \Omega r_e^2 v]\, dz\right\}_{\phi_m}^{\phi_{m+1}} + \left\{\int_{\phi_m}^{\phi_{m+1}} [\rho u r_e w]\, dy + \int_{\phi_m}^{\phi_{m+1}} [\rho \pi r_e^2 w]\, dy\right\}_{p_m}^{p_{m+1}} + \int_\sigma p r_e\, d\sigma + \int_{\phi_m}^{\phi_{m+1}} [r_e \mathbb{T}_x]\, dy \quad \cdots 2.4.$$

which may be expressed in terms of mean and eddy transfers.

The surface and frictional torque effects have been evaluated by Priestley (1950), and White (1949), respectively.

Tucker (1960), evaluated the mean fluxes of angular momentum directly and the eddy fluxes indirectly by means of estimates of the percentage of the net eddy transport effected at various levels (from Starr and White, 1952, 1954). The net eddy flux across a latitude circle was determined by subtracting the net mean transport from the total. The 200 mb. pressure interval used in the study gave sufficient resolution to show the mechanisms of tropospheric transfer but not those in the vicinity of the tropopause.

The study showed that in general there is a small contribution to the net horizontal flux of relative angular momentum from the mean circulation except in low latitudes where it was

the same order as the eddy flux. The mean meridional circulation was shown to transfer the angular momentum of terms involving the effect of the earth's rotation, in such a manner as to produce regions of convergence of advected angular momentum which balance corresponding regions of divergence of eddy flux or vice versa, so that the direction of vertical eddy flux is always downgradient.

We shall interpret these results in Chapter 8.

2.3.4 Correlations of Velocity Components and Their Relation to the Preferred Slope of Eddy Mixing

Given a large number of simultaneous vertical and meridional velocity components, the preferred slope of eddy mixing will lie between the regression lines of v and ω.

Since the mean values of both v and ω are an order of magnitude less than most individual observations, no significant loss of accuracy results from studying the observed components rather than their deviations from mean values.

A meridional section of vertical-meridional velocity covariance for January 1958, from values tabulated by Newell (1961), is presented in fig. 2.13. The values of ω are due to Jensen (1960), and are based on the adiabatic method, so that they have the usual limitations. We observe a pattern of positive covariance with maxima in the upper troposphere near 35°N and 70°N, and a negative covariance in the tropical lower stratosphere. These results imply northward moving parcels rising and southward moving parcels subsiding in the troposphere, and lower stratosphere in middle and high latitudes, and the reverse in the tropical lower stratosphere.

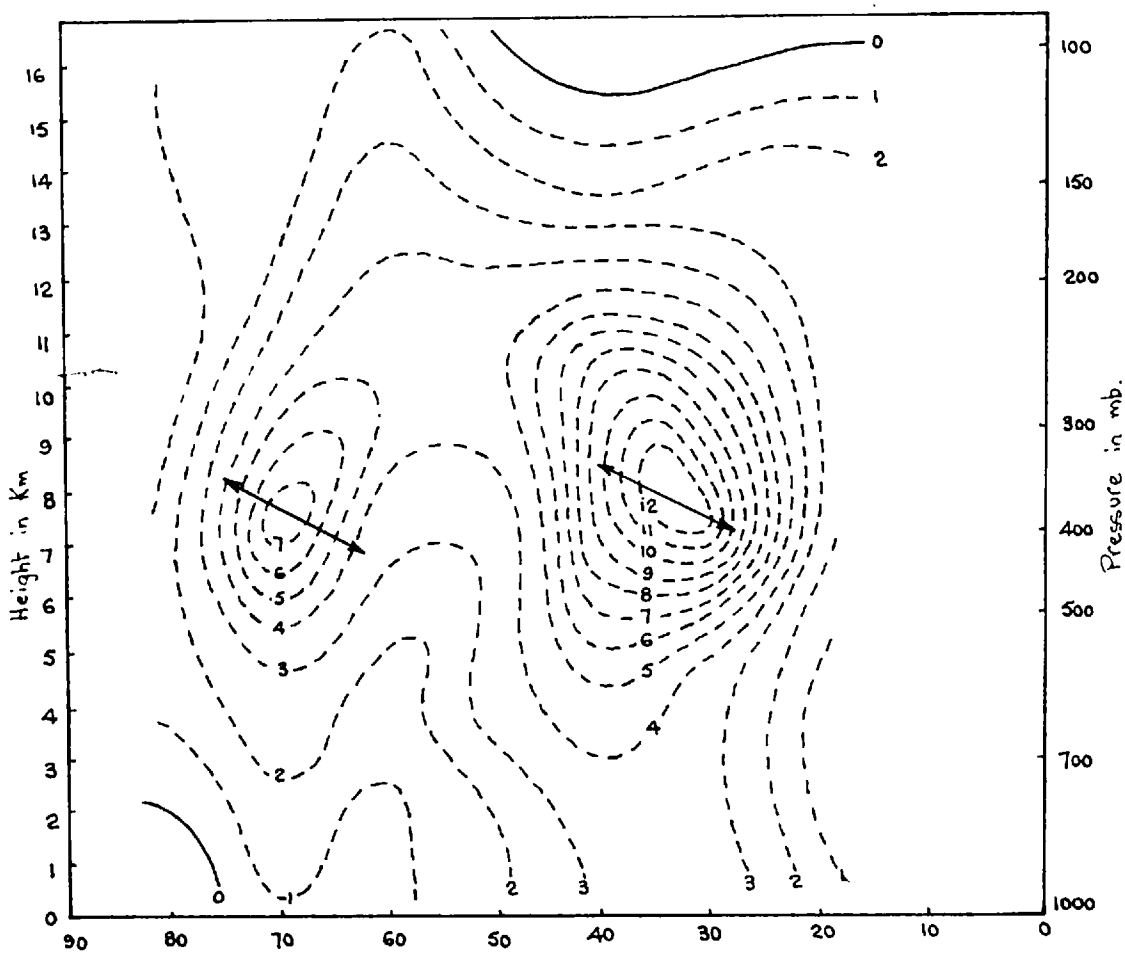

Figure 2.13. Meridional section of covariance of meridional and vertical velocities $[\overline{v'w'}]$ for the northern hemisphere for January 1958. Units are in $cm^2 sec^{-2}$ when multiplied by 10^2 (from Laisel & Molla data published by Newell 1961)

New Analysis of Vertical Velocities over the British Isles

Vertical velocities were calculated at the standard levels 100, 150, 200, 300, 400 and 500 mb., in the vicinity of Liverpool for 50 days in 1959 and 1960, selected for reasons discussed later in chapter 7. The method used was the thermodynamic method assuming adiabatic motion as described in Appendix 1.

Corresponding values of the meridional velocity at Liverpool were computed from observed winds and scatter diagrams were plotted of v versus ω for all levels.

Those for the 100, 200 and 400 mb. levels are shown in fig. 2.14. There is a substantial positive correlation at and below 300 mb., but at and above 200 mb., the pattern is more obscure. This might be a result of a seasonal change in the mixing angle but the sample is too small to establish numerical relations. The observations occurring in each quadrant (v, ω combinations, see fig. 2.14), were however tabulated, as given in Table 2.3, and the percentage frequency of observations by quadrant, level and season are plotted as 'vectors' in fig. 2.15, where the 'vector' direction simply indicates the quadrant in which the observations occur.

In all but five of the cases studied the jet axis lay between 200 and 300 mb., so the 300 mb., level and below may be considered characteristic of tropospheric motion and the 200 mb., level and above of stratospheric motion.

We observe in fig. 2.15 that below 300 mb. in all seasons, the percentage frequencies are, with one exception, greatest for

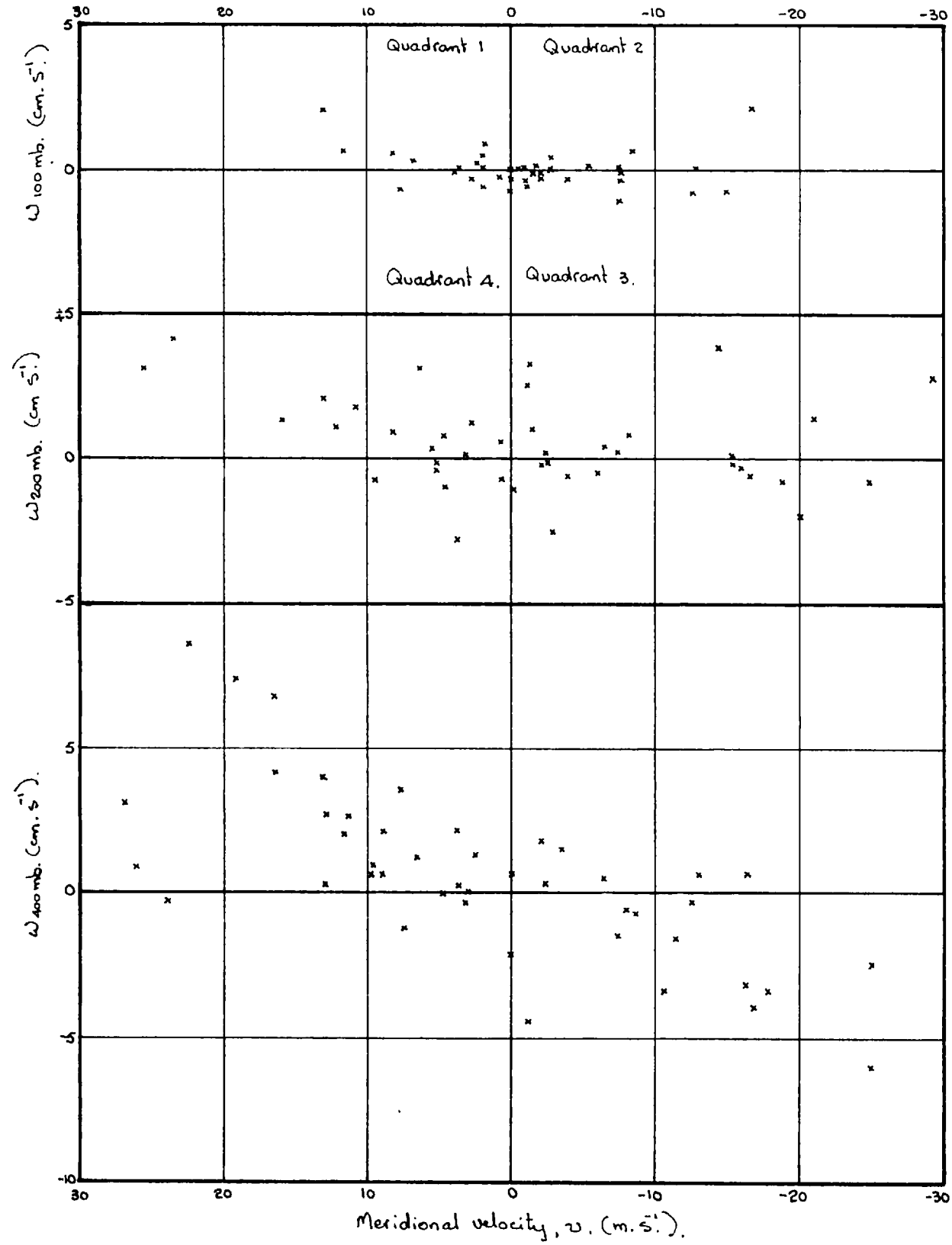

Figure 2.14. Scatter diagrams of vertical versus meridional components of velocity for the 100, 200 and 400 mb. levels. In the notation of v positive indicating a component towards the pole, observations in the various quadrants imply the following combinations of components:
1. $v+, \omega+$. 2. $v-, \omega+$, 3. $v-, \omega-$. and 4. $v+, \omega-$.

Table 2.3. Frequency of occurence of observations in various quadrants of scatter.

Season	Quadrant Number	No of observations per quadrant						No of obs" in diagonally opposite quadrants					
		100mb.	150mb.	200mb	300mb	400mb	500 mb	100 mb	150 mb	200 mb	300 mb	400 mb	500mb
Spring	1	2·0	1·5	3·0	3·0	4·0	4·0	6·5	4·5	5·5	4	7	6
	3	4·5	3·0	2·5	1·0	3·0	2·0						
	2	2·0	2·5	2·0	3·0	1·0	1·0	2·5	4·5	3·5	3	2	3
	4	0·5	2·0	1·5	0	1·0	2·0						
Summer	1	2·0	2·5	3·0	4·0	5·0	5·0	4	6·5	6	9	9	10
	3	2·0	4·0	3·0	5·0	4·0	5·0						
	2	5·0	4·5	5·0	2·0	3·0	1·0	8	5·5	6	3	3	2
	4	3·0	1·0	1·0	1·0	0·0	1·0						
Autumn.	1	1·0	2·0	3·0	4·0	5·0	5·0	3	5	6	7	7	7
	3	2·0	3·0	3·0	3·0	2·0	2·0						
	2	2·5	2·0	3·0	3·0	2·0	3·0	7	6	5	4	3	3
	4	4·5	4·0	2·0	1·0	1·0	0·0						
Winter.	1	5·5	4·5	7·0	7·0	7·0	3·0	7	8	11	10·5	11	5
	3	1·5	3·5	4·0	3·5	4·0	2·0						
	2	5·5	5·0	4·0	3·0	0·0	2·0	7	9	6	6·5	2	8
	4	1·5	4·0	2·0	3·5	2·0	6·0						

Quadrant 1. Ascending motion towards the pole.
2. Ascending motion towards the equator.
3. Subsiding motion towards the equator.
4 Subsiding motion towards the pole.

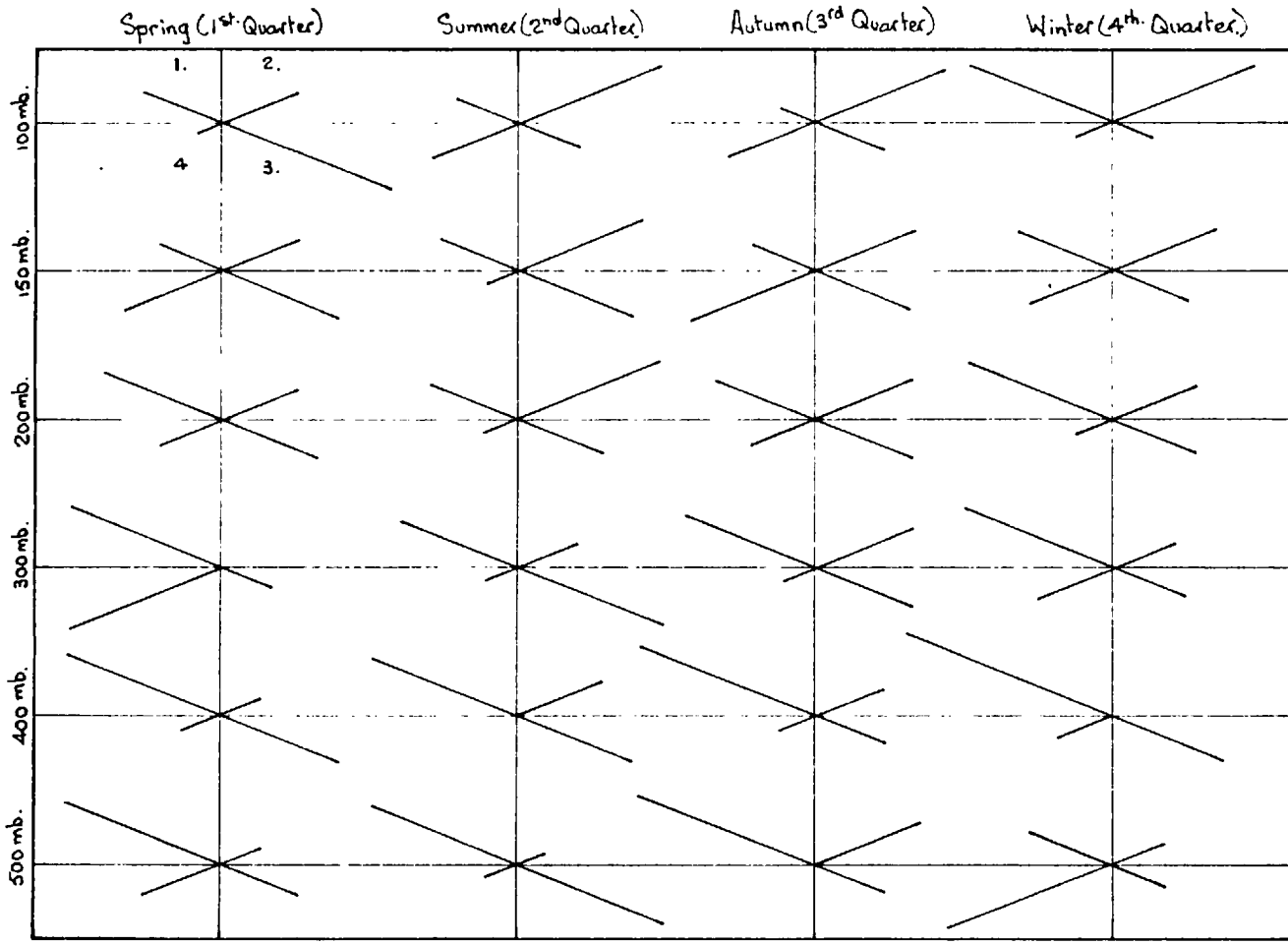

Figure 2.15. The percentage frequency of occurence of each combination of meridional and vertical component of velocity at various levels expressed as vectors. The vector direction simply indicates the quadrant in which the observations occur while the length represents the fraction of the total number of observations in that quadrant. The quadrant numbers imply the same velocity combinations as in fig. 2.13.

quadrants 1 and 3, that is northward moving parcels ascending and southward moving parcels subsiding. At the 200 and 150 mb. levels the correlation is not clear, but at 100 mb. there may be a positive correlation in spring and a negative correlation in summer and autumn. By comparison with seasonal sections of potential temperature in fig. 2.8 we see that the angle of mixing is generally in the same sense as the slope of the mean potential isotherms.

Summary

We have established that both mean and eddy transfers are necessary to maintain dynamical and energy balance in the atmosphere.

Direct evidence of mean toroidal circulations from wind observations are restricted to regions below 100 mb. and show a direct circulation in low latitudes and an indirect circulation in middle latitudes.

The preferred slope of eddy mixing was shown to be generally in the same sense as that of the mean potential isotherms in both troposphere and lower stratosphere though we have not established whether the magnitude is greater or less.

The relative contribution of the two types of motion in meridional transfers will of course depend on the sources and sinks of the property to be transported, but the evidence of energy transfer does suggest that the eddy motion is much less effective in low latitudes.

Meridional sections of wind and temperature have been presented for comparison with subsequent analyses of tracers.

CHAPTER 3

The Tropopause, Jet-Stream, Frontal Zone Complex

3.1 Intent

In this chapter we shall attempt to describe the temperature distribution in the atmosphere in terms of its major discontinuities. Having described the thermal structure, we incorporate the corresponding wind field in the model, since, both from considerations of dynamics and energy, the two are irrevocably linked.

Having presented the various models of the complex, a brief analysis of the mechanisms supposedly responsible for its formation and maintainance will be presented.

3.2 The Tropopause and Frontal Zone - a Descriptive Account of Their Thermal Structure

The tropopause is defined in terms of static stability. The W.M.O., definition being:

1. The first tropopause is defined as the lowest level at which the thermal lapse rate decreases to $2^{\circ}K\ km^{-1}$ or less, provided also that the average lapse rate between this level and all higher levels within 2 km. does not exceed $2^{\circ}K\ km^{-1}$.

2. When, above the first tropopause, the average lapse rate between any level and all higher levels within 1 km. exceeds $3^{\circ}K\ km^{-1}$, then a second tropopause can occur and is defined by the same criteria as in paragraph 1. This tropopause can either be within or above the 1 km. layer.

There exists an almost infinite variety of profiles in the region separating the two stability regimes and it is frequently difficult to distinguish where a meaningful boundary might exist.

This ambiguity has resulted in a variety of plausible interpretations of the thermal structure.

The front was initially conceived as an extensive surface at which there existed a zero order thermal discontinuity. This surface was thought to extend from the high latitude tropopause downwards to the surface in mid-latitudes. This concept was later modified to a zone of transition between two roughly isothermal regimes, the surfaces of this zone being marked by discontinuities in the thermal gradients.

The historical development of models of tropopause front cyclone relationships is presented in fig. 3.1

Figures 3.1 a) and c) illustrate the concept of the front as a zero order temperature discontinuity throughout the depth of the troposphere, while in 3.1 c) a 'fold' was introduced into the postulated continuous tropopause surface above the upper tropospheric frontal surface to explain the observed variations in temperature profiles. These variations are more consistent with the model 3.1 e) of Matthewman (1955), in which the upper and lower surfaces of the frontal zone are analysed as continuous with the tropical and polar tropopause surfaces respectively.

The model 3.1 d), showing a frontal zone extending through and reversing in slope at the tropopause which becomes less well defined in its proximity, lacks conviction, since there are many inconsistencies in routine analysis.

Figures 3.1 b) and f) illustrate the concept of the foliated tropopause. Palmén (1933), postulated a multiple tropopause structure with lapse rate discontinuities forming over large areas

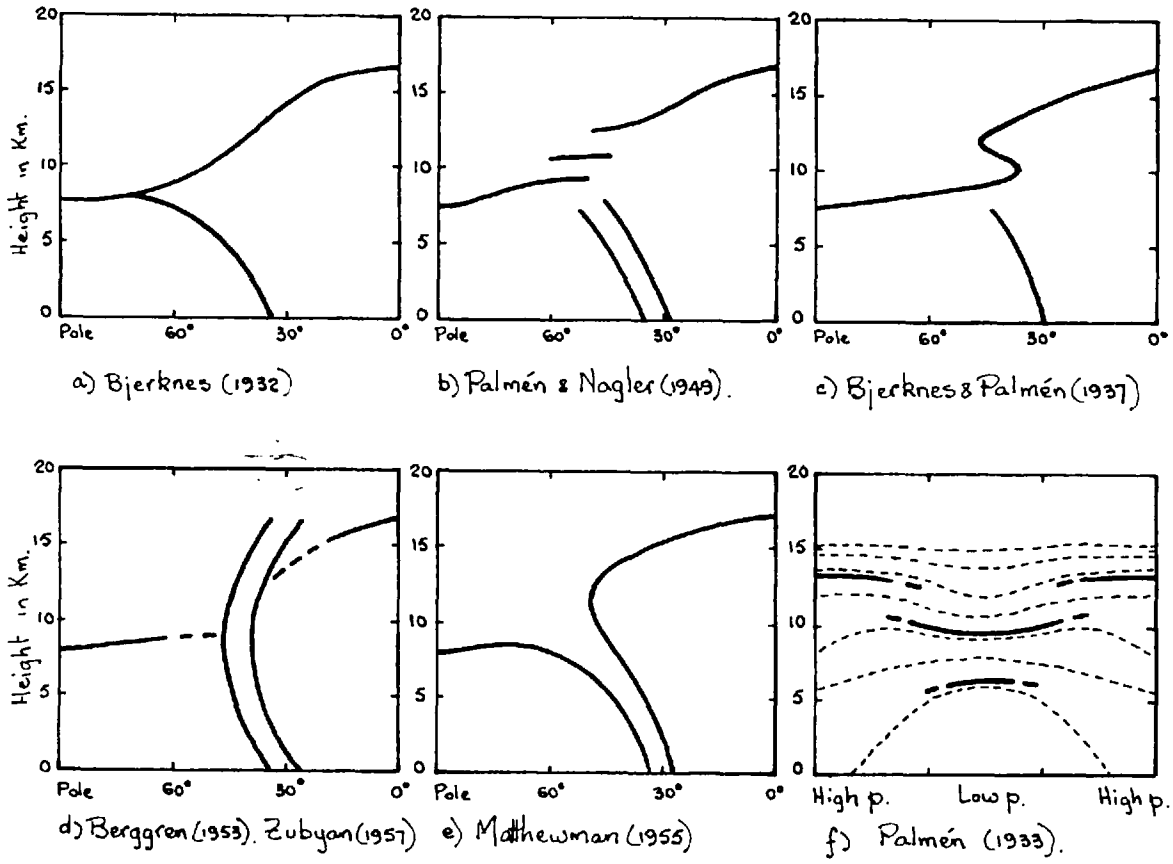

Figure 3.1. Alternative models of the tropopause-frontal zone complex.

at roughly the same potential temperature, above and below the old tropopause, above the cyclone wave, (i.e., the new folded tropopauses correspond closely with isentropic surfaces). If rapid cyclogenesis took place the tropopauses were depicted as symmetrical with respect to the cyclone centre, as shown in fig. 3.1 f). This introduced the idea of temporal as well as spatial variation of the tropopause structure and it became possible to consider mass transfer taking place between the two stability regimes by the process of reformation of the tropopause at a different level.

The role of the jet stream in this picture has been investigated by the Chicago school and Palmén (1948), showed the jet stream to be located just below the tropopause, directly above the 550 mb. position of the frontal zone. Several inconsistencies appeared in individual cross sections, and these were subsequently rectified by the Canadian school simply by postulating not just one but two and sometimes more jets, each associated with its own hyperbaroclinic zone. This work was reviewed by McIntyre (1959). Fig. 3.2 after Newton and Perrsen (1962), shows the characteristic distribution of the macro-scale features of the wind and temperature fields. This cross section was constructed from the study of a limited number of cases over the U.S.A., and so is representative of a section through the subtropical jet maximum which Krishnamurti (1961), showed corresponded to the semi-permanent low latitude upper level ridge position.

Riehl (1962), has pointed out that a strong jet may exist without a corresponding sharp frontal zone in the upper troposphere,

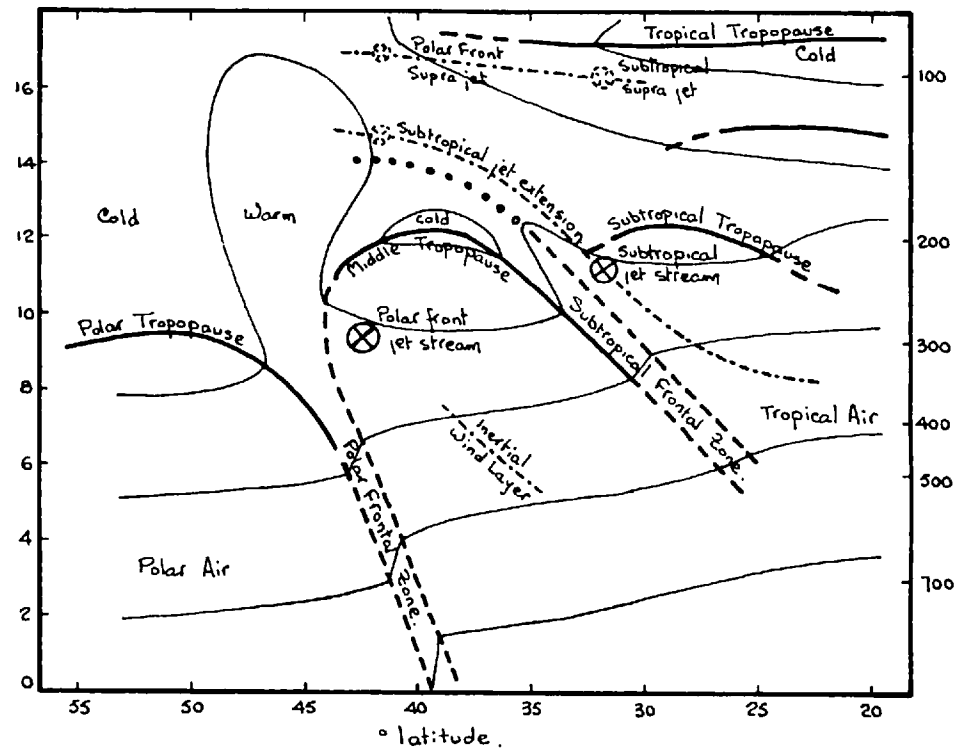

Figure 3.2. Meridional section showing the characteristic features of the wind and temperature fields over North America in winter from individual case studies. Isotherms (thin continuous lines) are schematic. (from Newton & Persson, 1962)

in fact many strong jets are observed when no stable layers are reported between 500-700 mb. and the tropopause.

A recent analysis of temperature and wind distributions relative to the jet by Brundidge and Goldman (1962), illustrated the lack of uniformity of pattern, but was restricted to too limited a number of cases to establish any definite evolution of the complex. On the basis of the cases considered, all unfortunately in the region to the east of the long wave trough over North America, they classified the jet stream frontal zone complex into three types illustrated in fig. 3.3. Types I and III they considered as fundamental, with type II possibly being a transition between them. Type III showed a laterally narrow jet of great vertical extent, associated with a strong polar front sloping steeply up to the tropopause, and was generally found in entrance zone situations. Type I showed an isotach pattern broad and vertically thin associated with a shallow baroclinic layer (usually warm frontal) in the lower troposphere. This was generally found in the far exit region of the jet.

In mid-troposphere the thermal structure, as revealed by Sawyer's (1955, 1957, 1958), analysis of Met. Research Flight transverses through frontal zones, is equally indefinite. Sawyer (1958), found, on examining the horizontal variation of temperature at 500 mb., that well defined frontal zones with quite sharp changes in horizontal temperature gradient could only be identified on about half of the cases studied, and the proportion fell to less than a third at 600 mb. Temperature

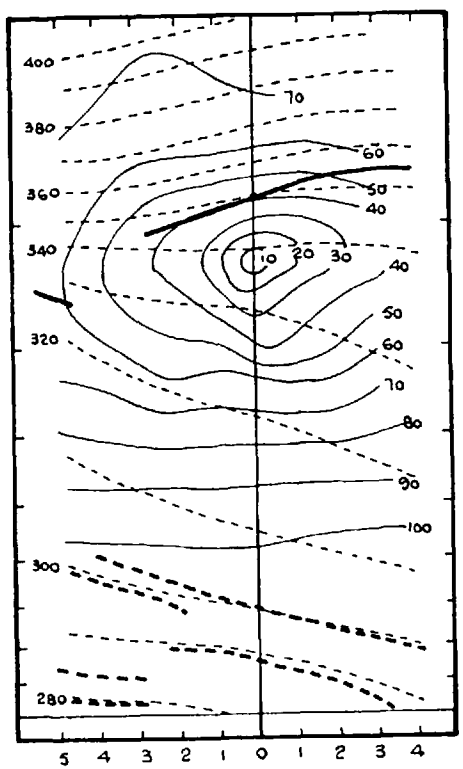

Type I Isotach pattern laterally broad and vertically thin In some cases two maxima side by side. Pattern associated with shallow warm front in a small amplitude wave system in the far exit region of the jet

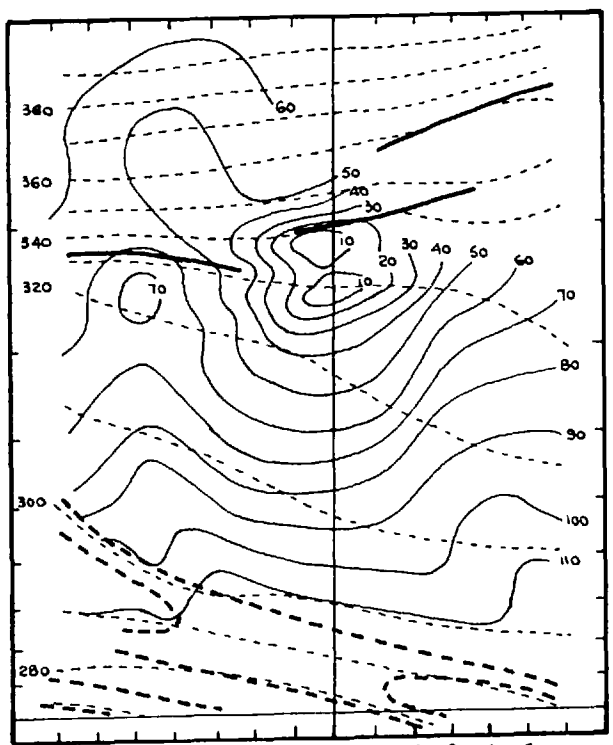

Type II. Possible transition between Type I and III This class has no clearly defined synoptic situation associated with it.

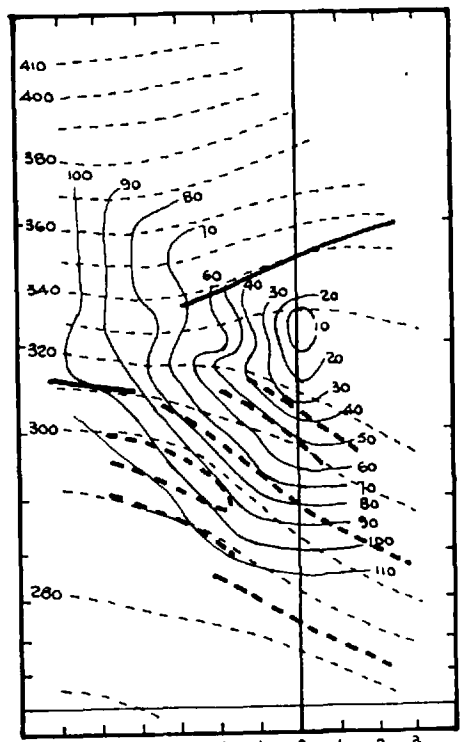

Type III. Strong polar front sloping up steeply to the tropopause. The isotach configuration laterally narrow and of great vertical extend. These cases were associated with entrance zones east of long wave troughs.

Figure 33 Model cross sections showing isotachs (continuous lines) labeled as departures from jet core values in knots, and potential isotherms (dashed lines) in °K divided into three types, constructed from radiosonde and flight data (from Brundidge and Goldman, 1962). Thick continuous lines represent tropopauses and frontal zones are enclosed by thick dashed lines.

changes across other zones were diffuse and showed no sharp boundaries.

The complex structure of many frontal zones and tropopauses has been thoroughly investigated over the U.S.A., by means of cross sections of potential temperature analysed on a meso-scale for selected storms. These analyses of Reed (1955), Danielsen and McLain (1955), and Reed and Danielsen (1959), and particularly that of Danielsen (1959), demonstrated that over large areas the arbitrary selection of a tropopause on macro-criteria was frequently ambiguous. This is illustrated by Fig. 3.4, which displays forcibly the laminar nature of the atmosphere with layers of large static stability separated by layers whose lapse rate is quasi-adiabatic. Danielsen (1959), demonstrated the temporal continuity of these stable layers over short periods by constructing isentropic trajectories and comparing the inversions on the final sounding with those on the original soundings at the initial points of the appropriate trajectories.

Since the terms troposphere and stratosphere imply a macro-scale division of the atmosphere Danielsen postulated that in order to apply the terms objectively, it is necessary to smooth out the micro and mesoscale thermal features revealed by his analyses. He smoothed the temperature by taking weighted running vertical mean values over nine successive pressure contacts (about 3,000') from the sonde record and defined a surface joining the maximum elevation of each smoothed isentropic surface as equivalent to the tropopause.

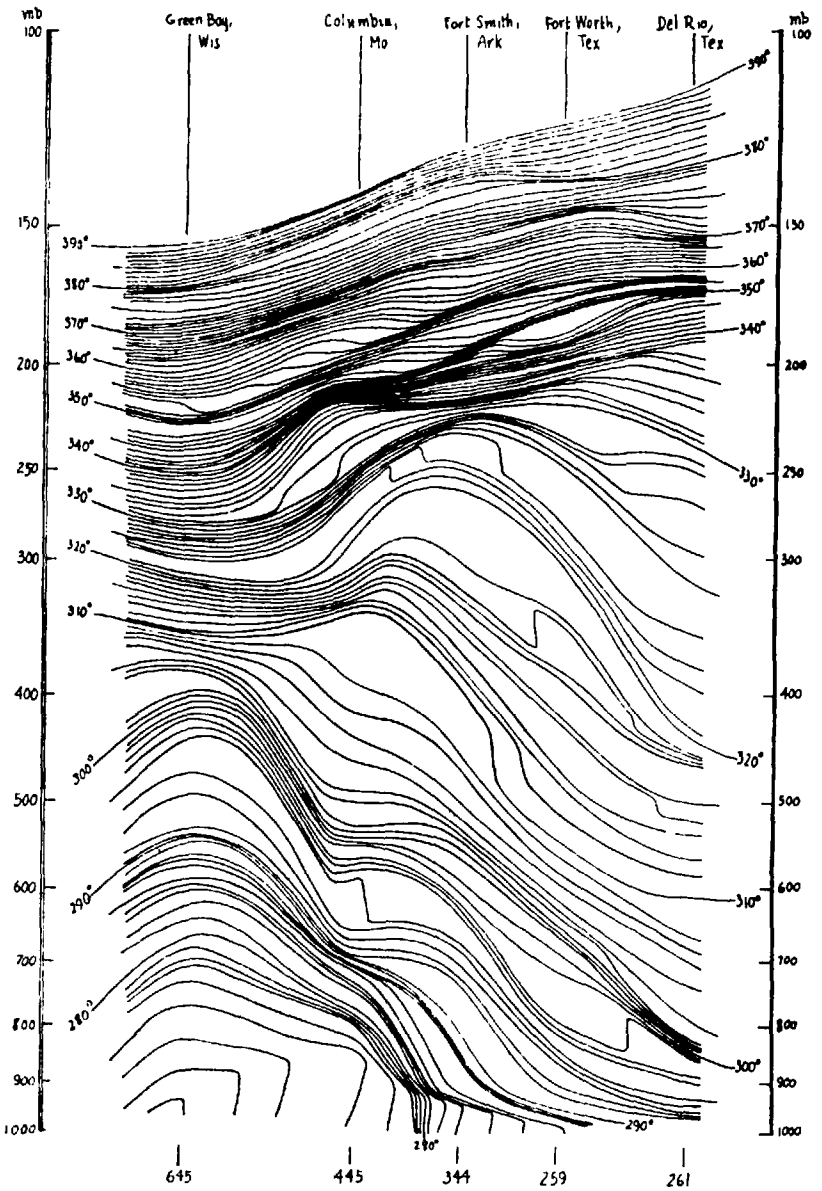

Fig. 3.4. Detailed vertical cross section from Green Bay, Wisconsin to Del Rio, Texas, 15.00 GMT, 29 March, 1956

This definition results in the selection of the tropopause being no longer ambiguous but the analysis of any one tropopause surface becomes a formidable and doubtfully meaningful task. The observation that, both in the meso-and the smoothed analyses, isentropic surfaces intersect the tropopause suggests that the tropopause need represent no barrier to adiabatic exchange between the stratosphere and the troposphere.

3.3 An Attempt to Formulate Criteria for the Unique Determination of a Tropopause

The time required to analyse the smoothed tropopause being prohibitive, we shall attempt to describe a set of criteria by which an objective unambiguous analysis of tropopause may be made. At present there is no consistent sequence of models of the thermal and wind fields in relation to the jet front complex under varying synoptic conditions. The fields may vary with position in relation to the jet maximum, except for broad quasi-geostropic consistency, and to the position with respect to the standing eddies. Analysis of winds and temperatures in situations of frontogenesis and cyclogenesis in these varying conditions might elucidate the evolution of the complex.

The absence of a well defined frontal zone at the 600 mb. level below a jet, on many occasions, may be plausibly interpreted as indicating two separate processes of formation of the frontal zone, one in the lower troposphere decreasing in efficiency with height, and another operating at least to some extent independently near the jet level. The subtropical jet might then be considered as a case where only the upper tropo-

spheric mechanism is operative while the other jets are linked in some fashion with corresponding low level mechanisms.

The analysis of Brundidge and Goldman (1962), relating isotach configurations with frontal types, may serve as a starting point in synthesising models of thermal and wind fields of characteristic types for various stages of evolution of the jet-tropopause-frontal zone complex.

Study of a large number of cross sections suggest there are a limited number of characteristic types. As noted above, the presence of a frontal zone in the lower troposphere is not a sufficient condition for the existence of a corresponding upper tropospheric front, and the absence of such a well defined frontal zone may or may not imply a continuous tropopause surface. The cases may be roughly divided into three classes of thermal structure as illustrated in fig. 3.5, but it should be understood that these criteria are subjective.

These models were evolved from study of cross sections through polar front type jets over Britain, but if, as postulated earlier, the subtropical jet differs from the mid-latitude jet systems by absence of a corresponding low level mechanism, it is plausible that the same models may serve for it simply by deleting the lower tropospheric frontal zones from the models. If this is so, it suggests that the effect of the lower troposphere may be quantitative rather than qualitative, and we may begin an analysis of this nature by neglecting its influence.

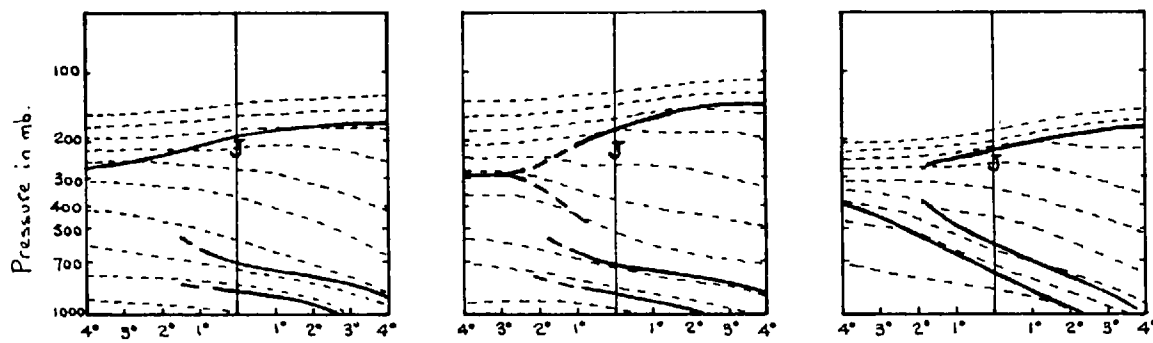

Figure 3.5 Models of tropopause - jet stream - frontal zone complexes suggested by the study of numerous individual cross sections. The dotted lines representing potential isotherms are qualitative and simply intended to show variations in stability. Thermal gradient discontinuities are indicated by thick solid lines.

We observe the similarity in tropopause and frontal structure between the models in fig. 3.5 and the corresponding Types in the isotach analysis of Brundidge and Goldman (1962), in fig. 3.3. In the limited number of cases studied by Brundidge and Goldman Type I was generally observed in far exit regions and Type III in entrance zone situations. Type II was postulated to be a transition between Types I and III. Many exceptions were noted to this general association in the cross sections examined in constructing the frontal zone models in fig. 3.5, but these may be due to uncertainty in deciding the appropriate jet criterion. The hypotheses thus require both statistical and case study confirmation.

From fig. 3.5 we observe there should be no ambiguity in analysing the tropopause on stability criteria to the right of the jet looking downstream. When the ascent lies to the left of the axis the following criteria are used to define the tropopause:

Model I - only one inversion at high level occurs so there is no ambiguity.

Model II - the upper of the two lapse rate discontinuities, shown by the thick dashed lines, is chosen in spite of its not satisfying the W.M.O. stability criterion of $2^{o}K\ km^{-1}$, though such a lapse discontinuity is satisfied at the lower level.

Model III - no ambiguity exists close to and far to the left of the jet, but when the lower level stable zone is superposed by a layer of reduced stability above which there is either another lapse discontinuity or a gradual increase in stability, this upper maximum of lapse rate curvature, indicated by the thick solid line above the jet is chosen.

3.4 Tropopause formation and Maintainance

The early attempts to explain the existence of a tropopause were based on theories of radiative equilibrium or in terms of a troposphere in convective equilibrium and a stratosphere in radiative equilibrium. These theories of Gold (1909), Emden (1913), Möller (1941), and Goody (1949), were critically appraised by Staley (1958). None satisfactorily explains the generation and maintainance of a discontinuity of lapse rate.

While the gradient of potential temperature in the troposphere is much less than that in the stratosphere, it is still in general statically stable but the additional feature of a horizontal temperature gradient implies that the troposphere may be dynamically unstable and a type of slantwise convection a common feature of the flow field (Charney, 1947, Eady, 1949).

A review of the various processes which might contribute to the generation and maintainance of a tropopause will now be given.

3.4.1 Radiation and the Tropopause

The mean radiative heating charts in fig. 2.9 show the uncertainty of the computations in the vicinity of the tropopause as a result of variations in the assumptions concerning the vertical variation of the component absorbers and the absorption spectra. While no quantitative conclusions may be drawn from these charts, it is instructive that where a continuous variation of absorbers is assumed, all calculations show a smooth vertical variation of cooling rates, suggesting no tendency for radiation, by itself, to produce a lapse rate

discontinuity, though calculations of seasonal distributions of radiative equilibrium temperatures by Manabe and Møller (1961), show minimum temperatures and maximum lapse rate curvature at levels consistent with the observed tropopause.

Möller (1941), and Staley (1958), show, by calculating the profiles of radiative transfer by water vapour for characteristic temperature and humidity distributions, that the tropopause is warmed relative to layers above and below, i.e., the radiative flux destroys the curvature of the lapse rate profile.

Möller (1941), suggested the tropopause might be maintained by infra red cooling above, by postulating the existence of a haze or cloud layer with its upper surface at the tropopause. In general, in a cloud layer the refraction and transmission of short wave radiation in stratus type cloud, greatly exceed absorption, for thicknesses up to 500 m. Computed values of heating by absorption of short wave radiation at the upper limit of cloud for particular values of cloud thickness, droplet size and vapour content, and of long wave cooling are $0.03^{o}c\ min^{-1}$, and $3^{o}c\ min^{-1}$ respectively. Thus if haze may be assumed to have similar radiative properties to stratus, the tropopause could be cooled by long wave radiation both night and day. Though there is some visual evidence - not well recorded - for such a haze top to the troposphere, there is no satisfactory evidence of the analagous radiative properties of haze and cloud layers, though Brewer and Houghton (1956), suggest from radiative flux measurements from aircraft, that the emissivity of cirrus clouds is little different from that of a layer of water vapour of the same

thickness. If such a discontinuity did exist, however, the vertical gradient of the rate of radiative temperature change would be negative, with maximum cooling at the top of the layer, producing a gradually increasing lapse rate with height, which might approach the adiabatic towards the top of the layer. Observed profiles seldom exhibit such properties.

A series of observations of radiative fluxes near the tropopause by Suomi et al (1958), and Bushnell and Suomi (1961), show no major changes of cooling rate in the region of the tropopause, and tend to confirm the view that radiation, in general, acts so as to reduce the curvature of the temperature profile at the tropopause.

3.4.2 Convection (Vertical Overturning) and the Tropopause

The concept of convection initially applied to the problem of tropopause formation was that of vertical overturning, resulting from an initially statically unstable lapse rate. The equilibrium profile would be a lapse rate between the dry and the saturated adiabatic because, while a parcel of air might ascend along the saturated adiabat above the condensation level, a subsiding parcel would warm at a rate intermediate between dry and wet adiabatic as a result of evaporation of rain in the descending current. The high static stability in the stratosphere, due broadly to radiation, precludes the existence there of such a motion, and a sharp boundary might result. Even in the arctic night, however, where large and deep surface thermal inversions are produced, a lapse rate discontinuity is generally in evidence aloft, moreover, in the tropics and subtropics there is considerable

spatial variability both in distribution and degree of cumulus activity, yet the tropopause height shows remarkable uniformity, so that tropopause formation and maintainance cannot be generally due to convection of this type.

3.4.3 Slantwise Convection and the Tropopause

Slantwise convection, i.e., overturning in sloping planes, is a common type of atmospheric motion. Profiles of the rate of temperature change by slantwise convection may be obtained by evaluating, then combining, the meridional and vertical components of eddy heat flux divergence.

Table 3.1 shows values of the function $\{(\overline{v'T'})_{\phi_1} - (\overline{v'T'})_{\phi-\Delta\phi}\}$, which is proportional to the flux divergence of mean meridional eddy transport of sensible heat at standard pressure levels and gives a measure of the rate of eddy heating $\left(c_p\bar{\rho}\,\frac{\Delta T}{\Delta t} = c_p\bar{\rho}\,\frac{(\overline{v'T'})_{\phi_1} - (\overline{v'T'})_{\phi_1-\Delta\phi}}{\Delta\phi}\right)$, obtained from Piexoto's (1960), zonally averaged eddy heat fluxes $(\overline{v'T'})$. We observe in fig. 3.6 that these values may be analysed (though not very convincingly) consistent with a relative maximum cooling in the vertical profiles near the mean tropopause levels as extracted from the analysis of Goldie et al (1957). At about 55°N a reasonable value of $\{(\overline{v'T'})_{60} - (\overline{v'T'})_{50}\}$ of about 1·7°K m.sec^{-1} near the tropopause would result in a net cooling of 14×10^{-2}°K day^{-1}.

Vertical fluxes have not been evaluated as a function of latitude. However, using the temperature and vertical velocity values for Liverpool computed in the current study for 50 days, an attempt was made to evaluate the vertical fluxes at the 200 and 300 mb. levels, since throughout the year these levels bounded the tropopause above and below. The mean vertical eddy flux divergence of heat was then converted to a mean rate of only 6×10^{-2}°K day^{-1} within the layer.

	Pressure mb \ °latitude	65	55	45	35	25	15
Yearly	300	-1.43	0.11	2.41	-0.30	-1.03	-0.99
	200	2.00	1.50	-0.34	-2.28	-3.99	-0.59
	100	2.74	-1.89	-5.04	0.00	-0.50	-0.52
Summer	300	-1.65	-2.17	1.09	-0.58	-2.55	-0.28
	200	0.65	1.61	0.35	-4.37	-4.49	+0.74
	100	0.93	0.88	-2.13	-0.59	+0.89	-0.87
Winter	300	1.55	2.07	1.85	-1.70	-1.36	-1.64
	200	3.06	1.86	1.79	-3.86	-3.67	-0.68
	100	5.37	1.25	-3.20	-3.43	-3.78	-1.60

Table 3.1. Zonally averaged values of the flux divergence of mean meridional eddy transport of heat $(\bar{T}'\bar{v}')_{\phi_1} - (\bar{T}'\bar{v}')_{\phi_2}$ in units of absolute degree meter sec^{-1} for yearly and seasonal data at specified latitudes from Peixoto (1960).

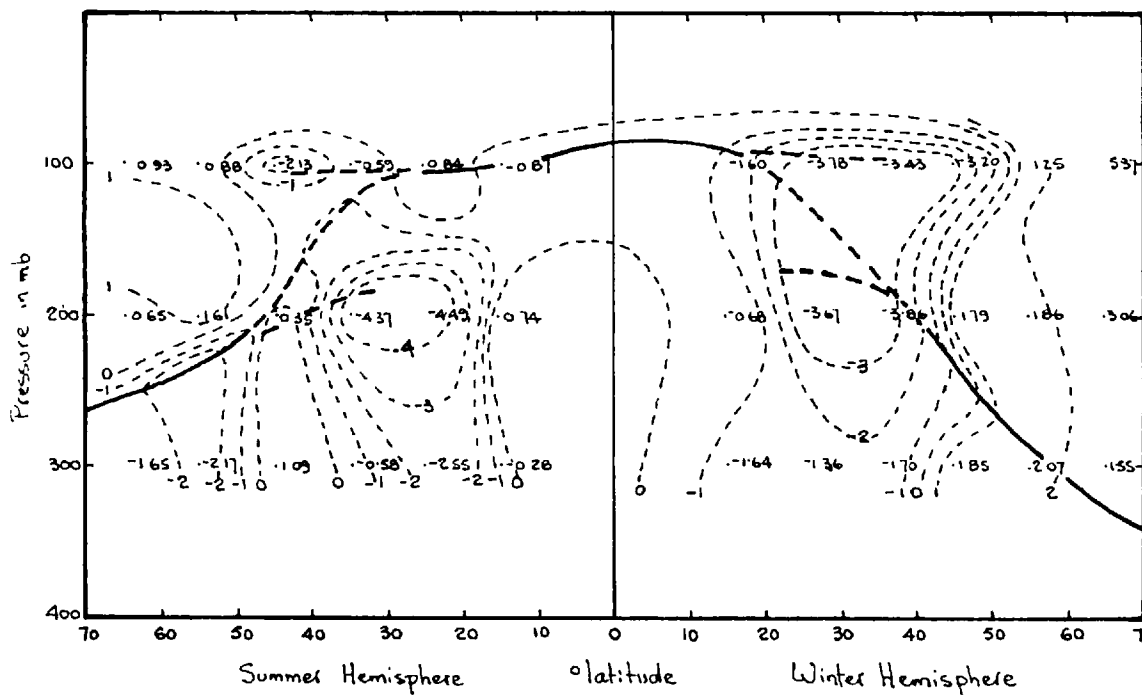

Figure 3.6. Meridional sections of $\{(\overline{v'T'})_{\phi} - (\overline{v'T'})_{\phi=10°}\}$ in units of °K m.sec^{-1} analysed in relation to corresponding mean positions of the tropopause (thick lines) in winter and summer.

Thus while both the vertical and meridional eddy heat fluxes in mid-latitude contribute to maintaining the tropopause, the values computed above suggest the cooling is small. These values are clearly under-estimates and more realistic estimates await greater resolution in estimating the individual profiles of vertical and meridional fluxes and calculation of mean values of the fluxes with respect to the tropopause.

3.4.4 Small Scale Turbulent Flux of Enthalpy

Staley (1957), has provided plausible arguments to support his thesis that small scale turbulent flux of enthalpy is divergent for positive curvature of the temperature profile, thus intensifying the existing curvature. He derived a formula for the rate of cooling by turbulence in the inertial sub-range, which showed the magnitude of the cooling by this mechanism to be several degrees per day, given an initial curvature of the lapse rate of $10^{\circ}K\ km^{-1}\ km^{-1}$.

3.4.5 Inference

It appears that the general location of the tropopause is determined by radiation and slantwise convection whereas the intensification of the lapse rate curvature may plausibly be attributed to the small scale turbulent enthalpy flux.

3.5 Transverse and Vertical Velocity Components in Relation to the Jet Axis

The component v of the wind vector normal to the jet axis was computed for wind data over the British Isles by Murray and Daniels (1953). They constructed mean vertical profiles of the transverse flow and found maximum values of 10 kt. near the jet

level decreasing to zero about 150 mb. below the jet. From crude sections constructed from these profiles in fig. 3.7, we observe the component to be directed towards lower and higher pressure in jet entrance and exit regions respectively.

A more recent analysis by Briggs and Roach (1963), of observations by the Met. Research Flight, illustrated by fig. 3.8, shows a qualitatively similar distribution of transverse flow (though somewhat greater components) to that of Murray and Daniels (1953).

Vertical velocities have been obtained using the adiabatic assumption by Endlich (1953), and from a simplified continuity equation $\frac{\partial v}{\partial y} + \frac{\partial \omega}{\partial p} = 0$, by Briggs and Roach (1963), applied to observations on jet traverse flights by Met. Research Flight aircraft, assuming the rate of change of velocity in the direction of the jet to be negligible.

Endlich (1953), found 3 hour average values of ω frequently exceeded 10 cm. $sec.^{-1}$ at both 500 and 300 mb., with the values being approximately equal at both levels. He further observed that the greatest velocities were to be found at or near the jet axis, and that values greater than 5 cm. $sec.^{-1}$ were seldom found more than 300 miles from the jet centre. Regions of greatest ascent over a 10 day period he found to the east of long wave troughs, while subsidence was most intense west of the troughs. He noted, moreover, that the distribution of regions of ascent and subsidence along the jet axis was irregular.

Briggs and Roach (1963), assumed negligible vertical velocities 3.6 km. above the jet core level (i.e., level of top

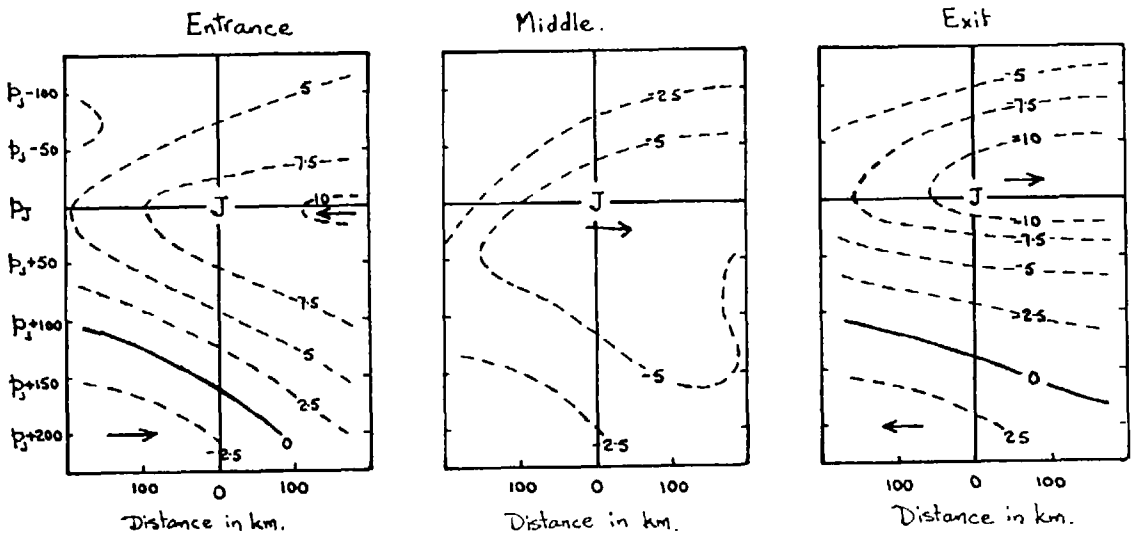

Figure 3 7 . Isopleths of transverse components of velocity constructed from mean values of observations made within 200 miles of the jet axis (from Murray and Daniels 1953) Units in knots, the direction indicated by the arrows.

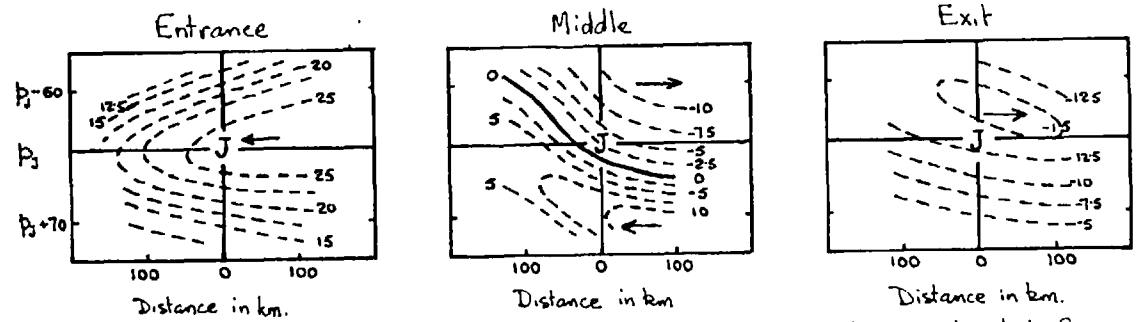

Figure 3.8 . . Isopleths of transverse component of velocity constructed from observations made by Met Research Flight within 200km of the jet axis (from Briggs and Roach 1963) Units in knots, the direction indicated by the arrows.

traverse), and computed velocities for a particular jet. (October 3, 1960). These indicate slight descent well to the cold side of the core but appreciable ascent near the jet axis and on the warm side of the core especially just below the core level. The bias towards large ascent rates may be a result of an appreciable positive constribution from $\int \frac{\partial u}{\partial x} dp$ or of bias as a result of position relative to the jet maximum. No data were provided on the relation of the section to the synoptic features, but the relevant contour analyses show it to be in the entrance zone to the right of a longwave trough and in Chapter 8 we find this is consistent with the proposed transfer model.

Thus it appears that a convincing evaluation of vertical velocity distribution relative to the jet complex is overdue.

3.6 New Analysis of Wind Components over the U.K., with Respect to the Jet

The profiles of vertical and meridional velocity components computed for 34 selected days in 1960, were roughly analysed in relation to the jet, to help formulate a model of transverse circulations.

The sample was divided into two groups - those to right and left of the jet axis - their respective mean vertical and meridional wind components calculated at standard pressure levels, and plotted in fig. 3.9. The isopleths are consistent with an indirect transverse cell centred below the jet axis. This agrees with the circulation suggested above for the exit zone, and in fact the observations in this study were biased in favour of exit

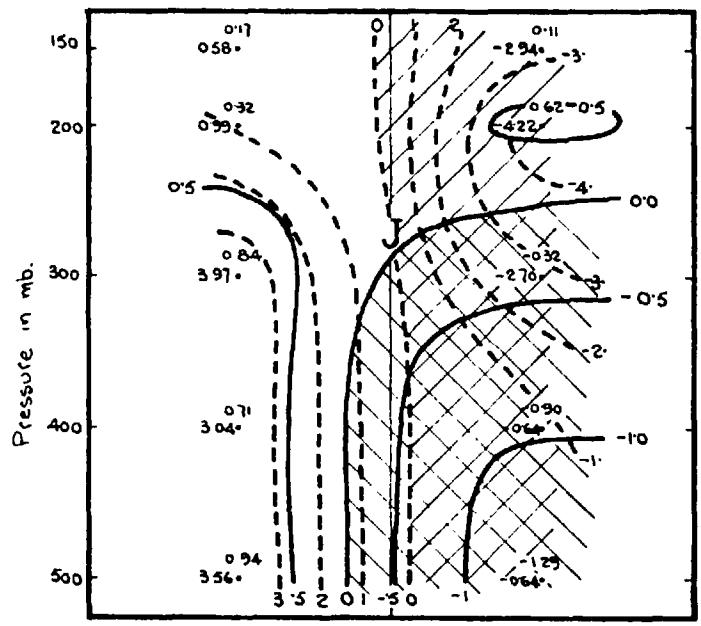

Figure 3.9. Mean values of vertical and meridional components of velocity, analysed from mean values calculated for standard levels on either side of the jet axis (plotted above and to the left of the appropriate points) are shown as solid and dashed lines. Units of w are cm. sec^{-1}, units of v are m. sec^{-1}. The jet is shown at its mean pressure of ~270mb.

zones in the ratio 21/13 but meridional, not necessarily transverse velocity components, were evaluated.

3.7 Conclusions

We have seen from the statistical analysis and case studies reviewed, that there is no model of the jet-tropopause-frontal zone complex which describes its development unequivocably, but a scheme for consistent analysis was presented.

Evidence has been presented of a direct transverse circulation in the entrance zone of the jet and an indirect circulation in the exit zone (and in the mean). In the upper troposphere, moreover, there appears to be an excess of subsidence to the left, and of ascent to the right, of the longwave trough positions.

CHAPTER 4 Tracers

An atmospheric tracer may be a conservative physical property of the atmosphere, a trace gas, or a finely dispersed particulate. These will now be discussed in some detail.

4.1 Physical Tracers

Various non-uniformly distributed physical properties of the atmosphere are shown in Table 4.1 with a note on regions wherein conservatism may not be a plausible assumption. Sources and sinks are defined as regions in which the non-conservative effects result in positive and negative increments respectively to the mean value for that region.

4.1.1 Potential temperature, θ, and wet bulb potential temperature, θ_ω.

In Chapter 1 we obtained:

$$\frac{\partial \theta}{\partial t} = -\underline{v}.\nabla\theta + \frac{1}{c_p}\left(\frac{p_o}{p}\right)^{\kappa}\left\{\frac{dq}{dt} + \alpha\left(\underline{\tau}_x \cdot \frac{\partial \underline{v}}{\partial x} + \underline{\tau}_y \cdot \frac{\partial \underline{v}}{\partial y} + \underline{\tau}_z \cdot \frac{\partial \underline{v}}{\partial z}\right)\right\} \quad \cdots\cdots 1.7.$$

where q is the diabatic heating per unit mass (see Table 4.1).

The potential temperature in the free atmosphere is of the order of 300°K and ranges over ten or more degrees at any level in a short period disturbance (36-48 hr). This rate of change is large compared with the average rates of heating or cooling, evaporation and condensation apart, of 1-2°K day^{-1} of Chapter 2 but the latter is mainly cumulative and so θ becomes increasingly non-conservative with time.

We discussed in section 3.2.1 how the radiative cooling is not seriously altered by large thermal and gaseous absorber gradients such as we expect near the tropopause. If, however, the upper limit of haze or cloud layers correspond to this lapse change, the radiative cooling may increase by orders of magnitude to a

Table 4.1. Physical tracers and their departures from conservatism.

Tracer	Source	Source Type	Sink	Sink Type
Potential Temp. θ	Atmosphere Earth	1. Radiation 2. Condensation 3 Frictional Dissipation	Atmosphere	1 Radiation 2 Evaporation
Wet Bulb Potential Temperature θ_w	As above but condensation-evaporation sources and sinks now incorporated in the tracer function.			
Absolute Vorticity	Atmosphere	Pressure-density solenoid field	Earth	Frictional Dissipation
Potential Vorticity	Atmosphere	Pressure-density solenoid field.	Earth	Frictional Dissipation.

degree or more per hour, swamping the other effects. Flux observations by Bushnell and Suomi (1961) have never suggested such excessive rates of cooling but it may not always be justifiable to assume conservatism for θ and θ_ω near the tropopause.

4.1.3 Absolute Vorticity

The equation for absolute vorticity $\bar{\eta}_t$ is:

$$\frac{d\bar{\eta}_t}{dt} = -\bar{\eta}_t(\nabla.\bar{V}) + (\bar{\eta}_t.\nabla)\bar{V} - \nabla\bar{\alpha}\wedge\nabla\bar{p} + \nabla\wedge\bar{\alpha}\underline{F} \qquad \text{.....1.4.}$$

so that $\bar{\eta}_t$ is conservative if:

1. the motion is non-divergent (incompressible fluid).
2. the tilting terms are zero (no deformation of the vorticity field).
3. the fluid has no α,p solenoids (autobarotropic).
4. the fluid is frictionless or $\underline{F}$ irrotational.

The equation for the vertical component ($\zeta+f$) of the absolute vorticity $\bar{\eta}_t$ is:

$$\frac{d(\zeta+f)}{dt} \doteq -(\zeta+f)\nabla_h.V_h + \left(\frac{\partial V_h}{\partial z}\wedge\nabla\omega\right).\underline{k} + \frac{\partial\omega}{\partial y}2\Omega\cos\phi - \frac{\omega f}{r_e} - \nabla_h\alpha\wedge\nabla_h p + \underline{k}.\nabla\wedge\alpha\underline{F} \qquad \text{.....4.1.}$$

(1. 2. 3. 4. 5. 6.)

The partial success of C.A.V. trajectories and barotropic forecasts suggests that for short periods the vorticity may be conserved in mid-troposphere ($\sim$ level of non divergence) in the absence of baroclinic development, but in the vicinity of the jet and in the frontal zones in the upper and lower troposphere the terms 1, 2 and 5, are each of magnitude 10^{-9} -10^{-10} sec.$^{-1}$, and would be capable of producing large departures from conservatism ($\zeta+f \sim 10^{-4}$ sec.$^{-1}$) in a period of 12 hours.

4.1.4 Potential Vorticity

The potential vorticity obeys the equation:

$$\frac{d}{dt}(\bar{\alpha}\nabla\bar{\theta}.\bar{\eta}_t) = \bar{\alpha}\bar{\eta}_t.\nabla\left(\frac{d\theta}{dt}\right) + \bar{\alpha}\nabla\bar{\theta}.\nabla\wedge\bar{\alpha}\underline{F} \qquad \text{.....1.5.}$$

It is only conservative if the motion is adiabatic and either frictionless, the frictional force irrotational, or the gradient of potential temperature perpendicular to the rotation of $\underline{F}$.

If $\underline{n}$ is a unit vector in the direction $\nabla\theta$, the equation may be written:

$$\frac{d}{dt}\left(\bar{\alpha}\frac{\partial\theta}{\partial n}\eta_n\right) = \bar{\alpha}\eta_t\cdot\nabla\left(\frac{d\theta}{dt}\right) + \bar{\alpha}\frac{\partial\theta}{\partial n}R_n \qquad \text{4.2.}$$

where η_n is the component of absolute vorticity normal to the isentropic surface and $R_n = \underline{n}\cdot\nabla\times\underline{F} \doteq \left(\frac{\partial F_y}{\partial x} - \frac{\partial F_x}{\partial y}\right)_\theta$ denotes the component normal to the isentropic surface of the rotation of the frictional force.

The component of absolute vorticity η_n may be written to a close approximation as $\eta_n \doteq \zeta_n + f \doteq \zeta_\theta + f$ where ζ_n is the component of relative vorticity normal to the isentropic surface and ζ_θ is the relative vorticity evaluated from the projections on the horizontal, of the horizontal wind components on the isentropic surfaces.

Now introducing the further excellent approximation $\frac{\partial}{\partial n} \doteq \frac{\partial}{\partial z} = -g\rho\frac{\partial}{\partial p}$

into equation 4.1 yields:

$$\frac{d}{dt}\left[\frac{\partial\bar{\theta}}{\partial p}(\zeta_\theta + f)\right] = -\frac{\bar{\alpha}}{g}\eta_t\cdot\nabla\left(\frac{d\theta}{dt}\right) + \frac{\partial\theta}{\partial p}R_n$$

or $$\frac{d}{dt}\left[-\frac{\partial\bar{\theta}}{\partial p}(\zeta_\theta + f)\right] = \frac{\bar{\alpha}}{g}\left\{\eta_z\frac{\partial}{\partial z}\left(\frac{d\theta}{dt}\right) + \eta_h\cdot\nabla_h\left(\frac{d\theta}{dt}\right)\right\} - \frac{\partial\theta}{\partial p}R_n \qquad \text{4.3.}$$

Staley (1960), has estimated the orders of magnitude of the terms on the right hand side for large scale diabatic heating and friction to be as follows:

$$\frac{\bar{\alpha}}{g}\eta_\theta\frac{\partial}{\partial z}\left(\frac{d\theta}{dt}\right) \doteq 10^{-14}\ {}^\circ\text{K cm.gm}^{-1}.$$

$$\frac{\bar{\alpha}}{g}\eta_h\cdot\nabla_h\left(\frac{d\theta}{dt}\right) \doteq 10^{-15}\ {}^\circ\text{K cm.gm}^{-1}.$$

$$\frac{\partial\theta}{\partial p}R_n \doteq 10^{-15} - 10^{-16}\ {}^\circ\text{K cm.gm}^{-1}.$$

Since a representative value of potential vorticity in the lower stratosphere or a frontal zone is 2 x 10^{-8}deg gm^{-1}cm sec, over a 12-hour period the largest non-conservative effect above would result in a change of at least an order of magnitude less than this value, implying that potential vorticity might be assumed conservative for periods of up to a day. Staley (1960), estimated the individual potential vorticity change by means of isentropic trajectories for an extratropical disturbance and inferred that in the vicinity of the frontal zones potential vorticity was not conserved. In fact, large positive potential vorticity changes occurred in the lower stratosphere and in the upper troposphere on the cold side of the front while large negative values occurred in the frontal zone and around the entire periphery of the cold trough in the upper troposphere.

4.1.5 Measurement

Vorticity measurements necessitate an accurate description of the wind field. The network of meteorological observing stations is sparse and the observational accuracy diminishes with height. These factors, together with the introduction of an arbitrary grid size from which the vorticity is calculated, introduce an upper limit to the resolution of vorticity estimates.

Thus all physical tracers may be seen to have severe limitations in application to periods exceeding a few days.

4.2 Gaseous Tracers

Various trace gases are shown in Table 4.2, and we briefly consider their suitability for use as tracers.

Table 4.2 Gaseous tracers and their departures from conservatism.

Tracer	Source	Source Type	Sink	Sink Type
Water Vapour	Earth	Evaporation	1. Troposphere 2. Above 70-80km.	Condensation, Precipitation Photochemical decomposition
Ozone	Stratosphere	Photochemical reactions	1 Earth 2. Stratosphere above 30-35km.	Reduction. Photochemical decomposition.
$C^{14}O_2$	Stratosphere	Nuclear explosions. Cosmic ray 'stars'	1. Atmosphere 2 Ocean	Radioactive decay Solution.

4.2.1 Water Vapour

Water vapour is conservative in the absence of condensation and mixing, as perhaps in the stratosphere and to a limited degree in the upper troposphere.

Measurements

The humidity sensors used in radiosondes are without exception inaccurate above the middle troposphere (Middleton and Spilhaus, 1953), because of their excessive lag at low temperature.

In the regions where water vapour is moderately conservative the temperatures vary within the range -40 to -90°C., and sampling may be carried out by the frost point hygrometer of Dobson et al (1946), and Easterbrook and Dinger (1961); by infra-red spectrometry of the sun at various heights and differencing, either from a balloon borne platform (Murcray et al, 1960), or from aircraft (Houghton et al, 1962); and finally by direct sampling using cooled vapour traps (Barclay et al, 1960, Brown et al, 1961).

4.2.2 Ozone

Ozone is produced by photochemical processes by ultra-violet light, as discussed by Chapman (1951). It has been shown fairly conclusively that ozone below 30 km. is protected from photochemical dissociation by the ozone above that level (Nicolet, 1958, Dutsch, 1956, Craig, 1950). The 50% recovery times at 30 km. are 3 days and a month for zenith and horizon sun respectively, and very much longer at lower levels. Thus ozone is essentially conservative for periods of at least a few days near 30 km. and for much longer below this height.

Measurements

Ozone measurements fall into two categories: -

1. Total ozone in a vertical column above the station (this is a crude form of tracer since most of it occurs in the stratosphere below the 30 km. level).

2. Vertical profiles of ozone concentration or mixing ratio.

Measurements of total ozone are made using the Dobson spectrophotometer on the sun, zenith sky either clear or clouded, and the moon, as radiation sources. The method utilises the differential absorption by ozone in two neighbouring wavelengths ~3,200 Å as described comprehensively by Dobson (1957).

Measurement of vertical profiles may be made either by remote sampling by surface-based instruments, or by direct sampling instruments carried aloft by balloons, aircraft or rockets.

The most used remote sampling method is the 'Umkehr' method which makes use of the differential absorption of ultraviolet from zenith sky light by ozone at various solar zenith angles. The technique has been described and methods recommended for interpreting the observations by Ramanathan and Dave (1957), Dütsch (1959), and Matteer (1960).

The profile may also be estimated for layers of finite depth from emission measurements in the 9.6μ infra-red band. The method was described by Goody and Roach (1958), and has since been modified and critically appraised by Walshaw (1960), Dave et al (1963), and Ooyoma (1962).

Direct observations fall in two subgroups - those measuring the total ozone above the instrument at any instant in its flight

and differencing, and those directly sampling the ozone in the air in the environment of the sampling device.

The former method, initiated by E. and V. Regener (1934), makes use of the differential absorption of ultra-violet by ozone. It has been used from balloons (Regener, 1951), and rockets (Johnson et al, 1954, Hulbert, 1955), and has been refined for use on a radiosonde by Paetzold (1954).

Environmental sampling may make use of the oxidation of potassium iodide by ozone (Regener, 1959, and Brewer and Milford, 1960), or the oxidation luminescence device of Regener (1960).

Comparison tests of the different instruments have recently been published by Moreland (1959, 1960), and Brewer et al (1960). These show considerable differences in simultaneous profiles from different types of instrument but good qualitative agreement between instruments of the same type.

4.2.3 Carbon-14 Isotope in Carbon Dioxide

C^{14} is produced from N by cosmic rays and by nuclear explosions, and becomes attached to form $C^{14}O_2$. Its rate of production by cosmic rays is closely proportioned to the number of cosmic ray stars, which is a function of latitude and height (fig. 4.1), but independent of time. Since the half life of C^{14} is 5,600 years it is conservative with respect to decay.

Measurement

A method of direct sampling has been used whereby a large volume of air is collected at a standard level compressed and analysed in the laboratory - Hageman et al (1959).

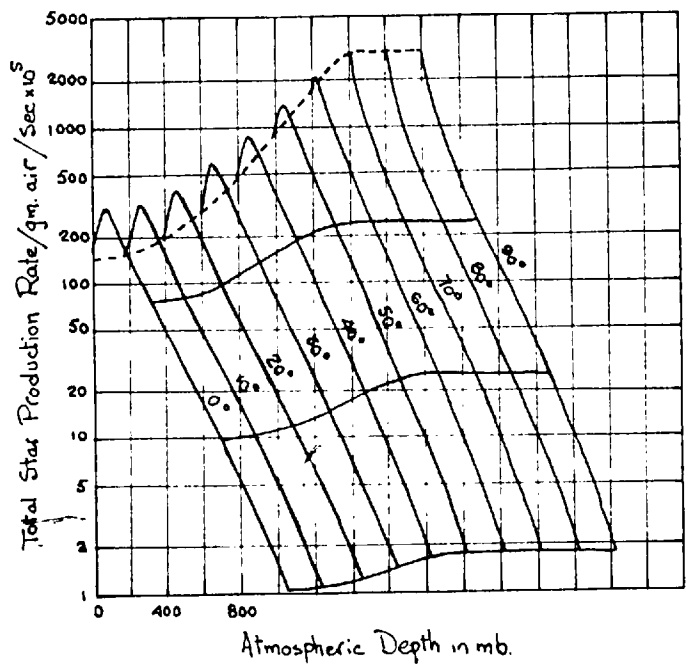

Figure 4.1. Star production rate as a function of pressure, curves for successive 10° lat. intervals are displaced 200 units along the abscissa.

4.3 Particulate Tracers

Among possible particulate tracers Table 4.3 shows a selection of those with most obvious application to the problem under study.

4.3.1 Aerosol Particles of Radius < 0.1μ.

Both the effects of sedimentation and coagulation place limitations on the use of particles as tracers.

Fig. 4.2 from Junge et al (1961), shows the gravitational settling rates for spherical particles, calculated from the Stokes-Cunningham formula. We observe that the sedimentation may be neglected for particles whose radius is below 0.1μ since the settling rates are less than vertical velocities commonly observed in the lower stratosphere. Junge et al (1961), also estimate the half life of particles as a result of coagulation with a background population of larger particles - self coagulation being neglected. The results, in Table 4.4, show that coagulation may be neglected in the size range 0.01 - 0.1μ.

Measurement

Vertical profiles of sub-decimicron particles are obtained using a balloon borne automatic recording Aitken-nuclei counter with a chamber pressurisation device described by Junge et al (1961).

4.3.2 Artificially produced Radioactive Isotopes

In addition to considerations of gravitational sedimentation and coagulation, radioactive isotopes depart from conservatism as a result of radioactive decay. Their sporadic injection in time and locality further complicates the interpretation of their four dimensional distribution.

Table 4.3. Particulate tracers and their departures from conservatism. (Half lives of radioisotopes are shown in brackets.)

Tracer	Source	Source Type	Sink	Sink Type
Aerosol Particles of radius < 0·1 μ	Troposphere	Uncertain	1 Stratosphere 2 Earth	Coagulation Wet, Dry deposition.
Bomb produced radioisotopes Sr^{89} (50·4d), Zr^{95} (65d), W^{185} (74d), Rh^{102} (210d), Sr^{90} (28y), Cs^{137} (30y)	Atmosphere	Nuclear explosions	Earth	Wet, Dry deposition.

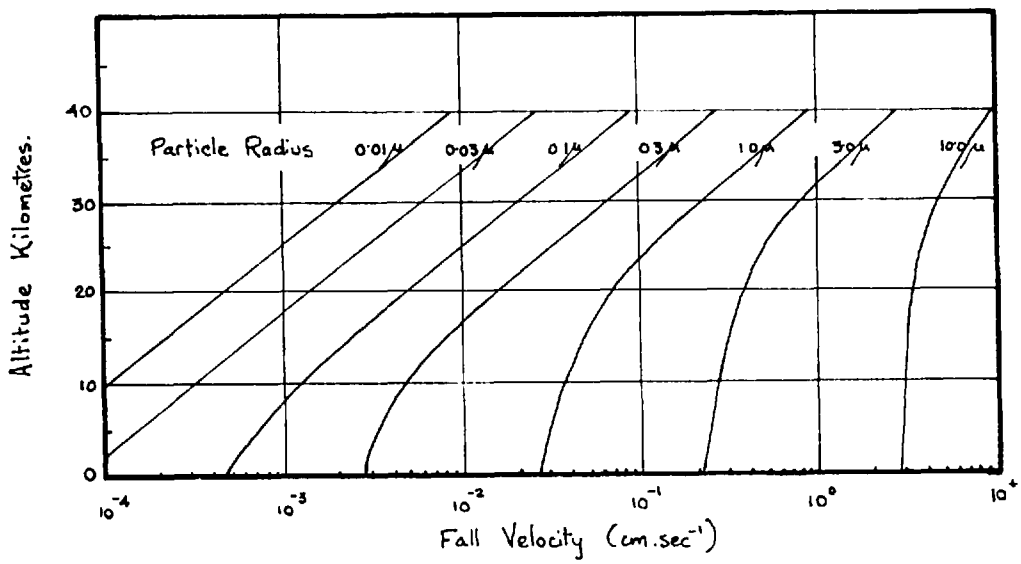

Figure 4.2. Velocity of gravitational settling for spherical particles of density 2 gm. $cm.^{-3}$

Table 4.4. Half lives of particles of various radii in days as a result of coagulation with the background population of particles for various altitudes.

Altitude in km. \ Radius in μ.	0·0025	0·005	0·01	0·02	0·04
27·5	1·6	6·4	24·	90·	340·
20·0	5·1	20·	80·	280·	1060·
12·5	17·	61·	210·	740·	2570·

In each nuclear explosion radioactive debris, produced by vapourisation and irradiation of the environment results, on subsequent recondensation, in an initial particle concentration spectrum probably heavily weighted towards small radius. In megaton bursts these particles are injected into the stratosphere where quasi-horizontal winds distribute them approximately in a zonal belt around the hemisphere and gravitational settling out of larger particles takes place.

As a result of the increase of sedimentation velocity with height (fig.4.2), at any instant the spectrum of debris concentration will be more biased towards larger radius with increase in pressure. This may result in a departure from conservatism, unless we limit sampling throughout the stratosphere to the same particle size range, and may aid in interpreting the results of W^{185} distributions later presented.

If the half-life is long compared with the period of the motion being studied, radioactive decay may be neglected, if not, provided the isotope concentration has not recently been disturbed by a fresh injection, the decay may be removed for a specific isotope by normalising all activities to a fixed time.

Particulates are removed from the atmosphere both by wet and dry deposition but the physical processes are not clearly understood (Greenfield, 1957, Small, 1960, Itagaki and Koenuma, 1962), and the relation of strength of sink to concentration is correspondingly lacking in precision.

Radioactive isotope concentrations are, in general, so minute that sampling requires time intervals of hours to weeks.

Deposition measurements have been made either by collection of the total deposition over a given area, including the precipitation during the period, or by exposing a one foot square gummed film 3 feet above the ground for 24 hour periods - the rainfall during the period washing over the film not being collected. Welford and Collins (1960), by analysing simultaneous samples from the various types of collectors, viz. tub, pot and funnel, together with gummed film, concluded that the various collection type samplers gave consistent results but there was no obvious correlation between them and the collection by gummed film.

Air concentrations are measured by passing a considerable volume of air through a filter at the earth's surface, on balloons (U.S.) and on aircraft flights (U.S. and U.K.). Attempts were also made to measure surface air activity by means of one foot square cheesecloth screens mounted in a vertical plane normal to the airstream, but Lockhart et al (1959), found little correlation with simultaneous sampling by the standard filter technique.

We have suggested earlier that conservatism may only be a plausible assumption for particulate tracers if a limited size range is collected at all levels. In fact, as we observe from Holland's (1959), efficiency height plots in fig. 4.3, the millipore filters commonly used remove the largest particles with highest efficiency, and the millimicron particles which form the bulk of the population with the least. We presented plausible

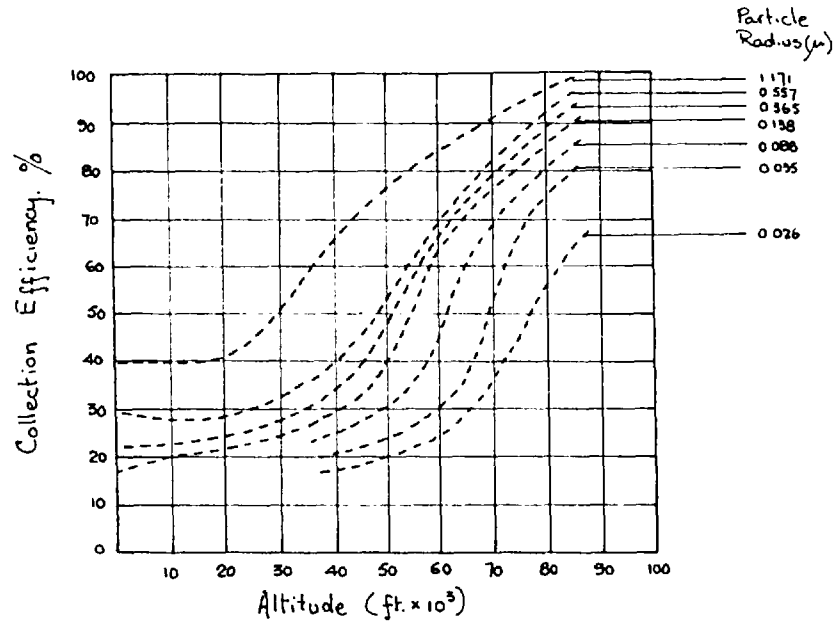

Constant Air Flow Rate of 100 ft min^{-1}.

Figure 4 3. Variation of Collection Efficiency with particle size for porous filter of General Mills Inc. design. (after Holland 1959).

reasons that the activity may be concentrated in larger mean particle size with increasing pressure and the variation in collection efficiency may further accentuate this non-conservative effect.

4.4 Data and Projected Analysis

Information now available on the distribution of potential temperature, water vapour, ozone and radioactive matter will now be presented; in Chapter 5 from a climatological viewpoint and in relation to the jet front complex in Chapter 6. A new analysis of U.K. data will follow in Chapter 7.

CHAPTER 5 A Climatological Analysis of Tracer Distributions

5.1 Intent

The various tracers will be analysed, where possible, in terms of meridional and zonal distributions, either for the year or season, but their interpretation in relation to the transfer through the tropopause will be postponed to Chapters 6 and 8. Some correlations of total ozone with features of the temperature field will be examined in investigating eddy transfer in the lower stratosphere.

5.2 Water Vapour

A summary of the water vapour observations in the upper troposphere and stratosphere is presented in Tables 5.1 and 5.2.

From flights listed in Table 5.1 between the equator, England and Iceland, meridional sections for winter and summer have been constructed in figs. 5.1 and 5.2 (after Roach and Murgatroyd, to be published).

The observational sample is limited but should give a reliable qualitative description of the distribution in low latitudes. In high latitudes there was a period in January and February, 1962, when much higher frost points than usual were observed during Met. Research Flights from Leuchars. The approximately fivefold increase in mixing ratio suggests the observations might have been unreliable, but they are not inconsistent with other mixing ratios throughout the lower stratosphere, nor with the transfer model discussed in Chapter 8. Moreover, Tucker (1957), evaluated mean profiles of frost point for observations in various tropopause height ranges over southern England, and showed the frost point

Table 5.1. Observations made within the troposphere and lower stratosphere by instruments mounted in aircraft of the British Meteorological Research Flight.

Observation Reference	Locality	No of Flights	Season	Observational Method.
Bannon et al. (1952)	Vicinity of England	130	all	
Murgatroyd et al (1955)	Vicinity of England	35	all	Frost point hygrometer mounted in Meteorological Research Flight aircraft.
Goldsmith (1954)	Sudan		Summer	
Helliwell et al (1956)	Vicinity of England	46	all	
Tucker (1957)	Vicinity of England	399	all	
Helliwell & Mackenzie (1957)	Farnborough south to Idris	17	Summer	
Helliwell (1960)	40° to 67°N.		Spring, Summer	
Kerley (1961)	Malta to Niarobi	12	Summer	
Houghton & Seeley (1960	England & Malta	7	winter	Solar spectrometer in aircraft.

Table 5.2. Observations of vertical profiles, and values at about 30km. made with balloon-borne instruments.

Observation Reference	latitude	longitude	No. of Profiles	Season	Observational Method.
Barrett et al. (1950)	37°N	100°W.	3	1-7-49, 26-8-49 7-1-50	Dew point radiosonde.
Brasefield (1954)	40°N	75°W	>7	All	Dew point radiosonde.
Mastenbrook & Dinger (1960)	U.S.A		11	All	Dew point radiosonde
Mastenbrook & Dinger (1961)	40°N 39°N	105°W 75°W	1 2	28-4-59 8-4-60, 27-6-60	Dew point radiosonde.
Murcray et al (1960)	40°N	105°W	1	19-6-59.	Solar spectrometer.
Murcray et al (1962)	40°N	105°W	1	18-5-60	Solar spectrometer.
Barclay et al (1960)	52°N	0°W	1	2-5-58.	Vapour trap
Brown et al (1961)	52°N	0°W	9	Summer Autumn.	Vapour trap

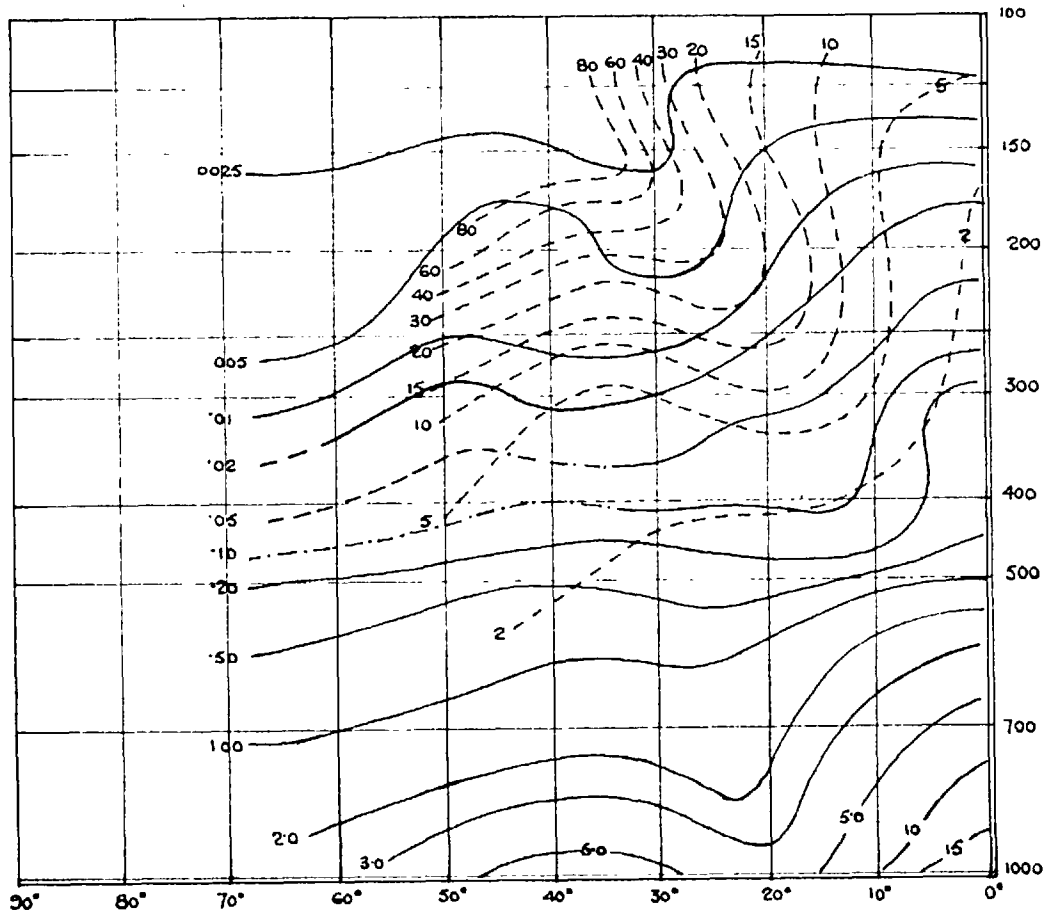

Figure 5.1. Meridional Section of ozone and humidity mixing ratios in Winter

---- Ozone volume mixing ratio (units of 10^{-8})

——— Humidity mixing ratio (units gm kgm^{-1})

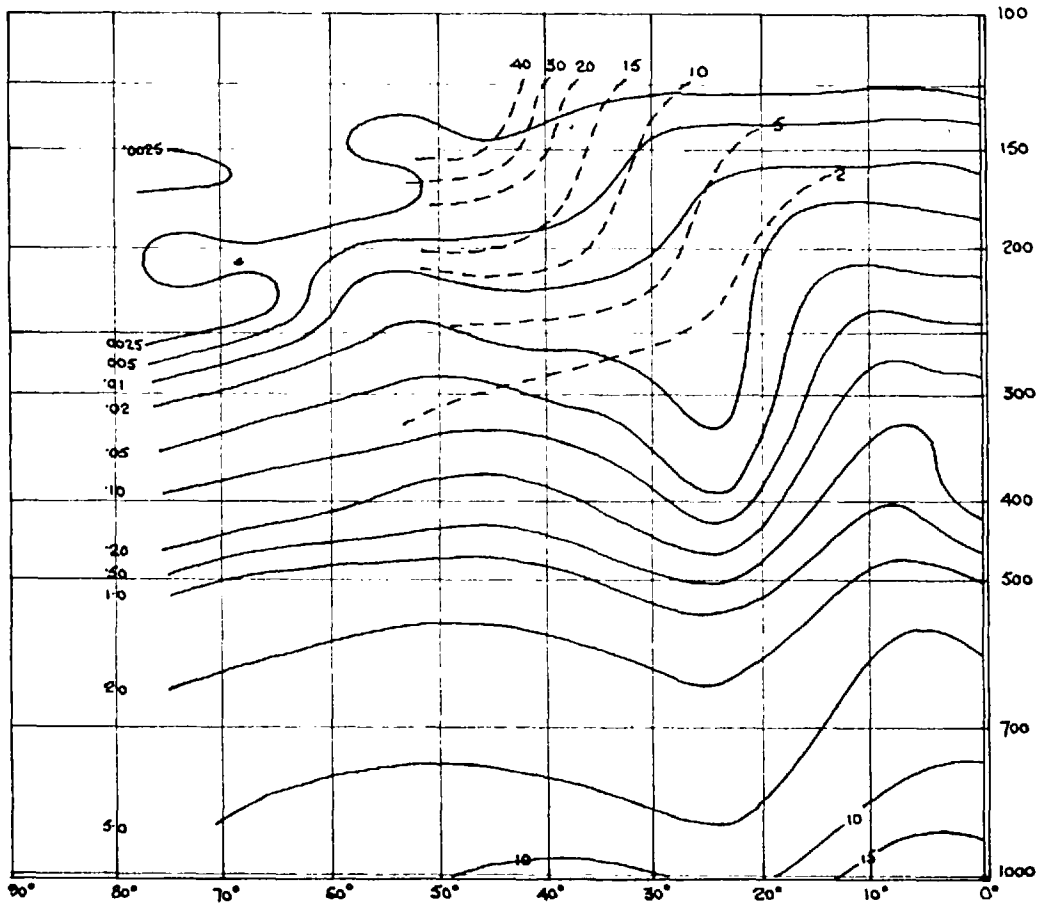

Figure 5.2. Meridional Section of ozone and humidity mixing ratios in Summer

--- Ozone volume mixing ratio (units of 10^{-8})

—— Humidity mixing ratio (units gm.kgm^{-1})

at a given level in the lower stratosphere to range over 15°K, with changes in tropopause height, and it is to be expected that this variation will be at least as noticeable in higher latitudes.

No information is currently available on zonal variations in water vapour.

The series of observations of water vapour up to the middle stratosphere in Table 5.2, are restricted to a 15° latitude belt about 45°N and between 0° and 105°W, and are presented in fig. 5.3 with M.R.F. for comparison.

In general the humidity mixing ratio appears to fall with height to a level between 150 and 200 mb, then increases once more to a value at a height of 50-25 mb, about an order of magnitude greater than the mean value at the tropopause over England. Mastenbrook (1963), has shown, by comparing ascent and descent vapour profiles in August, September, October and April, over the U.S., that the apparent increase in mixing ratio in middle stratosphere probably results from contamination from the balloon, and casts reasonable doubt on all balloon observations. He shows the mixing ratio to vary between .01 and .04 gm kg^{-1}, to at least 30 km.

The results of Houghton and Seeley (1960), using a spectroscopic method appear consistent with the concept of the dry middle stratosphere.

While the absolute values of humidity measured by balloon-borne instruments may be unreliable, qualitative seasonal variations were investigated by plotting mixing ratio values at 20 and 30 km levels extracted from all available profiles on a

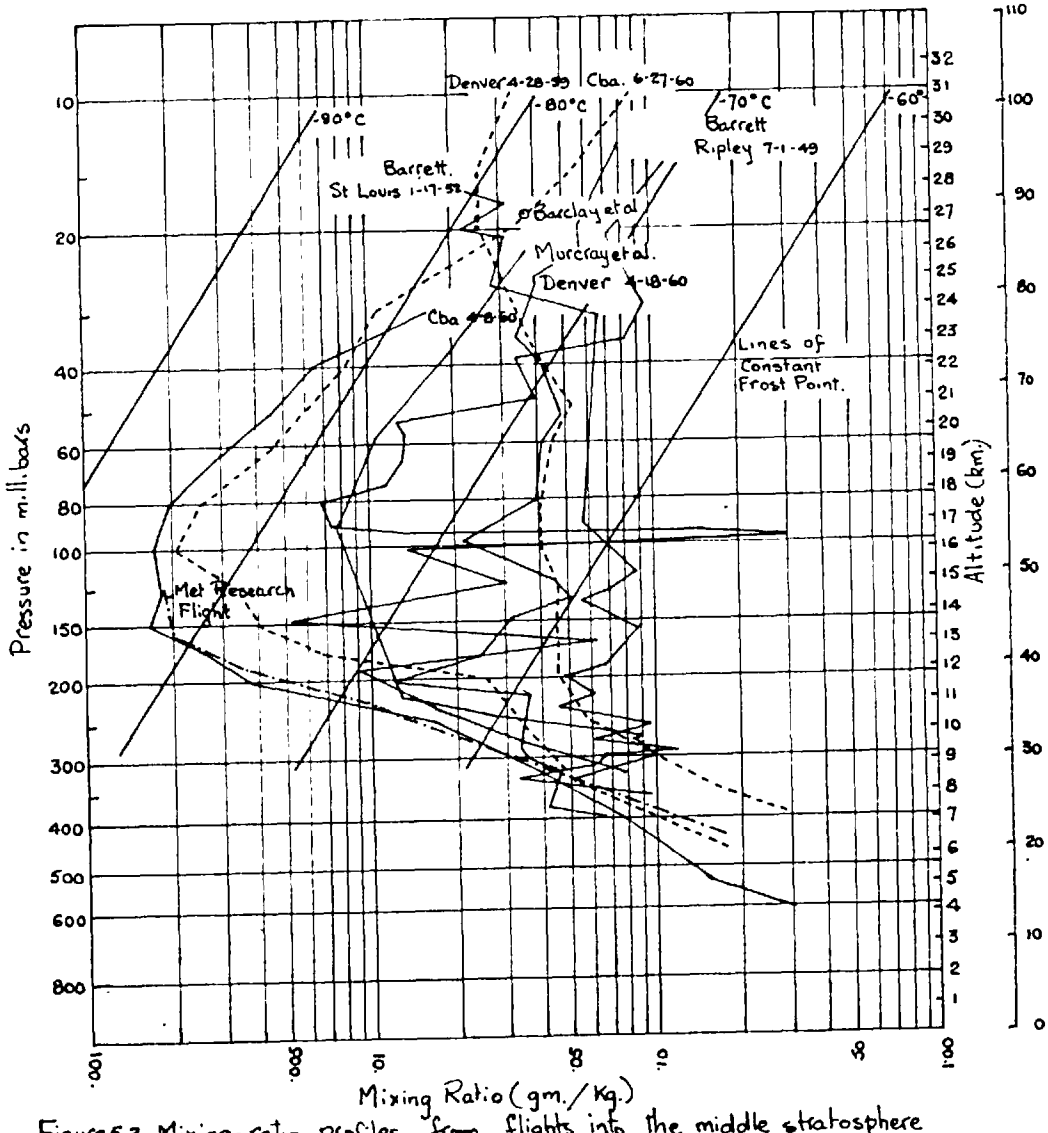

Figure 53. Mixing-ratio profiles from flights into the middle stratosphere

seasonal abscissa, and it was apparent that little variation in mixing ratio occurred at the higher level but at 20 km. there appeared to be a distinct maximum of mixing ratio in the winter-spring seasons.

5.3 Ozone

In the following treatment we will be concerned with total ozone, O_z, in the vertical, and with vertical profiles expressed in terms of mixing ratio, χ_{o_p}, at pressure level p.

5.3.1 Total Ozone, .

The meridional and zonal variations in the total ozone amount, O_z, are best illustrated by London's (1962) seasonal northern hemispheric analysis in figs. 5.4 - 5.7. The ozone amount is observed, at almost all longitudes and seasons, to increase with latitude to 50-80°N, then remain constant or decrease slightly northwards to the pole. This is consistent with McDowall's (1963) time latitude section of ozone in fig. 5.8, constructed from observations made at different longitudes, and with such differences as are shown in simultaneous observations at Srinugar (35°N, 80°E), and Tateno (35°N, 135°E), as discussed by Ramanathan and Kulkarni (1959). In section 5.5 such differences will be shown to be related to the position of the standing eddies.

5.3.2 Vertical Profiles of Ozone and Three-Dimensional Distributions

The most intensive investigation of ozone distribution in the upper troposphere and lower stratosphere has been carried out, as with humidity, by the British M.R.F., using a modified Brewer type chemical sampler.

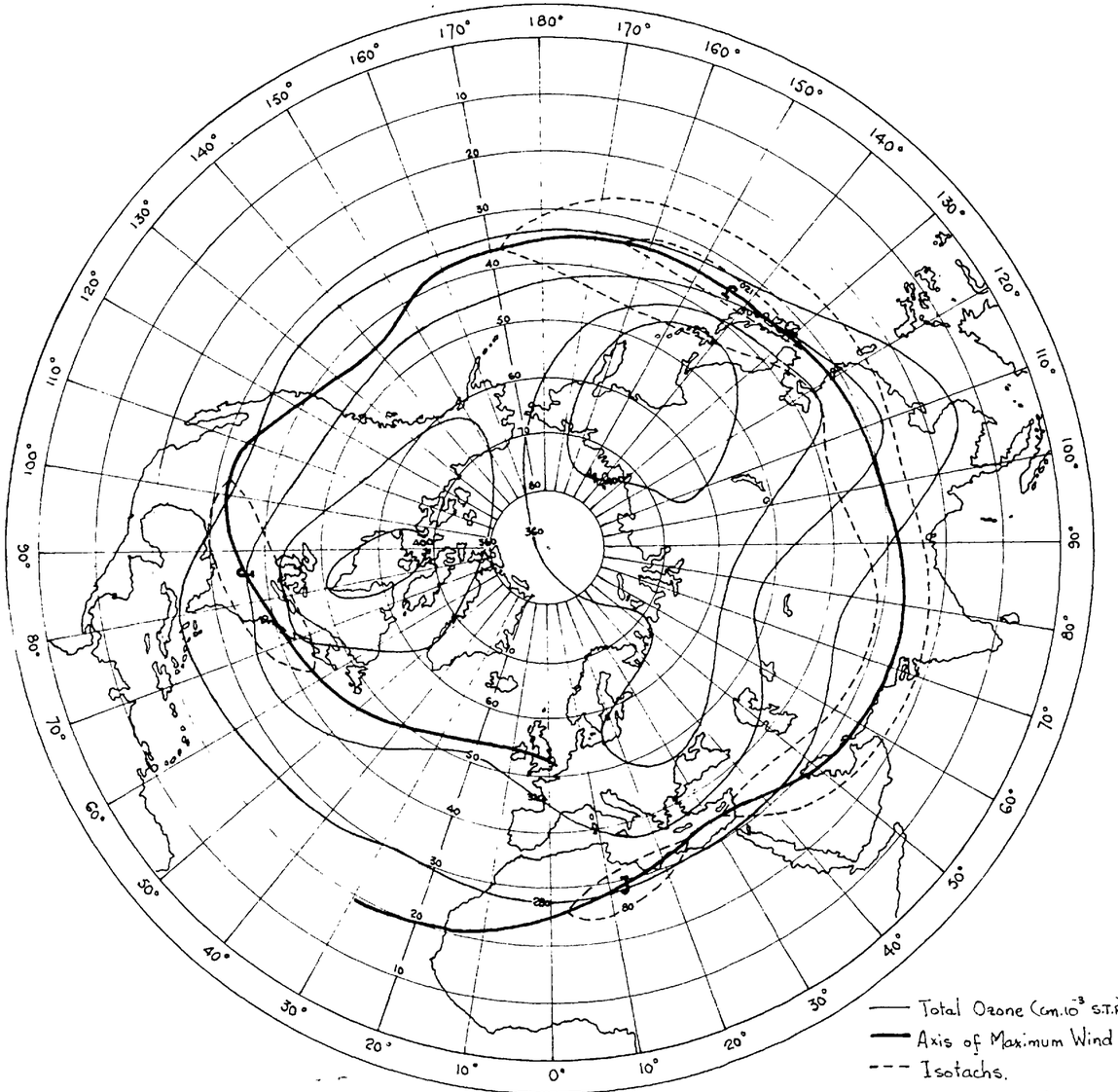

Figure 5.4. The distribution of 3 monthly mean values of total ozone in winter, (London 1962), is shown together with the axis of maximum wind from the seasonal mean values of Crutcher (1962).

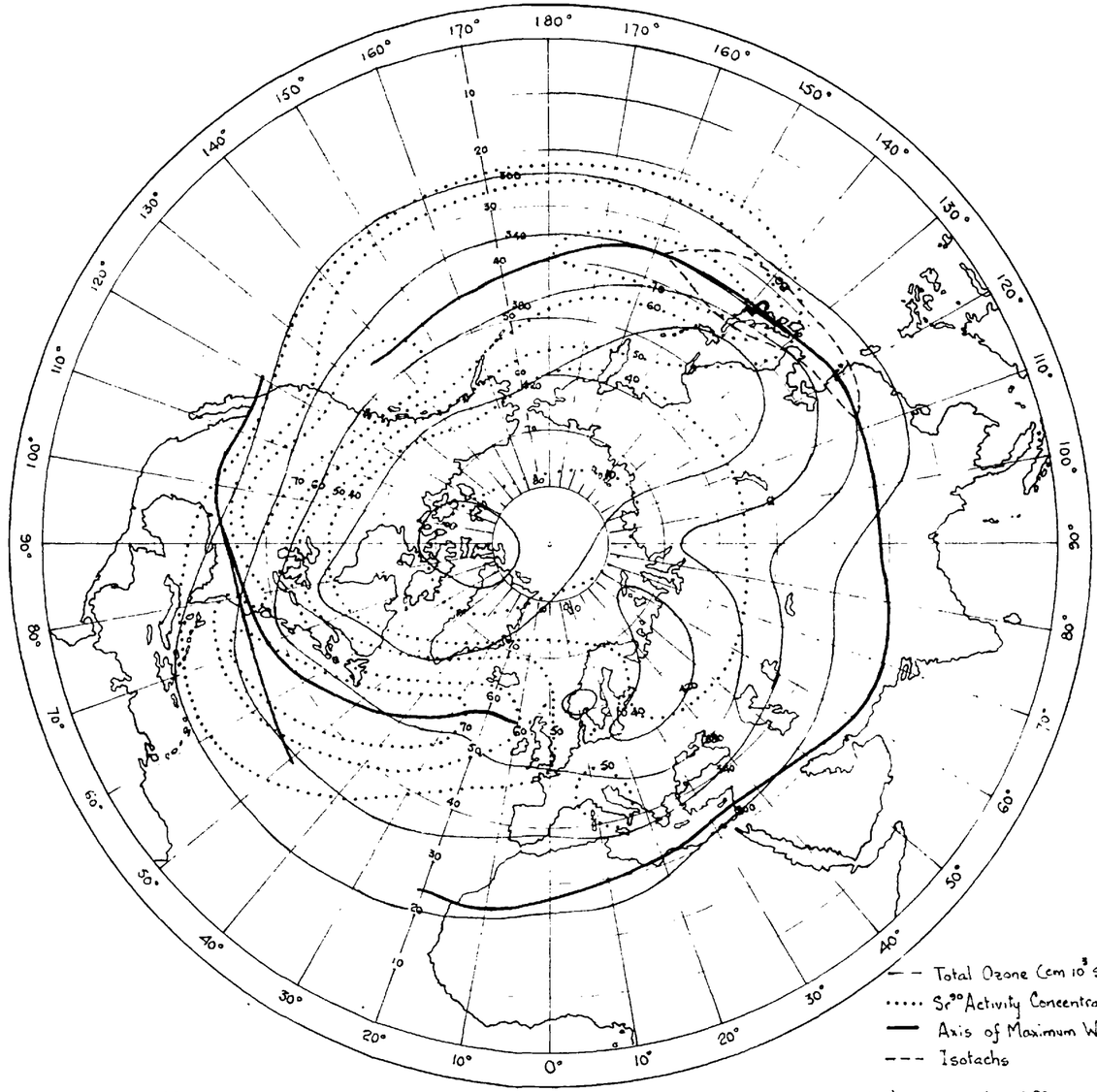

Figure 5.5. The distribution of 3 monthly mean values of total ozone in spring, and the annual Sr^{90} activity concentration are shown, together with the axis of maximum wind from the calculated seasonal mean values of Crutcher (1962).

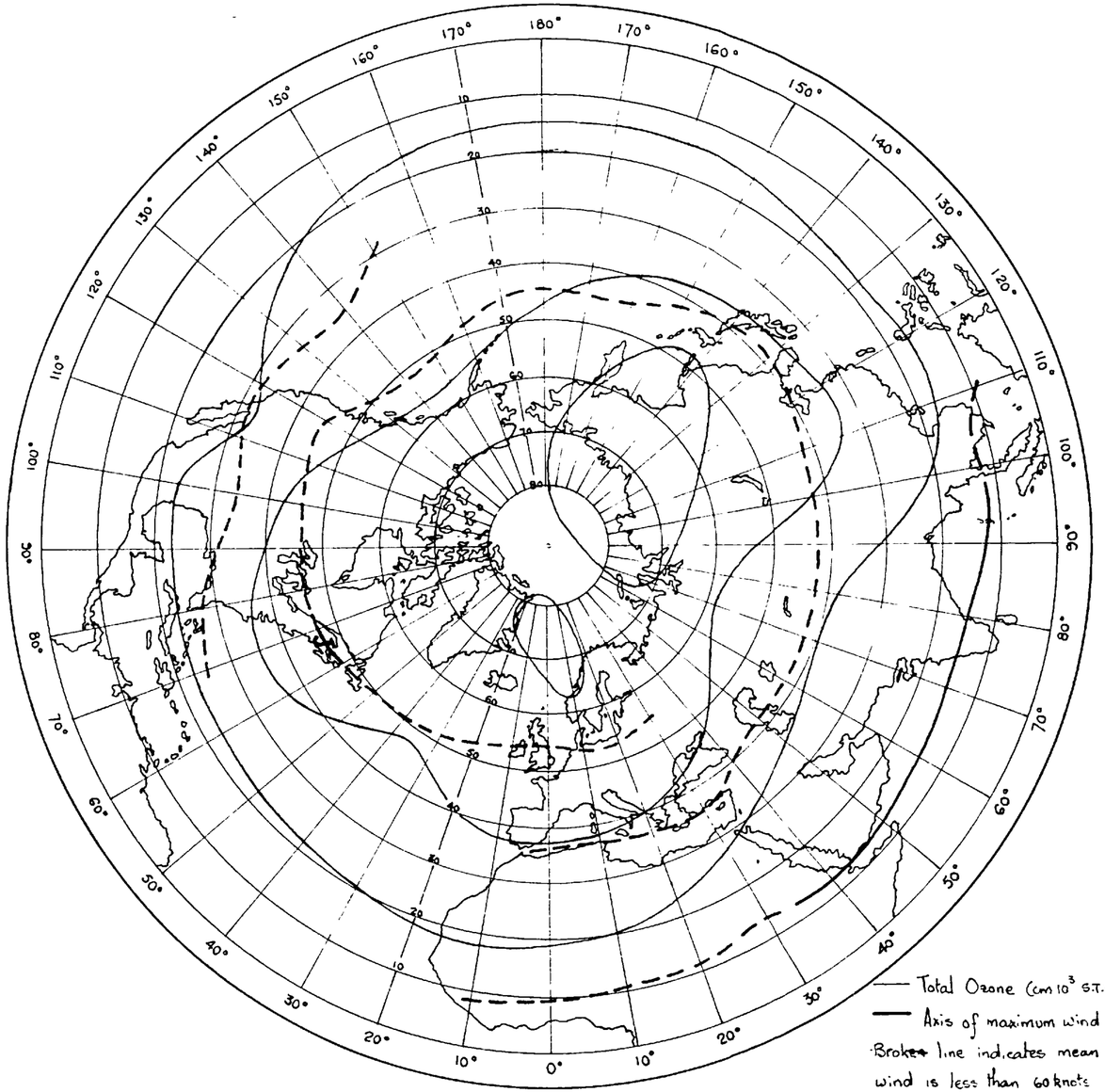

Figure 5.6. The distribution of 3 monthly mean total ozone for summer, (London 1962), is shown together with the axis of maximum wind from the seasonal mean values of Crutcher 1962

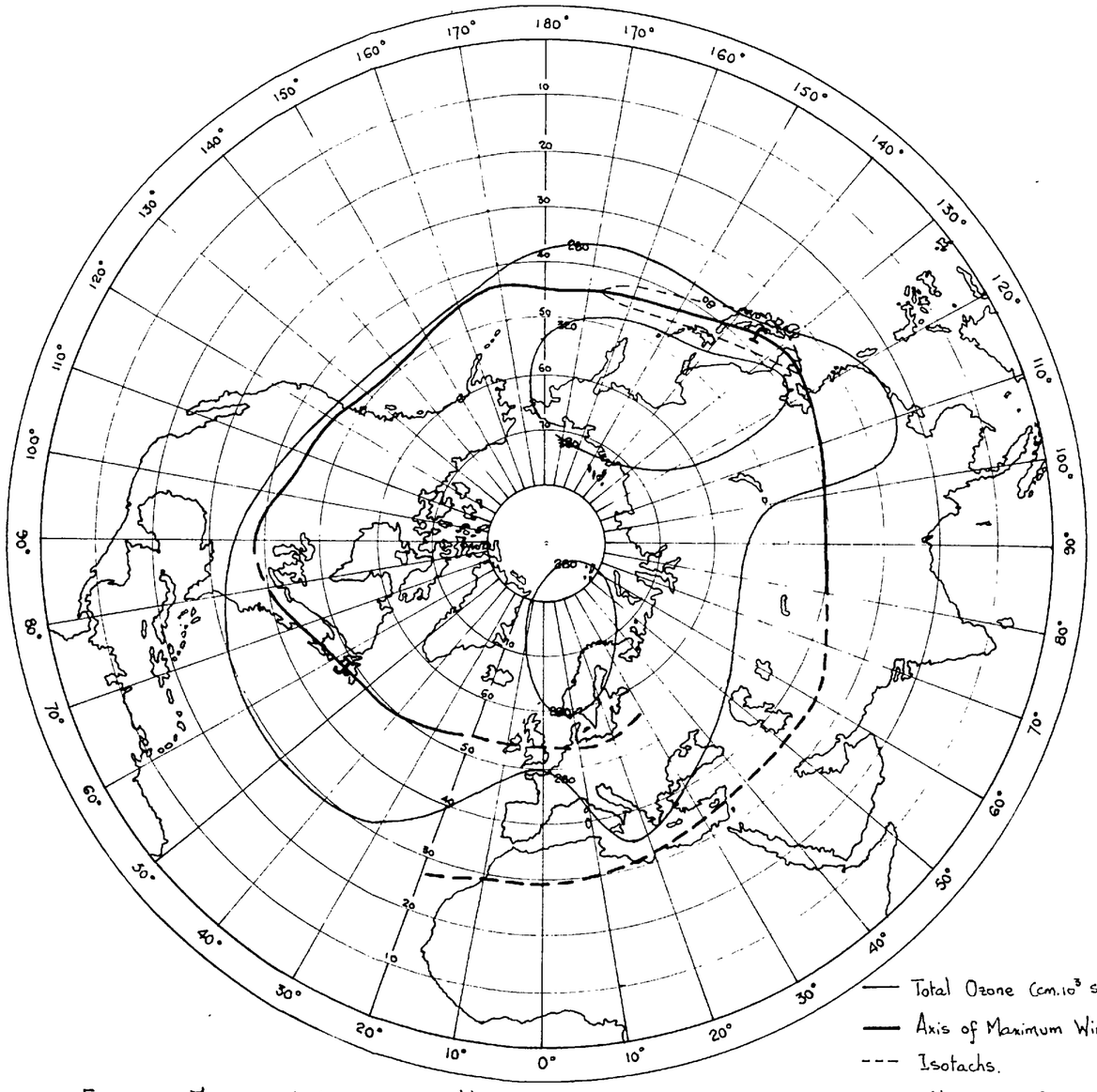

Figure 5.7. The distribution of 3 monthly mean values of total ozone in autumn. (London 1962), is shown together with the axis of maximum wind from the seasonal mean values of Crutcher 1962,

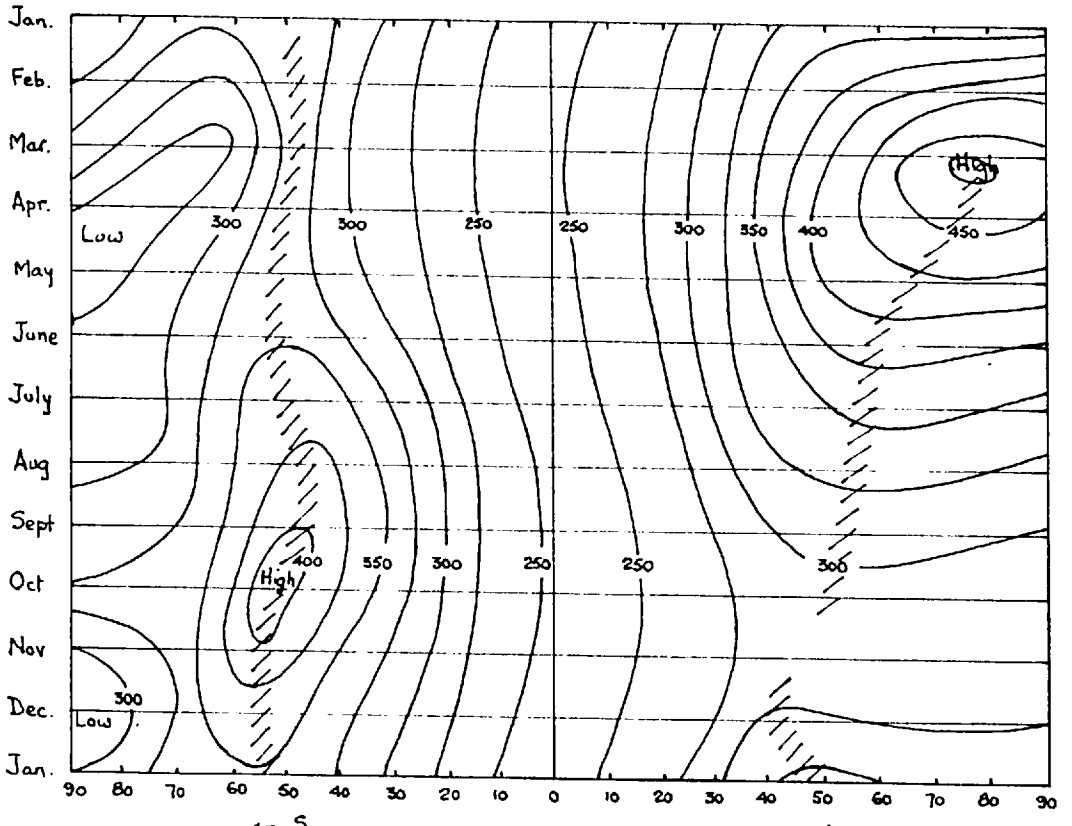

Figure 5.8. Smoothed Ozone results of 17 stations during I G Y. (after McDowall 1960)
Hatched Areas indicate approximate meridional Maximum.

From data collected in summer and winter detatchments from England south to the tropics, tentative seasonal meridional sections have been prepared, (figs. 5.1 and 5.2 after Roach and Murgatroyd unpublished).

A summary of ozone vertical profile measurements is presented in Table 5.3.

The inconsistency between ozone profiles measured by different devices was illustrated by the intercomparison tests of Brewer et al (1960), and is even observed in 'Umkehr' profiles derived using different computation techniques, (Dütsch, 1960). Ramanathan and Kulkarni (1960), assembled spectra for nine stati ons extending from 10 - 70°N latitude, inferred profiles by a uniform technique and presented the results as cross sections for March, July and November (fig. 5.9).

Fig. 5.10 shows representative summer and winter cross sections obtained by modifying the high latitude distributions in fig. 5.9 by introducing the mean profiles for Churchill and Moosonee from Matteer and Godson (1960). The secondary maximum, which is not nearly so prominent over European stations, is thus introduced into the sections, making them more representative of zonal mean sections. The concentrations have been converted to mixing ratios below 30 km. in fig. 5.11.

5.4 Radioactive Isotopes from Nuclear Weapons

5.4.1 General

The irregular distribution of nuclear explosions in space and time makes special caution necessary in seeking the meteorological

Table 5.3. Observations of vertical profiles of ozone specifying the measurement technique used in each case.

Observation Reference	Approximate Location	No. of Observations	Season	Observational Method.
Götz, Meetham & Dobson (1934)	47°N, 10°E	46	All	'Umkehr' method
E & V. Regener (1934)	37°N, 100°W	1	Summer	Spectrograph ascent in an unmanned balloon.
Meetham & Dobson (1935)	70°N, 19°E	13	Summer	'Umkehr' method
O'Brien et al (1936)	44°N, 100°W	1	Winter	Spectrograph in manned balloon – Explorer II
Tonsberg & Olsen (1944)	70°N, 19°E	64	All but Autumn	'Umkehr' method
Coblentz & Stair (1939)	39°N, 77°W	4	Summer	Ultra-violet intensity meter in unmanned balloon
Coblentz & Stair (1941)	39°N, 77°W	19	All	Ultra-violet intensity meter in unmanned balloon.
Newell & Siry (1947)	37°N, 105°W	1	Winter	Spectrograph in rocket
Ramanathan & Karandikar ('48)	28.5°N, 77°E 18.5°N, 73.9°E		All	'Umkehr' method
Karandikar (1952)	28.5°N, 77°E 18.5°N, 73.9°E		All	'Umkehr' method
Ramanathan (1953)	10-30°N, ~75°E		All	'Umkehr' method
Hulbert (1955)	37°N, 105°W	7	All	Spectrographs in rockets.
Paetzold (1953)	Collected Profiles for European Stations (Bibliography)			'Umkehr' method.
Paetzold (1955)	51°N, 10°E	17	All	Ultra-violet intensity sonde
Paetzold, P. scalar (1961)	4°S, 48°N, 70°N, ~0°W.	8	Spring, Winter	Optical sonde
Dütsch (1959)	47°N, 10E	30	All	'Umkehr' method
Brewer & Milford (1960)	55°N, 5°W	32	All	Chemical sonde
	70°N, 19°E	3	Autumn	Chemical sonde
	47°N, 10°E	12	Autumn	Chemical Sonde
Godson & Matteer (1960)	51°N, 81°W 74°N, 95°W	27 4	All	'Umkehr' method
Kulkarni (1962)	38°S, 145°E	15	All	'Umkehr' method

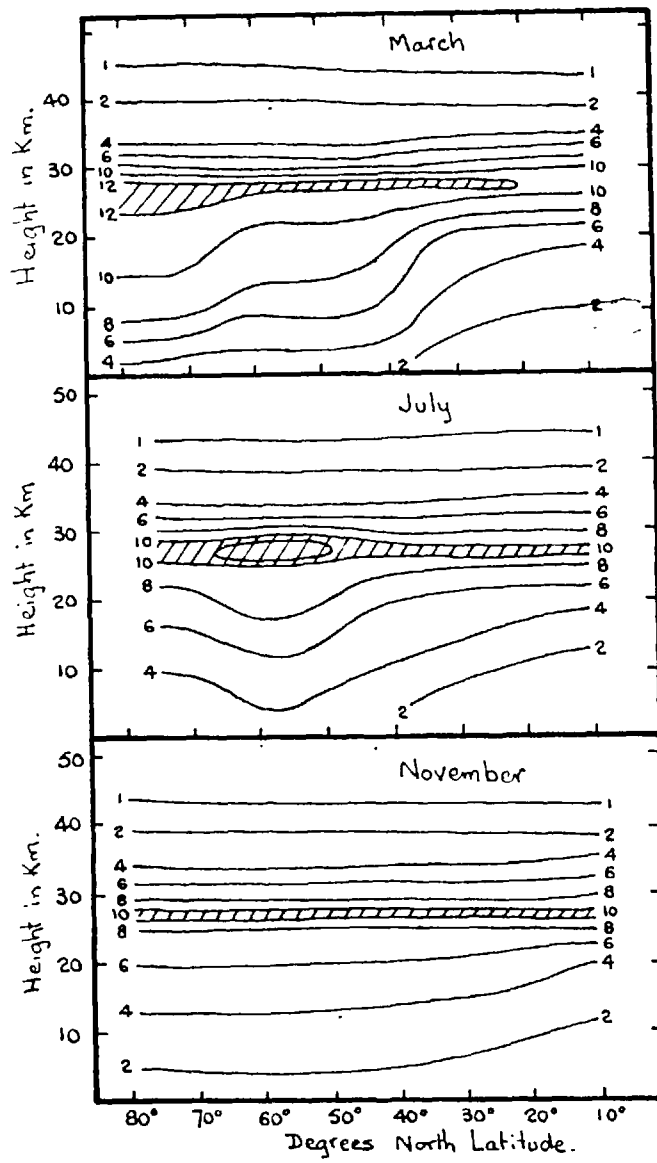

Figure 5.9. Distribution of ozone concentration in units of 10^{-3} cm.atm^{-1} for March, July and November (after Ramanathan & Kulkarni, 1960.) Hatched area indicates region of maximum concentration.

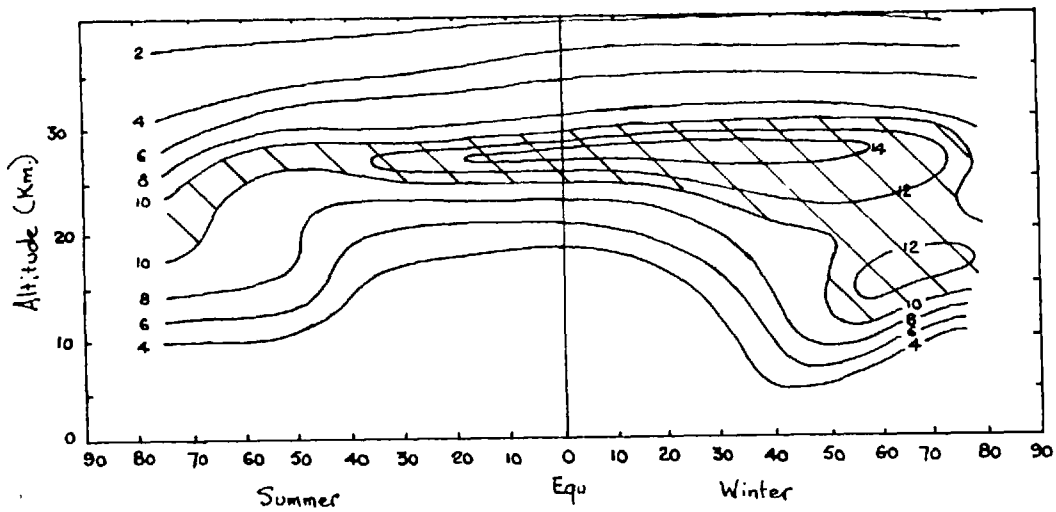

Figure 5.10. Representative Meridional Sections of Ozone Concentrations. (10^{-3} cm km^{-1})

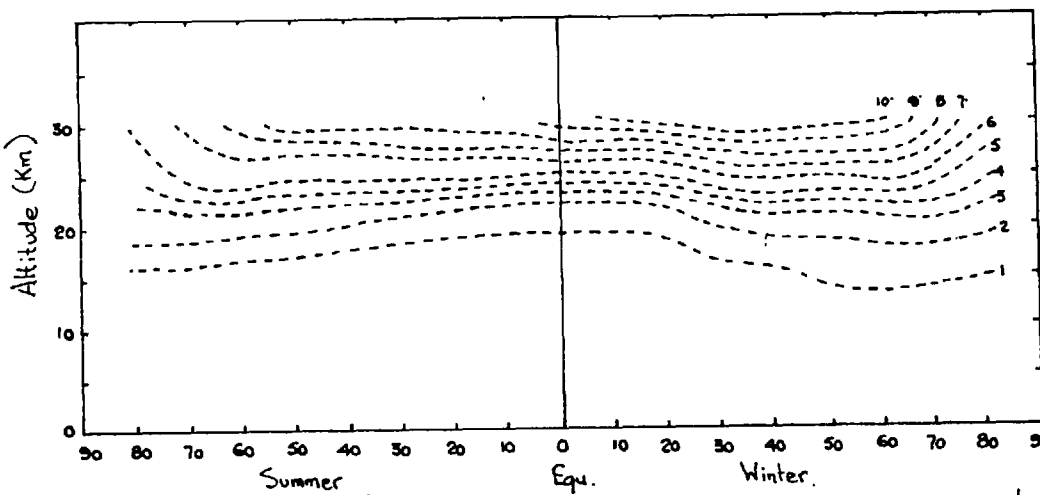

Figure 5.11. Meridional Cross Sections of Ozone Mixing Ratio derived from the above concentrations and temperatures from Murgatroyd (1957.)

significance of observed distributions of the isotopes produced. It will, however, appear that certain distributions are unquestionably of high meteorological significance.

5.4.2. Activity at and Near the Ground

Both air and rain samples may be evaluated for total activity or better for individual isotopes. Unfortunately there has been little consistency in sampling by the various measuring agencies, with resulting difficulty in synthesising the results into a useful four dimensional distribution.

The meridional distribution of radioactive fallout over a year may be estimated either by soil sampling or, if dry deposition is negligible, from rain sampling. The former method, used extensively since 1955, as reported by Martell (1959) and Alexander et al (1960), while not a particularly good technique has the advantage of being the one method from which rapid estimates of the world-wide deposition may be made, without an extensive programme of instrument standardisation and considerable computation. For this reason no attempt has been made to tabulate the extensive data sources but only to present consistent data analysis.

We observe a similar pattern (fig. 5.12) of meridional deposition of Sr^{90} obtained from soil sampling in successive years (Alexander et al, 1960), and from measurements of Sr^{90} in rain (Stewart et al, 1958), - a mimimum at the equator bounded by distinct maxima in the 30 - 50° latitude belt in both hemispheres with values decreasing thereafter with latitude to at least 70°N and 60°S.

The meridional variation of mean annual rainfall is shown as a histogram in fig. 5.12. The mid-latitude maximum corresponds

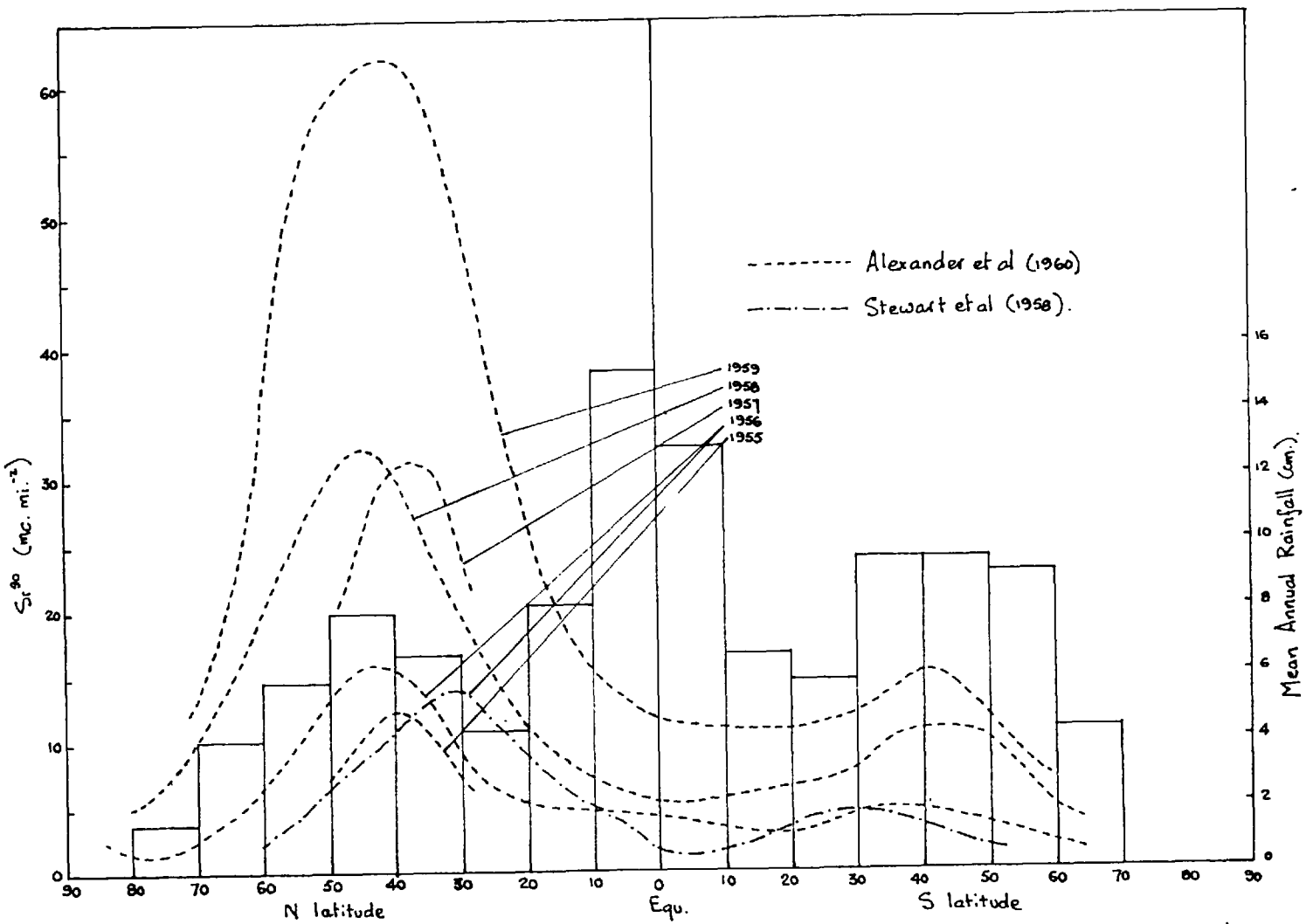

Figure 5.12. The continuous curves show Sr^{90} deposition in successive 1 year periods from 1955-1959. and the histogram shows the meridional variation of mean annual rainfall

closely with that of deposition but the high tropical rainfall has no obvious counterpart in the deposition pattern. Thus the deposition is not solely a function of the rainfall amount, and if we are to interpret these and other deposition results unambiguously in terms of activity in air, we must detect the relation between them.

The meridional variation of annual values of Sr^{90} concentration in rainwater in fig. 5.13 for different sets of years from Stewart et al (1958), and Crooks et al (1960), shows a minimum in the tropics, a maximum near 40°N, a decrease to 60-70°N and a final increase towards the pole.

The empirical studies of Stewart et al (1959), Crooks et al (1960), Bliechrodt et al (1959), Storebo (1959), Small (1960), and Alexander et al (1960), are in general agreement with Stewart (1958), that the monthly mean values of specific activity in rainfall are approximately proportional to the concentration in the air through which it falls, so that the former can be taken as a climatological measure of the latter, except in low latitudes. The close correspondence in the meridional and seasonal variations in the gross fission product activity in surface air along 80°W (Lockhart et al, 1959, 1960 a,b), and in specific activity in rain (Staley, 1962), in fig. 5.14, provide further confirmation of this relation.

We observe the position of the meridional mid-latitude maximum of both properties exhibits a seasonal N - S fluctuation.

The concentration of Sr^{90} in rain at mid-latitude stations from 1954 - 1962, is shown in fig. 5.15 (from Crooks et al, 1961, 1962).

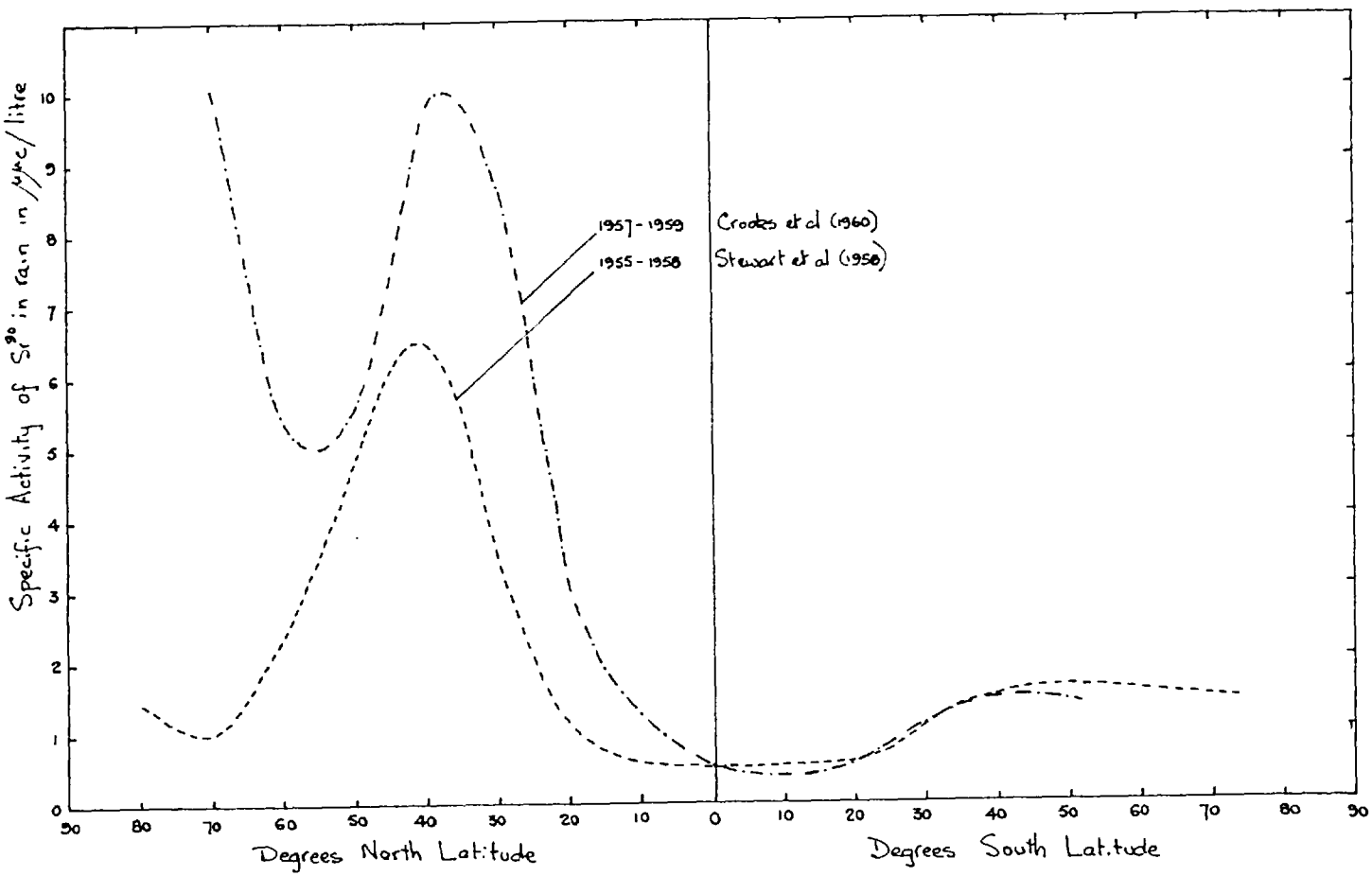

Figure 5.13. Meridional Variation of Sr^{90} concentration in rainwater.

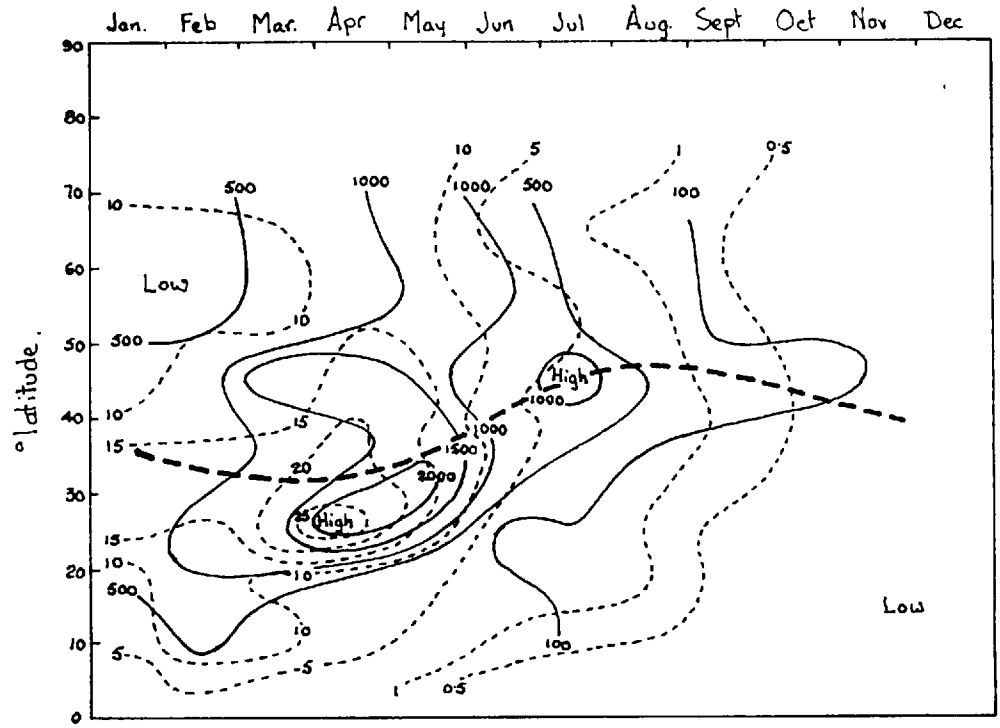

Figure 5.14. ------ Time-Latitude Section of Gross Fission Product Activity in air from data published by Lockhart et al (1959, 1960 a) b)) Units Disintegrations $min^{-1}/100 m^3$. S.T.P.

——— Time-Latitude Section of Rain Fission Product content from Staley (1962). (Units $\mu c.m^{-2}$ per inch of rain).

– – – Position of mean zonal wind maximum for 80°W from Crutcher (1961).

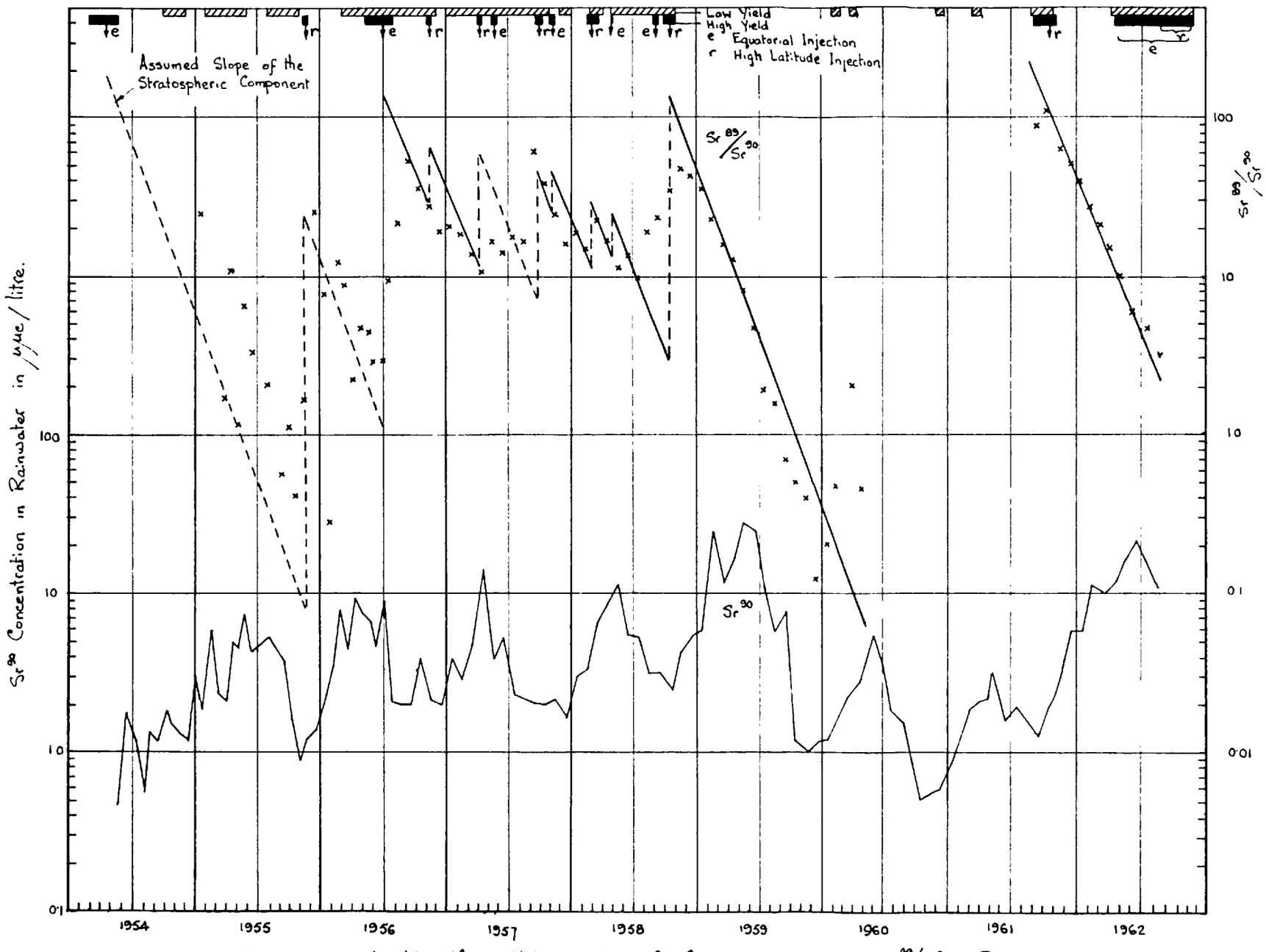

Figure 5.15. Time Series of Monthly Mean Values of Sr^{90} Concentration and Sr^{89}/Sr^{90} Ratio in rainwater at Milford Haven (South Wales). Schedule of injections is shown at the top

A seasonal variation with strong spring maximum and autumn minimum is evident throughout the period and is apparently little influenced by the incidence of injections. From the inventory of nuclear explosions presented graphically at the top of fig. 5.15, we see that there were no high yield stratospheric bursts in the years 1955, and 1959 - 1961, yet the spring maximum remained obvious in each year.

5.4.3 Activities in the Free Atmosphere

In fig. 5.16 we observe a fairly distinct negative correlation between the mean monthly Cs^{137} concentration over England in the lower stratosphere at 47,000' (Peirsen et al, 1960), and in the air near the ground (Cambray et al, 1962), with maxima in the lower troposhere in May and minima in October and vice versa at 47,000'. The mean tropopause pressure is not simply related to the Cs^{137} values. The positive correlation observed with Cs^{137} at 47,000' in 1958 and 1959 becoming negative in 1960.

Two specific radioisotopes were injected during the testing schedule as detailed below:

1. Tungsten 185 isotope, W^{185}, was injected at a height close to 25 km during the Hardtack series of tests at 12°N in summer 1958.
2. Rhodium 102, Rh^{102}, was injected at 30 km during the Orange test at 17°N latitude in August, 1958.

They were sampled later in the stratosphere from aircraft and balloons, together with Sr^{90} which was injected in all tests, and their distributions are shown in figs. 5.17 - 5.22. Distributions of excess C^{14} from balloon sampling of CO_2 by Hageman et al (1959), are shown in figs. 5.23 and 5.24. We observe the following features:

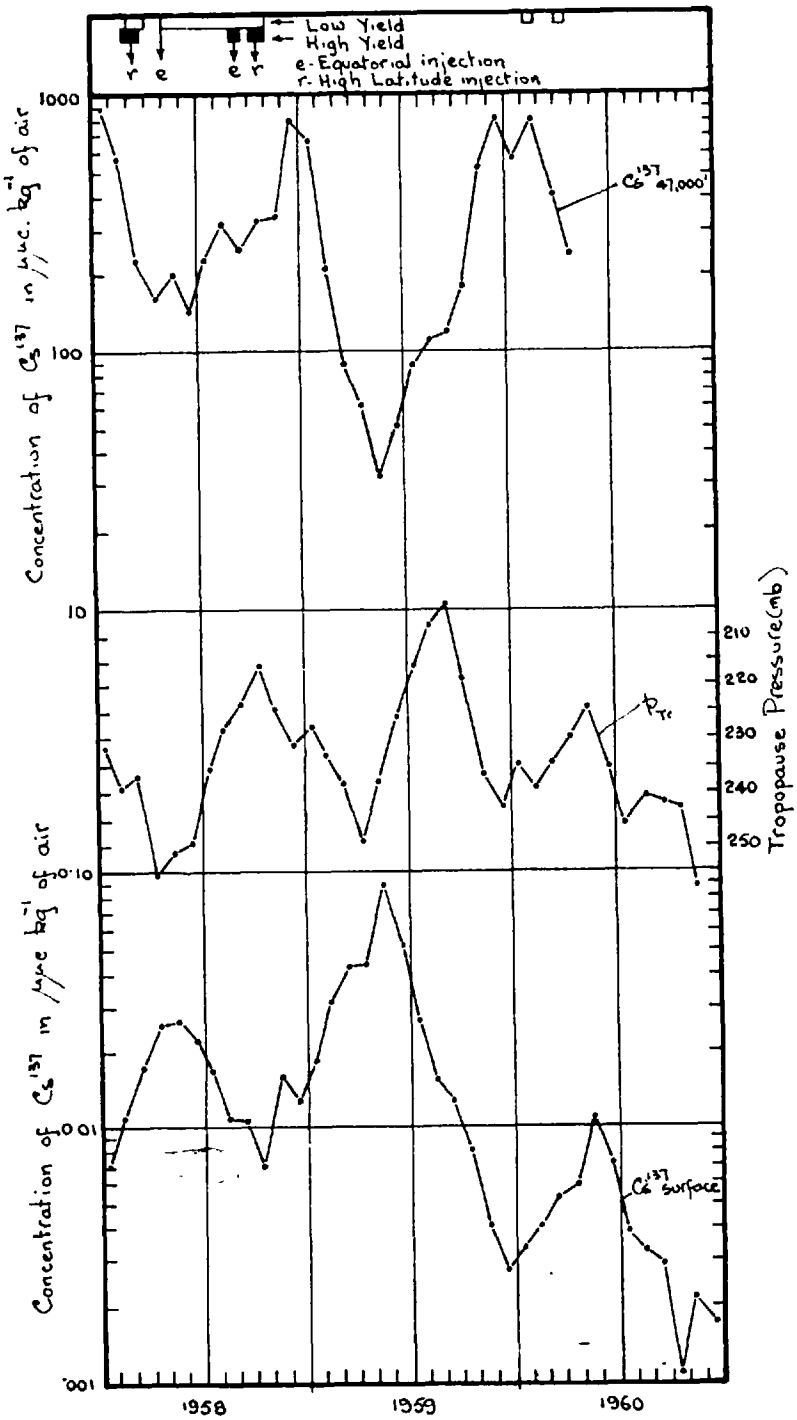

Figure 5.16. Time series of monthly mean values of Cs^{137} concentrations in air over England, in the lower stratosphere (47,000') and near the ground, and corresponding mean tropopause pressure, for the period 1958 - 1960.

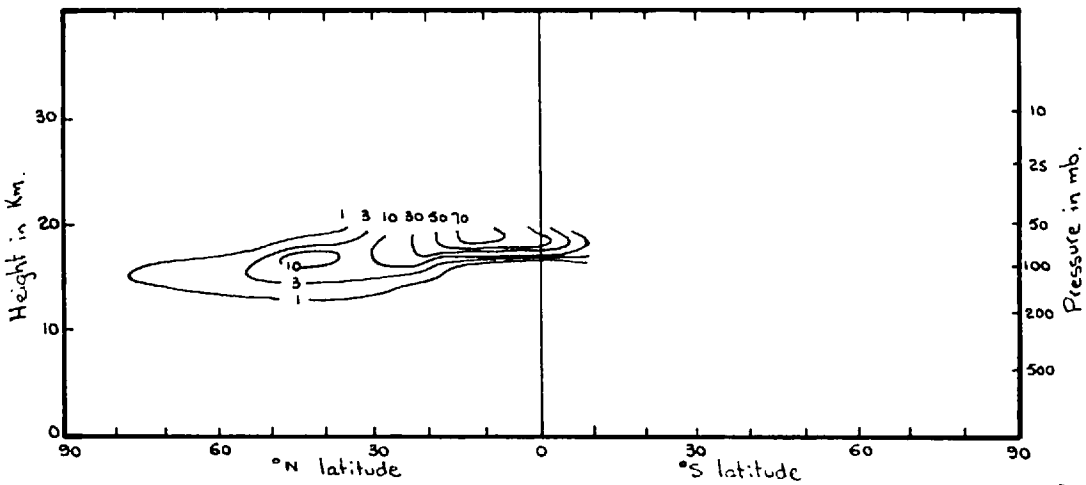

Figure 5.17. Meridional distribution of ω^{185} for September-October, 1958 (Newell, 1961)

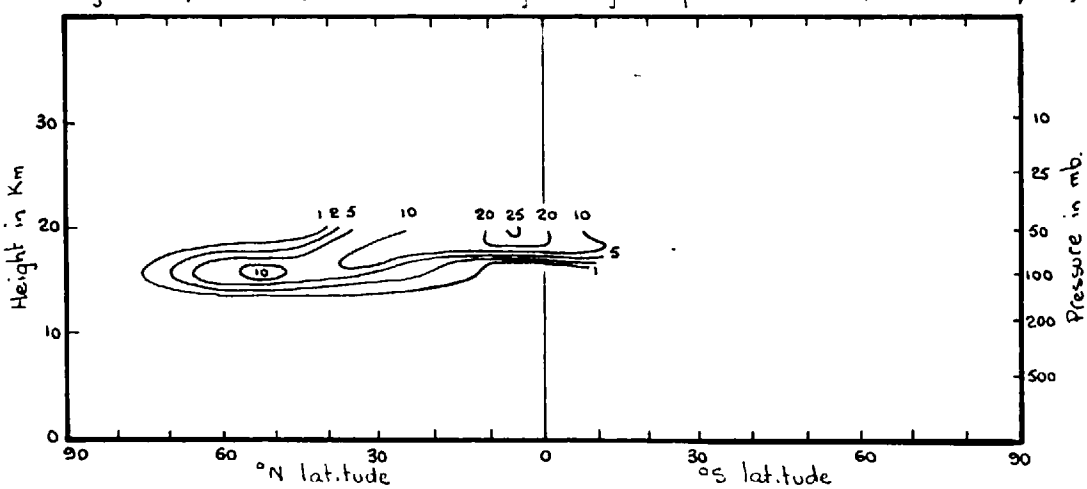

Figure 5.18. Meridional distribution of ω^{185} for November-December, 1958 (Newell, 1961)

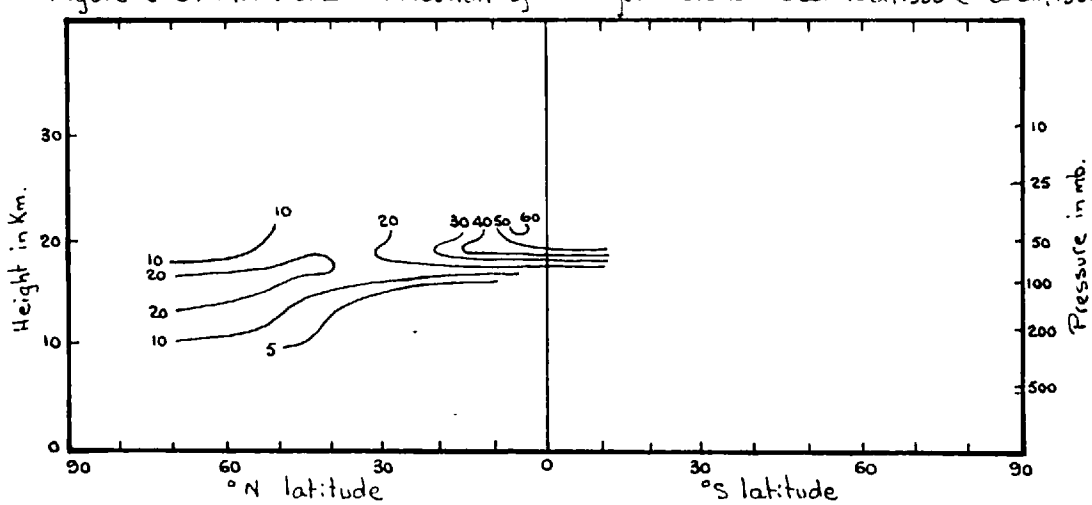

Figure 5.19. Meridional distribution of ω^{185} for November-December, 1959 corrected to 15-8-58 (Feely & Spar, 1960).

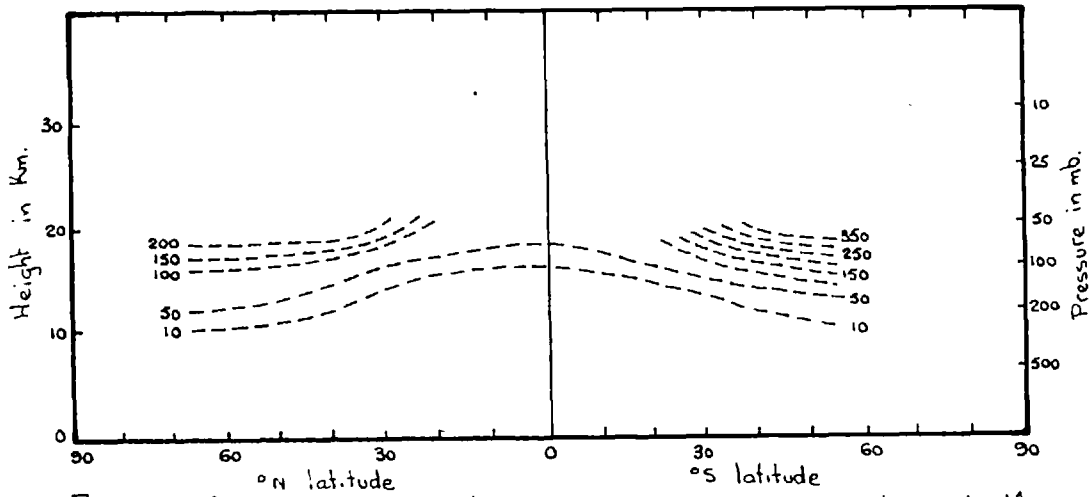

Figure 5.20. Meridional section of mean Rh^{102} concentrations in May 1961 from high level injection of 'Orange' test (17°N, altitude 30km burst) corrected to the date of the explosion - 12-8-58.

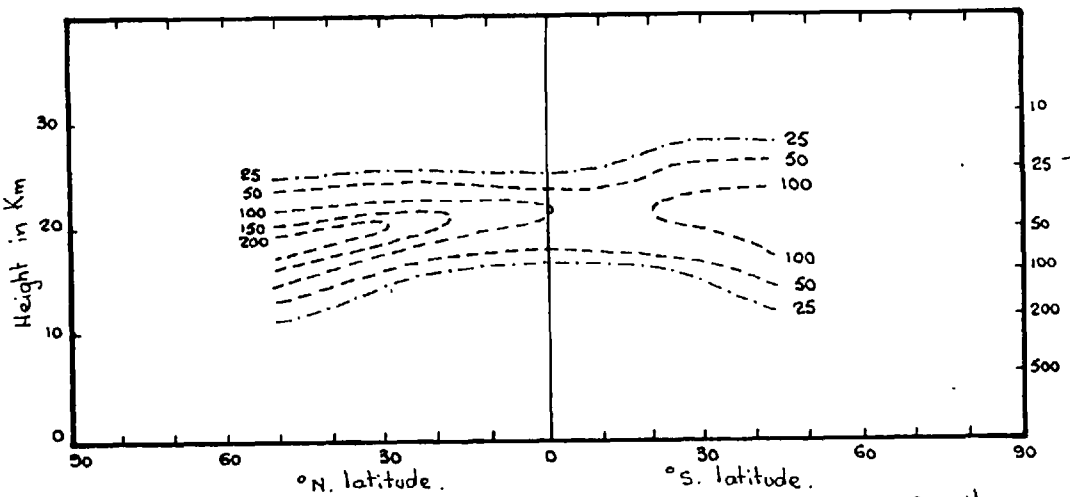

Figure 5.21. Meridional section of mean Sr^{90} concentrations for the period Jan.- Jun. 1957

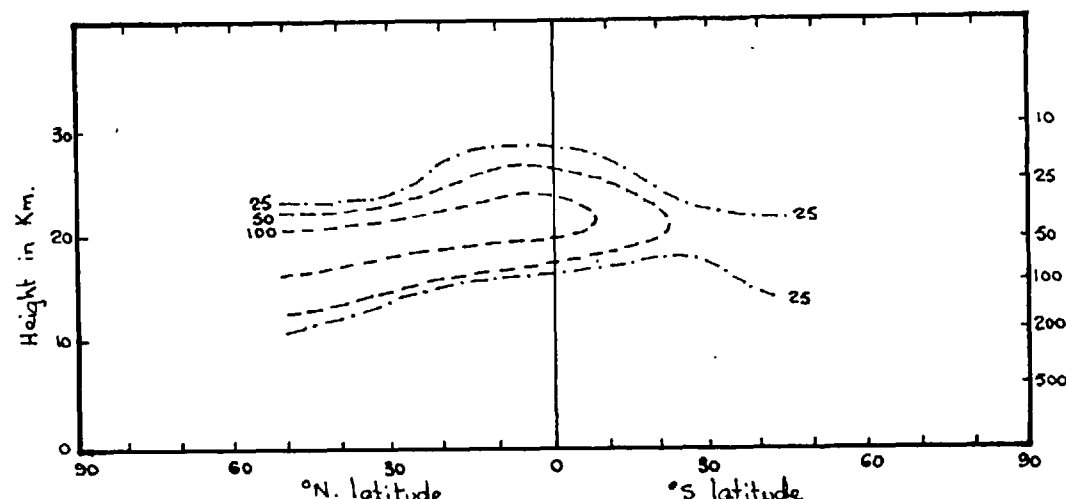

Figure 5.22. Meridional section of mean Sr^{90} concentration for the period Jan. - Jun. 1958.

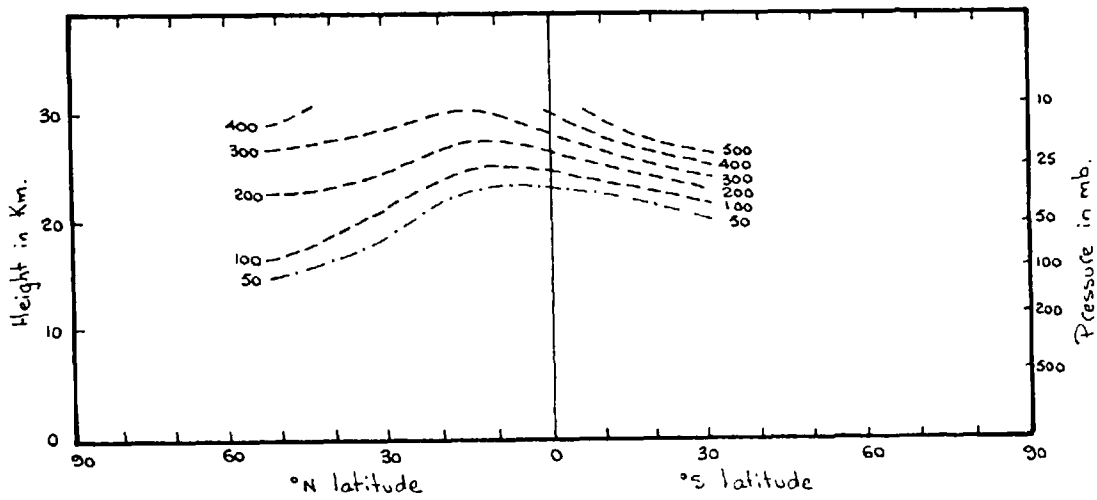

Figure 5.23 Meridional section of 6monthly mean values of excess C^{14} for winter, 1956, computed from data of Hageman et al (1959)

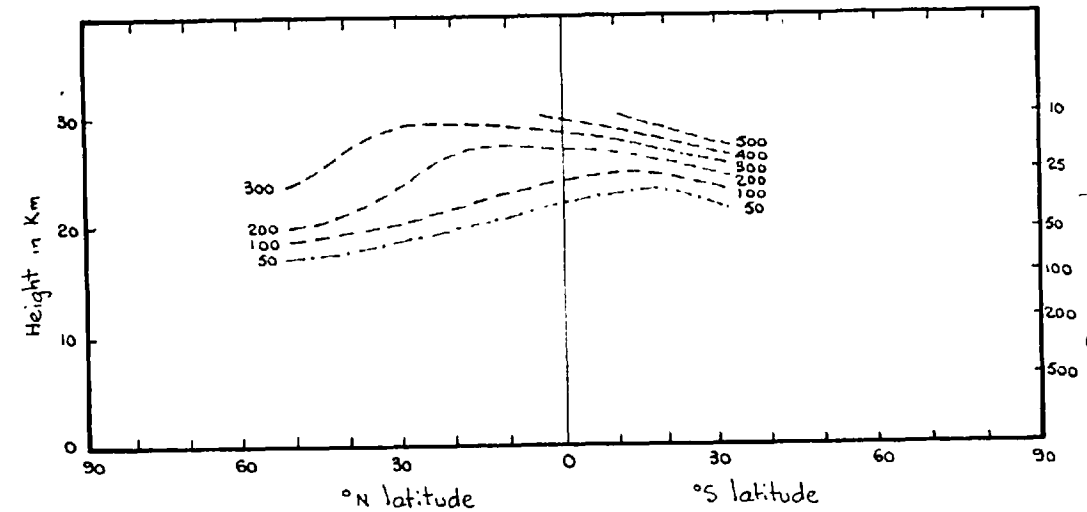

Figure 5.24 Meridional section of 6monthly mean values of excess C^{14} for summer, 1955, from Hageman et al (1959)

1. Where a maximum exists in the vertical profile the height of this maximum varies little with time, and rises toward the equator.

2. Concentrations are barely detectable in the tropics to a height of 15 - 16 km.

3. The tropical lower stratosphere appears to be relatively poor in Sr^{90} and excess C^{14} in winter compared with summer.

These figures give no direct information on the transfer from stratosphere to troposphere, however, their interpretation will assist in forming an integrated picture of the general transfer problem.

5.5 Correlation Studies and Deductions Concerning Eddy Transfer in the Lower Stratosphere

Analyses relating the total ozone with features of the upper tropospheric and lower stratospheric temperature fields have been carried out by Meetham (1937), Normand (1951, 1953, 1954), Gowan and Leppard (1953), and Johansen (1955), to name a few, and the current view may be stated as follows:

1. The high correlations between total ozone, O_z, and either temperature, T, or potential temperature, θ, in the lower stratosphere, suggest that variations result from the same mechanisms. This assumption is supported by the drop in correlation coefficient with the introduction of a 48 hour time lag either way between the respective types of data, as shown in Table 5.4. The higher correlation observed with θ than T suggests the vertical advection is important since the horizontal advection will be similar for each.

Table 5.4. Correlation coefficients of total ozone O_z with various parameters of the thermal distribution from results of Normand (1954) for Oxford, and Johansen (1955) for Tromso where subscripts denote the height in km and H_{trop} is the tropopause height.

Correlated parameter	No specific season			Period considered						Station of Analysis
	Oxford	Arosa	Tromso	Dec Jan	Feb Mar.	Apr May	Jun Jul	Aug Sept	Oct Nov	
T_{12}				-0 29	0 47	0 594	0 536	0 517	0 339	Tromso
T_{15}	+0 60	+0 65	+0 52	0·52	0·59				0 60	O_z Oxford, T·Larkhill
T_{18}	+0 69									
θ_{15}	+0 73	+0·72	+0 56	0 54	0 53				0·59	Oxford
θ_{18}	+0·83		+0·37							
$(\theta_{18})_{-48hr}$	+0·39									
$(\theta_{18})_{+48hr}$	+0 39									
$H_{Trop.}$	-0 67	-0 52	-0·45	-0·123	-0 434	-0·642	-0 524	-0 557	-0 317	Tromso

2. The correlation between O_z and temperature just above the tropopause diminishes in winter. This might either be the result of a seasonal variation of the ratio of the horizontal to the vertical gradients of ozone and potential temperature or the varying influence of more than one transfer mechanism.

3. The correlation with the tropopause height is significantly lower in winter, during the time of the polar night vortex, than in summer, moreover, Normand (1951), found that in winter the correlation coefficient with temperature may increase or decrease with height for successive 26 day periods, suggesting variations in winter may not be associated with tropospheric disturbances. Ohring and Meunch (1960), found O_z was generally more highly correlated with temperature at 100 mb. than 50 mb. for European stations during 1956 and 1957, but the sample was not sufficiently representative to detect seasonal variations in the correlation coefficients.

Normand (1953), took 3 day mean values of O_z at Oxford and temperature in the upper troposphere (300 - 500 mb. thickness) and found a close relation between the deviations from their respective seasonal mean values, but noted some major inconsistencies in winter. Johansen (1955), found similar results for Tromso.

Godson (1960), computed ten day running mean values of total ozone and 100 mb. temperature at several stations for four winters and showed a distinct relation between the time series of the smoothed parameters. The wave number of the stratospheric system associated with the polar night vortex is generally two

(Hare, 1960, 1962), compared to that of three to six (Saltzman and Peixoto, 1957), predominant in tropospheric circulations, so the rate of propagation of the former, (and the associated local temperature change), if both systems are of Rossby wave type, would be expected to be much slower, and the high correlation between longer period systems in winter suggests an association with the polar night vortex system.

4. The highest positive O_z, θ correlation was found (see Table 5.4), by Normand (1951), at 18 km., and Ohring and Meunch (1960), using 100 mb. charts ($\sim$ 16 km.), found that high total ozone was associated with high temperature, low geopotential height, south winds and cyclonic curvature at that level. The horizontal gradient of O_z is generally directed equatorward over the range 35° - 65°N, so an ozone increase with south wind implies a simultaneous subsidence which over-compensates the negative meridional advection (i.e., predominant mixing slope is poleward and downward). The correlation coefficients showed little seasonal change.

Ohring and Meunch (1960), concluded from the above analysis, and from a study of average departures of total ozone from the spatio temporal mean in relation to the standing eddies, that the total ozone maxima and minima occurred slightly in advance of the long wave troughs and ridges respectively.

CHAPTER 6 Tracer Distribution Relative to Synoptic Features

6.1 General

The obvious lack of uniformity in tracer distributions observed in Chapter 5, may be used to elucidate atmospheric transfers either climatologically by noting associations between the tracer distributions and corresponding features of the fields of wind and temperature, and establishing correlations between such parameters, or by individual case studies.

6.2 Associations in the Mean Distributions with Respect to Axes Fixed on the Earth's Surfaces

In the cross sections of ozone mixing ratio and water vapour from Meteorological Research Flight information, shown in figs. 5.1 and 5.2, we observe that the tongue of ozone-rich air with low water vapour content dips down rather markedly in subtropical latitudes from levels normally in the stratosphere to levels more characteristic of tropospheric air. By comparison with the independently drawn mean cross sections of wind and potential temperature in figs. 2.3 and 2.14, we observe that the tongue apparently coincides with the region in the vicinity of the wind maximum, where the isentropic surfaces sweep down from the more stable stratosphere into the troposphere, which may be interpreted as corresponding to the upper tropospheric frontal zone on individual cross sections. Unfortunately no section for another longitude than that of figs. 5.1 and 5.2 is available to support or contradict this apparent relationship.

The middle latitude maximum of annual Sr^{90} concentration in rain, shown in fig. 5.13, also suggests some connection between

the stratosphere-troposphere transport and the tropopause-jet stream-frontal zone complex. This is further supported by the coincidence of the mean maximum wind position for 80°W and the maximum in surface air activity at that longitude shown in fig. 5.14.

We observe a distinct relation between the distribution of Sr^{90} deposition on a hemispheric chart (fig. 5.5) after Alexander et al (1960), and the position of the mean wind maximum from Crutcher (1961). While the wind maximum in the Crutcher sections is probably more closely related to the sub-tropical jet than the polar front, the regions of maximum deposition correspond to the regions of confluence of the two jet systems, i.e., to the southeast of the troughs of the middle latitude standing eddies. It seems plausible that the mechanisms of transfer may be qualitatively similar in both systems, combining where the jets become indistinguishable.

While the meridional variations in deposition and in air activity may be related tentatively to the mean position of the jet front complex, the seasonal variation remains to be related to the wind distribution.

It seems plausible to look for similar transfer mechanisms associated with the jet complex of the polar night vortex to those in the troposphere, and it does appear that transfer there is also associated with the westerly jet maximum. The polar stratospheric jet is a winter-spring phenomenon and it is during this period that the lower polar stratosphere shows its

highest ozone values of the year, (see fig. 5.11). Figs. 6.1 and 6.2, obtained by subtracting successive seasonal mean total ozone amounts, from London (1962), also show a general increase in middle and high latitudes in the 1st and 4th quarters. Moreover, the correspondence between the disproportionately high ozone increase in fig. 6.1, and the region of greatest baroclinity in the polar night vortex over arctic Canada in spring (Hare, 1960, b) where short period thermal waves have been observed (Boville et al 1961), suggests that a major part of the downward transfer may be effected by eddy rather than mean motion.

6.3 Associations Between Tracers and Synoptic Features

6.3.1 Water Vapour

Analyses of M.R.F. data on water vapour distribution have been carried out relative to such features as the tropopause by Bannon et al (1957), Murgatroyd et al (1954), Helliwell et al (1956), and Tucker (1957); fronts by Sawyer (1955, 1957), and Miles (1962); and jet streams by Tucker (1957), Murray (1956), and Briggs and Roach (1963).

Vuorela's (1957), analysis of dewpoint depression below 400 mb. in selected jet-front complexes over western Europe, suggests that air in the frontal zone is frequently subsiding relative to its environment, and this inference is supported for mid-tropospheric levels by Sawyer's (1957). observation from M.R.F. frontal traverse data, that the frontal zone is frequently dry relative to its environment.

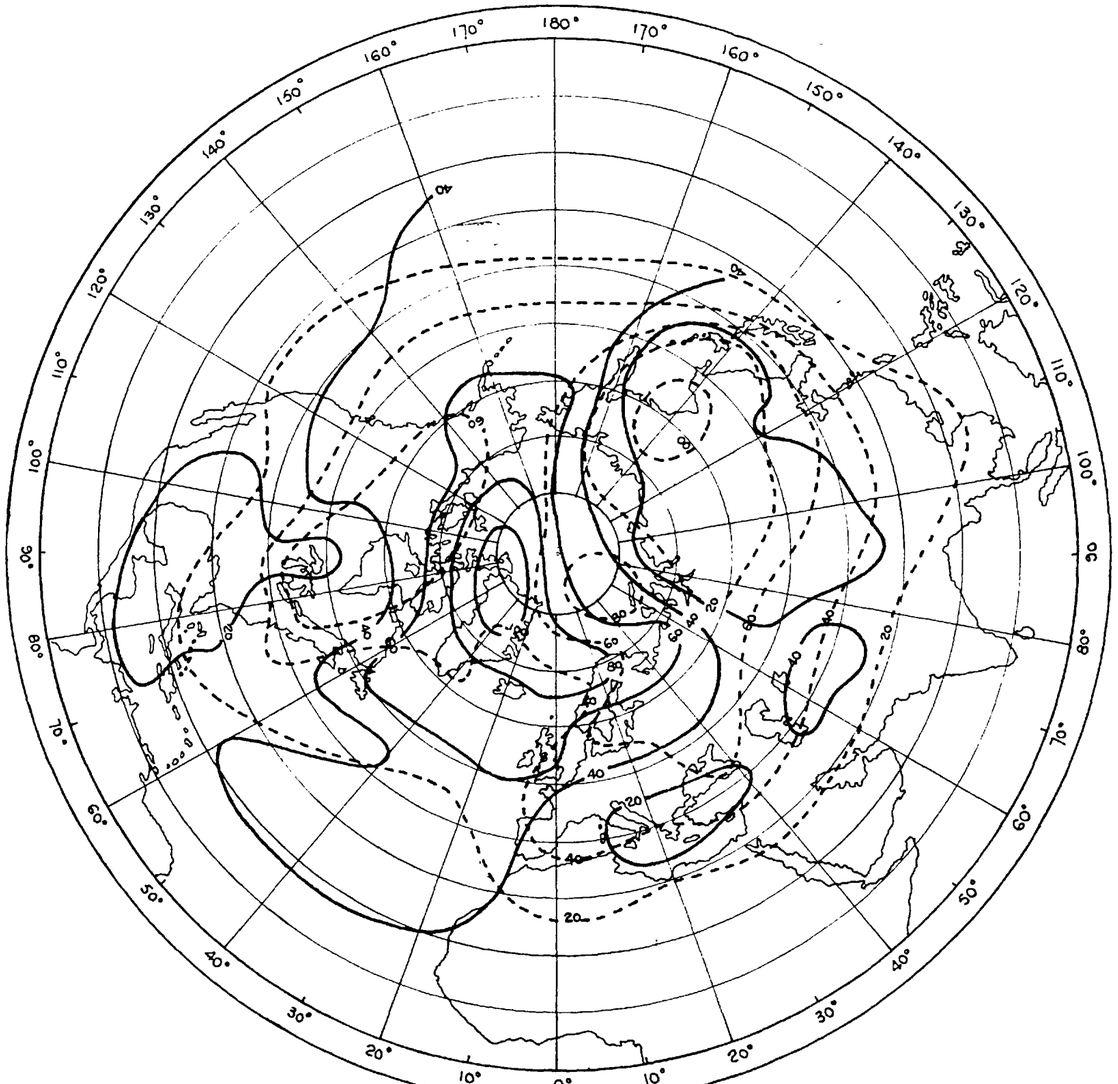

Figure 6.1. Isopleths of the mean increase in vertically integrated ozone amounts over the northern hemisphere from autumn to winter (dashed lines) and from winter to spring (continuous lines) in cm. atm. S.T.P. 10^{-3}.

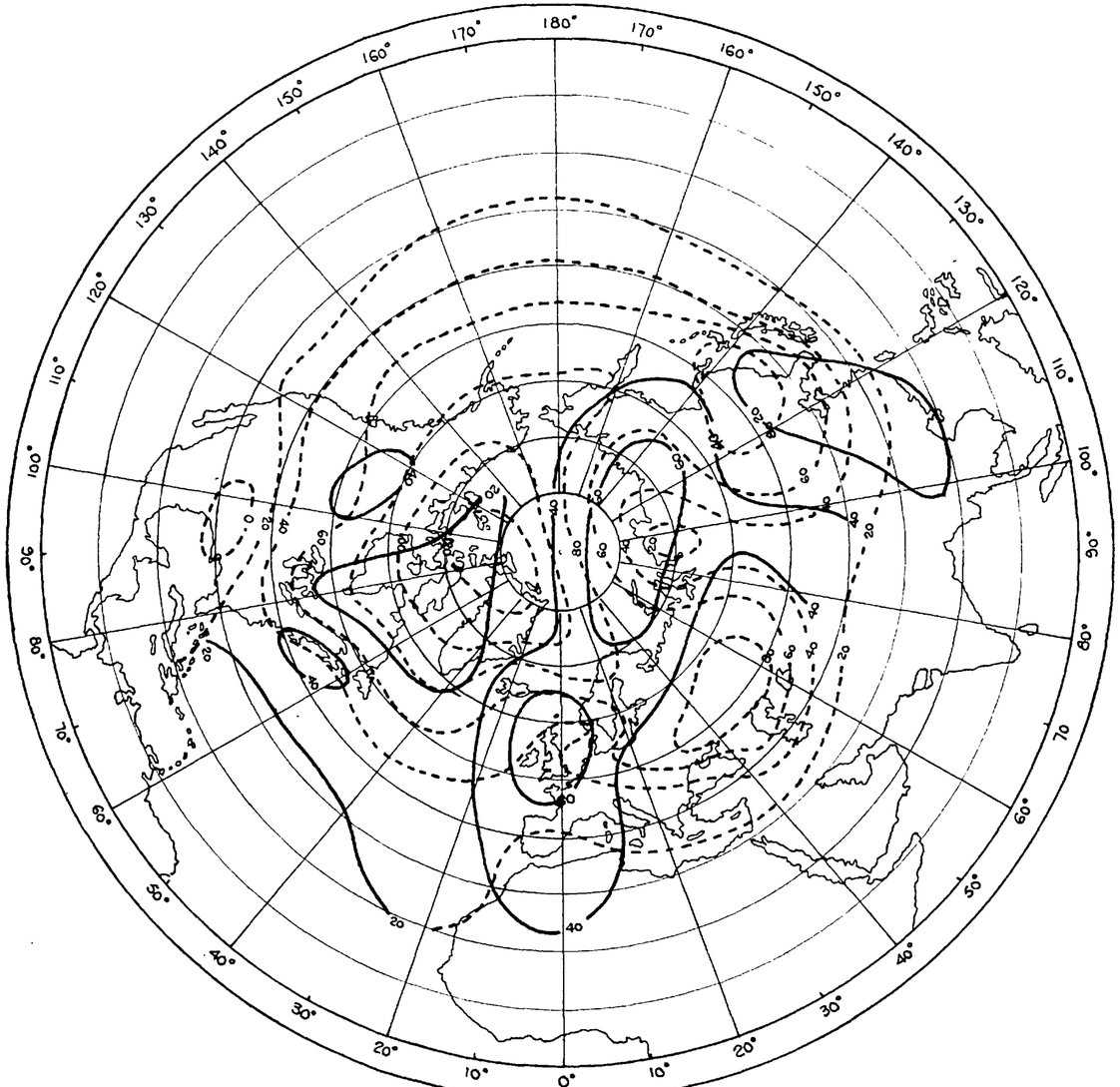

Figure 6.2. Isopleths of the mean decrease in vertically integrated ozone amounts over the northern hemisphere from spring to summer (dashed lines) and from summer to autumn (continuous lines) in cm. atm. S.T.P. 10^{-3}.

In the upper troposphere, information from jet traverse flights have been analysed by Murray (1956), and Briggs and Roach (1961), and indicate the existence on many flights of a fold in the mixing ratio isopleths suggesting an intrusion of relatively dry polar stratospheric air into the troposphere below the jet axis in the region corresponding closely to the frontal zone.

On some flights only two traverses were flown resulting in considerable subjectivity in analysis, but on flights like that shown in fig. 6.3, the resolution was sufficient that this would not radically alter the pattern.

Tucker (1957), inferred a direct transverse circulation about the jet axis in entrance zones and an indirect circulation in exit zones, from an analysis of average frost point departure from the mean value for standard levels above and below the jet axis in fig. 6.4.

6.3.2 Ozone

Brewer (1960), presented a series of ozone sonde ascents together with simultaneous temperature profiles in all seasons indicating discontinuities in the ozone concentration lapse rate at the tropopause level on many individual flights, but a coherent three dimensional analysis was not attempted.

Briggs and Roach (1963), analysed the ozone distribution with respect to the jet-front complex for individual cases (e.g., fig. 6.3) and statistically, as previously discussed in relation to humidity. The mean distributions shown in fig. 6.5 suggest that the intrusion of stratospheric air down the frontal zone below the jet is not a persistent feature of the pattern of transport.

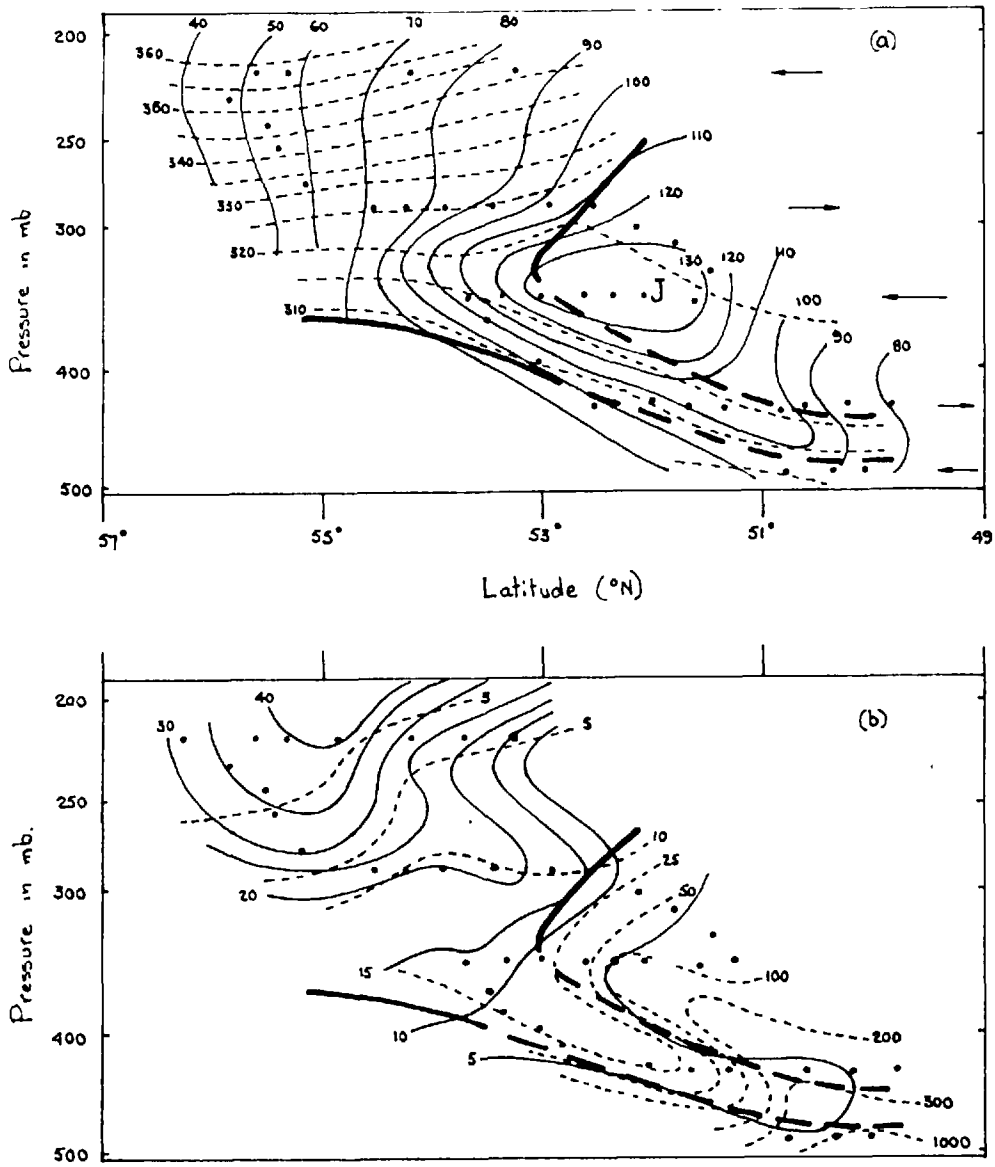

Figure 6 3. Analysis of aircraft observations on flight of 8 May 1961 (Briggs & Roach 1965.)

(a) ——— Isotachs in knots.
----- Potential isotherms in °K
(b) ——— Ozone mixing ratio in mol./10^8 mol.
----- Humidity mixing ratio in $\mu g/g$.

The flight path is indicated by the arrows and the dots represent the points of observation. The thick solid lines represent Tropopauses and frontal boundaries.

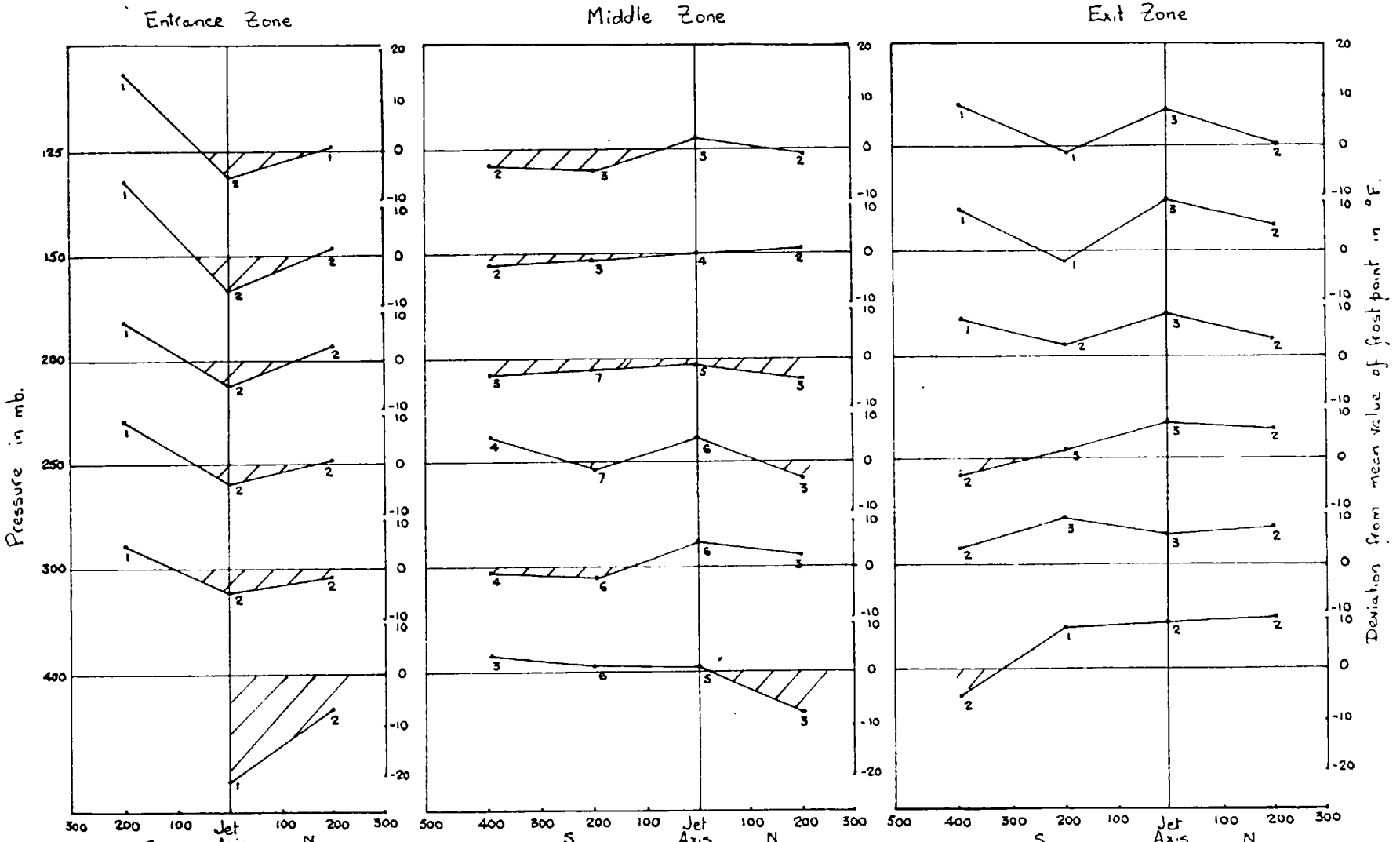

Figure 6.4. Mean frost point deviations from average values at selected pressure levels above and below the jet axis in Entrance, Middle and Exit zones. Negative deviations suggest subsidence relative to the average jet level. Figures alongside points show the limited numbers of cases considered Distances on the abscissa are in miles from the 300 mb jet axis.

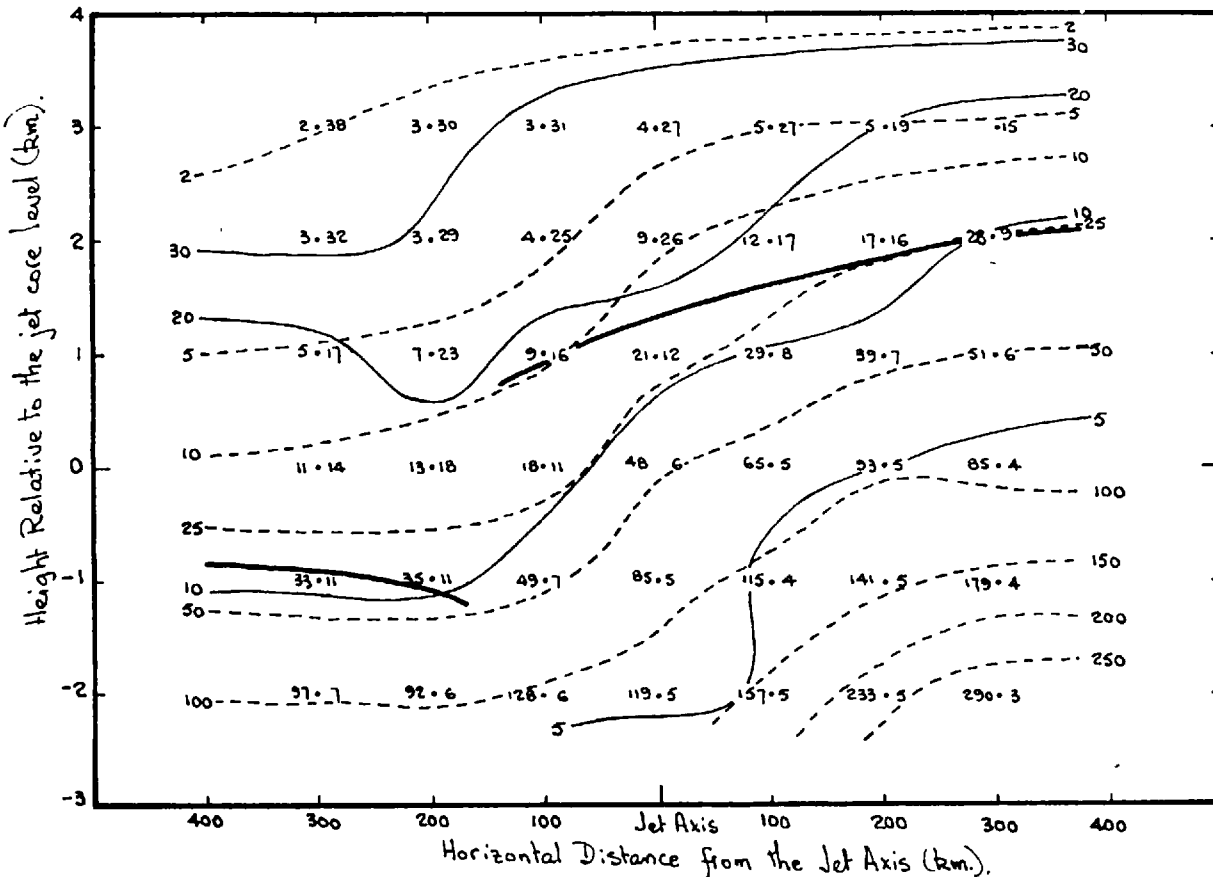

Figure 6.5. Average distribution of water vapour and ozone about the jet core from M.R.F. data. (Briggs & Roach, 1963) The thin solid lines represent ozone mixing ratio (mol./10^8 mol.), the thin dashed lines show humidity mixing ratio (μg./g.), and the thick solid lines tropopauses. Mean ozone and humidity mixing ratios are plotted to the right and left of the relevant grid points respectively.

6.3.3 Artificially Produced Radioactive Isotopes

Miyake et al (1960), could detect no systematic variation in the integrated activity 'C' in the tropospheric air column associated with the changes in surface weather conditions (see Table 6.1), but found it to be related to the position of the jet axis and the presence or absence of a marked 500 mb. cold trough. The integrated activity 'C' in the rain bearing tropospheric layer is plotted, on an abscissa of distance from and ordinate of pressure of the neighbouring jet axis, as a circle whose area is proportional to 'C' in figs. 6.6 and 6.7 for cases with or without a 500 mb. trough in the vicinity. The highest values of 'C' are observed to occur when the jet is situated above or a little north of the sampling station and when the jet axis occurs at lower levels.

During the month of March, 1960, an extensive series of observations of S_r^{89}, S_r^{90}, ω^{185} and β_e^{7} concentrations in the upper troposphere and lower stratosphere was made over the U.S.A. Danielsen et al (1962), analysed these observations together with simultaneous values of potential temperature and potential vorticity statistically and by means of case studies, in the investigation of stratospheric-tropospheric exchange processes.

The S_r^{89} which was injected into the troposphere largely within a stable layer between potential temperatures of 330-350°K in the French tests in the Sahara, shows a maximum in this θ range throughout the sampling programme (fig. 6.8), but we observe a minimum in the ratio of ω^{185} to P_e within this θ range in fig. 6.9, implying that although air from which these samples were extracted was classified as stratospheric, much of it must have had tropospheric origin.

Table 6.1 Radioactivity 'c' in the air column of the tropospheric rain bearing layer, as related to the types of rain during the period March - August 1955. (after Miyake et al. 1960.)

Type of Rain	Radioactivity 'c' in the rain bearing air column (d.p.m/$m^2 \times 10^{-2}$)
Cold Frontal	58 ± 17
Warm Frontal	44 ± 14
Intermediate of above two	58 ± 17
Stagnant warm frontal	53 ± 19
Typhoon	45 ± 22

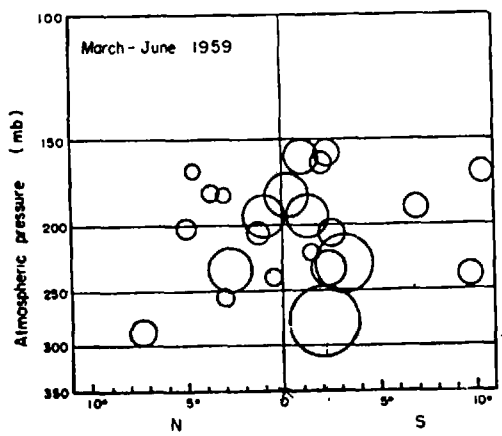

Fig. 6.6. Air activity in rain bearing layer and position of a jet stream accompanied by a trough at 500 mb.
Surface area of each circle shows relative activity.
0 indicates the position of observation.

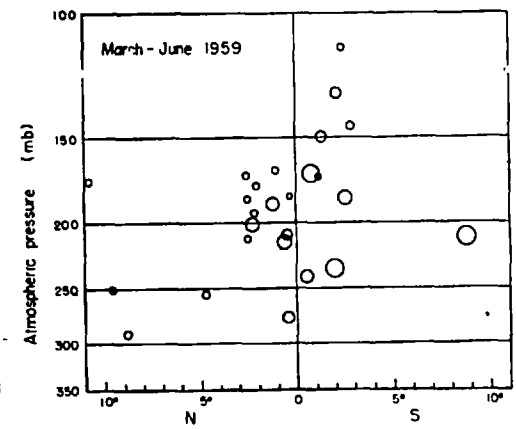

Fig. 6.7. Air activity in rain bearing layer and position of a jet stream which has no neighbouring trough at 500 mb.
Surface area of each circle shows relative activity.
0 indicates the position of observation.

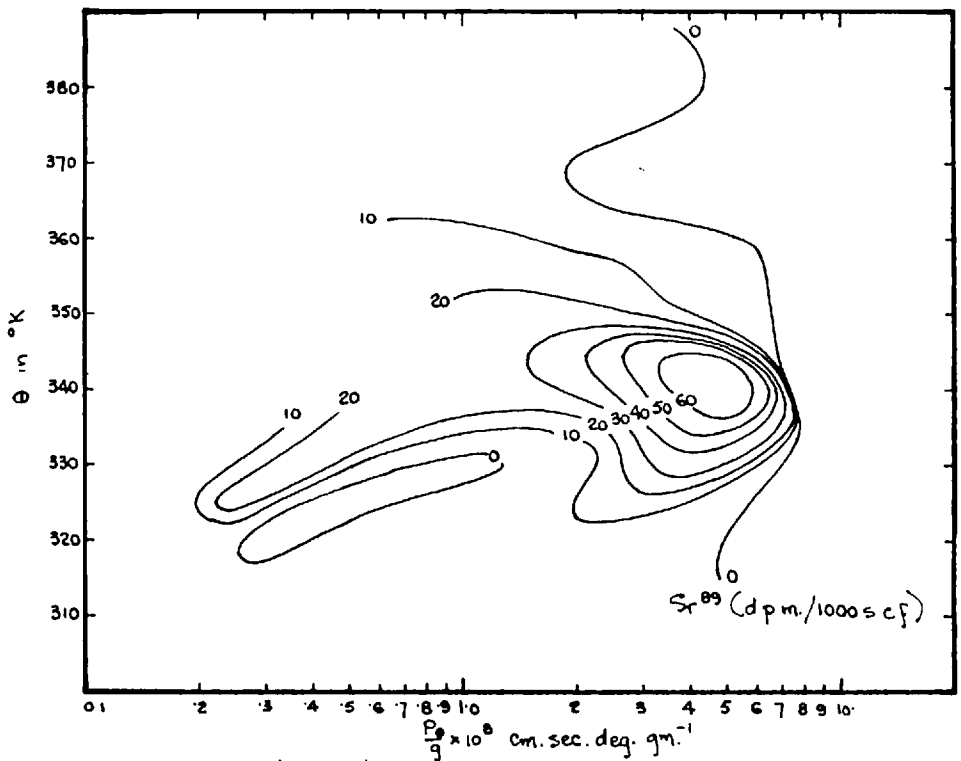

F.gure 6 8. Relation between Sr^{89} concentrations and simultaneous values of potential temperature, θ, and potential vorticity, P_θ, for observations made at various heights over a period of a month (Danielsen et al, 1962)

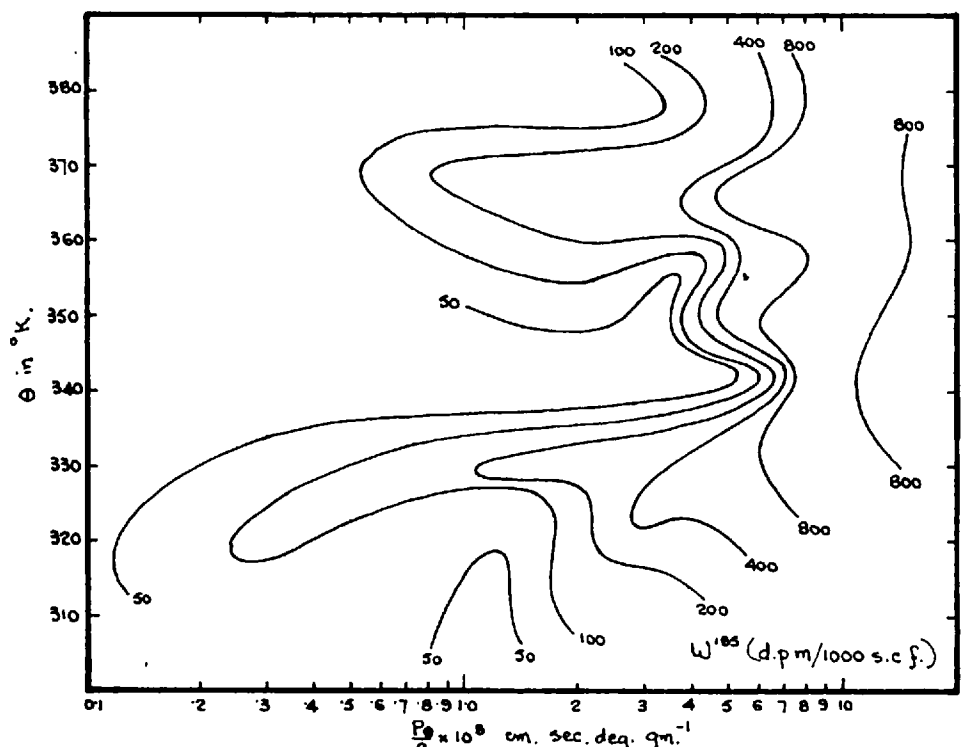

Figure 6.9. Relation between W^{185} concentrations and simultaneous values of potential temperature, θ, and potential vorticity, P_θ, for observations made at various heights over a period of a month, over the U S A. (Danielsen et al, 1962).

The isopleths of Sr^{90} activity in figs. 6.10 and 6.11, drawn consistent with the values plotted over the regions sampled in flight paths normal to the cross sections as indicated by the heavy bars, show a tendency for air of stratospheric origin to intrude into the troposphere in the region below the jet on some occasions.

6.4 Case Studies and Analyses of Particle Trajectories

Case studies require an accurate four dimensional description of the atmosphere in order that individual parcels may be followed through successive stages of their history and related to the persistent features in analysis, viz. fronts, tropopauses and jet streams.

The case studies of Reed and Sanders (1953), and Reed (1955), investigating the thermal structure of particular cyclones in the upper troposphere and lower stratosphere at successive stages of development, showed that a pre-existing frontal zone was not a prerequisite for cyclogenesis. In fact, frontogenesis and cyclogenesis took place simultaneously associated with large horizontal gradients of vertical velocity which tilted the isentropic surfaces in the vertical.

Reed (1955), Danielsen (1959), Staley (1960), and Danielsen et al (1962), showed cases of mass transfer from stratosphere to troposphere within the stable layer below the jet, tracing specific air parcels by trajectories based on conservation of potential temperature and potential vorticity over 12 hour intervals. Staley (1960), moreover, noted the existence of exceptionally dry air as measured by standard humidity elements

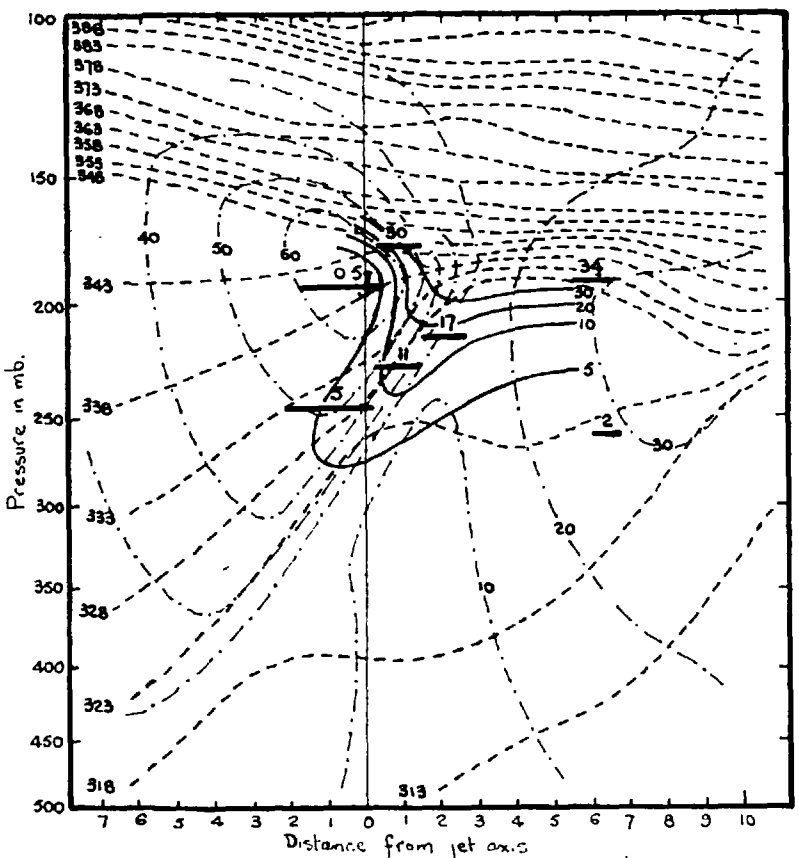

Figure 6 10. Transverse section, with respect to the jet axis, of Sr^{90} concentration in d.p.m./1000 s.c.f. (continuous lines), potential temperature in °K. (dashed lines), and isotachs in knots (dash-dot lines). Heavy dashes represent sampling traverses. Unit distance ~ 60 nautical miles. (Danielsen et al, 1962)

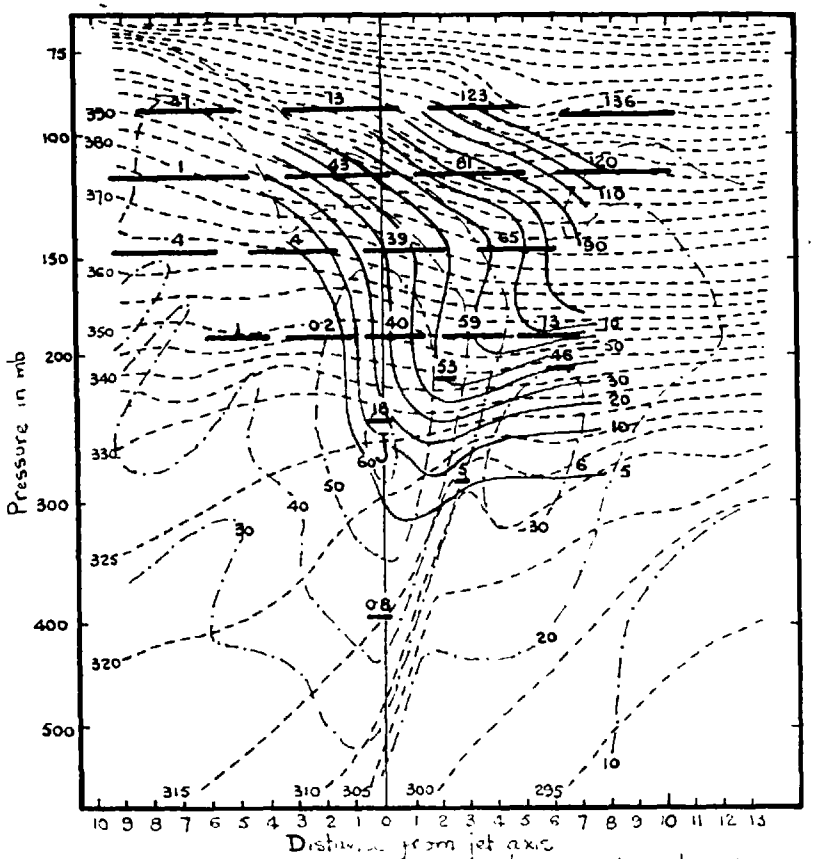

Figure 6 11 Transverse section, with respect to the jet axis, of Sr^{90} concentration in d.p.m./1000 s.c.f. (continuous lines), potential temperature in °K (dashed lines), and wind component in knots (dash-dot lines). Heavy dashes represent sampling traverses. Unit distance ~ 60 nautical miles. (after Danielsen et al, 1962)

in routine radiosonde ascents, at the final point of those trajectories suggesting subsidence from the lower polar stratosphere.

Staley (1962), interpreted vertical profiles of β-ray activity, made from aircraft observations on days when a dry baroclinic zone either existed or was anticipated within the troposphere, in terms of transfer. Where maxima in the β-ray activity profiles occurred, they were roughly equivalent in height to the stable layer, but, as shown in Table 6.2, maxima were only noted on about half the cases, suggesting that the existence of an upper tropospheric frontal zone was not a sufficient condition for subsidence to take place from stratosphere to troposphere. Isentropic trajectories were constructed, on those days when observations were suitable, to verify the origin of air at the edges and the middle of the baroclinic zone. The results in Table 6.3 show that in each case of observed high activity in the frontal zone, at least part of the air in the stable layer was of stratospheric origin, whereas in cases showing no activity maximum the air was found to originate within the troposphere.

6.5 Summary

There is considerable evidence of adiabatic transport from the lower polar stratosphere into the troposphere down the frontal zone below the jet stream and this appears to be the only region of rapid concentrated intrusions.

Table 6 2. The association between the presence of a significant maximum in the vertical profiles of β-ray activity over the U.S., sampled by aircraft, and of dry layers of above average stability in the troposphere. (after Staley, 1962.)

Date	Sampled Levels in 10^3 ft	Significant Max^m in β-Activity	Dry, Stable Layers in sampled height range	Height of Max^m Activity	Wind directions in sampled height range
7 Feb. '61	9, 11, 13	No	None	–	W, W.N.W,
8 Feb. '61	8, 10, 11, 12, 14, 16	No	Several thin layers.	–	W.S.W., W.N.W.,
9 Feb '61	9, 10, 11, 12, 14, 16	No	None	–	N W, N N.W,
20 Feb. '61	10, 13, 15, 16, 17, 20	No	None	–	N W, N E,
24 Feb. '61	7·5, 11, 12, 16	No	dry inversion 6-8 kft.	–	N, E N.E,
8 Apr '61	9, 14, 17, 20	No	dry inversion 11-13 kft.	–	W N.W, N N W.,
6 Feb. '61	9, 11, 13, 15	Yes	dry inversion 11-13 kft	13 kft.	N, N E,
17 Feb '61	11, 15, 17, 18, 20	Yes	dry, above average stability	15 kft.	W.S W, N.W.
27 Feb. '61	6, 7·5, 9, 12, 14	Yes	dry inversion 7-9 kft	7·5 kft.	S W., N.W.
3 Mar '61	13, 15, 17, 19	Yes	dry – no stable layers	17 kft.	W.S.W.
16 Mar. 61	18, 21, 24, 27	Yes	dry above 17 kft, few stable layers	18 kft.	N.W.
30 Mar. 61	7, 15, 18, 20, 22, 24	Yes	thin dry inversion near 11 kft.	18 kft.	N W.
2 Apr '60	8, 10, 11, 12, 14, 16	Yes	dry inversion 11-12 kft.	10-12 kft.	N N W., N N E.

Table. 6 3. Source regions of air parcels in the stable layer as inferred from β-activity profiles and as determined by the technique of isentropic trajectories. (after Staley, 1962.)

Date	θ-Trajectory Traced.	Apparent Recent Source of Air from β-Activity	Apparent Recent Source of Sampled Air from Isentropic Trajectories.
20 Feb. '61	311	No Max^m. – Troposphere	Troposphere – west of Port Hardy in 48 hours.
	303	No Max^m. – Troposphere	Troposphere – off coast of Washington in 48 hours.
	299	No Max^m – Troposphere	Troposphere – southwest coast of Washington in 36 hours
8 Apr. '61	317	No Max^m. – Troposphere	Troposphere – vicinity of Port Hardy & Tattoosh in 24 hrs
	311	No Max^m – Troposphere	Troposphere – vicinity of Port Hardy & Tattoosh in 24 hrs.
	301	No Max^m – Troposphere	Troposphere – between Spokane & Great Falls in 24 hours.
6 Feb. '61	305	No Max^m. – Troposphere	Troposphere – east of Prince George in 48 hours.
	301	Max^m. – Stratosphere	Troposphere – eastern and southeastern Wyoming in 48 hrs.
	295	No Max^m. – Troposphere	Troposphere – eastern and southeastern Wyoming in 48 hours.
30 Mar. 61	313	Max^m. – Stratosphere	Vicinity of Tropopause, west of Annette Island in 48 hrs.
	305	No Max^m. – Troposphere	Troposphere, northeast of Edmunton in 48 hrs.
	301	No Max^m. – Troposphere	Troposphere. north of Great Falls in 48 hrs.
2 Apr. '61	315	No Max^m. – Troposphere	Troposphere – southwest of Annette Island in 24 hours
	307	Max^m. – Stratosphere	Stratosphere – between Prince George & Fort Nelson in 24 hrs.
	303	Max^m. – Stratosphere	Stratosphere. between Annette Island & Port Hardy in 36 hrs.

Such intrusions are not apparent on mean distributions and appear on rather less than a half of the individual sections suggesting such transport only takes place under limiting synoptic conditions.

There is no direct evidence of transport in the opposite sense in the region of the front on any occasions, though this would be less easily detectable appearing as a relatively moist ozone poor region over an ill-defined region to the left of and about level with the jet axis. The excessively high humidity values observed in the winter sampling, by M.R.F., of humidity in the lower stratosphere in high latitudes, from Leuchars, (Roach personal communication), may be evidence of this effect.

The evidence of transverse circulations from analyses of velocity components in Chapter 3, and from Tucker's analysis of humidity in section 6.3.1, suggest the circulation is direct in entrance zones and indirect in exit, thus the dry ozone rich intrusions are anticipated in entrance zones and possibly a mass transport from troposphere to stratosphere via the frontal zone in exit zones.

CHAPTER 7 New Analysis of U.K. Data

7.1 General

This chapter will follow a similar pattern to that of the preceeding two chapters, a climatological study of the temporal variations of selected tracers over the U.K., the relation between such tracers and the flowfield, then an investigation of the cycle of transfer associated with the jet stream by means of representative cross sections constructed by incorporating all available consistent data.

7.2 Data - Consistency and Preliminary Analysis

The data available for analysis were listed in Chapter 4, and we shall first examine them for consistency.

From Table 7.1 we see that on less than ten days out of the entire sample do any two types of data sampling take place simultaneously. Furthermore, the different types of sampling take place at locations separated, at times, by over a hundred kilometers.

The nature of the various sampling techniques results in highly variable data smoothing. The airborne radioactivity measurements over the U.K., required flight passes of 1 - 4 hours, in order to collect a measurable sample, depending on the sampling level. Horizontal smoothing resulting from this sampling procedure was consequently over a minimum distance of 100 km. and frequently much more. These flight paths were oriented randomly with respect to the macro-features of tropospheric structure. Since sampling involved such prolonged flights, it was seldom practicable to sample more than two levels on any day. The lack of vertical

Table 7.1.

Tracer observations made over Great Britain during the years 1957-1960

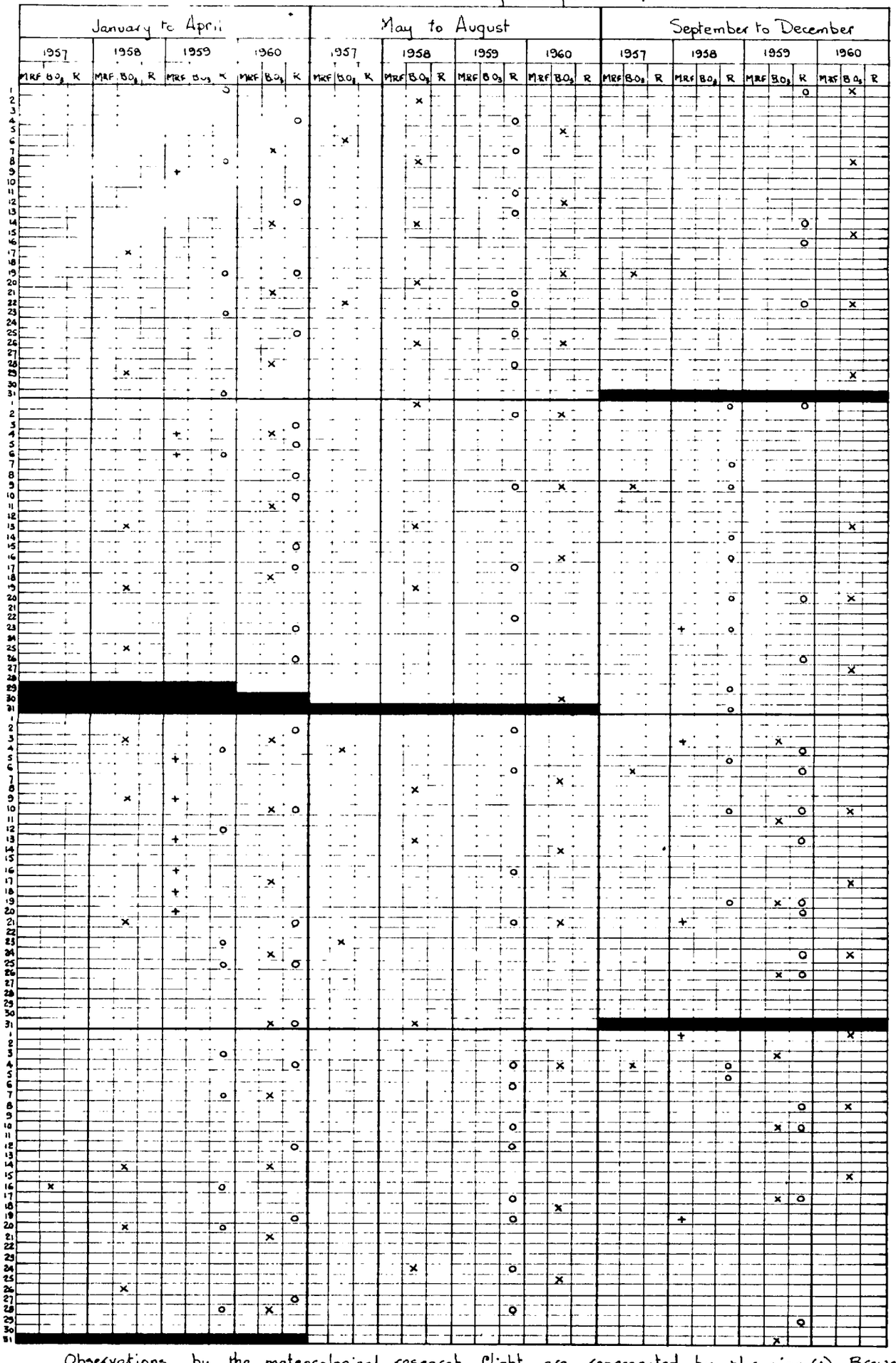

Observations by the meteorological research flight are represented by plus sign (+), Brewer ozone profiles by cross (x) and radioactive isotope sampling in air by circles (o).

consistency in sampling is illustrated by Table 7.2.

These imperfections in sampling led us to concentrate initially on ozone and temperature leaving appeal to radio-debris to special cases.

The original data were converted to ozone mixing ratio, χ_o, and potential temperature, θ. Temperatures were extracted from Daily Weather Reports and the potential temperatures read off T-ϕ-grams directly. The Brewer ozone sonde (bubbler-type) data, over Liverpool, give concentration ρ_o in units of cm.S.T.P. km^{-1}, so that mixing ratio, $\chi_o = \rho_o . 5{\cdot}86 \frac{T}{P} . 10^{-5}$ and the ozone in a finite vertical column is $\int_{z_1}^{z_2} \rho_o \, dz$ or $\frac{1}{g}\int_{p_2}^{p_1} \chi_o \, dp$. The choice of the most suitable method of evaluating the total ozone in a finite column is dependent on the section of the profile over which it is desired to carry out the integration (Appendix 2).

Observations of total ozone, made with Dobson spectrophotometers, were also available for Oxford and Eskdalemuir. While we have shown in section 5.3 that the vertical profile for a given total ozone for different locations may be extremely variable, there is some evidence to the contrary (Mateer and Godson, 1960), for specific locations. The correlation coefficient between total ozone at Edmonton and Moosanee, and the ozone in the 12 - 18 km. layer from Umkehr profiles was + 0.97. Mateer and Godson (1960), noted a small apparent negative correlation (- 0.36) with the ozone between 0 - 12 km., which may be considered as the tropospheric layer, so it is reasonable to investigate the possibility

Table 7.2

Radioactive isotope sampling over Great Britain analysed in terms of vertical consistency.

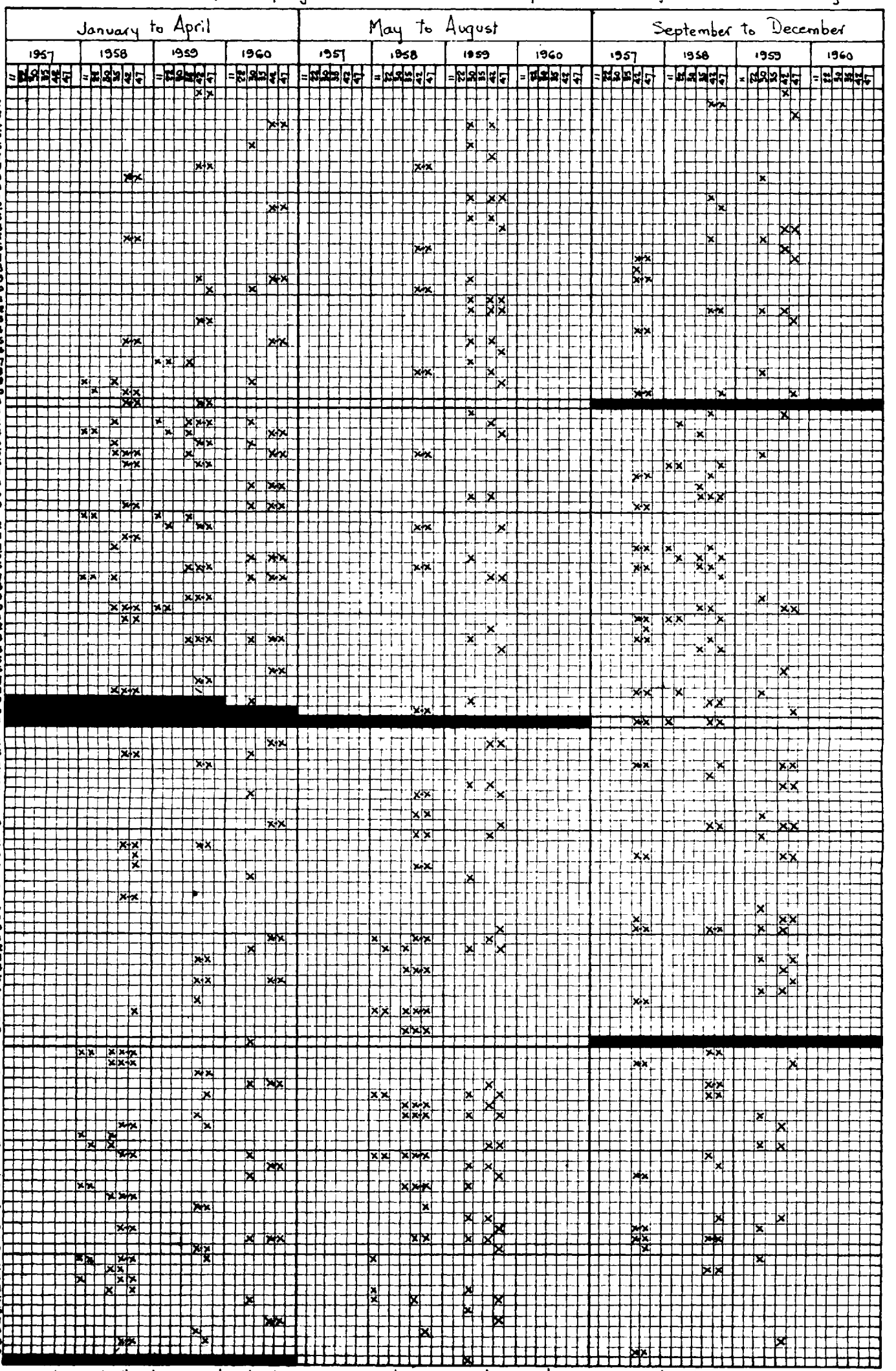

The numbers to the left of the table represent the day of the month and months follow a sequence from top left to bottom right of the table. The crosses show levels sampled on any given day and are connected by a dash when sampling was carried out at two levels without changing the filter.

of increasing the information on profiles from the larger sample of total ozone observations.

In addition to the data on tracers, information on the synoptic situation was extracted and tabulated on each day on which an ascent was made. Cross sections of potential temperature and wind speed were drawn in a plane through Liverpool orthogonal to the nearest jet axis.

The following parameters were then extracted:

1. The tropopause pressure at Liverpool (using the criteria stated in section 3.2).
2. The pressure at the level of the jet axis.
3. The distance from Liverpool to the jet axis, positive values to the right of the axis looking downstream.
4. The location of Liverpool with respect to jet entrance (confluence) jet maximum and jet exit (difluence) zones.
5. The location of Liverpool with respect to long wave troughs and ridges.

These data were extracted using 500 mb., 300 mb., and 200 mb., contour analyses and tropopause height charts of M.O., which were re-analysed where necessary to maintain temporal continuity and spatial consistency, and the above cross sections.

7.3 Investigation into the Relationship Between Total Ozone Amounts and Vertical Distributions over Liverpool.

While observations of the total ozone amount at Oxford (53°N) and Eskdalemuir (55°30'N), were made over the period of this study many of the values at Eskdalemuir were missing on days of the Liverpool (53°20'N) ozone sonde ascents, so for consistency the

Oxford values were used.

The profiles were defined for this study by integrating the ozone over the following layers:

1. The surface to the tropopause , $[O]_{P_o}^{P_T}$.
2. The 50 mb. and 100 mb. layers directly above the tropopause $[O]_{P_T}^{P_T-50}$ and $[O]_{P_T}^{P_T-100}$ respectively.
3. The surface to the 50 mb. level , $[O]_{P_o}^{50}$.
4. The 50 mb. level to the top of the atmosphere, $[O]_{50}^{\circ}$, was obtained by subtracting 3. from the total ozone amount for Oxford.

The techniques used are presented in Appendix 2.

Inspection of the time series in fig. 7.1, suggests the total ozone is most strongly positively correlated with the tropopause pressure and with the ozone in the column below 50 mb. as other workers have found. The correlation with the ozone above 50 mb. is negative, consistent with, though less than, Mateer and Godson (1960) values for Moosanee and Edmonton of - 0.79 and - 0.76 with ozone in the 24 - 36 km., and 36 - 54 km., layers respectively. The tropospheric ozone shows no simple relation with the other integrated ozone amounts or with the tropopause pressure.

These time series, together with scatter diagrams, not shown, suggest the correlation could be improved by removing the seasonal variations. Three monthly running mean values of the various parameters were plotted, and a smoothed curve drawn through them in fig. 7.1. The deviations of individual values were then abstracted and plotted on scatter diagrams in fig. 7.2.

We observe that while a positive correlation exists between

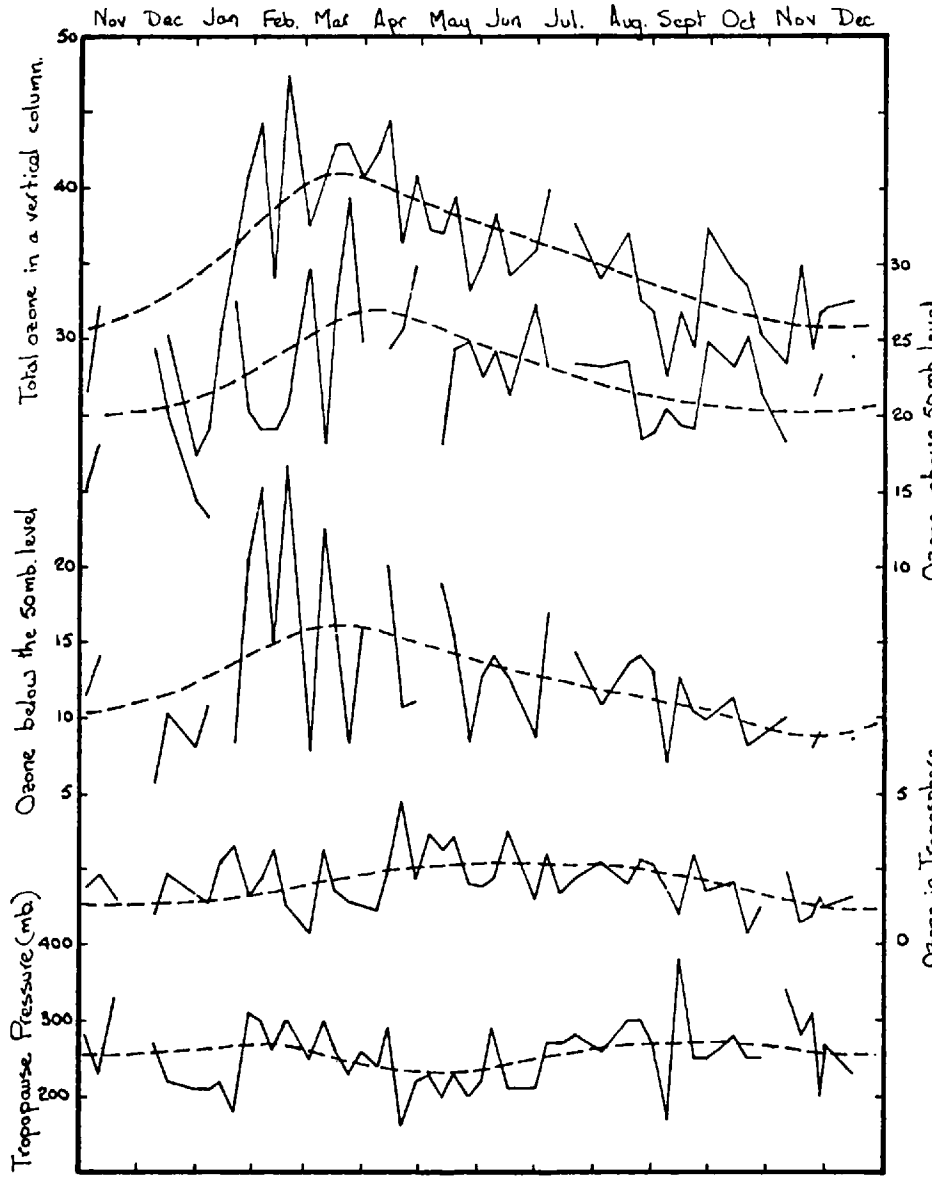

Figure. 7.1. Time series of integrated ozone in layers of arbitrarily defined depth (units $\cdot 10^2$ cm. S.T.P), and corresponding tropopause pressures. The continuous dashed lines represent seasonal mean values.

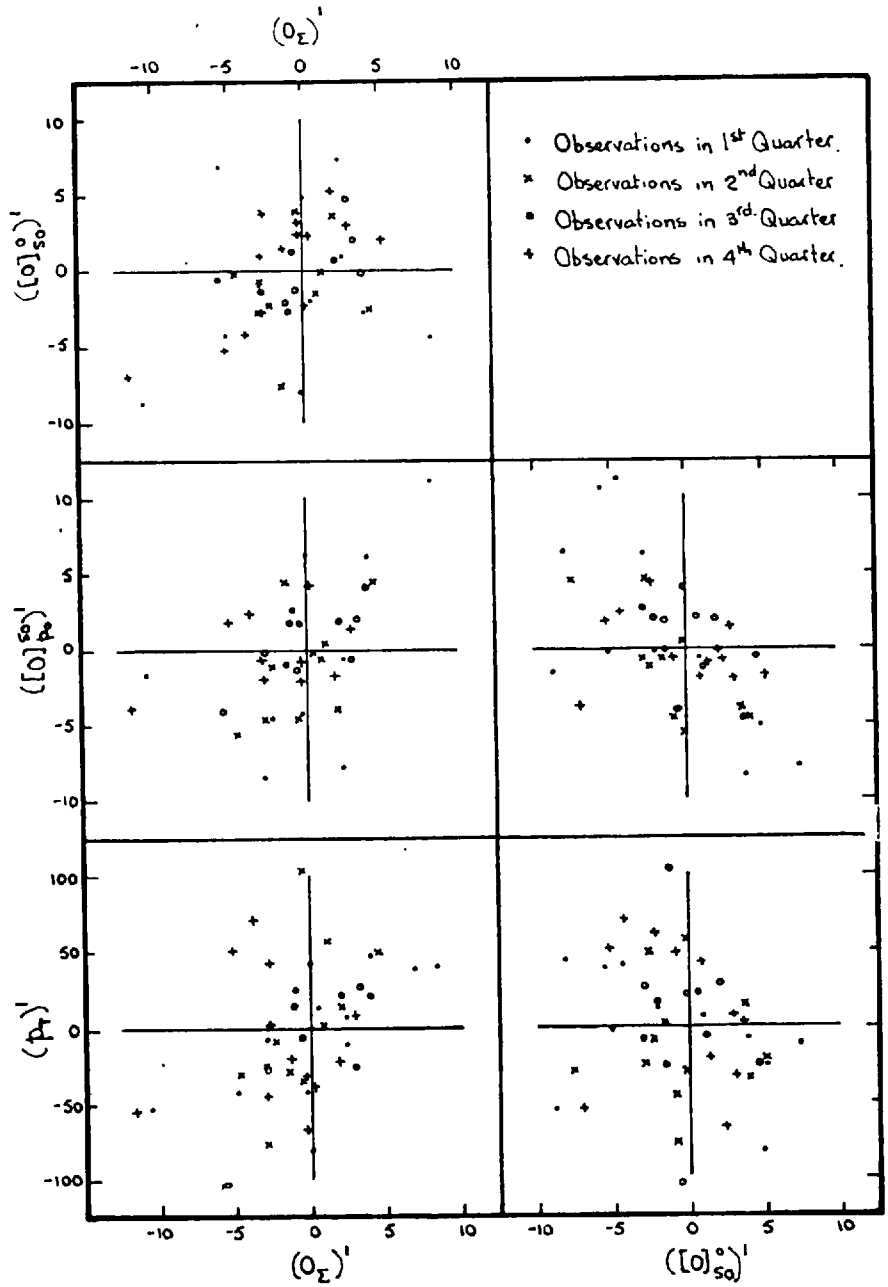

Figure 7.2. Scatter diagrams indicating correlations between deviations from their respective three monthly mean values, of total ozone, O_Z, ozone above and below the somb. level ($[O]^{\circ}_{so}$ and $[O]^{so}_{p_o}$ respectively) in cm. atm. S.T.P. 10, and tropopause pressure in mb..

the deviations from seasonal mean values of total ozone, ozone below 50 mb, and tropopause pressure, the regression factors vary with season, and the correlation is not sufficiently high to infer one variable from another. In any case in investigating the problem of transtropopause exchange the tropospheric ozone is an important factor and it bears no obvious relation to the total ozone.

7.4 Climatological Analysis in Relation to Transfer Within the Lower Stratosphere

7.4.1 Total Ozone

Observations of total ozone amount, O_Σ, for Oxford, measured by Dobson spectrophotometer, are presented in a time series, together with simultaneous observations of potential temperature at several levels for Liverpool throughout 1960, in fig. 7.3

We observe in fig. 7.3, that from March to November, of the observed fluctuations of O_Σ and θ those of short period (few days) show greatest correlation. The magnitude of the temperature fluctuations decreases with pressure suggesting the origin of the systems to be the troposphere.

In winter and spring the highest correlation appears to be with systems of 2 - 3 weeks period whose amplitude increases with decreasing pressure suggesting dominant influence of systems of stratospheric origin.

These time series, together with the interpretation of correlation coefficients of O_Σ and features of the temperature and wind fields in section 5.5 suggest that the ozone changes in the lower stratosphere may or may not be associated with tropospheric disturbances.

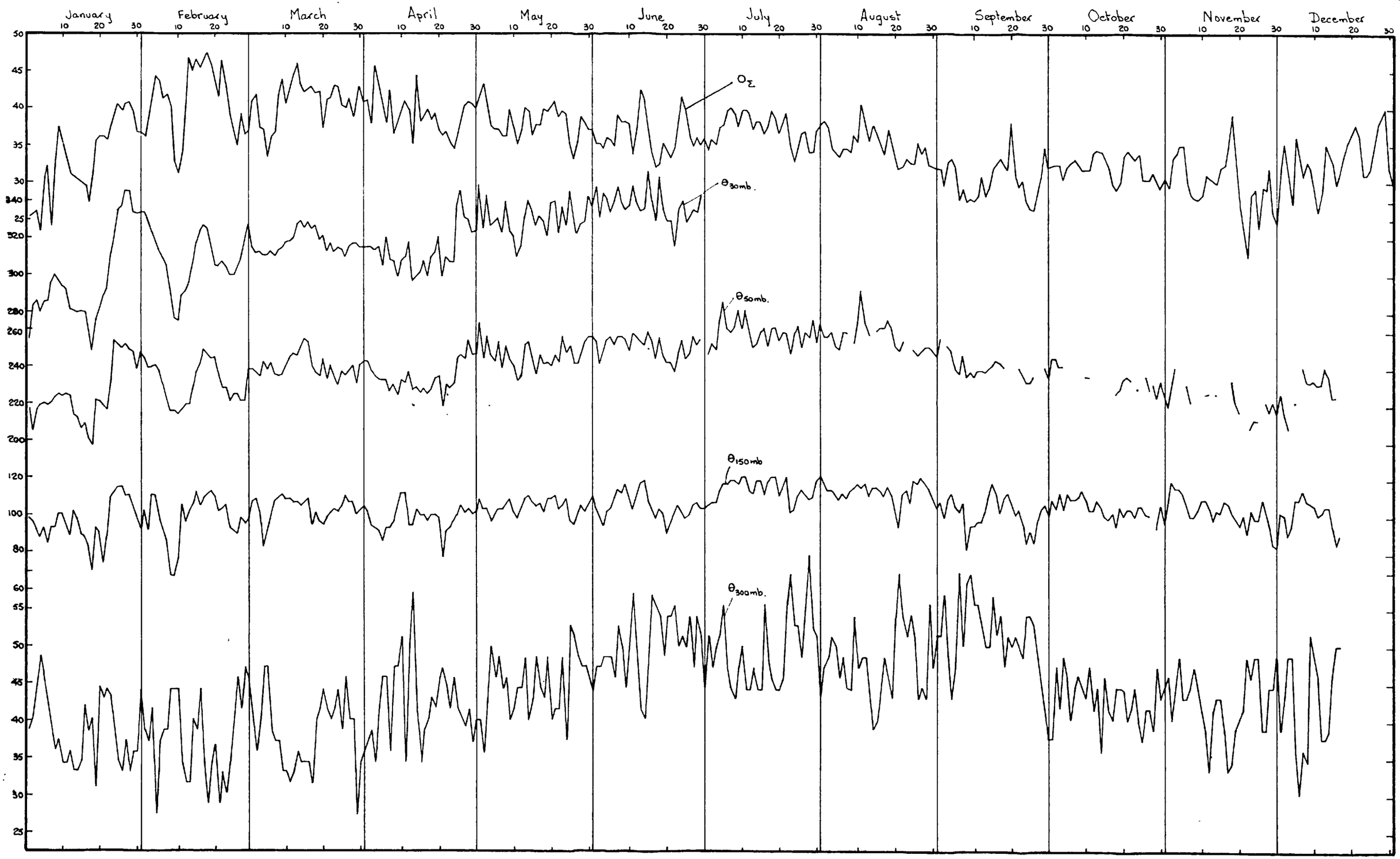

Figure 7.3. Time series of total ozone (cm atm S.T.P 10^{-2}) and potential temperature (°K) at standard levels above Liverpool during 1960. Ozone values are obtained taking the average of simultaneous observations from Oxford and Eskdalemuir.

7.4.2 Ozone Mixing Ratio and Potential Temperature at Selected Levels

Observations of ozone mixing ratio, χ_o, and potential temperature, θ, were extracted from the original profiles for the standard levels - 50, 70, 100, 150, 200, 250 and 300 mb. Time series of both individual values and of three monthly mean values are shown in fig. 7.4. Many ascents failed to reach the higher levels so two sets of mean values were computed for test of consistency, the first including only values from the ascents reaching the 50 mb. level and a larger sample reaching 150 mb. The mean values computed from the two different samples, while exhibiting the same general features, showed differences, particularly in winter and spring, amounting to 30-60% of the amplitude of the seasonal variation at the levels considered. This lack of consistency illustrates the danger in evaluating a seasonal mean value from such a restricted sample.

Considering only the consistent data of ascents reaching 50 mb, we note in fig. 7.4 a tendency for the maximum observed in March and April at 70 mb (-18 km) to become less obvious as we proceed downwards, while another maximum in June/July becomes more pronounced close to the tropopause level, and indeed dominates at the 300 mb level. Since two distinct maxima are present at 150 and 300 mb, the retardation in occurrence of the dominant maximum at higher pressure does not appear to be a result of a downward propagation of the same maximum. Dütsch (1962), computed monthly mean ozone concentrations for Arosa from an extensive series of Umkehr ozone profiles for

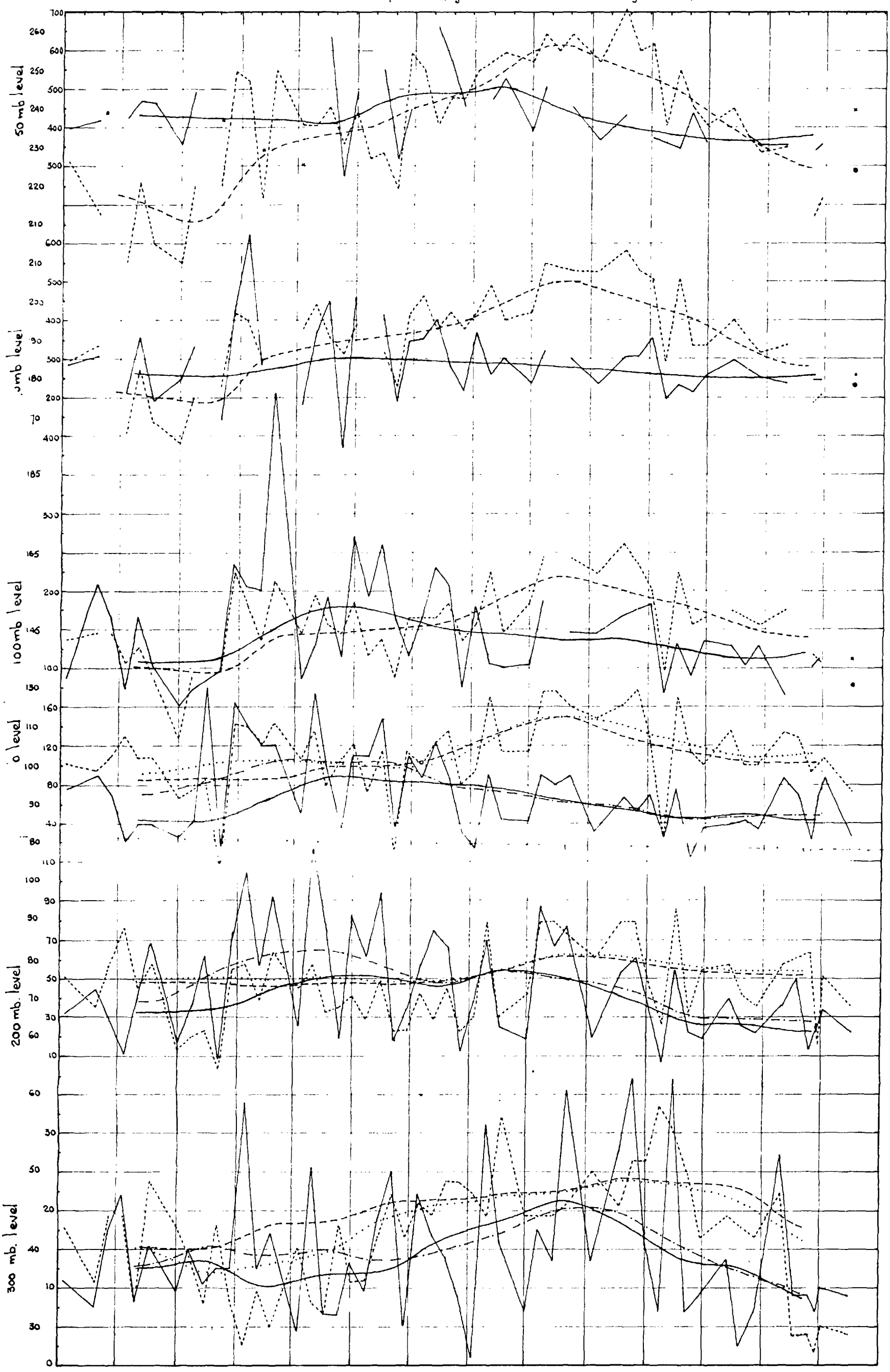

Figure 7.4. Time series of ozone mixing ratio, x_o, and potential temperature, θ, at standard pressure levels are shown for Liverpool, with breaks in the series at higher levels indicating malfunction of the sampling device at these levels. Three monthly running means of ozone, $\bar{x}_o$, and potential temperature, $\bar{\theta}$, are shown as smooth curves, the various line types representing the following:

------- θ, ——— x_o, (units θ - °C, x_o - $\mu g\ g^{-1}$)
- - - - $\bar{\theta}$, ——— $\bar{x}_o$, evaluated from centres reaching 50 mb.
..... $\bar{\theta}$, -·-·- $\bar{x}_o$, evaluated from ascents reaching 150 mb.

the 6, 12.5, 17, 21.5 km, and higher levels. His seasonal curves in the lower stratosphere for 21.5 km (45 mb), 17 km (70 mb), and 12.5 km (180 mb), indicate the maximum at the same time as observed above, but the tropospheric maximum (6 km) occurred in mid May.

In Chapters 3 and 6 we presented evidence that the dominant transfer through the jet is probably linked to the jet axis, so the delay in occurrence of the tropospheric ozone maximum at Oxford (56°N) to that at Arosa (47°N) may be a result of the jet axis being later in reaching the more northerly station.

We now infer the origin of disturbances in the lower stratosphere from variations in ozone mixing ratio, χ_o, at standard levels, as represented most simply by the range, R_o, i.e., the difference between the highest and lowest values occurring during the period.

The variance (or range R_o) of ozone over three monthly periods may be expected to be a function of the mean mixing ratio gradient, $\frac{\partial \bar{\chi}_o}{\partial p}$, ($\frac{\partial \chi_o}{\partial p}$ being evaluated over the intervals 50 - 70, 70 - 100, 100 - 150, 150 - 200, and 200 - 250 mb, for each profile) of the horizontal gradient, $\nabla_h \bar{\chi}_o$, not available, and the wave disturbance activity at that level. The normalised variance, represented by the ratio $R_o / \frac{\partial \bar{\chi}_o}{\partial p}$, will be a function of the activity of fluctuations and fig. 7.5 shows the seasonal variation of this function throughout the lower stratosphere.

The lack of correspondence between the times of maximum activity at 50 and 70 mb, and closer to the tropopause suggests

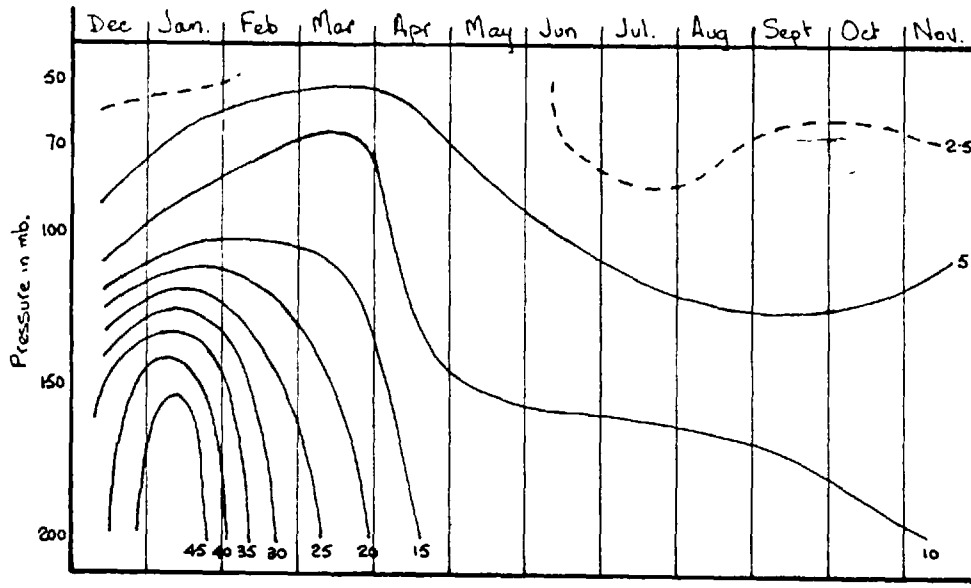

Figure 7.5. Time section of normalised variance of ozone mixing ratio $R_o/\overline{\frac{\partial z_o}{\partial p}}$.

the origins of the fluctuations to be different, though it is not possible to deduce from fig. 7.5 whether the high values in March are or are not a result of tropospheric disturbances.

The variation of mean ozone mixing ratio, $\overline{\chi}_o$, and normalized ozone variance, $R_o/\frac{\partial \overline{\chi}_o}{\partial p}$, throughout 1960, are shown in fig. 7.6. We observe a delay of one or two months between the period of maximum variance, in fig. 7.6, and the maximum ozone at all levels, which suggests the eddy transfer is only partly responsible for the spring build-up over Liverpool. The secondary maximum ozone in June - July, which increases with proximity to the tropopause, is not associated with any wave activity maximum, implying a meridional circulation to be its cause. The circulation model deduced in Chapter 8 will be shown to provide a plausible explanation of this maximum.

We conclude from fig. 7.6 that the mean ozone mixing ratio, $(\overline{\chi}_o)_p$, at a given level, p, is the net effect of seasonal variation of the transfer mechanisms, resulting from both variation of the different jet complexes with which they are probably linked, and seasonal variation in their relative transfer efficiency.

Representative mean values, $\overline{\overline{\chi}}_o$, were estimated assuming a fluctuation of wave number one, drawn as a best fit through all individual, χ_o, plotted on a seasonal abscissa, so that the maximum and minimum corresponded approximately with their positions on the curves of computed unrepresentative means, $\overline{\chi}_o$, and in such a way that continuity of vertical profile was maintained. Seasonal values of $\overline{\overline{d}}_j$, (d_j is the shortest distance from Liverpool to the jet axis), were estimated from the most probable position of the jet axis in 1957 and 1958, (Crossley, 1961).

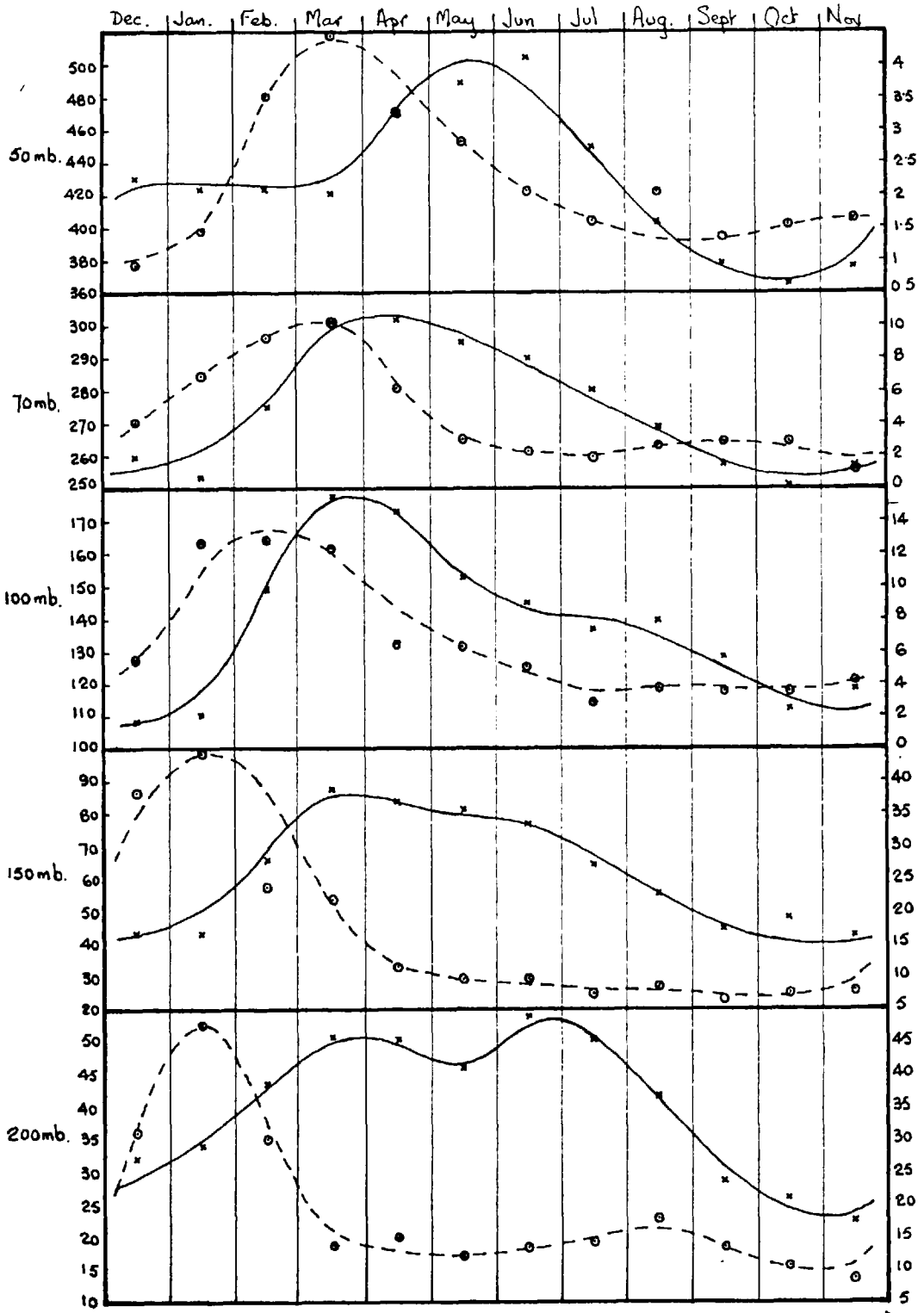

Figure 7.6. Seasonal variation of mean ozone, $\bar{x}_o$, (continuous lines), and normalised ozone variance ($R_o/\frac{\partial \bar{x}_o}{\partial p}$) dashed lines, at standard pressure levels. Monthly values of $\bar{x}_o$ are plotted as crosses and of $R_o/\frac{\partial \bar{x}_o}{\partial p}$ as encircled dots.

The corresponding deviations of potential temperature ($\bar{\bar{\theta}} - \bar{\theta}$) and tropopause pressure ($\bar{\bar{p}}_T - \bar{p}_T$) were extracted and are shown with the other deviations in fig. 7.7.

We observe a good correlation between the tropopause pressure deviation, and the potential temperature and ozone in the lower levels in the stratosphere, but the relation between the tracers and the jet axis is obscure. The lack of association between ($\bar{\bar{\chi}}_o - \bar{\chi}_o$) and ($\bar{\bar{\theta}} - \theta$) values at different levels suggests the transfers in the lower stratosphere are not the result of a single mechanism.

7.5 Climatological Analysis in Relation to Transfer Between Stratosphere and Troposphere

Ozone mixing ratios and potential temperatures analysed in this section were smoothed over 40 mb. intervals. Ozone values were smoothed by evaluating total ozone over 40 mb. layers ($\propto$ mean mixing ratio), and corresponding values of potential temperature extracted from T-ϕgrams.

Data were extracted at 40 mb. intervals from 80 to 400 mb., thus spanning the tropopause on all ascents. Time sections of individual values and three monthly running mean values, together with corresponding values of tropopause pressure, are shown in figs. 7.8 and 7.9 respectively. There is no obvious relation between the mean values in fig. 7.9, but individual values in 7.8 show negative correlations between the tropopause pressure and both tracers throughout the lower stratosphere, the correlation being greatest in each case close to the tropopause, and greater for θ than for ozone. Where a jet is present within 1000 km.

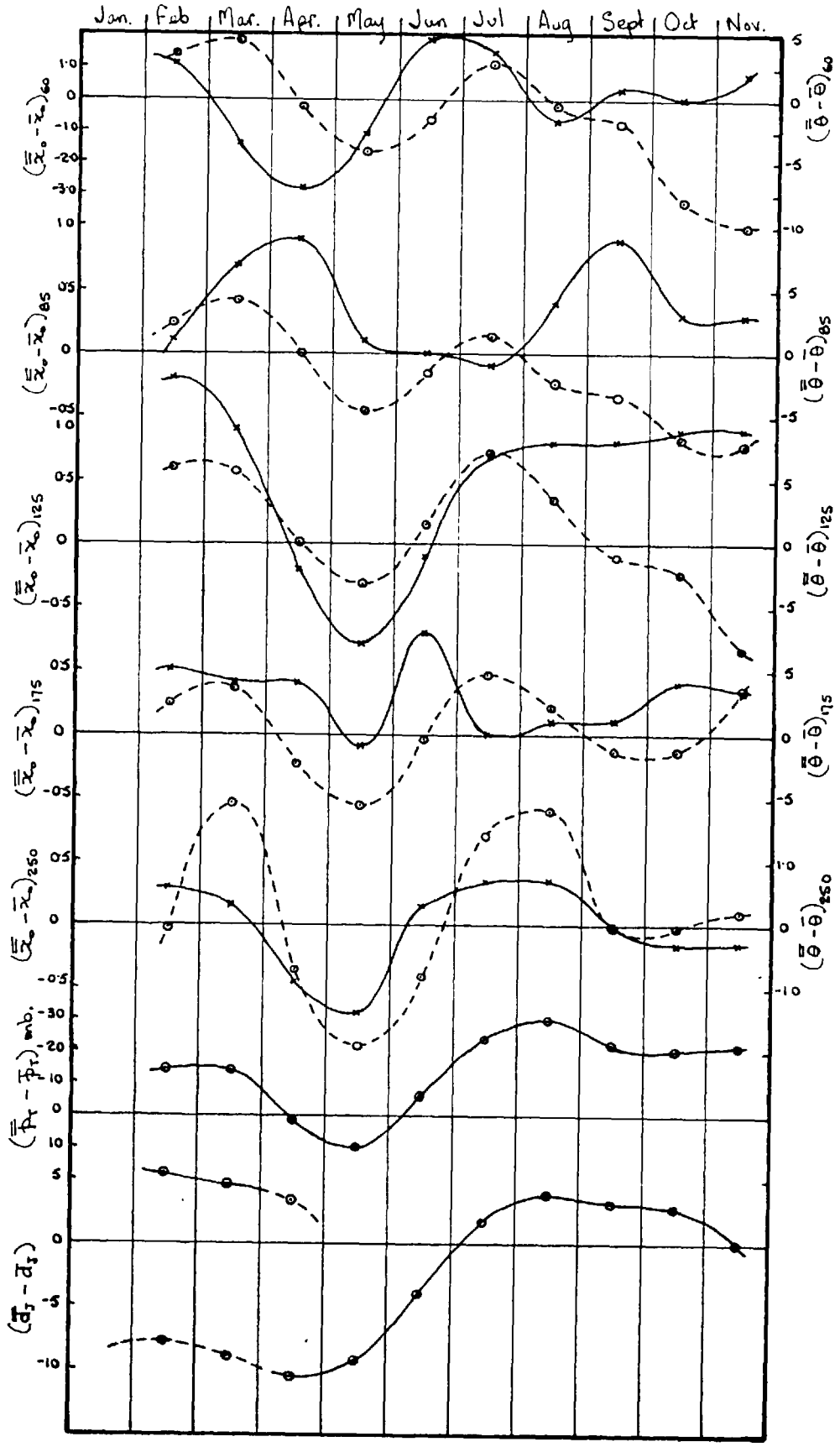

Figure 7.7. Seasonal variation in the deviations of computed mean values of various properties from estimates of their respective representative means, at levels denoted by subscripts following brackets. $(\bar{\bar{x}}_o - \bar{x}_o)$ and $(\bar{\bar{\theta}} - \bar{\theta})$ are shown as continuous and dashed lines respectively, p_T is the tropopause pressure and d_T the shortest distance from the jet axis.

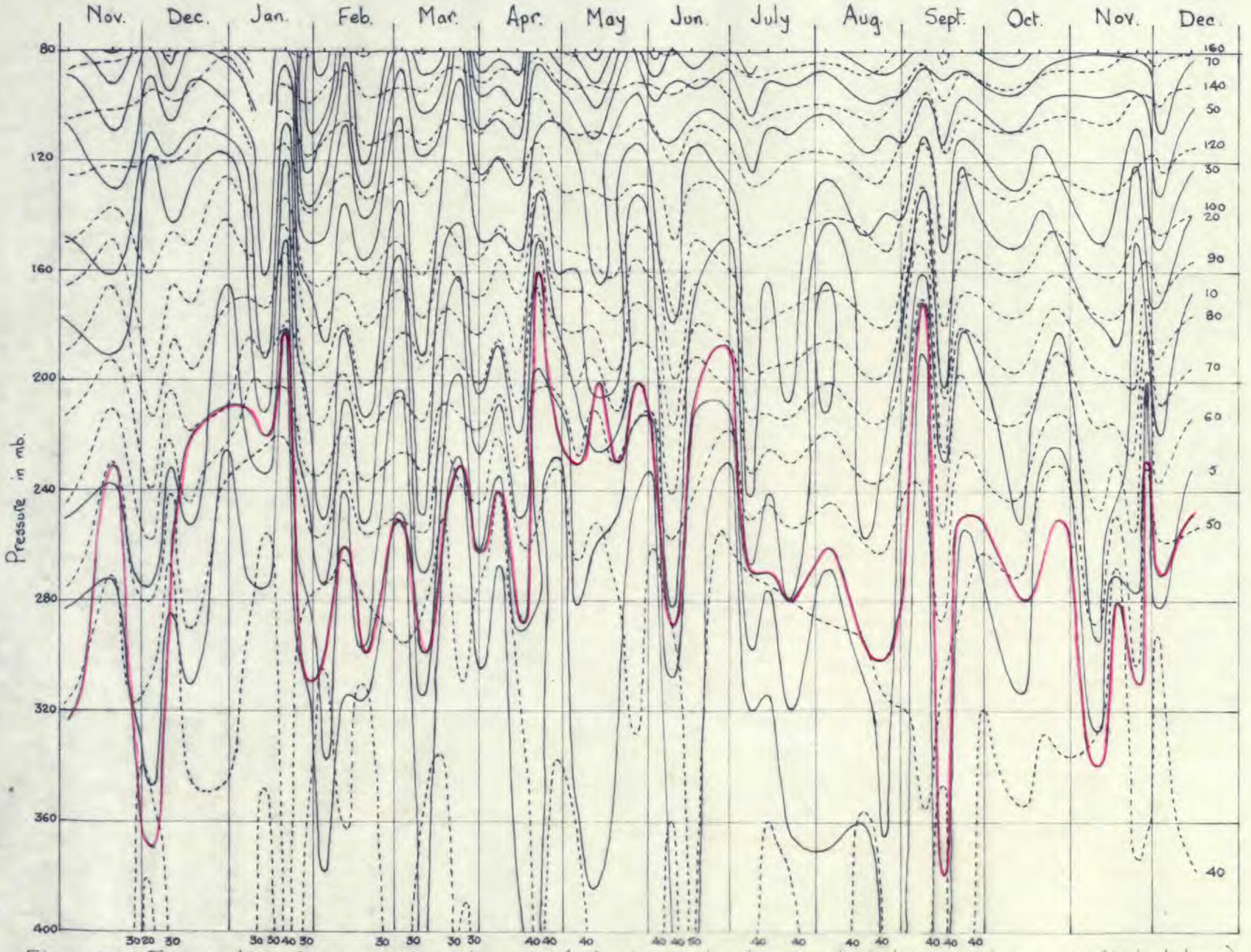

Figure 7-8. Time section of ozone mixing ratio in $\mu g/g$ (continuous lines) and potential temperature in °c (dashed lines), together with tropopause height (red line) from November 1959 to December 1960.

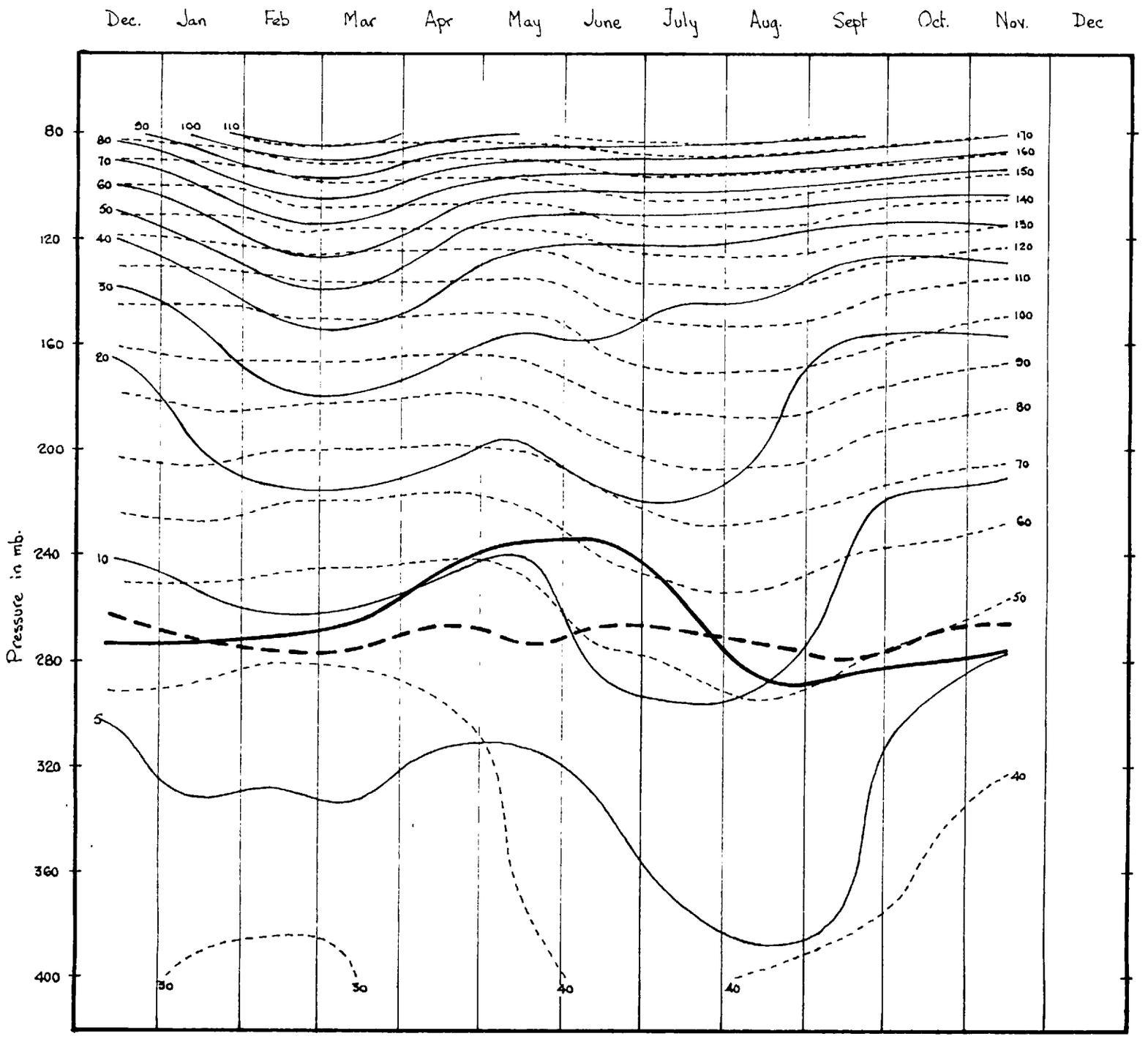

Figure 7.9. Time section of three monthly running means constructed from profiles reaching 80mb. maintaining vertical consistency. The same sample was used in calculating the mean tropopause and jet levels. The thin solid line represents mean ozone mixing ratio, the thin dashed line mean potential isotherms, the thick solid line the mean tropopause level and the thick dashed line the mean jet level. The jet does not occur at Liverpool so the jet level is not consistent with the other parameters.

of Liverpool, the height of the axis was estimated from cross sections, and the mean value (which is not, of course, consistent with the other parameters for Liverpool), is shown in fig. 7.9.

To analyse transfer through the tropopause it was decided to extract and analyse data relative to the Liverpool tropopause height, and relative to the jet axis. The ozone mixing ratio and potential temperature values were smoothed as before over 40 mb layers from 140 mb below, to 140 mb above the corresponding tropopause height and jet axis level. The values, plotted as time series in figs. 7.10 and 7.11, respectively, show a fairly good positive correlation between the deviations from their respective mean values at all levels. The variance is, however, large, and we proceed, in subsequent sections, to investigate possible causes.

7.6 A Rough Analysis of Transfer with Respect to the Jet Axis Using Ozone Integrated over Specific Layers

7.6.1 Intent

In this section we investigate transfer capacity with respect to the jet axis, by studying the mean horizontal profiles of mean ozone mixing ratio in the troposphere and in a 100 mb layer above the tropopause. The scatter of individual observations about the mean value is shown to be marginally reduced by removing the effect of seasonal variations. Indirect evidence is provided that the instrumental errors do not seriously effect the mean distributions and that the greatest changes in transfer capacity along the jet axis occur on its left side.

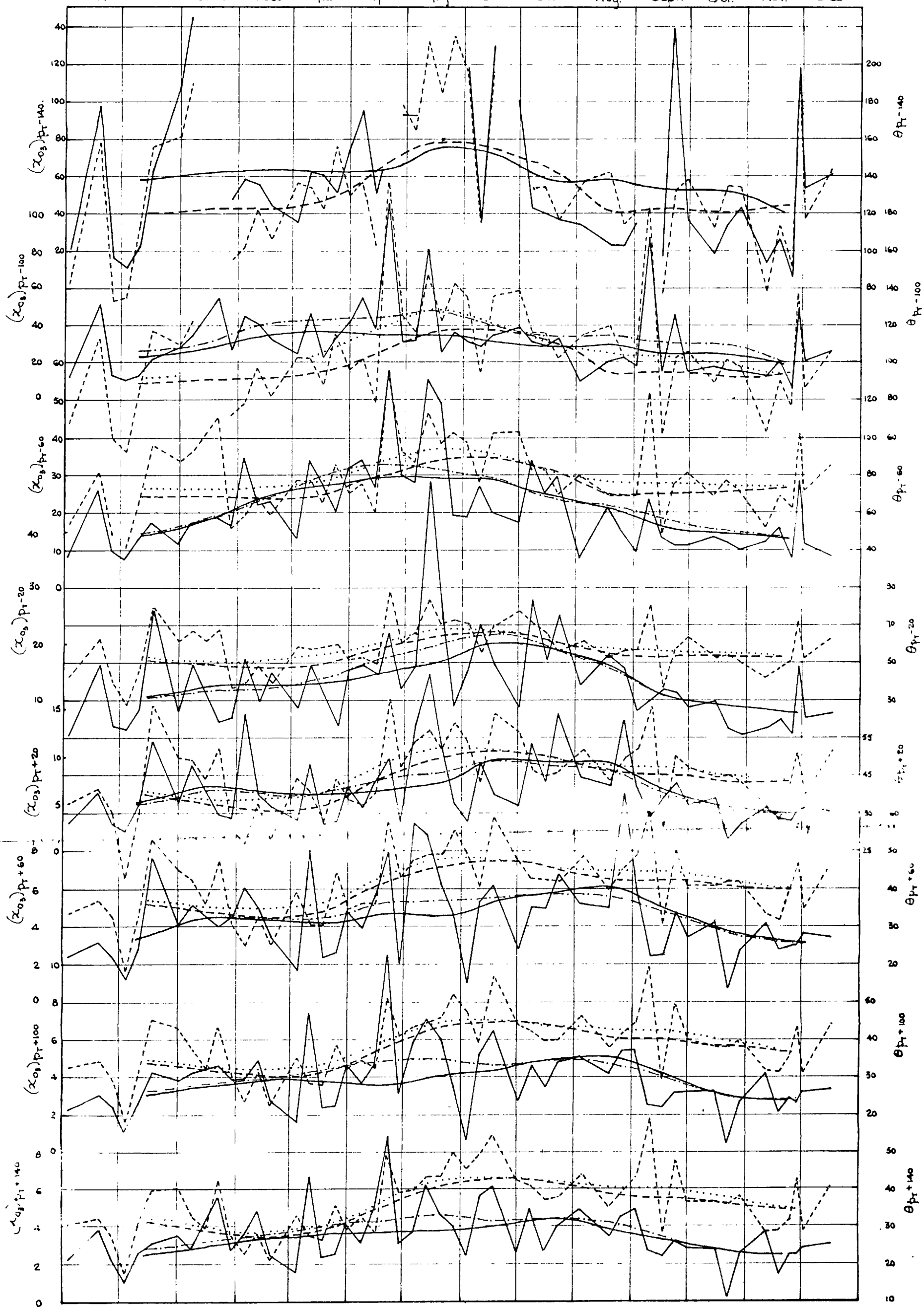

Figure 7.10. Time series of vertically smoothed ozone, x_o, and potential temperature, θ, for Liverpool and curves drawn through their respective mean values, are shown for levels differing from the tropopause by constant pressure intervals as denoted by the appropriate subscripts.

-------- θ, ——— x_o, (Units: θ - °C, x_o - $\mu g/g$)

– – – – – $\bar{\theta}$, ——— $\bar{x}_o$, computed from only profiles reaching p_T - 140 mb. level

..... $\bar{\theta}$, -·-·- $\bar{x}_o$, computed from all available profiles.

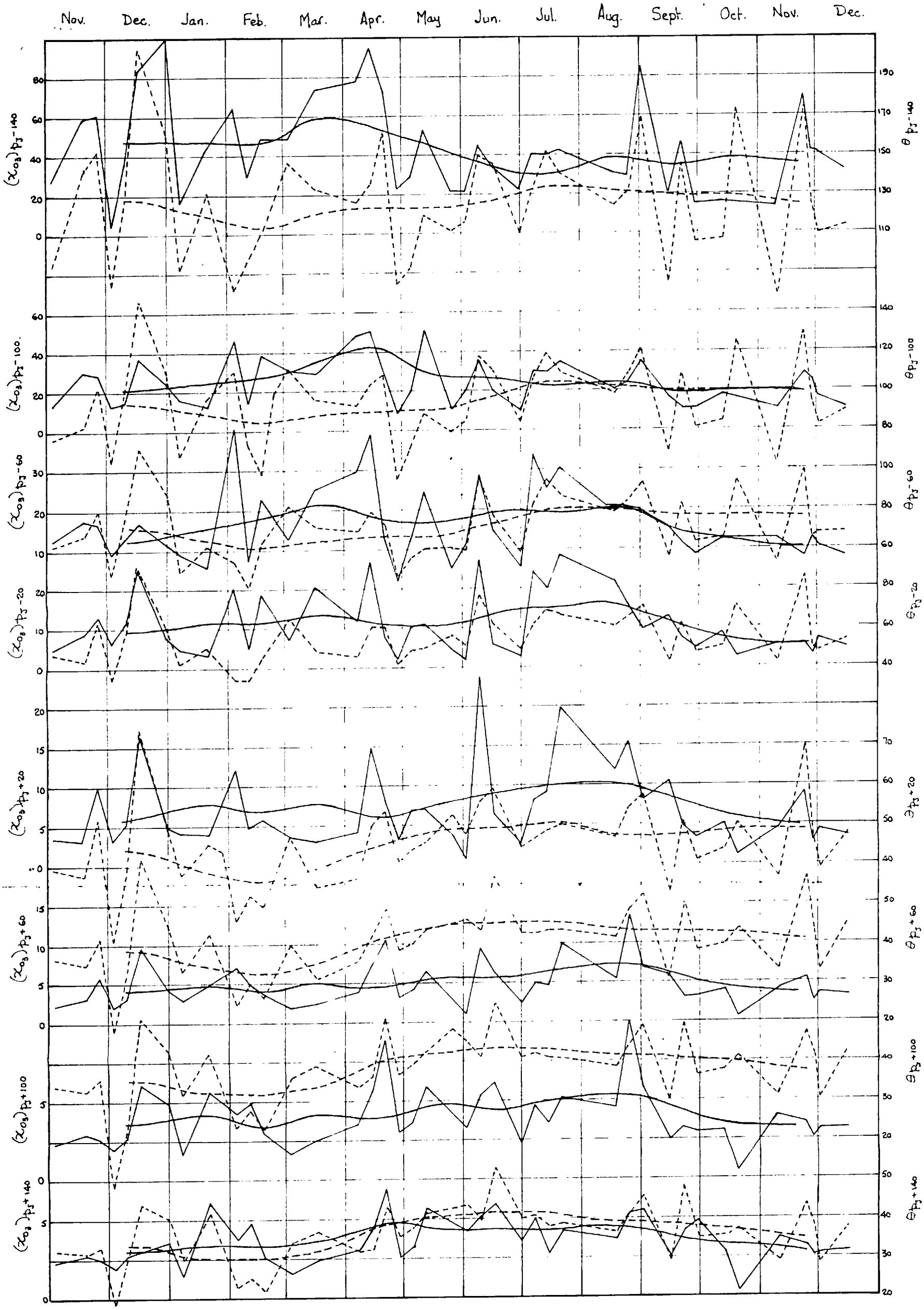

Figure 7.11 Time series of individual observations and three monthly running means of vertically smoothed values of ozone mixing ratios and potential temperatures at levels differing by constant pressure intervals from that of the nearest jet axis. The straight lines represent the series of individual observations while the continuous smooth curves represent the three monthly running mean values computed from these observations. The continuous lines represent ozone mixing ratio and the dashed lines potential temperature (Units: θ - °C, χ_{O_3} - $\mu g/g$.)

7.6.2 Investigation of Horizontal Profiles of Mean Ozone Mixing Ratio in the Troposphere and in the 100 mb Super-Tropopause Layer

The integrated ozone within the troposphere, O_T, and the 100 mb super-tropopause layer, O_S, were converted to mean mixing ratios by the equations $(\chi_o)_T = \frac{g \cdot O_T \cdot 10^{-3}}{(1010 - p_T)}$ and $(\chi_o)_S = g \cdot O_S \cdot 10^{-5}$ respectively, where p_T is the tropopause pressure in mb and O_T and O_S are in gm cm^{-2}.

Figure 7.12 shows all values of $(\chi_o)_T$ and $(\chi_o)_S$ respectively, plotted against an abscissa of distance from the jet axis. Throughout the analysis one unit distance will be equivalent to 60 nautical miles (111 km). The thick dashed lines in the figures are the smoothed horizontal profiles obtained from mean values for three adjacent units of distance. (e.g. mean value at a distance i from the jet axis $= \frac{1}{n_{i+1}+n_i+n_{i-1}} \left(\sum_{1}^{n_{i+1}} \chi_o + \sum_{1}^{n_i} \chi_o + \sum_{1}^{n_{i-1}} \chi_o \right)$.)

The maximum tropospheric ozone mixing ratio, $(\chi_o)_T$, was found at over 200 nautical miles (370 km) to the right of the jet axis, the minimum (about half the magnitude of the maximum) 60-100 nautical miles (150 km) to the right of the jet, and values slightly greater than the minimum value ($\sim \frac{2}{3}$ maximum), but fairly uniform in magnitude to the left of the jet.

The maximum stratospheric mean mixing ratio, $(\chi_o)_S$, is also greatest at over 400 km to the right of the axis with a minimum value ($\sim \frac{2}{3}$ maximum) at the jet and increases to the left to a value $\frac{4}{5}$ of the maximum value500 km left of the jet axis.

The horizontal profile of the ratio of the spatially smoothed values of tropospheric to the stratospheric mixing ratios is shown in fig. 7.13, and may be considered to give the tropo-

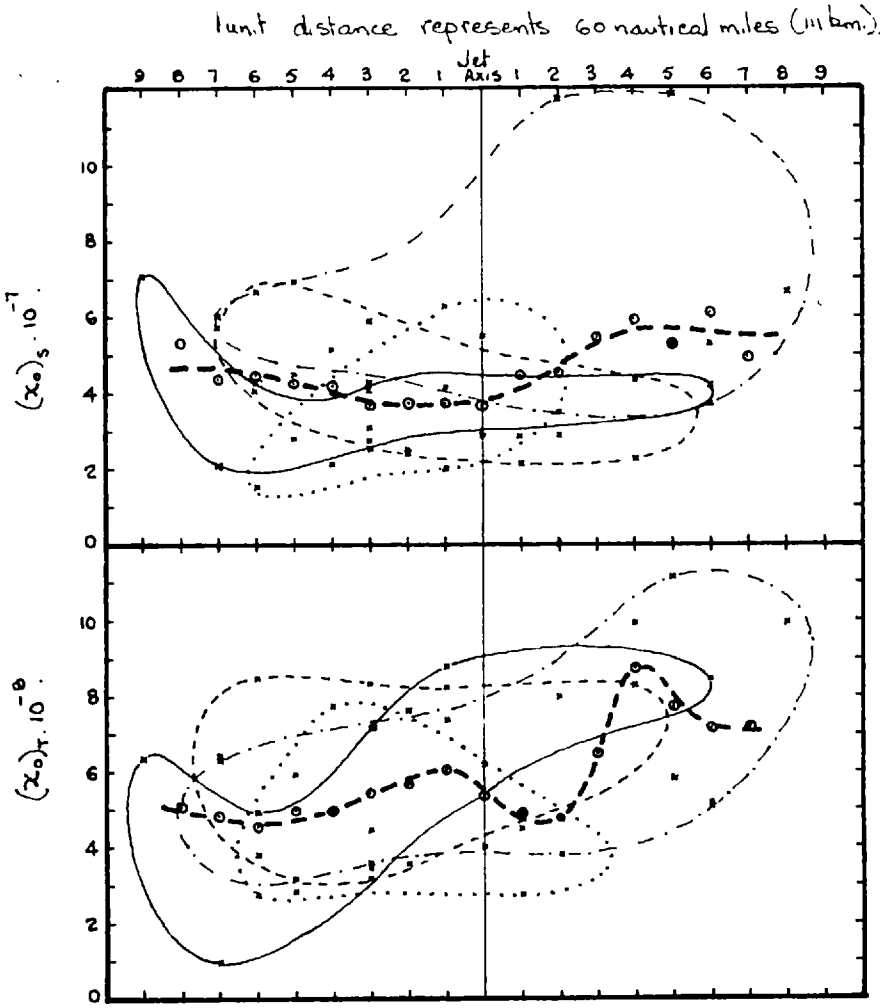

Figure 7.12. Observations of mean ozone mixing ratio in the troposphere $(x_o)_T$, and in the 100mb. super-tropopause layer are shown with respect to the jet axis. Each value is represented by a cross (×) and mean values over three units of distance, by encircled dots (⊙). The thick dashed lines show the mean horizontal profiles across the jet.

Observations occurring in different seasons are enclosed within the following envelopes:

——— 1st Quarter, ----- 3rd. Quarter,

-.-.- 2nd Quarter. ·····: 4th Quarter.

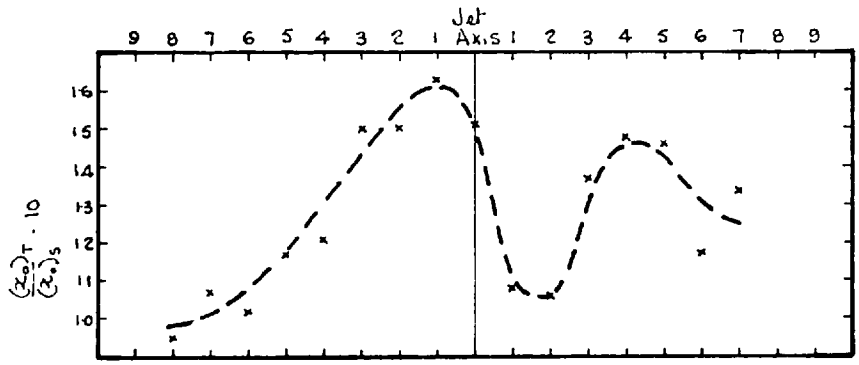

Figure 7.13. Ratio of spatially smoothed mean mixing ratio of ozone in the troposphere to that in the 100 mb super-tropopause layer

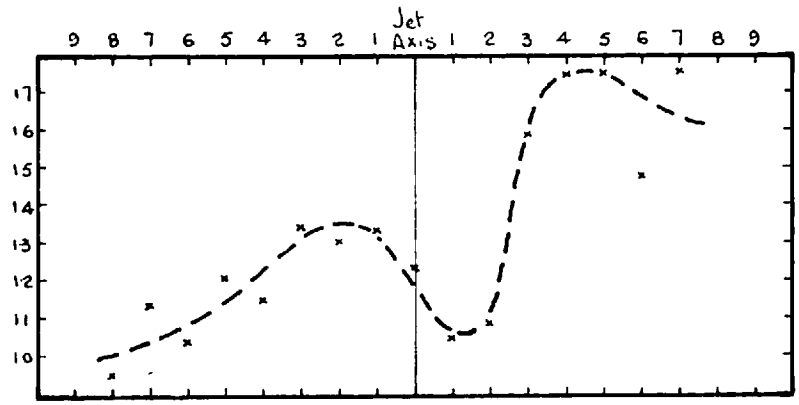

Figure 7.14. Ratio of spatially smoothed mean mixing ratio of ozone in the troposphere to that in the 100 mb super-tropopause layer, after subduing the effect of seasonal variations.

sphere mixing ratio which would result from a hypothetical uniform source above the tropopause. This diagram suggests that the vertical transfer process is most effective just to the left of, and over 400 km to the right of, the jet axis.

The scatter of observations in fig. 7.12 is attributable to three factors:

1. Seasonal variations.
2. Instrumental errors.
3. Variations along the jet front complex.

and we consider these factors in order.

The envelopes on fig. 7.12, enclosing the observations in each quarter, strongly suggest both variance and mean values, at a given distance from the jet axis, vary with season, as is to be expected on the basis of earlier work, and we proceed to eliminate seasonal effects by multiplying each observation by the ratio of the appropriate annual to seasonal mean value.

Estimates of consistent seasonal mean values with respect to the jet axis for different months are derived by dividing the sample into four ranges of distance from the jet axis, (the mean values within each range being about equal and each range containing about the same number of observations), drawing best fit curves of seasonal variation for each range, then adjusting the horizontal profiles in each month drawn through the average range values so derived, for consistency with the annual mean profiles in fig. 7.12. Values are tabulated for each month and unit distance from the jet axis and corresponding annual mean values computed.

The scatter of observations about the new mean horizontal profiles (not shown) is about the same as that before eliminating the seasonal variation, but the horizontal profile of the ratio of the tropospheric to stratospheric ozone mixing ratios, shown in fig. 7.14, suggests that the most effective transfer appears to take place well to the right of the jet axis.

Brewer and Milford (1960), claim instrumental errors throughout any one flight are mainly systematic, i.e., error at any level will be a constant percentage of the observed value , $\varepsilon_p = e.(\chi_o)_p$, where ε_p represents the instrumental error at level p , and e is a constant for a given profile.

The relative importance of variations in $(\chi_o)_p$ due to changes in instrumental error will be studied. On any single profile the ratio of $\frac{\varepsilon_p}{(\chi_o)_p}$ for any two levels p_1 and p_2 will be unity, and this applies equally to the mean values in the troposphere and in the 100 mb super-tropopause layer.

If we abstract mean values $(\bar{\chi}_o)_T$ and $(\bar{\chi}_o)_S$ corresponding to each individual observation, from the values tabulated by month and distance from the jet, as described above, the deviations $(\chi_o)'_T$ and $(\chi_o)'_S$ will be composed of instrumental error, ε , and non-systematic deviation $(\chi_o)^*$ attributable to changes along the jet-front complex. i.e., $(\chi_o)'_T = (\chi_o)_T - (\bar{\chi}_o)_T = (\chi_o)^*_T + \varepsilon_T$.

The ratio $$\frac{\frac{(\chi_o)'_T}{(\bar{\chi}_o)_T}}{\frac{(\chi_o)'_S}{(\bar{\chi}_o)_S}} = \frac{\frac{(\chi_o)^*_T}{(\bar{\chi}_o)_T} + e}{\frac{(\chi_o)^*_S}{(\bar{\chi}_o)_S} + e} = R.$$

is unity if $$\left|\frac{(\chi_o)^*_T}{(\bar{\chi}_o)_T}\right| \ll |e| \gg \left|\frac{(\chi_o)^*_S}{(\bar{\chi}_o)_S}\right|$$

We can draw no conclusions on the relative importance of the two contributions to the deviation in a given profile, but individual

values of the ratio R plotted versus an abscissa of distance from the jet axis in fig. 7.15, show large departures from unity implying large variations in distribution take place along the jet complex. Of particular interest is the large scatter in the vicinity of, and to the left of the jet axis, implying - to the extent that the sample is adequate - that this is the region of major variation along the jet front complex, i.e., the region where most rapid, possibly localised, transfers between stratosphere and troposphere take place. The smaller variance to the right of the jet suggests that large departures from the mean values are more likely attributable to instrumental error and that transfer between the two regions is there more diffuse.

The implications are thus:

1. Major transfer from stratosphere to troposphere takes place well to the right of the jet axis.

2. This transfer appears to be effected by rather slow processes over a large area.

3. A second region of maximum exchange is left of the jet axis and transfers in this region appear to be more intense, though possibly localised, than those to the right of the axis.

7.7 Construction of Normalised Cross Sections for Characteristic Situations

In cross sections relative to the jet axis, we wish to incorporate, as well as isopleths of ozone mixing ratio and potential temperature, a wind field either in isotachs or some function of the wind in terms of its value at the jet axis.

From inspection of the individual profiles and the time

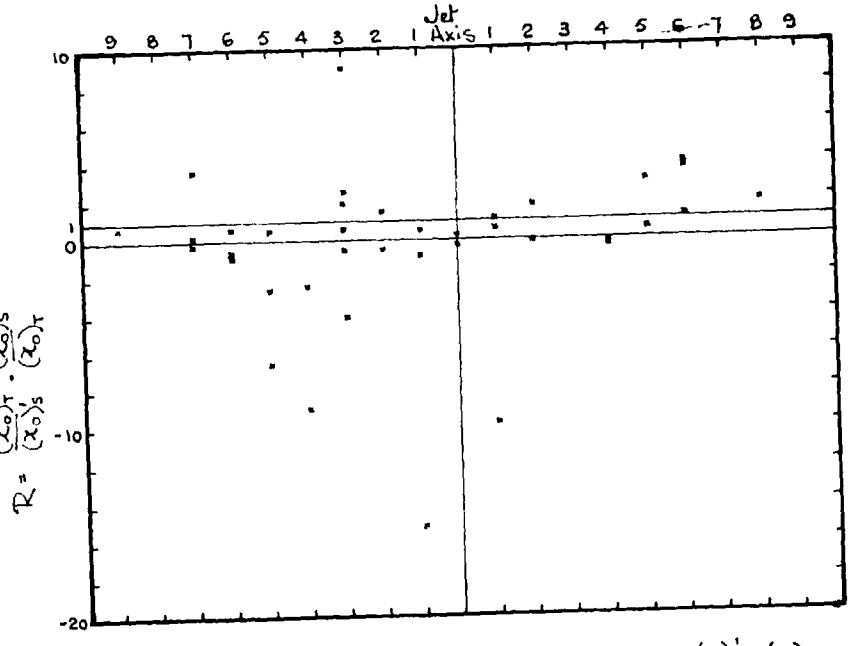

Figure 7.15. Relation of the function $R = \frac{(x_0)'_T}{(x_0)'_S} \cdot \frac{(x_0)_S}{(x_0)_T}$ to the jet axis.

series in figs. 7.10 and 7.11, it is obvious that the height of the jet axis or tropopause strongly influences the profiles of ozone and potential temperature. The profiles were plotted in the tropopause ranges - above 250 mb, 250-300 mb inclusive, and below 300 mb, and the scatter was seen to increase with jet height, and with height above the axis.

Fig. 7.16 gives distribution of mean ozone mixing ratio and potential temperature with respect to jet pressure and we observe that both tracers increase rapidly with height. Profiles were plotted on a new vertical logarithmic scale ($z^* = \log \frac{P}{P_s}$) and values extracted for arbitrary levels equispaced relative to the jet level. The new profiles still showed considerable scatter. The possible causes of this variance are instrumental error, seasonal variations, and variations relative to the jet axis.

Neglecting instrumental error, (c.f. results in section 7.6), we attempt to isolate the transfers relative to the jet by removing the variations which result from changes in jet level and season.

This process of normalisation requires three stages:

1. Determination of characteristic jet stream profiles of ozone properties as a function of season and jet level.

2. Taking the ratio of values of a property at standard levels to the corresponding values on the characteristic profile, i.e: - quotient is then unity in the vicinity of the characteristic profile.

3. Re-introducing the vertical gradients by multiplying each quotient by the annual mean value for that level, for a jet at 270 mb.

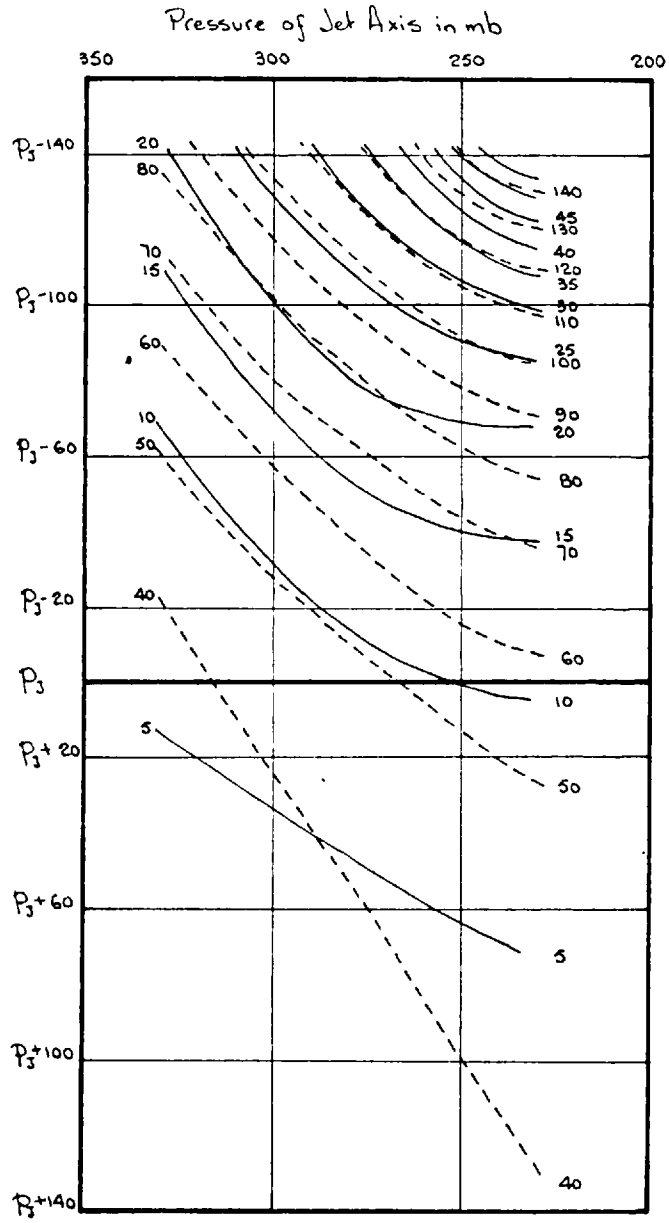

Figure 7.16. Mean distribution of ozone mixing ratio (mol./10^8 mol) and potential temperature in °C, shown by continuous and dashed lines respectively, relative to the jet level for varying jet axis pressure.

We require that the characteristic profiles be representative of the same column, preferably close to the jet axis. This is likely to be so if only profiles at the jet axis are considered, or the property gradients are continuous and similar on either side of the axis.

The latter qualifications may be considered as roughly satisfied for ozone and potential termperature, (c.f. Briggs and Roach, 1963), however, this is patently not so for scalar wind or wind components. The vertical profiles of wind through the jet axis were available and the characteristic jet profiles for wind were constructed from these values.

7.7.1 Cross Sections of Ozone Mixing Ratio and Potential Temperature

The characteristic jet stream profiles were estimated by a method of successive approximation utilising seasonal and vertical continuity.

Observations in each quarter, for a given level relative to the jet axis on the z^* height scale, were plotted on an abscissa of jet level pressure. Plausible best fit curves were drawn for each season.

A first approximation was then obtained of the seasonal variation of the property considered, for specific jet level pressures, by drawing curves through the best fit values just determined, and removing any obvious departures from smooth curves as unrepresentative of seasonal variations.

Any necessary corrections were then made to the original best fit curves. When required, the process of approximation was repeated to produce a family of seasonal mean values corresponding

to different jet pressure levels for the particular height ($z_1^* \pm \Delta z^*$).

Vertical profiles were then drawn to ensure vertical consistency, and values tabulated for each month and jet level pressure. Of the ten levels considered in the analysis, six were evaluated directly as described, and the remaining four obtained by interpolating between these values.

The normalised values were plotted on an abscissa of distance from the jet axis. There was considerable scatter but after smoothing, as in section 7.4, a fairly distinct pattern emerged for ozone mixing ratio and potential temperature and the results are presented graphically on a linear pressure scale in fig. 7.17, for three jet criteria - entrance zones, exit zones, and the complete group of observations. The distribution of these profiles in relation to the jet axis, from which the sections were prepared (Table 7.1), indicates that the section to the right of the jet in the entrance zone is most unreliable.

7.7.2 Cross Sections of Scalar Wind Field

In section 3.2 we postulated characteristic isotach patterns in entrance and exit zones which would result in different vertical profiles for the two regions.

Study of the individual wind profiles through the jet axis plotted for consistency on the z^* vertical scale, showed no obvious grouping of profiles of characteristic form in a particular class of jet region. Mean profiles were computed of wind speed relative to the jet value for each class and are given in fig. 7.18 a).

Mean profiles of fractional wind speed at the jet axis for

Distance from Jet	9	8	7	6	5	4	3	2	1	Jet	1	2	3	4	5	6	7	8	9	Total
Entrance				1		1	2	2	3	1				1						11
Exit	1		3	3	3	1	2			1	3	1		1	1	1				21
All Observ^ns	1		3	4	3	2	6	2	3	2	3	2		2	2	3			1	39

Table 7.1. Distribution of profiles in relation to the jet axis for entrance and exit zones and for all available observations.

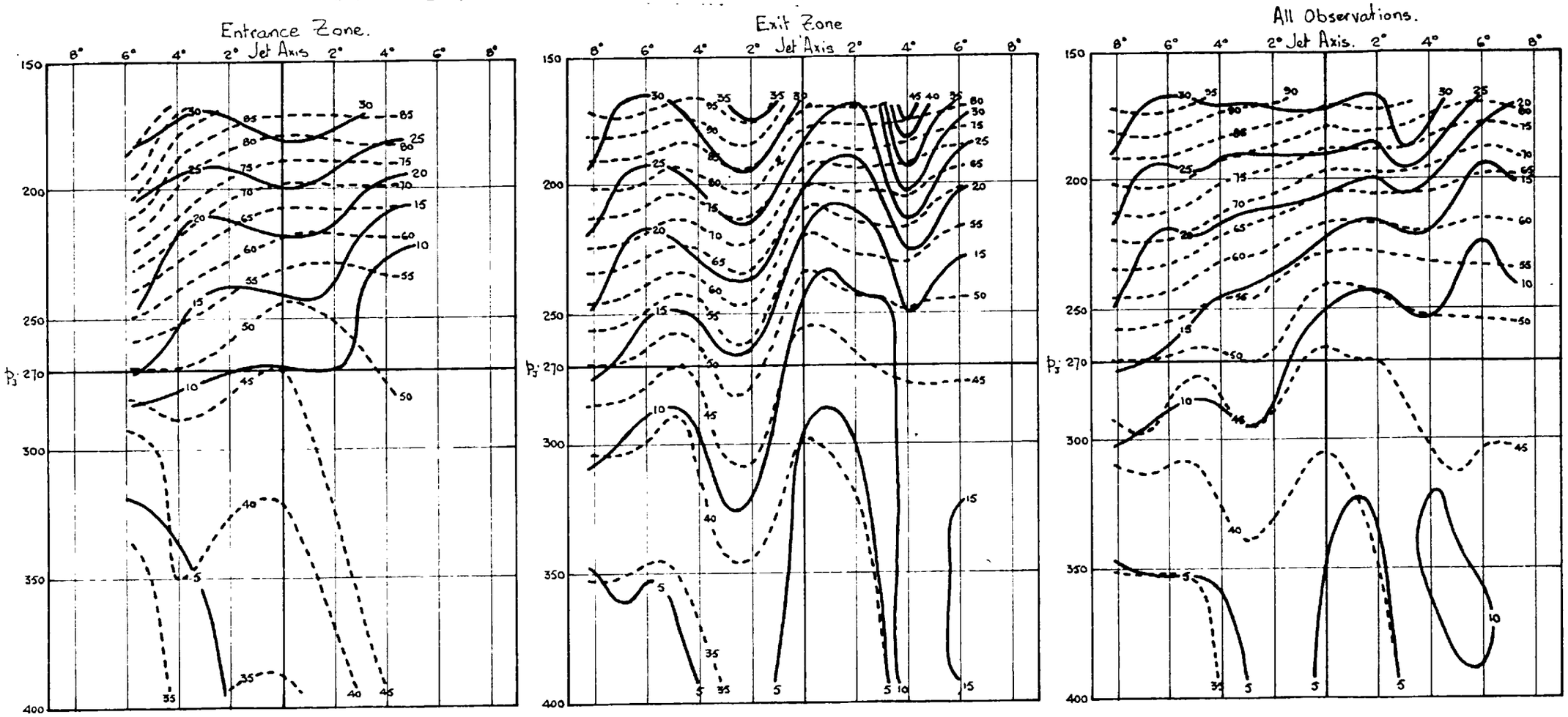

Figure 7.17 Characteristic cross-sections of ozone mixing ratio (solid lines) and potential temperature (dashed lines) normalised relative to characteristic jet profiles, and presented with respect to a 270mb jet axis for entrance and exit regions, and for all observations, irrespective of the region of the jet for which the observations are considered representative. Units x_o - $\mu g/g$, θ - °C.

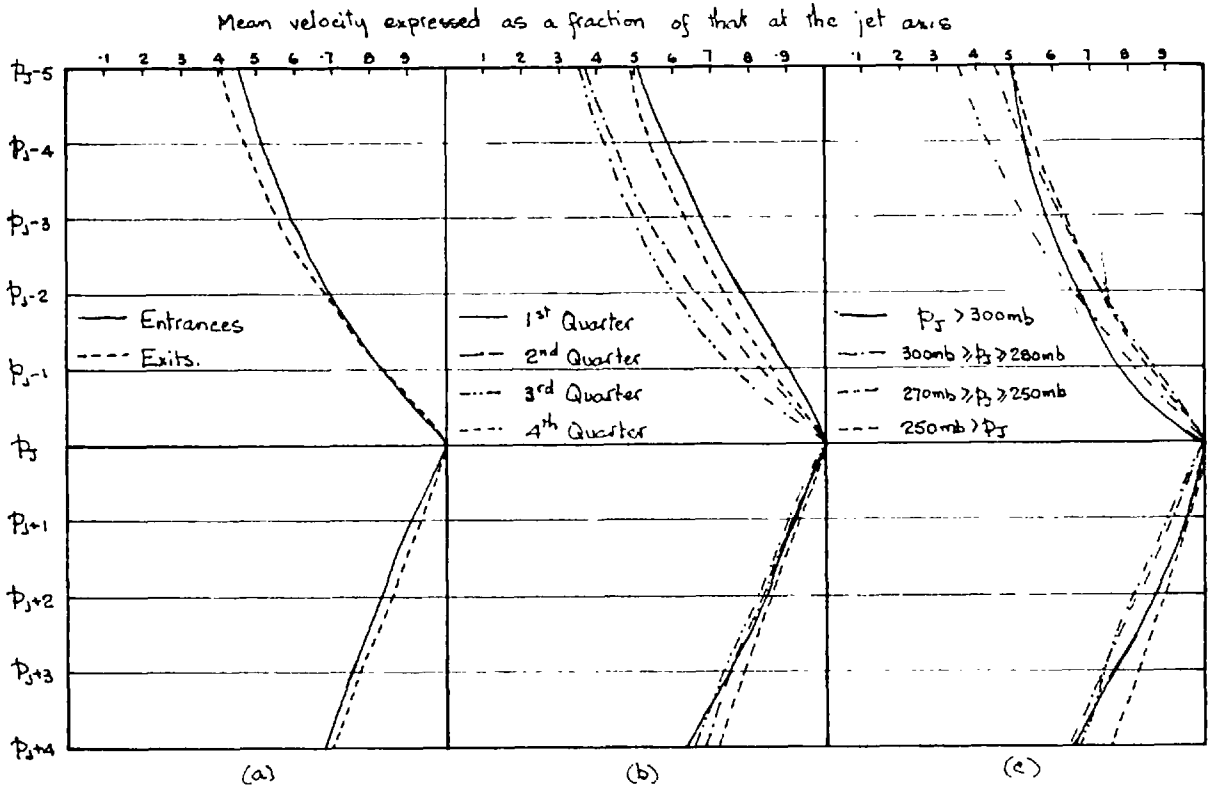

Figure 7.18 Mean profiles of wind relative to that at the jet axis, on the z^* height scale for the following conditions: a) observations in entrance and exit zones b) observations in different seasons and c) observations in different jet level classes.

each quarter and for various groups of jet levels are shown in figs. 7.18 b) and c). We observe greater variation in these profiles than in fig. 7.18 a), which suggests the variations expected in changing synoptic situations may be obscured by seasonal and jet pressure effects.

The procedure followed in determining the characteristic profiles from fractional wind speed at the jet axis, for different months and jet levels, and the subsequent normalisation and analysis of the fractional winds, was identical with that described in section 7.7.1 for ozone. The results are presented graphically in fig. 7.19.

7.7.3 Cross Sections of Vertical Velocities

The vertical velocities computed in Chapter 3 were smoothed over 24 hour intervals and so are not strictly consistent with the data so far studied in this section. However, a corresponding analysis was attempted.

Profiles were drawn through the values of vertical velocities computed for standard levels and values from these converted to the Z^* height scale as before. Individual values extracted at any given level were generally found to be much greater than the corresponding mean value. Since the latter was less than the error in evaluating the vertical velocity, it was decided to ignore the seasonal effects in computing the spatial mean values. The computed values are shown on a linear pressure scale in fig.7.20.

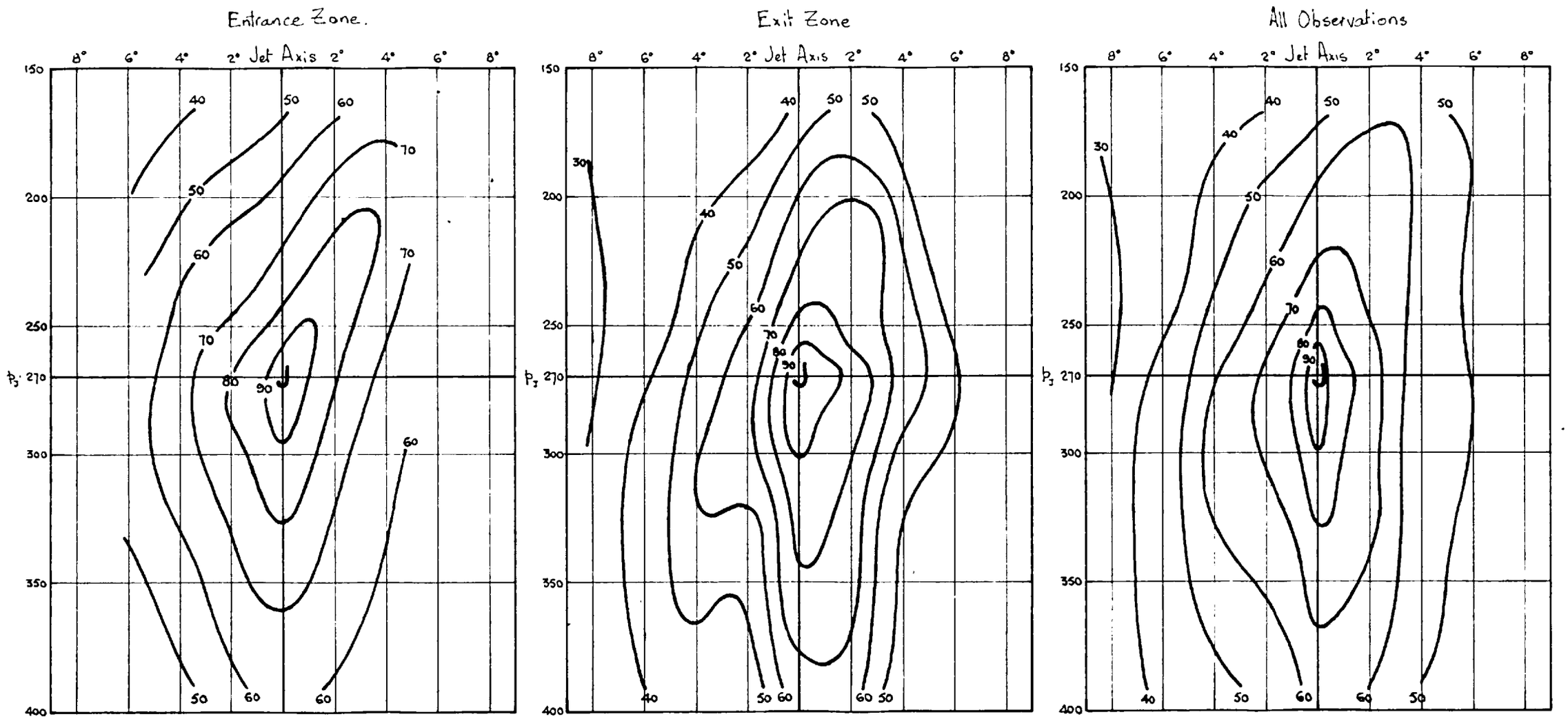

Figure 7.19. Characteristic cross sections of percentage horizontal wind normalised with respect to a 270 mb jet axis, for entrance and exit regions of the jet, and for all observations irrespective of the region of the jet for which the observations are considered representative.

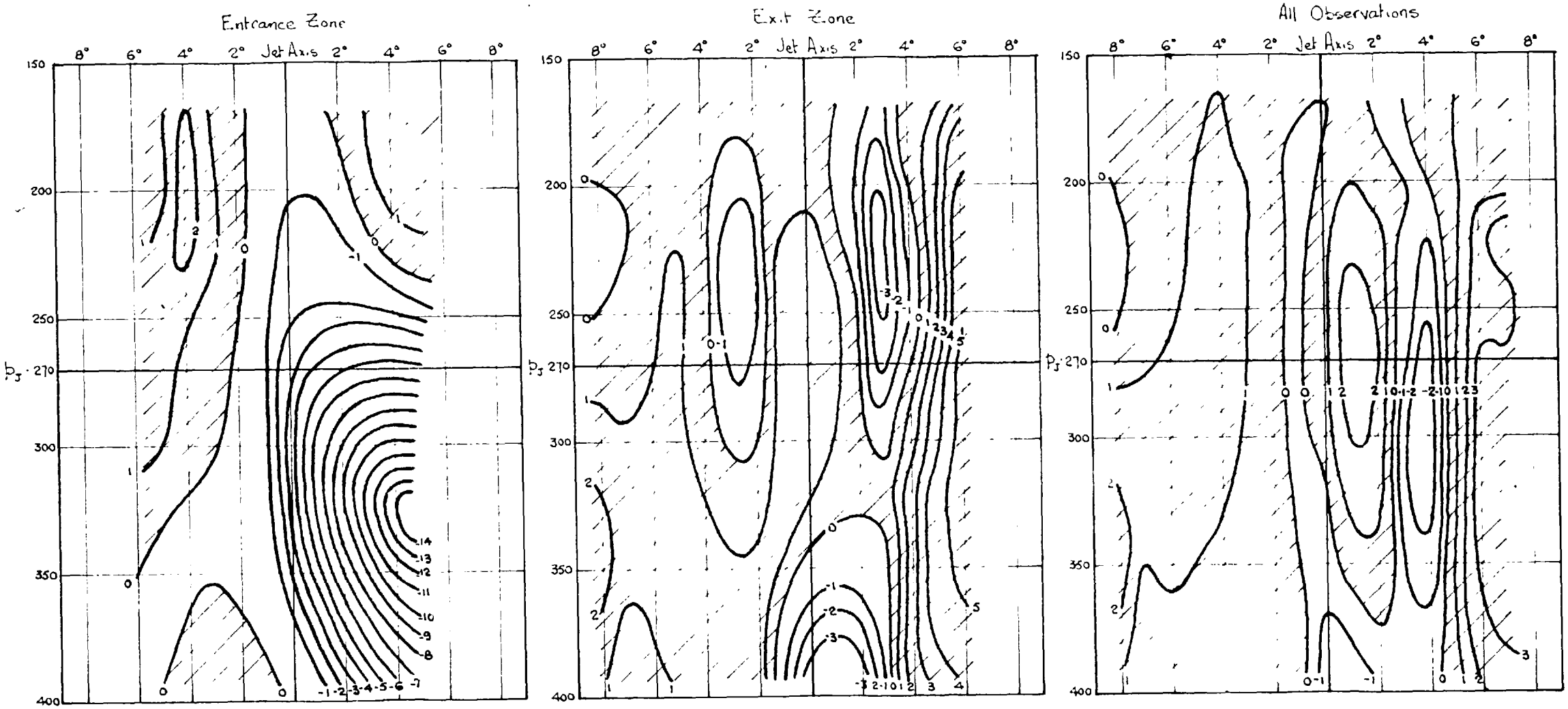

Figure 7.20. Characteristic cross sections of computed vertical velocities normalised and presented relative to a jet axis at the 270mb pressure level, for entrance and exit regions of the jet and for all observations irrespective of the region of the jet for which the observation is considered representative. Units ω cm sec^{-1}.

CHAPTER 8 Exhange of Air Between the Troposphere and the Stratosphere

8.1 General

We now attempt a synthesis of the data presented in earlier chapters.

The possible processes of exchange of air between troposphere and stratosphere are:

1. Mean transverse circulations through the tropopause.
2. Dissolution of the tropopause at one level and reformation at another.
3. Vertical exchange by small scale eddy transfer.
4. Slantwise exchange by large scale mixing.

We proceed from a climatological analysis of the transfer mechanisms in the troposphere, lower stratosphere, and between troposphere and stratosphere to a formulation of a physical model of exchange as related to the jet stream,frontal zone complex.

8.2 An Analysis of General Circulation in the Troposphere and Lower Stratosphere

A qualitative estimate of the variation in dominance of mean meridional and large scale eddy transfers with latitude, in the troposphere, may be inferred from energy balance and energy conversion studies.

We may infer from fig. 2.10, showing the net poleward energy transfer required for meridional heat balance, and the eddy heat transfers of Starr and White (1954), that the transport is almost entirely due to eddy flux in middle and high latitudes, but a meridional cell is necessary in low latitudes.

Lorenz (1955), estimated the energy generation, conversion and dissipation, integrals over the northern hemisphere and showed the potential to kinetic energy conversion of eddies was much greater than that of mean motion. Tucker (1959), estimated the energy conversion in low latitudes by mean meridional circulation to be the same order as the total, implying the contribution of mean meridional motion in higher latitudes must be small or possibly energy consuming.

These combined results suggest the Hadley cell exists almost undisturbed by eddy mixing in the tropics, but slantwise convection contributes strongly to the net transfers elsewhere.

In the stratosphere we shall attempt to account for observed tracer distributions by transfers excluding large scale eddy turbulence, then see how its incorporation in the model will resolve many apparent inconsistencies.

Seeking to interpret the observed meridional gradient of total ozone and the absence of diffusive separation in the stratosphere, Dobson (1929), postulated a model of transfer incorporating slow large scale meridional overturning and small scale vertical eddy diffusion. He proposed (fig. 8.1) that air rose through the equatorial tropopause, spread polewards and downwards through the middle and high latitude tropopause, and that vertical eddy mixing took place through the tropopause and lower stratosphere.

Brewer (1949), estimated mean velocities for this circulation from profiles of water vapour in middle latitudes.

The balance equation for a conservative property in the middle to high latitude lower stratosphere, neglecting horizontal advection

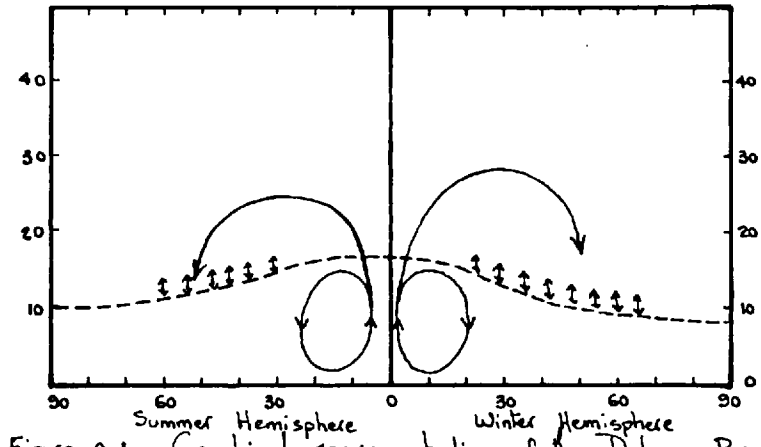

Figure 8.1. Graphical representation of the Dobson-Brewer model of stratospheric circulation

may be expressed by:

$$K \frac{\partial^2 S}{\partial z^2} - \bar{\omega} \frac{\partial S}{\partial z} = 0 \quad \ldots\ldots\ldots\ldots\ldots\ldots \quad 8.1$$

where K is the vertical eddy diffusivity and S the value per unit mass of any conservative tracer.

Neglecting vertical variation in $\bar{\omega}$ and K, and integrating, the equation becomes:

$$\frac{S - S_o}{S_t - S_o} = e^{\frac{\bar{\omega}}{K} z} \quad \ldots\ldots\ldots\ldots\ldots\ldots\ldots\ldots \quad 8.2$$

where z is the height measured from the tropopause, and S_t and S_o are the values of S at the tropopause and in the upper part of the descending current respectively.

Brewer (1949), applied this equation to humidity profiles in middle latitudes, and found reasonable agreement in many cases for a value of $\frac{\bar{\omega}}{K}$ of about -3×10^{-5} cm^{-1}. In the absence of any measured value of K in the lower stratosphere, he proposed a reasonable value of 10^3 cm^2 sec^{-1}, which implies $\bar{\omega} \doteq -3 \times 10^{-2}$ cm sec^{-1} or 25 m day^{-1}. This would result in adiabatic warming by subsidence of about 0.25°K day^{-1}, which might reasonably be compensated by radiative cooling as indicated by fig. 2.9. The complementary heating required in the tropical stratosphere does not appear consistent with the radiative heating rates in fig. 2.9, but the computations of mean annual rate of temperature change, by Manabe and Moller (1961), in fig. 2.10, indicate a possibility of slight heating in this region.

Murgatroyd and Singleton (1961), calculated a meridional circulation sufficient to transport heat between the mean radiative sources and sinks, as evaluated theoretically, in the stratosphere. Below 30 km they found rising air over the equator with

outflow towards both poles and descent towards the tropopause in high latitudes in both hemispheres.

The suggestion in section 5.2 that the stratosphere is almost uniformly dry (.01 - .04 gm kg^{-1}) to an altitude of 30 km throughout the year (Mastenbrook, 1963), is consistent with the Brewer-Dobson circulation model. The apperent winter-spring maximum of humidity in the middle latitude lower stratosphere suggests the meridional circulation may be stronger during this period.

The meridional velocity in the lower stratosphere which would provide continuity with the subsidence rates derived by Brewer, is of the order of 0.2 m sec^{-2} which would generate zonal motion by conservation of angular momentum at a few metres per second per day. This could conceivably be disposed of by eddy diffusion so is not obviously inconsistent.

Interpreting the ozone distribution quantitatively demands a knowledge of the source strength and the rate of leakage of ozone through the tropopause. The latter is unlikely to be greater in summer than in winter, nor is there much seasonal variation in the source strength and distribution, so differences in seasonal distribution are likely to be due to variations in transfers. The observed spring build-up of ozone in the winter lower stratosphere is thus consistent with maximum circulation strength in winter and spring, and little or no circulation in summer which is apparently consistent with the interpretation of humidity. The generally lower ozone mixing ratios in the summer lower stratosphere (fig. 5.11), in spite of the seasonal increase of source

strength at a given level, could be accounted for by the poleward arm of the meridional cell being confined to a lower level during this season, and consequently the descending current being relatively poor in ozone. Moreover, the decrease in slope of the ozone isopleths in summer (fig. 5.11), implies a weakening of the circulation.

The low ozone concentrations in the tropical lower stratosphere (Ramanathan and Kulkarni, 1960) in all seasons, which are less than would be expected from photochemical equilibrium (Dutsch, 1956), strongly suggest a slow ascending current.

The obvious features of the analysis of radioisotopes presented in section 4.3 may be summarised as follows:

1. Low concentrations in the lower stratosphere relative to the tropopause of Sr^{90}, W^{185}, Rh^{102}, and excess C^{14}, are observed in low latitudes, in figs. 5.17 - 5.24, consistent with the slow ascending current of the Brewer-Dobson model.

2. Figs. 5.23, 5.24, from Hageman et al (1959), show the tropical lower stratosphere to be poorer in excess C^{14} in winter than summer, in each hemisphere, implying that the mean ascent, and consequently the meridional cell, is stronger in winter than summer.

3. The axis of maximum concentration of Sr^{90} in figs. 5.21 and 5.22, slopes downward from the equator towards the poles in both hemispheres, and shows little vertical displacement with time, in spite of being injected by all nuclear bursts, and consequently having a highly variable source. This is apparently inconsistent

with the Brewer circulation since the ascending and descending currents of the meridional cell would be expected to advect the levels of maximum S_c^{90} along with them.

4. The axis of maximum concentration of ω'^{85} in figs. 5.17 - 5.19, like S_c^{90}, slopes downwards from the equator towards the poles in both hemispheres and shows little vertical displacement with time. A plausible resolution of this apparent inconsistency with the Brewer circulation lies in the discussion of sampling technique and variation in sedimentation rates in section 4.3. From fig. 4.2 we observe the sedimentation rate increases with height and with increase in particle size with a resulting tendency for only the smaller particles to be advected upwards in the ascending current. The 22 km level of maximum ω'^{85} in the tropics could represent the equilibrium level between mean ascent and sedimentation of the larger particles. The relatively higher collection efficiency of the sampling filter for larger particles shown by fig. 4.3, will further accentuate the maximum. This possibility fails to account for the meridional spread of the ω'^{85}, the lack of meridional movement of the concentration maximum, and the lack of subsidence in the middle latitude level of concentration maximum over the period considered.

Stebbins (1960), from analysis of the rate of change of vertical profiles of ω'^{85}, estimated values of the vertical eddy diffusivity of 10^3 cm sec^{-1} in the tropical stratosphere, and 4×10^4 cm^2 sec^{-1} in middle latitudes. This latter value is over an order of magnitude greater than the value assumed by Brewer (1949), and would result in a much faster meridional cell.

Eliassen (1952), has shown that zonally symmetric thermal and momentum sources and sinks induce meridional overturning. These two mechanisms are linked in a complex non-linear fashion and make a general theory relating the zonal flow and the meridional circulation extremely difficult.

We now invoke the concept of large scale eddy mixing in an attempt to explain any inconsistencies. In section 2.3.4 we presented evidence of eddy mixing in the lower stratosphere from an analysis of zonally averaged covariance of vertical and meridional wind components, and showed the mixing angle implied by the correlations was consistent with the slope of the mean isentropic surfaces. The slope of the mean potential isotherms is downward towards the pole over the entire hemisphere in the summer lower stratosphere but reverses in higher latitudes in winter. The analysis of the limited observations for Liverpool in section 2.3.5 strongly suggests a seasonal variation of mixing slope in the lower stratosphere consistent with the reversal of horizontal gradient of potential temperature.

The counter gradient eddy heat fluxes noted in the lower stratosphere by White (1954) and Peixoto (1961), suggest these eddies to be energy consuming, i.e., forced so the mixing slope will be greater than that of the mean isentropic surfaces.

No such direct evidence of eddying motion exists in the middle stratosphere, however, by analogy with the tropospheric systems, transfer by waves associated with the polar night vortex seems plausible, and in section 6.2 seasonal mean distributions of ozone were interpreted as evidence of eddy transfer by transient eddies.

The Brewer-Dobson model of stratospheric circulation is modified in fig. 8.2 to incorporate a pattern of large scale eddy mixing consistent with the preceeding data interpretation.

The apparent spring maximum in the seasonal variation of humidity in the middle latitude lower stratosphere (section 5.2) may now be interpreted as due to both increased eddy mixing above the tropopause and increased moisture transport from the troposphere.

The meridional sections of ozone mixing ratio in fig. 5.11 are also consistent with the pattern of eddy mixing shown in fig. 8.2. The generally lower values observed in the summer lower stratosphere might then be partially accounted for by the lower levels to which the stratospheric eddy mixing was confined in the absence of the polar night jet.

Newell (1961), has estimated the horizontal flux of ozone by transient eddies in the lower stratosphere. In the absence of a sufficient number of vertical profiles of ozone, he assumed the total ozone anomaly to approximate that in the lower stratosphere (12-24 km). In section 7.3 we showed that the correlation between ozone in the lower stratosphere over Liverpool was much less than over Canada, in fact both the correlation coefficient and the regression factors vary with locality and season, but the flux estimates should be of the correct order. Newell estimated the horizontal eddy flux from 25 stations, for three monthly periods throughout the I.G.Y., using for alternative estimates, the winds at the 50 mb and 100 mb levels. In middle latitudes he found the eddy flux directed polewards for both estimates, with

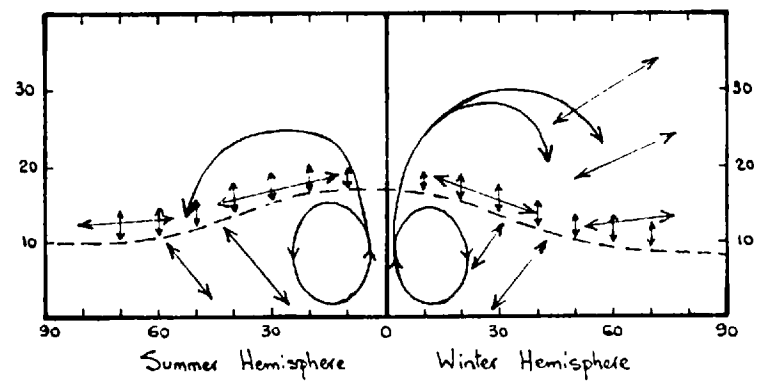

Figure 8 2. The Brewer-Dobson model of stratospheric circulation incorporating, in addition, macro-eddy mixing. The short arrows represent vertical eddy diffusion, and the long oblique arrows, macro-eddy mixing.

strongest flux in the 1st and 4th quarters, but for three stations north of 60°N, where the stratospheric isentropes reversed their slope in winter, it was found to be southward. These results are consistent with the proposed eddy transfer pattern.

Newell (1961), attempted to evaluate the relative contributions of the various transfers to the lower stratospheric spring build-up of ozone in high latitudes, examining the ozone budget north of 55°N. The evaluation of both mean meridional transport $[\bar{o}][\bar{v}]$ and that by standing eddies $[\bar{o}\,\bar{v}] - [\bar{o}][\bar{v}]$ require an accurate evaluation of mean meridional velocity and mean ozone. The sample used by Newell is clearly too small to be representative and so the results can at best only represent a rough approximation, and might even be incorrect in sign. Newell estimates a zonal temporal mean meridional velocity for the 100-25 mb layer, directed poleward, of 6 cm sec^{-1} during the first quarter. His reasons for adopting such a value are unconvincing, (he takes estimates of the wind in this layer in summer by Barnes (unpublished), which are directed equatorward, reverses their direction, but keeps the same magnitude). However, since this value is consistent with an upward extrapolation of the value at 100 mb of Palmen and Vuorela (1963), and the computed value of Murgatroyd and Singleton (1961), it may not be unreasonable. On the further assumption that a third of the total ozone in a vertical column is involved in the lower stratospheric transport processes, Newell estimates the transports across 50°N due to transient eddies, mean advection and standing eddies to be 9.0×10^9

1.6×10^9 and 2.5×10^9 atm cm cm^2 sec^{-1} respectively.

Furthermore, Newell estimated the net mean rate of change in integrated mean ozone within the polar cap, from Godson's (1960), meridional profiles of total ozone, as 9.0×10^9 atm cm cm^2 sec^{-1}, which is somewhat less than the amount transferred by total eddy flux. This too suggests eddy transfers exert a dominant influence in the middle and high latitude lower stratosphere.

Finally, the introduction of the scheme of large scale eddy mixing helps to explain the distribution of certain radioisotopes. The W^{ies} debris which was injected at 12°N in summer 1958 appeared to spread polewards and downwards in a manner consistent with eddy mixing along a slope somewhat greater than that of the mean isentropes, implying the eddy motion to be energy consuming.

The evidence presented then appears consistent with the model in fig. 8.2.

8.3 Transfer Across the Tropopause

8.3.1 Relative Contributions to Transfer from a Climatological Viewpoint

The mean tropopause height in fig. 8.3 (from data of Goldie et al, 1957, and Staley, 1962), is considerably lower in winter than in summer except in low latitudes. The surface pressures also show an annual variation with maximum in January and minimum in July, the amplitude of the change varying with latitude as shown in fig. 8.4. (Zonal mean values in January and July were computed from hemispheric charts of mean monthly pressure in Brunt, 1934.)

The seasonal change in stratospheric mass due to mean tropopause height was computed by means of the formula:-

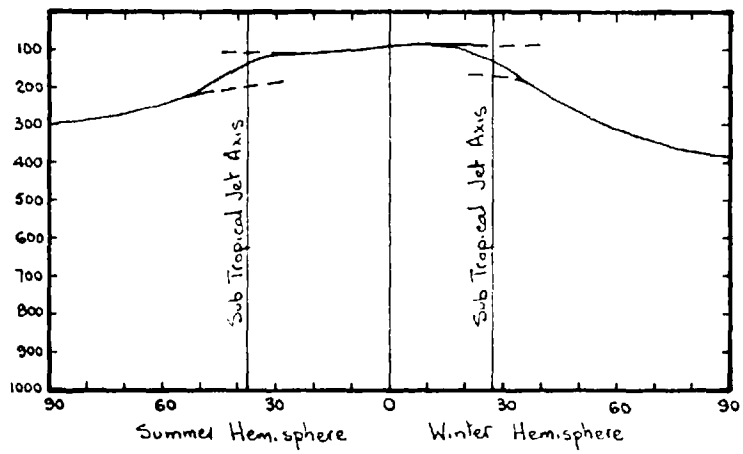

Figure 83. Meridional variation of mean tropopause pressure in summer and winter and corresponding positions of the sub-tropical jet axis.

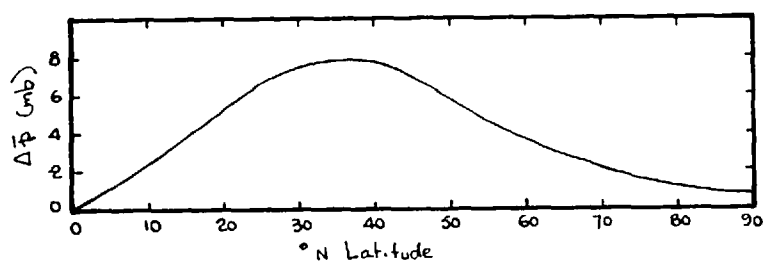

Figure 84. Meridional variation of the amplitude of the seasonal change in the zonal mean surface pressure. (mb.) Pressures increase from summer to winter.

$$\text{Mass change} = \int_0^{\frac{\pi}{2}} \frac{2\pi r_e^2 \cos\phi}{g} (\Delta p_T) d\phi$$

where Δp_T is the seasonal change in tropopause pressure and ϕ latitude. Summation is carried out over 5° intervals in Table 8.1 and the total seasonal change is $2\pi r_e^2 . 30.3$ g. The corresponding mass change in the column from the surface to the top of the atmosphere resulting from trans-equatorial transfer, is also shown in Table 8.1 ($2\pi r_e^2 . 4.82$ g) and only amounts to 15% of the change in the stratosphere. So even if the entire trans-equatorial transfer was effected within the stratosphere, there must still be a net mean mass transfer upwards through the tropopause in winter and downwards in summer of $2\pi r_e^2 . 25.5$ g.

New interpretation of ozone and radioisotope distributions in the tropical stratosphere (see section 8.2) indicates mean ascent takes place in both summer and winter hemispheres, but is less in summer than winter. If we assume the seasonal mean mass transfer from troposphere to stratosphere in winter to take place within 20° latitude of the equator, the mean rate of ascent necessary to effect a transfer of $2\pi r_e^2 . 25.5$ g ($2\pi r_e^2 . 30.3$ g) would be 0.29×10^{-1} cm sec^{-1} (0.35×10^{-1} cm sec^{-1}). These values do not allow for the ascent due to the Hadley-Brewer cell in summer, but a mean ascent in the tropical lower stratosphere consistent with Brewer's (1949), estimate of subsidence in mid-latitudes would be about $.35 \times 10^{-1}$ cm sec^{-1} which would suggest transtropopause velocities of about 0.2×10^{-1} and 0.5×10^{-1} cm sec^{-1} in summer and winter respectively.

The evidence in section 8.2 justifies our asserting that

Latitude ϕ	87.5	82.5	77.5	72.5	67.5	62.5	57.5	52.5	47.5	42.5	37.5	32.5	27.5	22.5	17.5	12.5	7.5	2.5
Cos ϕ	·0436	·1305	·2164	·3007	·3827	·4617	·5373	·6088	·6884	·7373	·7934	·8434	·8870	·9239	·9537	·9763	·9914	·9990
Δp_T (mb)	90	85	85	85	80	75	67	56	48	45	50	43	30	10	-8	-12	-8	-3
$\frac{\cos\phi\, d\phi\, \Delta p_T}{g}$	348	·985	1·632	2·270	2·717	3·068	3·195	3·030	2·93	2·94	3·52	3·22	2·36	0·82	-·677	-1·038	-·703	-·266
Total mass change associated with tropopause height change $= \sum_{0}^{30} \frac{2\pi r^2 \cos\phi\, d\phi\, \Delta p_T}{g} = 2\pi r^2 30.3$ gm																		
Δp (surface)	0·8	1·0	1·5	2·0	2·6	3·3	4·1	5·3	6·5	7·5	8·0	7·7	7·1	6·0	4·6	3·0	1·7	0·6
$\frac{\cos\phi.\, d\phi\, \Delta p}{g}$	003	·012	·029	·053	·088	·135	·196	·286	·397	·490	·561	·674	·559	·490	·387	·259	·149	·053
Total mass change associated with surface pressure change $= 2\pi r^2 .482$ gm.																		

Table 8.1. Computation of seasonal change in mass in the stratosphere as a result of changes in the tropopause pressure, and in the complete depth of the atmosphere as reflected in changes in the mean surface pressure.

vertical transfer in both troposphere and lower stratosphere, in the tropics, is due predominantly to a mean direct meridional circulation and there is some evidence in sections 2.2.1, 3.5 and 3.6, of an indirect cell associated with the jet complexes. The relative contributions of the mean transfer by these systems to the net transfer are evaluated from meridional sections of $[\bar{\omega}]$.

Palmen and Vuorela (1963) computed zonal mean values of the mean meridional wind $[\bar{v}]$ to a height of 100 mb from Crutcher's (1961) cross sections of three monthly mean values at successive 10° longitude intervals around the globe for winter. No similar summer section of $[\bar{v}]$ is available so consistent values were computed for the 100, 200 and 300 mb levels from the equator to 55°N latitude from Crutcher's original sections. Mean values of horizontal divergence were then obtained from the equation:-

$$\nabla.[\bar{v}] = \frac{\partial[\bar{v}]}{r_e \partial\phi} - \frac{[\bar{v}]}{r_e}\tan\phi \qquad \text{8.3.}$$

Profiles of $\nabla.[\bar{v}]$ were then drawn from $p=0 (\nabla.[\bar{v}]=0)$ down to the 300 mb level and the vertical velocities $[\bar{\omega}]$ were estimated by graphically integrating downwards by means of the equation:-

$$[\bar{\omega}] = \frac{1}{g\rho_z}\int_0^{p_z} \nabla.[\bar{v}]\, dp \qquad \text{8.4.}$$

We observe from the results in fig. 8.5 that mean ascent rates at the tropical tropopause are qualitatively consistent with the preceeding indirect estimates.

The general features of fig. 8.5 are incorporated in the model of meridional circulations in fig. 8.6. In this figure the vertical transfers α, β, γ, are the mean vertical mass fluxes through the tropopause in high middle and low latitudes

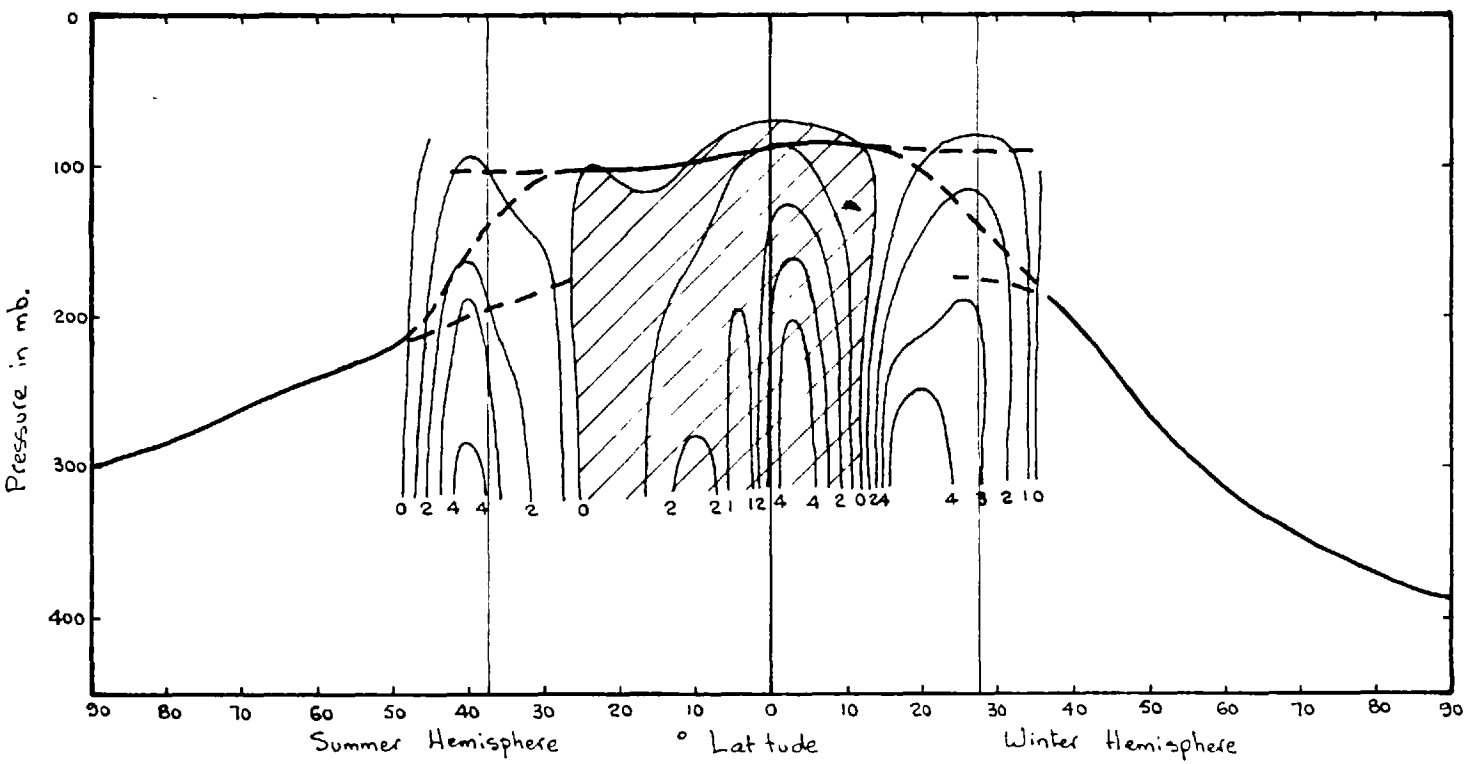

Figure 8.5. Meridional section of mean vertical velocities in low latitudes in the vicinity of the tropopause, computed from Crutcher's (1961) sections of mean meridional wind. Units are 10^{-1} cm. sec^{-1}. Thick lines represent mean tropopause levels.

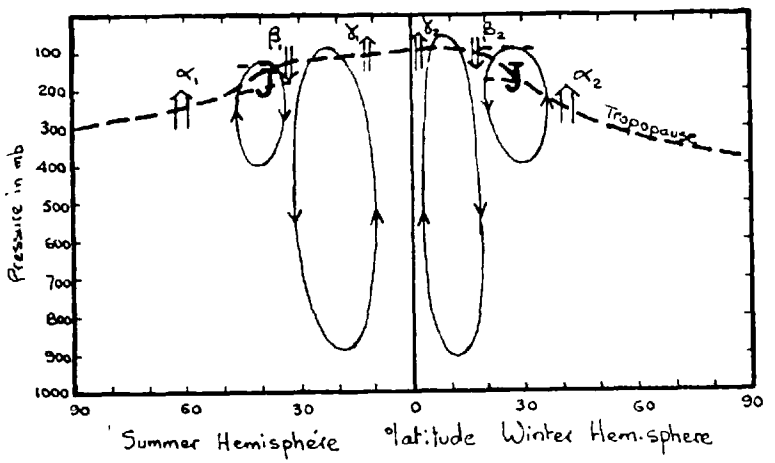

Figure 8.6. Graphical representation of mean transfers near the tropopause and plausible mean meridional circulations.

Latitude ϕ	50	45	40	35	30	25	20	15	10	5	0	5	10	15	20	25	30	35
$\cos\phi$	·623	·707	·766	·819	·866	·906	·940	·966	·985	·996	1·00	·996	·985	·966	·940	·906	·866	·819
$\bar{\omega}_T$ (10^{-1} cm sec^{-1})	0·3	-1·0	-1·9	-0·9	-0·1	0·2	0·0	-0·4	0·2	0·7	1·0	0·8	0·4	-0·3	0·0	-2·1	-2·2	-0·8
$\bar{p}_T$ (mb)	220	190	155	125	110	105	105	102	99	94	90	88	89	92	106	125	145	170
$\bar{T}_T$ (°K)	217	215	213	209	205	202	200	200	198	197	196	195	195	196	199	201	206	210
$\frac{\Delta t \cos\phi \, d\phi \, \bar{p}_T \bar{\omega}}{R\bar{T}_T}$	+9·1	-30·1	-51·1	-22·2	-2·2	+4·5	0·0	-9·5	+4·8	+16·0	+22·1	+17·3	+8·7	-6·6	-24·0	-57·0	-64·6	-25·4
Mass Transfers	$\beta_1 = 2\pi r^2 1056$ gm					$\gamma_1 = 2\pi r^2 269$ gm						$\gamma_2 = 2\pi r^2 381$ gm		$\beta_2 = 2\pi r^2 1776$ gm				

Table 8.2 Evaluation of mean vertical mass transfers across the tropopause in summer and winter from estimates of the mean vertical velocities.

respectively, associated with the circulations in fig. 8.6, and Σ is the seasonal stratospheric-tropospheric mass exchange reflecting tropopause pressure changes already calculated to lie between $2\pi r_e^2 30.3$ g and $2\pi r_e^2 25.5$ g, so that the tropospheric-stratospheric balance is maintained in accord with the following equations:

In winter $\alpha_2 + \gamma_2 + \Sigma = \beta_2$ 8.5

In summer $\alpha_1 + \gamma_1 = \Sigma + \beta_1$ 8.6

The northern limits of the descending mean current in winter and summer at the 200 mb level, from fig. 8.5, are 37°N and 47.5°N respectively. The mean position of the subtropical jet, evaluated from the Crutcher (1961) cross sections of scalar wind speed, were 27.5°N (consistent with the estimate of Krishnamurti, 1960), and 37.5°N. It appears reasonable to assume the vertical velocity reversal is associated with the jet.

The mean mass fluxes γ_1, γ_2, and β_1, β_2, as defined above, have been evaluated and are given in Table 8.2. Corresponding values of α_1, and α_2, were deduced from equations 8.5 and 8.6, giving:

$\gamma_1 : \beta_1 : \alpha_1 = 26.9 : 105.6 : 109.2$ (or 114.0)

$\gamma_2 : \beta_2 : \alpha_2 = 38.1 : 177.6 : 109.0$ (or 104.2)

The alternative values of the α transfers, represent limits encompassing the actual value. The bracketed values representing the transfers if the total seasonal transequatorial transfer is assumed to take place entirely in the stratosphere, and the other if entirely in the troposphere.

The ratio $\frac{\alpha}{\gamma}$ suggests the postulated indirect circulation associated with the jets is responsible for the greater part of

the total transfer by mean vertical transfers, (three times as much as the tropical circulation in winter and four times in summer).

There is only about 10% seasonal variation in the mass transfer by the indirect cell and the maximum transfer is in winter. This is consistent with the seasonal and meridional variations in radiodebris concentrations shown in fig. 5.14.

Information presented in section 1.1 suggests that the mean residence time of air in the lower and middle stratosphere is somewhat less than a year - ranging from a few months in the lower extratropical stratosphere (Martell, 1959), to a year or more in the tropical middle stratosphere. If then the stratospheric air is completely changed in nine months there is an annual mass exchange between troposphere and stratosphere of $2\pi r_e^2 .250$ gm.

The mean mass exchange by mean vertical transport over a year may be estimated, from Table 8.2, by $\beta_1+\beta_2 = 2\pi r_e^2\ 280$ gm, which suggests that the total annual transfer may be accomplished by mean motions.

The estimate of total mass transfer from stratospheric residence times may be somewhat low since there may well be an exchange of air in the vicinity of the jet between troposphere and stratosphere without depletion of the lower stratospheric radioisotope concentration, the transverse circulations about the jet axis simply causing an oscillation of much the same air between the two regimes.

8.3.2 Trans-tropopause transfer as inferred from evidence of tracers.

The evidence on trans-tropopause transfer presented in the last section derives from our evaluation of the field of mean vertical velocity in the neighbourhood of the tropical and near extratropical tropopause, and of seasonal mass transfer between stratosphere and troposphere deriving from the fields of mean pressure and from estimates of stratospheric residence times.

We have seen, moreover, (Chapters 2 and 3), that the direct evidence on the extratropical meridional circulation from observations of wind is inconclusive. Tucker (fig. 2.6) found evidence of an indirect cell, Palmen and Vuorela (fig.2.5) of a direct out to 10°-20° poleward of the subtropical jet, and our own (limited) analysis for Liverpool suggested an indirect cell centred beneath the jet. Murray and Daniels (fig. 3.7) and Briggs and Roach (fig. 3.8), distinguishing between entrance and exit zones of middle latitude jets, found direct circulation about the former and indirect about the latter.

We shall now, in conclusion, summarise the further evidence which has been extracted in the present research (and otherwise) which lends support to the ideas expressed in figs. 8.2, 8.6, and Table 8.2, and may be used to help resolve the inconsistencies concerning circulation models noted in the last paragraph. We shall also point out where further elucidation is called for.

One of the most important of our present findings is the maximum of mean tropospheric ozone observed to the right of the jet axis in fig. 7.14. It suggests (to the extent that tropospheric transfer adds no complication) that stratospheric-tropospheric transfer is greater to the right of the jet axis. This inference is supported by the distributions of integrated tropospheric radiodebris of Miyake et al (1960), in figs. 6.6 and 6.7, which also exhibit maxima to the right of the jet axis.

Such distributions are consistent with a mean indirect circulation about the jet in which the transverse transfers across a sloping or broken tropopause may be as important as the vertical transfers. Upon this circulation may perhaps be superposed a largescale circulation of the Brewer-Dobson pattern. The contribution to net transfer close to the middle latitude jets of the latter circulation, is inferred to be minimal since - a further important finding - the secondary seasonal ozone maximum in the lower stratosphere in June/July (fig. 7.6) increases with proximity to the tropopause and is dominant near 300 mb (fig. 7.4), implying greater intensity of circulation near the tropopause than well above it. The June stratospheric ozone maximum in fig. 7.6 may be explained by assuming the ozone in the lower polar stratosphere to be increased in spring by the processes discussed in Section 8.2, which would result in a greater meridional ozone gradient in the late spring and, for the same transverse circulation, an increase in ozone in the lower stratosphere in the vicinity

and to the right of the jet axis from increased equatorward advection. This secondary maximum should be absent at more northerly stations remote from the jet axis and this requires confirmation. (The summer maximum cannot be explained by seasonal motion of the jet axis neglecting meridional circulations. The observation in the mean sections (fig. 7.17) that ozone at constant pressure is greater to the left than right of the jet axis would then suggest the inconsistent result that ozone at constant pressure in the middle latitude lower stratosphere should be a minimum in summer when the mean jet axis is furthest north.)

Sporadic intrusions of stratospheric air from the lower polar stratosphere into the troposphere in the vicinity of the frontal zone below the jet axis have been inferred from humidity and ozone data by Briggs and Roach (1963) - fig. 6.3; from S_r^{90} by Danielsen et al (1962) - fig. 6.10 and 6.11; and from β activity maxima on vertical profiles by an isentropic trajectory technique (Staley, 1962) - Tables 6.2 and 6.3. These are clearly inconsistent with transfers by a mean indirect circulation. The secondary maximum in $\frac{(\chi_o)_T}{(\chi_o)_S}$ to the left of the jet axis in fig. 7.14, suggests that direct cells alternate with indirect about the jet, an inference supported by Tucker's (1957) analysis of humidity in relation to the jet in fig. 6.4, and the interpretation of velocity components in Section 3.7. The combined evidence suggests that these intrusions may take place in a direct circulation in entrance zones, and a simple dynamical analysis by Sawyer (1958), supports this inference. Simple models of such transverse circulations are shown in fig. 8.7.

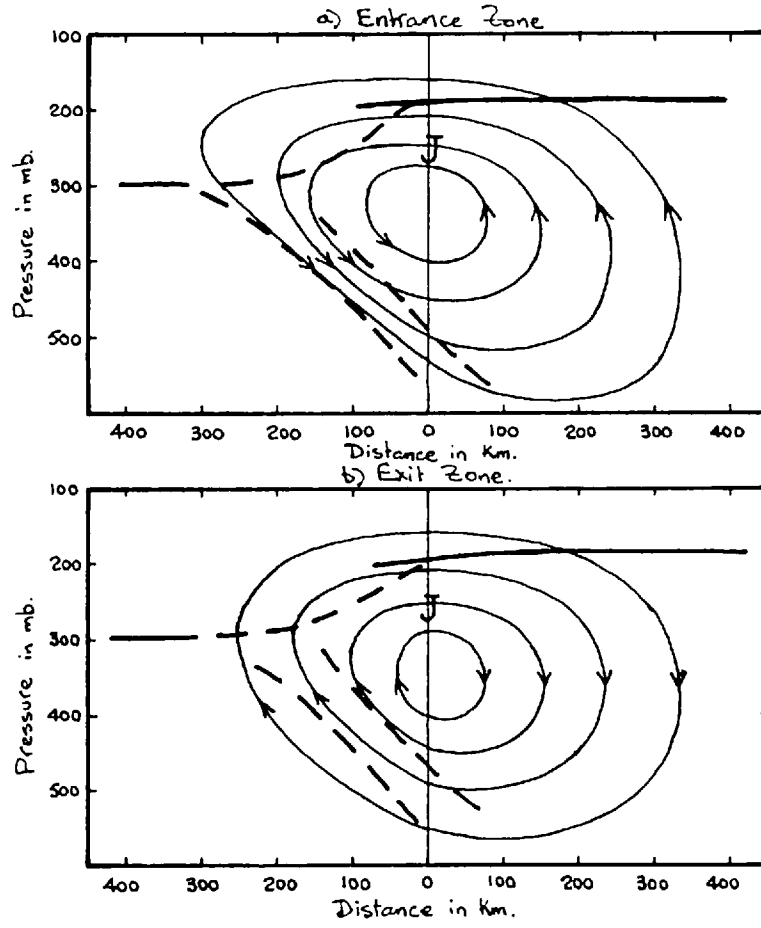

Figure 87. Circulations in entrance and exit zones of a straight jet, and their resulting mass transfers, are represented by plausible isopleths of Stokes' stream function.

In spite of the postulated dominant influence of the indirect circulation, we lack conclusive direct evidence of its importance from tracers. Transfer will, in all cases, be more readily detectable over short periods to the left of the jet where it takes place across greater tracer gradients, but there is no evidence of a marked ozone poor region in the lower stratosphere to the left of the jet maximum as we would anticipate in exit regions.

Confirmation of the transfer models in fig. 8.7 was attempted by construction of characteristic cross section but neither the vertical velocity nor the tracer distributions with respect to the jet in figs. 7.20 and 7.17 suggest a simple single cell circulation in any of the jet regions considered, though there is a good correlation in all sections between these parameters. The lack of distinct circulation patterns is probably a consequence of the unrepresentative sample. Sawyer's (1958) dynamical analysis showed that curvature vorticity advection is capable of producing a field of vertical velocities in the upper troposphere and lower stratosphere of the same order as those produced by sheer vorticity advection, and that increasing the cyclonic (anticyclonic) curvature of the jet axis would produce a field of vertical velocities resulting in upper tropospheric frontogenesis (frontolysis) and downward (upward) mass transfer to the left of the jet. This deduction, supported empirically by Endlich's (1953) finding that greatest subsidence (ascent) in the upper troposphere occurred west of the long wave troughs (ridges) and east of the long wave ridges (troughs) implies, as does the analysis of wind components in section 7.7, that the jet

front model proposed in Section 3.3 (p.52) is inadequate unless we restrict the analysis to straight jets or consider a more statistically representative sample.

In summary therefore we regard the wind and tracer studies undertaken here and previously to imply the following modes of stratospheric-tropospheric transfers:

A mean direct (Hadley) cell penetrating the tropopause in the tropics and subtropics, and an indirect cell, centred about 150 mb below the polar front jet maximum in middle latitudes, and large scale eddy transfers by transverse circulations about the jet axis in entrance and exit zones of the jet together with transverse transfers to the left of the jet axis associated with the long wave trough and ridge systems.

There is little evidence of a Brewer-Dobson type circulation making an appreciable contribution to the net transfer.

We regard the following aspects of the problem as unresolved:

1. The relative contributions of the mean and eddy motion to the net transfer, since the horizontal profile of mean tropospheric ozone across the jet axis is inconsistent with the results of the mean vertical mass transfer analysis in Section 8.2. Independent estimation of the magnitude of the exchange by eddy mass transfer directly, by means of characteristic cross sections, was not practicable since the sample was not representative.
2. The relationship of the subsidiary ozone maximum in the time series in the lower stratosphere in relation to latitude (and mean jet position).

8.4 Maintainance and Movement of the Tropopause in Relation to Proposed Circulations.

The present study has not contributed any notable clarification of the problem of tropopause formation and maintainance. But we should examine briefly whether the exchange processes discussed above are consistent with what we know of tropopause structure.

A tropopause formed in low latitudes as a result of radiation and wet convection would presumably be advected poleward by the upper limb of the Hadley cell as far as the subtropical jet. Similarly a tropopause formed by convection and radiation in colder air north of the polar front jet - at a lower level than in low latitudes, partly because of the smaller buoyancy from latent heat and greater stratospheric ozone - would presumably be advected equatorward as far as the jet to the south by an indirect circulation about the polarfront jet. (There is no evidence of a mean indirect cell associated with the subtropical jet though we have postulated similar local transverse circulations.) The tropopause is not an isentropic surface and so it is reasonable to expect air to move freely through it, the lapse curvature being maintained by radiation and the motion processes discussed quantitatively by Brewer - and probably, on a scale comparable with cyclone eddies, by a field of divergence associated with the jet circulations. This is broadly consistent with the observed tropopause structure. Moreover, in the jet entrance, where the transverse circulation about the jet is reversed, we would expect to find some

characteristic difference in tropopause structure and limited analysis in Section 7.7 supports this contention. The radiation field and its effect on tropopause reformation will change with change in circulation because of the dominant importance of cloud distribution. These are matters for further investigation.

ACKNOWLEDGEMENTS

The author wishes to thank the appropriate members of the Meteorological Office Staff for access to analysed charts, for generous use of Meteorological Office Library facilities, and for valuable assistance in processing data (M.R.F. and Ozone); Professor Brewer for providing his ozone profiles for Liverpool; and A.E.R.E., Harwell, for access to airborne radisotope sampling data.

I am indebted to Professor Sheppard for suggesting the general problem of this thesis and would like to express my appreciation of his constructive criticism throughout its development.

Finally, I should like to thank the Meteorological Branch of the Canadian Department of Transport for providing me with the incentive and the resources for this period of study.

BIBLIOGRAPHY

Alexander (1960)	N.A.S.L. 88
Bannon, Frith & Shellard (1952)	Geophys. Mem. 88
Barclay, Elliot, Goldsmith & Jelley (1960)	Quart. J.R. Met. Soc. 86
Barrett, Herndon & Carter (1949)	J. Met. 6
Barrett, Herndon & Howard (1950)	Tellus 2
Berggren (1952)	Tellus 4
Bjerknes (1932)	Geophys. Publ. 9, No. 9
Bjerknes (1934)	Hydrodynamique physique avec applications a la meteorologie dynamique, Paris, Les Presses Universitaires.
Bjerknes & Palmen (1937)	Geophys. Publ. 12.2
Bleichrodt, Blok, Dekker, Lock (1959)	Tellus 11
Bleichrodt, Bleeker & Schmidt (1960)	Tellus 12.2
Boville, Wilson & Hare (1961)	J. Met. 18.5
Brasefield (1954)	J. Met. 11
Brewer (1949)	Quart. J.R. Met. Soc. 75
Brewer & Houghton (1956)	Proc. Roy. Soc. A.236
Brewer (1960)	The transfer of atmospheric ozone into the troposphere. M.I.T. Planetary Circulation Project.
Brewer, Dutsch, Milford, Migeotte, Paetzold, Piscalar, Vigreox (1960)	Ann. de Gephys. 16
Brewer, Milford (1960)	Proc. Roy. Soc. A256

Briggs & Roach (1963)	Quart. J.R. Met. Soc. 89
Brooks (1953)	J. Met. 15.2
Brown, Goldsmith, Green, Holt, Parkham (1961)	Tellus 13.3
Brundidge & Goldman (1962)	J. Applied Met. 1
Brunt (1934)	Phys. & Dyn. Met., Cambridge Press.
Bushnell & Suomi (1961)	J. Geophys. Res. 66
Cambray, Fisher, Spicer, Wallace, Webber (1962)	A.E.R.E. R.4094
Chapman (1951)	Compendium of Met. A.M.S.
Charney (1947)	J. Met. 4
Coblentz & Stair (1939)	J. Res. Nat. Bur. Stand. 22
Coblentz & Stair (1941)	J. Res. Nat. Bur. Stand. 22
Craig (1950)	Met. Monograph V.1-2
Crooks, Osmond, Owers, Fisher, Evett (1960)	A.E.R.E. R.3349
Crocks, Evett, Fisher, Lovett, Osmond (1961)	A.E.R.E. R.3766
Crossley (1961)	J. Inst. Navig. 14.4
Crutcher (1961)	Tech. Paper 41 U.S. Weather Bur.
Danielsen & McLain (1955)	J. Met. 12.314
Danielsen (1959)	Archiv. fur Met. Geoph. Brokl. 11.3
Danielsen (1962)	
Dobson, Harrison, Lawrence (1929)	Proc. Roy. Soc. A.122
Dobson, Brewer, Cwilong (1946)	Proc. Roy. Soc. A.185
Dobson (1957)	W.M.O.

Dutsch (1956)	Archiv. fur Met. Geoph. Biokl. A.9.1
Dutsch (1959)	Archiv. fur Met. Geoph. Biokl. A.11.2
Dutsch (1962)	Archiv. fur Met. Geoph. Biokl. A.13.2
Eady (1949)	Tellus 1
Eady (1950)	Cent. Proc. Roy. Met. Soc.
Eliassen (1952)	Astrophys. Norvegia. 5.2
Emden (1915)	Sitzungeber k Bayer Acad. Wies. Math. Phys. Klasse 55.142
Endlich (1953)	J. Met. 10
Feely, Spar (1960)	Nature V.188.4756
Feely (1960)	Science 131.645
Fultz, Long, Owers, Bohan, Kaylor, Weil (1959)	Met. Monograph 4.21 A.M.S.
Godson (1960)	Quart. J.R. Met. Soc. 86.369
Gold (1909)	Proc. Roy. Soc. A.82
Goldie, Moore, Austin (1958)	Geophys. Mem. 101
Goody (1949)	Proc. Roy. Soc. A.197
Goody, Roach (1958)	Quart. J.R. Met. Soc. 84
Gotz, Meetham, Dobson (1934)	Proc. Roy. Soc. A.145
Gowan, Leppard (1953)	Canadian J. Phys. 31.5
Greenfield (1957)	J. Met. 14.2
Hageman, Gray, Machta, Turkevich (1959)	Balloon Sampling U.S.A.E.C. TID.5555
Hageman, Gray, Machta, Turkevich (1959)	Science V.130.3375
Hare (1960)	Quart. J.R. Met. Soc. 86.368
Hare (1960)	J. Met. 17.1

Hare (1962)	Weather 17.8
Heastie, Stephenson (1960)	Geophys. Mem. 103
Helliwell, Mackenzie, Kerley (1956)	M.R.P. 976
Helliwell, Mackenzie (1957)	M.R.P. 1024
Helliwell (1960)	Sci. Paper 1, Air Ministry, Met. Office, London.
Hess (1946)	J. Met. 5
Holland (1959)	U.S.A.E.C. TID.5555
Houghton, Seeley (1960)	Quart. J.R. Met. Soc. 86.369
Houghton (1962)	Proc. Roy. Soc. A.258
Hulbert (1955)	N.R.L. Report 4600
Itagaki, Koenuma (1962)	J. Geophys. Res. 67
Jeffreys (1926)	Quart. J.R. Met. Soc.52
Jensen (1960)	Sci. Rpt. No.1 Planetary Circulations Project, M.I.T.
Johansen (1955)	Geophys. Publ.1915
Johnson, Purcell, Tousey, Watanabe (1952)	J. Geophys. Res. 5.7
Joint Scientific Advisory Group of Met, Rocket Network (1961)	J. Geophys.RRes. 66
Junge, Chagnon, Manson (1961)	Science 133.3463
Aumf Kampe (1960)	Weatherwise 13
Karandikar (1952)	Proc. Ind. Acad. Sci. A.35
Kochmanski (1955)	J. Met. 12
Krishnamurti (1961)	J. Met. 18
Kroening, Ney (1961)	J. Geophys. Res. 67

Langlo, (1952)	Geophys. Publ. Oslo, 18.6
Lockhart, Baus, Blifford (1959)	Tellus 11
Lockhart, Patterson, Saunders, Black (1960)	J. Geophys. Res. 65.3987
Lockhart, Patterson (1960)	Tellus 12.3
London (1957)	A.F. 19(122)-165
London (1962)	N.Y.U. Final Rpt. AFCRL-62-672
Lorenz (1955)	Tellus 7
Machta (1959)	TID.5555
Manabe, Moller (1961)	Mon. Weather Rev. 89
Martell (1959)	Science V.129
Mastenbrook, Dinger (1960)	U.S.N.R.L. Rpt. 5551
Mastenbrook, Dinger (1961)	J. Geophys. Res. 66
Masterson, Hubert, Carr (1961)	J. Geophys. Res. 66
Matteer, Godson (1960)	Quart. J.R. Met. Soc. 66
Matteer (1960)	Met. Branch Toronto Circ. 3291
Matthewman (1955)	Met. Office Prop. Notes No. 7.114
McDowall (1960)	Proc. Roy. Soc. A.256
McIntyre (1959)	Geophysica 6.3-4
Meetham (1937)	Quart. J.R. Met.Soc. 63
Meetham, Dobson (1935)	Proc. Roy. Soc. A.148
Met. Office Discussion (1954)	Met. Mag. 85
Middleton, Spilhaus (1953)	Met. Instruments, U.of T. Press
Miles (1961)	Quart. J.R. Met. Soc. 88
Mintz (1954)	Bul. A.M.S. V.35.5
Miyake, Saruhashi, Katsuragi, (1959)	Papers in Met. & Geophys. V.IX.3-4
Miyake, Saruhashi, Katsuragi, Kanazawa (1960)	Papers in Met. & Geophys. V.XI.1

Molla, Loisel (1962)	Geophys. Pura a Applicata 50.166
Moller (1941)	Die Warmstrahlung des Wasserdampfes der Atmosphere, Gerl. Beitr. Geophys. 58
Moreland (1959)	Bul. A.M.S. 40.373
Murcray D. Murcray F. Williams, Leslie (1960)	J. Geophys. Res. 65
Murgatroyd, Goldsmith, Hollings (1954)	M.R.P. 877
Murgatroyd (1957)	Quart. J.R. Met. Soc. 83.358
Murgatroyd, Goody (1958)	Quart. J.R. Met. Soc. 84.361
Murgatroyd, Singleton (1961)	Quart. J.R. Met. Soc. 87
Murray, Daniels (1953)	Quart. J.R. Met. Soc. 79
Murray (1956)	Geophys. Mem. 97
Newell, Siry (1947)	Naval Res. Lab. Rpt. R.3120
Newell (1961)	Geophys. Pura a Applicata 49
Newton, Persson (1962)	Tellus 14.2
Nicolet (1958)	Sci. Rpt. 102 Penn. State U.
Normand (1951)	Quart. J.R. Met. Soc. 77.333
Normand (1953)	Quart. J.R. Met. Soc. 79.339
Normand (1954)	Proc. Toronto Met. Conf. 1954
Obrien, Mahler, Stewart (1936)	Nat. Geo. Soc. Stratosphere Series 2
Ohring (1958)	J. Met. 15
Ohring, Meunch (1960)	J. Met. 17.2
Ooyama (1962)	NYU Dept. Met. & Ocean Rept. AF19(604)-5492
Paetzold (1953)	J. Atmos. Terr. Phys. V.3
Paetzold (1954)	Geophys. Res. 59
Paetzold (1955)	J. Atmos. Terr. Phys. V.7

Palmen (1935)	Commentations Physico-Mathematicae Soc. Scient. Fennica 7.6
Palmen (1948)	J. Met. 5
Palmen, Nagler (1949)	J. Met. 6
Palmen, Vuorela (1963)	Quart. J.R. Met. Soc. 89
Pant (1956)	J. Geophys. Res. 61.3
Peirson, Crooks, Fisher (1960)	A.E.R.E. R.3358
Piexoto (1960)	Sci. Rpt. 4 Plan. Circ. Project
Priestley (1950)	Australian J.Sci. Res.45
Ramanathan, Dave (1957)	Annals of IGY 5.1
Ramanathan, Karandikar (1949)	Proc. Ind. Acad. Sci. A.29
Ramanathan, Kulkarni (1959)	Quart J.R. Met. Soc. 86.368
Reed, Saunders (1953)	J. Met. 10
Reed (1955)	J. Met. 12
Reed, Danielsen (1959)	Archiv. fur Met. Geophys. Brokl. A.11.1
Regener, E & V. (1934)	Phys. Zeita 35
Regener (1951)	Nature 167
Regener (1959)	Advances in Chemstry Ser.21 A. Chem. Soc.
Regener (1960)	J. Geophys. Res. 65.12
Riehl (1962)	Tech. Rpt. 32, Colorado State U.
Saltzman, Piexoto (1957)	Quart. J.R. Met. Soc. 85
Sawyer (1957)	M.R.P. 1964
Sawyer (1958)	Quart. J.R. Met. Soc. 84.362
Serebreny, Eldon, Weigman, Hadfield (1962)	J. Applied Met. 1.2
Sheppard (1954)	Proc. Toronto Met. Conf. 1954
Sheppard (1963)	Rpts. on Progress in Physics V.XXVI
Small (1960)	Tellus 12.3

Staley (1957)	Beitr. Phys. freien Atmos. 29.4
Staley (1958)	Archiv. fur Met. Geoph. Biekl. A.10
Staley (1960)	J. Met. 17.6
Staley (1962)	J. Atmos. Sci. 19.6
Starr & White (1952)	Tellus 4
Starr & White (1954)	Geophys. Res. Paper 35 GRD
Stebbins (1960)	D.A.E.A. 532-B, Wash.DC.
Stewart, Osmond, Croose, Fisher (1958)	A.E.R.E.MP/R 2554
Stewart, Osmond, Crooks, Fisher, Ower (1959)	A.E.R.E. MP/R 2790
Storebo (1959)	J. Met. 16.6
Suomi, Staley, Kuhn (1958)	Quart. J.R. Met. Soc. 84
Toneberg, Olsen (1944)	Geophys. Publ. 13.12
Tucker (1957)	M.R.P. 1052
Tucker (1959)	Quart. J.R. Met. Soc. 85.365
Tucker (1960)	Tellus 12.2
Vuorela (1957)	Geophys. Helsinki, 6.2
Walshaw (1960)	Quart. J.R. Met. Soc. 86
Wege, Klaue (1957)	I.fur Met. Geoph. U. Berlin Met. Abh.5.4
Wege, Leese, Greening, Hoffmann (1958)	Berlin freie U.I. fur Met. Abh.6.4
Welford, Collins (1960)	Science V.131.3416
Widger (1949)	J. Met. 6
White (1949)	J. Met. 6
White (1954)	Tellus 6
Willet (1944)	Desc. Met. N.Y. Acad. Press
Zubyan (1957)	Canadian Met. Translations No.4.

Appendix 1

Evaluation of smoothed vertical velocities in the upper troposphere and lower stratosphere:

The thermodynamic equation for unsaturated air may be written:-

$$\frac{dT}{dt} = \frac{1}{c_p}\frac{dq}{dt} - \omega\Gamma_d \quad \ldots\ldots\ldots\ldots\ldots\ldots 1.$$

where $\Gamma_d = -\left(\frac{dT}{dz}\right)_d > 0$, represents the temperature profile of the atmosphere with which a parcel undergoing dry adiabatic motion would remain in thermal equilibrium,

giving : $$\omega = \frac{\frac{\partial T}{\partial t} + \underline{V}.\nabla_h T - \frac{1}{c_p}\frac{dq}{dt}}{-\left(\Gamma_d + \frac{\partial T}{\partial z}\right)} \quad \ldots\ldots\ldots\ldots 2.$$

On the infrequent occasions where the atmosphere is statically unstable, i.e., $\frac{\partial T}{\partial z} < -\Gamma_d < 0$, the denominator $-\left(\Gamma_d + \frac{\partial T}{\partial z}\right) > 0$, otherwise it is negative. In the troposphere $\frac{\partial T}{\partial z} \doteq -\Gamma_d$ so care must be taken in estimating the lapse rate there, but in the stratosphere $\frac{\partial T}{\partial z} \doteq 0$ and the denominator tends to $-\Gamma_d$ and may be derived more conveniently from potential temperature profiles.

Since realized values of $\frac{\partial T}{\partial t}$ in the upper troposphere and lower stratosphere are generally large compered with the likely rate of radiative heating or cooling ($\sim 1^{\circ}K\ day^{-1}$) we shall neglect the latter in our evaluation of ω.

Equation 2 refers to instantaneous values and becomes after smoothing: $$-\bar{\omega}\left(\Gamma_d + \frac{\partial \bar{T}}{\partial z}\right) \doteq \frac{\partial \bar{T}}{\partial t} + \bar{\underline{V}}.\nabla_h \bar{T} + \overline{\underline{V}'.\nabla_h T'} \quad \ldots\ldots 3.$$

Vertical velocities were evaluated smoothed over a 24 hour interval and an area about the size of Great Britain, and layers of 40 mb thickness. Temporal mean values were obtained by taking averages of the observations 12 hours preceeding and succeeding the required time, i.e., $t \pm 12hr$.

$$\bar{T} = \frac{T_i + T_f}{2}, \quad T_i = T_{t-12}, \quad T_f = T_{t+12},$$

Evaluation:
Denominator $$\left(\Gamma_d + \frac{\partial \bar{T}}{\partial z}\right) = \frac{1}{2}\left\{\left(\Gamma_d + \frac{\partial T_i}{\partial z}\right) + \left(\Gamma_d + \frac{\partial T_f}{\partial z}\right)\right\}$$

$\left(\Gamma_d + \frac{\partial \bar{T}}{\partial z}\right)$ was evaluated directly from radiosonde profiles in the troposphere, but in the stratosphere where a time section of Θ had already been evaluated on a linear p scale, it was estimated from the equation:

$$\frac{\partial \theta}{\partial p} = \frac{R\theta}{gp}\left(\Gamma_d + \frac{\partial T}{\partial z}\right) \quad \ldots\ldots\ldots\ldots\ldots\ldots 4$$

i.e.,

$$\Gamma_d + \frac{\partial \bar{T}}{\partial z} = \frac{1}{2} \cdot \frac{g}{R}\left\{\frac{p_i}{\theta_i}\frac{\partial \theta_i}{\partial p} + \frac{p_s}{\theta_s}\frac{\partial \theta_s}{\partial p}\right\} \quad \ldots\ldots 5$$

The ratio $\frac{p}{\theta}$ was assumed constant since $p_i = p_s$ and the range of θ (305-335°K at 300 mb) is about 10% of its mean. The vertical gradient of θ was evaluated over a layer from 20 mb above to 20 mb below the required level. (Smoothing over a 40 mb vertical interval is consistent with that over a horizontal distance of 3-400 km, and a time of about 12-hr.).

Local change term: $\frac{\partial \bar{T}}{\partial t} = \frac{1}{\Delta t}\left(\bar{T}_s - \bar{T}_i\right)$ where $\bar{T}_s$ and $\bar{T}_i$ are the temporal mean values at times $t \pm 12$-hr. The temperatures were spatially smoothed over a 250 km 'square', Leuchars-Hemsby-Camborne-Aldergrove, by combining their respective values with four times that at Liverpool and dividing the total by eight.

Horizontal advection term: $\bar{\underline{V}} \cdot \nabla_h \bar{T}$. The mean vector wind was evaluated from the Liverpool values $\underline{V}_i$ and $\underline{V}_s$, no spatial smoothing was considered necessary since $\underline{V}$ was not highly variable over the 300 km spatial smoothing area.

Charts of $\bar{T}$ were analysed over an area incorporating the British Isles and Northern Europe - the analysis procedure of drawing smooth isotherms introducing some degree of spatial smoothing. $\nabla_h \bar{T}$ was extracted from these charts. The eddy transfer term $\overline{\underline{V}' \cdot \nabla T'}$ was neglected though it may be as large as the mean advection in cases of rapidly moving waves.

Appendix II

Integration of ozone in finite vertical columns.

Tropospheric Integrated Ozone. In the troposphere $\frac{\partial T}{\partial p} \neq 0$ but $\frac{\partial \theta}{\partial z} \doteq 0$. Now $x_o = 5{\cdot}86 \times 10^{-5} \times \frac{T}{p} \times \rho_o$

and $T = \theta \left(\frac{p}{p_o}\right)^{K}$ where $K = \frac{R}{C_p}$

$$x_o = 8{\cdot}10 \times 10^{-6} \times \theta \times \frac{\rho_o}{p^{1-K}} \qquad \ldots\ldots\ldots\ldots\ldots\ldots\ldots\ldots 6.$$

Consequently the ozone in the troposphere may be evaluated as follows:

$$O_T = [O]_{p_o}^{p_{Tr}} = \int_{p_o}^{p_{Tr}} \frac{8{\cdot}10 \times 10^{-6} \times \theta \times \rho_o \times 10^3}{p^{1-K} \times g}\, dp$$

$$\doteq 8{\cdot}26 \times \theta \times 10^{-6} \sum_{p_o}^{p_{Tr}} \frac{\rho_o}{p^{1-K}} \cdot \Delta p \qquad \ldots\ldots\ldots\ldots 7.$$

In the troposphere $\theta \doteq 300^{\circ}K$ and the summation was carried out over small intervals of p (i.e, small c.f. the variations in p^{1-K} and ρ_o which are independent functions of p).

Now over the range 1000-100 mb, p approximates to a straight line and sums were evaluated over layers diminishing in thickness from 300 mb in the lower troposphere to 50 mb near the tropopause where the vertical ozone concentration profile is liable to greater changes.

Stratospheric Integrated Ozone. Ozone in a layer between the tropopause and a pressure p_s in the stratosphere

$$[O]_{p_{Tr}}^{p_s} = \frac{1}{g} \int_{p_{Tr}}^{p_s} x_o \cdot dp = \frac{5{\cdot}86 \times 10^{-2}}{g} \int_{p_{Tr}}^{p_s} T \cdot \rho_o \frac{dp}{p} \qquad \ldots\ldots\ldots 8$$

In the stratosphere $\overline{T} \doteq$ constant on any given day

$$\therefore [O]_{p_{Tr}}^{p_s} = \frac{5{\cdot}86 \times \overline{T} \times 10^{-2}}{g} \int_{p_{Tr}}^{p_s} \rho_o\, d\ln p.$$

$$= \frac{5{\cdot}86 \times \overline{T} \times 10^{-2}}{g} \sum_{p_{Tr}}^{p_s} \rho_o \ln\left(\frac{p}{p-\Delta p}\right)$$

But $\ln\left(\frac{p}{p-\Delta p}\right) = \frac{1}{\log_e}\left\{\log\left(\frac{p}{p-\Delta p}\right)\right\} = 2{\cdot}3 \log\left(\frac{p}{p-\Delta p}\right)$

$\therefore$ Ozone in column $= 1{\cdot}36 \times 10^{-4} \times T \sum_{p_{Tr}}^{p_s} \rho_o \cdot \log\left(\frac{p_i}{p_i - \Delta p}\right)$.

The area on a $\rho_o, \log_{10} p$ chart was estimated in such a way that $\Delta \log_{10} p = \log_{10}\left(\frac{10^n}{10^{n+1}}\right) = 1$ unit. Since 1 unit represents the ratio of 1000 to 100 mb an overlay scale was constructed to read off the area directly in terms of this unit.